Bacterial Mucin Degradation in the Cystic Fibrosis Airways: A Potential Regulator of *P. aeruginosa* Pathogenicity.

A DISSERTATION
SUBMITTED TO THE UNIVERSITY OF MINNESOTA BY

Alex Ruben Villarreal

IN PARTIAL FULLFILLMENT OF THE REQUIREMENTS
FOR THE DEGREE OF
DOCTOR OF PHILOSOPHY

ADVISOR: Ryan Hunter, PhD

May 2023

ACKNOWLEDGMENTS

First and foremost, I would like to acknowledge the Hunter laboratory and its many iterations over the years, starting with my advisor Ryan Hunter. Thank you for your continued support and for always being quick to offer understanding and compassion through some of the most difficult chapters of my life thus far. Thank you for always providing me with the attention and mentorship I required even during your tenure process and sabbatical. Lastly, thank you for not taking my commonly worn “I am unwell” and “I hate it here” text baseball caps personally. You are truly a fantastic advisor.

Thank you to the several post-docs I have had the pleasure of working with – Jeffrey Flynn, Ben Bonis, Patrick Moore, and Joshua Fletcher. I can attribute most of my technical knowledge directly to your collective guidance. I appreciate all of your listening ears, feedback, and tolerance of my never-ending repetitive questions. The completion of this Ph.D. would not have been possible without each of you.

Thank you to my fellow graduate students in the Hunter laboratory – Sarah Lucas, Richard Martinez, and Carlo Castillo. I am happy to have been able to share knowledge, feedback, and joint misery with each of you throughout the years, and I wish you the best in all of your endeavors.

Special thank you to the all-knowing and all-seeing Adam Gilbertsen who materialized at the formation of this institution and will dissipate in turn with the fall of it. Thank you for your begrudging aid in everything including but not limited to - technical support, material acquisition, instrument repair, method development, and bureaucratic loopholes. Thank you for always lifting my spirits by reminding me things could always be significantly worse. You were dearly missed after your departure from the laboratory.

Thank you to Lydia Cameron for your kind words and encouragement, and for always volunteering to make the hard phone calls that involved yelling. Thank you to Talia Wiggen for providing me with my sole source of nutritional intake (sausage penne pasta) during my second year in the program. Thank you to Mitchell Penningroth for quickly learning to wear many hats and ensure the laboratory remained functional during Ryan's sabbatical. Finally, thank you to Kayla Hoffman for providing bioinformatics support and generally being cool.

Outside of the Hunter laboratory, thank you to Megan Ruf. You were always there to answer my questions, send me reminders, and guide me through the many hoops of this graduate program. I would also like to acknowledge my cohort members – Katrina Jackson, Megan Smith, Jordan Naumann, and Lucy Sjaastad. You were always there for me to grab a drink, go on a hike, plan a mini getaway, and, above all, vent. I am the last to finish, but we did it!

Thank you to my deluge of friends from elementary school, high school, and college that I still keep in touch with regularly – you know who you are. Coming home and spending time with you always offered a reprieve from my never-ending workload and allowed me to recharge. Each of you have helped me more than you will likely ever know.

Last, and certainly least, thank you to the University of Minnesota and general graduate school complex for requiring our productivity stay high while our wages remain low throughout repeated “unprecedented times” and record-breaking inflation. You provided me with the spite I needed to fuel my escape.

DEDICATION

I dedicate this body of work to my mother Margaret Villarreal and brother Adam Villarreal. Thank you for your lifelong and unwavering support. This entire journey was done in part for you and would not have been possible without you. I love you both dearly.

ABSTRACT

Cystic fibrosis (CF) is characterized by impaired mucociliary clearance, leading to mucus accumulation and chronic bacterial respiratory infections. Pseudomonas aeruginosa (PA) is a canonical pathogen in these infections and is found to nutritionally benefit from cross-feeding interactions with co-colonizing mucin-degrading bacterial genera. However, the impact of these cross-feeding interactions on the regulation of PA virulence remains unclear. Implementing a reductionist experimental approach, this thesis aims to investigate the proposed cross-feeding model to identify key exchanged metabolites and elucidate mechanisms underlying PA virulence.

To successfully isolate and analyze variables of the multifaceted cross-feeding model, several specialized experimental tools and techniques were developed and described in Chapter 2. These tools were employed in Chapter 3 to fully characterize the growth profiles of several individual representative mucin-degrading bacterial species and investigate the effects of their secondary metabolites on PA physiology. Chapter 4 builds upon this by characterizing complex mucin-degrading bacterial communities enriched from clinical CF sputum samples, and again investigating their effects on PA physiology *in vitro*. These data establish validated methods for the field of CF research, expand our understanding of PA physiology, and pave the path for future development of novel targeted CF therapeutic strategies.

TABLE OF CONTENTS

† Reprinted in part or in full from a manuscript currently in preparation for publication, a manuscript currently under review for publication, or a publication in which I am listed as a contributing author.

LIST OF TABLES

LIST OF FIGURES

CHAPTER 1: Introduction

Cystic Fibrosis

Cystic fibrosis (CF), first described in 1938 (Navarro, 2016), is a multisystem autosomal recessive genetic disease that affects over 30,000 people in the United States and approximately 100,000 people worldwide (Shteinberg et al., 2021). 1 in 2,500 Caucasian newborns are diagnosed with the disease before the age of two (Scotet et al., 2012), ultimately contributing to an estimated annual average of over $467,130,000 dollars spent on direct CF healthcare expenditures in the United States alone (Gool et al., 2013). While advancements in treatment of this disease have drastically increased mean life expectancy of patients in the United States to the age of 56 compared to 38 just a decade ago (Cystic Fibrosis Foundation, 2022), research continues in an effort to increase patient quality of life and conclusively remedy the condition (Rowe et al., 2023).

CF etiology is a result of mutations in the CF transmembrane conductance regulator (CFTR) gene, encoding the CFTR protein that functions as anion-selective channel in epithelial cells (D'Amore et al., 2022). These channels transport chloride and bicarbonate ions across epithelial membranes and are vital in maintaining ionic homeostasis in environments such as the respiratory, pancreatic, intestinal, and reproductive epithelial tissues (Hanssens et al., 2021). There are five recognized classes of CFTR gene mutations (class I – class V), the most common being a class II mutation known as the F508Δ mutation which results from a single amino acid deletion and perturbs appropriate localization of the CFTR protein (Marson et al., 2016; Alfonso-Sanchez et al., 2010). Other

mutation classes involve premature translational termination, improper trafficking, misfolding, and altered gating. Regardless of mutation classification, deleterious mutations to the CFTR gene invariably lead to the loss of presence or function of CFTR ion channels in relevant tissues (Marson et al., 2016; Rowntree et al., 2003). As a result, CF is associated with a range of body-wide comorbidities that significantly impact quality of life. Effects on pancreatic function can lead to CF-related diabetes (Marshall et al., 2005). Effects on the liver can lead to CF-related liver disease (Scott-Jupp et al., 1991). Effects on the gastrointestinal tract can not only lead to chronic constipation and gastroesophageal reflux, but also malnutrition as a result of severely decreased nutrient absorption by intestinal epithelia (Pencharz et al., 2000). A variety of factors contribute to infertility in both male and female CF patients (Lyon et al., 2002). Additionally, chronic rhinosinusitis and lung inflammation are hallmarks of those with the condition (Chaaban et al., 2013).

While CF is a multisystem disease, the root of patient morbidity and mortality primarily lies in chronic airway complications. Loss of chloride ion transport across the airway epithelium leads to the dehydration and thickening of mucus. Mucus is a secreted gel matrix that coats epithelial cell surfaces in the airways, contributing to airway homeostasis (Tildy et al., 2015). In healthy human respiratory systems, this thin and fluid mucus layer is in perpetual motion via the coordinated beating of epithelial cilia. In the CF airways, this mucus layer is abnormally viscous and impairs ciliary beat, impeding mucociliary clearance – a physiological defensive mechanism responsible for the expulsion of foreign bodies and excess mucus from

the lungs (Robinson et al., 2002). Without this mechanism, the accretion of a thick and viscous mucus layer not only physically obstructs airflow, but also leads to the establishment of non-transient complex microbial communities and chronic bacterial infections punctuated by periods of decreased lung function known as pulmonary exacerbations (Carmody et al., 2015). Repeated pulmonary exacerbations cause excessive fibrosis of lung tissue and an overall decrease in lung function as measured by forced expiratory volume in one second (FEV1) – a measure of the volume of air an individual can forcibly expel from their lungs in one second (Taylor-Robinson et al., 2012; Sanders et al., 2010). While FEV1 values often recover to baseline following successful treatment of an exacerbation, values tend to trend downward over the course of a patient's life and ultimately contribute to pulmonary failure (Taylor-Robinson et al., 2012).

While bacterial infection is most commonly attributed to the onset of pulmonary exacerbations, viral infections, environmental pollutants, stress, and malnutrition can also lead to airway inflammation and contribute to the condition (Bhatt. 2013; Goss et al., 2003). Regardless, the first line of treatment for CF pulmonary exacerbations is the use of oral, inhaled, and/or intravenous antibiotics. Young patients are more likely to respond to treatment with first line β-lactam class antibiotics (i.e., penicillin, cephalosporin, carbapenem) that target peptidoglycan synthesis in the cellular envelope of common CF airway pathogens such as *Staphylococcus aureus* and *Pseudomonas aeruginosa* (Hahn et al., 2021). However, as a patient ages and is exposed to repeated rounds of antibiotic

treatment, the incidence of multi-drug resistant infections increases (Glen et al., 2021). This results in treatment plans becoming less targeted and often requiring the administration of multi-class antibiotic cocktails (Conway et al., 2012). There is growing evidence that antibiotic susceptibility testing in clinical laboratories offers little utility in accurately predicting patient response to an antibiotic regimen (Smith et al., 2003; Hurley et al., 2012; Waters et al., 2019). As a result, clinicians may work with patients to identify which combination of drugs works best for the individual (Flynn et al., 2020; Zemanick et al., 2020).

Outside of periods of pulmonary exacerbation, CF patients follow a multifaceted treatment plan to relieve symptoms, prevent complications, and increase quality of life. Daily antibiotics (i.e., azithromycin) aid in the reduction of airway infection occurrence and severity (McCormack et al., 2007). Bronchodilators (i.e., albuterol) and mucolytic agents (i.e., dornase alfa) are also regularly used and work to widen airways and thin mucus, respectively (Konig et al., 1995; Konstan et al., 2012). Periodic use of high-frequency chest wall oscillation via a specialized vest unit, works synergistically with prescribed medications by mechanically loosening airway mucus through intense vibration, ultimately helping some patients breathe and expectorate sputum more easily (Morrison et al., 2020). In severe cases or in late-stage lung disease, single or bilateral lung transplants are often a last resort when patient lung damage causes pulmonary function to fall below viable levels (Grossman et al., 1990; Force et al., 2011).

Next generation precision combination medicines such as Trikafta (ivacaftor, tezacaftor, and elexacaftor) have led to monumental improvements in CF patient airway health by correcting the root cause of malfunctioning CFTR proteins rather than treating subsequent symptoms (Bear, 2019). Tezacaftor and elexacaftor are classified as CFTR correctors which bind to CFTR proteins and facilitate their transport to epithelial cell membranes, where they can function properly. This benefits those with class II CFTR processing mutations, such as the common F508 deletion (Bear. 2019; Zaher et al., 2021). Ivacaftor is classified as a CFTR potentiator, which binds to membrane bound CFTR proteins and facilitates increased translocation of chloride ions across the channel protein. This benefits those with class III CFTR gating mutations such as G551D substitutions (Zaher et al., 2021). Together, these medications synergistically function to greatly improve CFTR channel protein localization and function, consequently improving airway homeostasis and reducing patient morbidities (Zaher et al., 2021; Liessi et al., 2020). Despite this recent advancement, Trikafta is not an effective treatment option for all CF patients. Those with CFTR mutations outside of the classes II and III, may produce faulty CFTR proteins (class IV), not enough CFTR proteins (class V), or no CFTR proteins at all (class I) – rendering the medications ineffective (Bear. 2019). Accordingly, **chronic mucus accretion and bacterial infections of the airways remain a burden on the CF population.**

Mucins

The mucus of the respiratory system, as well as other human tissues, is primarily composed of mucins; high molecular weight glycoproteins consisting of a polypeptide (protein) backbone structure that is heavily decorated with N- and O-linked glycans (carbohydrate). While the general structure of mucins can vary based on type, they generally range from 10 to 300nm in size and between 200 kDA to 200 MDa in molecular weight (Kesimer et al., 2011). The large masses are primarily due to the glycan components which comprise up to ~90% of total content by weight (Rose et al., 2006). The dense heavily glycosylated regions are hydrophilic, contributing to the high water-binding capacity and steric shielding of the polypeptide backbone from proteolysis (Hansson. 2019). The polypeptide backbone plays a role in polymerization of mucin monomers, conferring unique gel-forming properties that are central to the biological functions of mucin (Demouveaux et al., 2018).

The molecular structure of mucins consists of a large central PTS (proline, threonine, serine) domain that is rich in proline, threonine, and serine tandem repeats. This domain is flanked by cystine rich regions that promote polymerization of mucin molecules though the formation of disulfide bonds. The PTS domain is heavily glycosylated with O-linked glycans attaching directly to the hydroxyl groups of threonine and serine residues (Brockhausen et al., 2009). The proximal sugar residue of each O-linked glycan is one of four core structure patterns composed of a combination of five monosaccharides (galactose, N-acetylglucosamine, N-

acetylgalactosamine, fucose, and sialic acid) (Bansil et al., 2006). These cores are variably modified or terminated by a fucose, sialic acid, or blood group epitope (Varki et al., 2022). The result is an immense and complex biomolecule rich in glycan diversity and presenting in a characteristic “bottle-brush” structure (**Figure 1.1**).

This “bottle-brush” structure confers many biological benefits; however, it can also impede the analysis of mucin glycoproteins through traditional methods such as protein gel separation. The glycosylation of mucin core proteins precludes their proteomic analysis via conventional 1D or 2D polyacrylamide gel-based approaches (Kesimer et al., 2016). Similarly, glycomic analysis presents challenges. Chromatography-based approaches to analyze mucins or mucin-containing samples are complicated as the large glycoproteins are prone to clogging or damaging sensitive analytical chromatography columns (Jaggi et al., 1987). Despite this, the development of improved mucin characterization methods continues to push the field of glycobiology forward.

Mucins are highly conserved and are primarily produced by goblet cells of non-keratinized epithelia in most animals – including mammals, birds, reptiles, fish, and invertebrates. Irrespective of organism, mucins effectuate the same general key biological roles – hydration and lubrication of mucosal surfaces and immune function (Lagow et al., 1999; Bar-Shira et al., 2014; Madrid et al., 1989; Perez-Sanchez et al., 2013; McDermott et al., 2021). In humans, mucins coat epithelial

tissues in the respiratory, gastrointestinal, reproductive, urinary, and ocular systems (Audie et al., 1993). This layer prevents desiccation of tissue surfaces while also acting as a potent lubricant for vital functions such as intestinal peristalsis (Herath et al., 2020) or ciliary beat within the lungs (Bustamante-Marin et al., 2017). This lubrication also lends itself to roles in immune function, as it is required for the previously described debridement of foreign bodies and infectious agents via the process of mucociliary clearance in healthy human airways (Bustamante-Marin et al., 2017; Munkholm et al., 2013).

The mucus layer acts as a component of the innate immune system most notably by acting as a physical barrier to host cells preventing adhesion and invasion by infectious agents. While mucin glycan chains physically occlude microbes from accessing epithelial surfaces, the chains also act as a scaffold for the inclusion of host antibodies and antimicrobial molecules throughout the mucus layer (Sheng et al., 2022). In some cases, mucins themselves have been found to directly bind pathogens – restricting their proliferation (Tu et al., 2008). In the case of *Pseudomonas aeruginosa*, the canonical CF airway pathogen, intact high molecular weight intestinal mucins were found to impact the behavior of reference strain *PAO1* (Wheeler et al., 2019). In addition to inhibiting adhesion to culture and cell surfaces, intact mucins and select mucin-glycans dispersed *PAO1* biofilms and downregulated transcription of key virulence genes responsible for quorum sensing (*lasR*), siderophore biosynthesis (*pvdA*), and type-three secretion (*pcrV*). No significant change in growth rate was observed following mucin-elicited effects,

suggesting mucins may modulate bacterial virulence via a growth-independent signaling mechanism (Wheeler et al., 2019). Similar repression of virulence by intact mucins has been observed in a range of other organisms (Wang et al., 2022), including fungal opportunistic pathogens such as *Candida albicans* (Takagi et al., 2022; Kavanaugh et al., 2014).

In regard to the host, recent findings indicate that mucins play an understated role in signal transduction – signaling environmental changes to epithelial cell layers via membrane bound mucin intracellular domains (Sheng et al., 2022; Hollingsworth, 2006). Mucin signal transduction pathways influence host response to tissue injury and infection (Sheng et al., 2022; Singh et al., 2006). As a result, structural or chemical changes to the mucosal layer can lead to perturbed mucin expression and contribute to cancers via increased cellular proliferation and downregulated apoptosis (Sheng et al., 2022; Sheng et al., 2017).

Human *MUC* genes are responsible for the differential expression of mucin types. While many putative *MUC* genes have been identified, fourteen have been described and of those, eight have been well characterized (Ringel et al., 2003). The MUC protein family consists of two primary classification types – transmembrane mucins and secreted mucins (**Figure 1.1**). Heavily O-glycosylated transmembrane mucins form a scaffolding known as the glycocalyx – the epithelial cell proximal mucin layer that acts as the underlying base of a healthy stratified mucus environment in which secreted mucins can bind and gel upon.

Transmembrane mucins (MUC1, MUC4, MUC12, MUC13, MUC15, MUC16, MUC17, MUC21) (Bafna et al., 2010) contain a membrane-spanning domain and cytoplasmic tail that anchor them to cellular surfaces and allow them to form this scaffolding (Bafna et al., 2010). Secreted mucins contribute to the fluid gel-like layer covering the glycocalyx and are present in higher abundance in mucus secretions compared to transmembrane mucins (Gipson et al., 2003). The secreted mucin category is sub-categorized into gel-forming mucins (MUC2, MUC5AC, MUC5B, MUC6, MUC19) and non-gel forming mucins (MUC7, MUC8, MUC9, MUC20) (Zaretsky et al., 2018). The respiratory system is known to express MUC1, MUC4, and MUC16 transmembrane mucins. However, MUC5AC and MUC5B are considered to be most abundant of these mucin species (Lillehoj et al., 2013; Zanin et al. 2016).

Hypersecretion of airway mucus is a defining characteristic of CF. Accordingly, the abundance of MUC5AC and MUC5B are thought to be increased in CF airway secretions. Immunohistochemical staining (Groneberg, et al., 2002) and transcriptional analysis (Voynow, et al., 1998) support this claim, suggesting goblet cell hyperplasia and significant transcriptional increases in MUC expression as driving factors of hypersecretion. However, other studies employing Western blot approaches convey conflicting findings, suggesting significant decreases in both MUC5AC and MUC5B in CF mucus – instead proposing CF mucus secretions contain a higher abundance of non-mucin components such as DNA compared to mucus in relatively healthy individuals (Henke, et al., 2006). While *in vitro* addition

of DNA to mucus has been found to increase mucus viscosity (Picot, et al., 1978), the recalcitrance of mucin to protein gel methods impedes its thorough analysis and obfuscates definitive interpretation of results. Ultimately, it is agreed upon in the literature that the abundance of MUC5AC and MUC5B in CF airway secretions are variable between disease states (stable, exacerbation onset, exacerbation resolution) (Kirkham, et al., 2002). Regardless of mucin species abundance - pH, hydration, and salinity of the CF airway environment differs from that of healthy airways and disrupt post-secretory unpacking and folding of secreted mucin glycoproteins (Abdhllah et al., 2017). Disruptions to mucin maturation can impact its structure and gelling properties, increasing its viscosity, and leading to its accumulation in the airways.

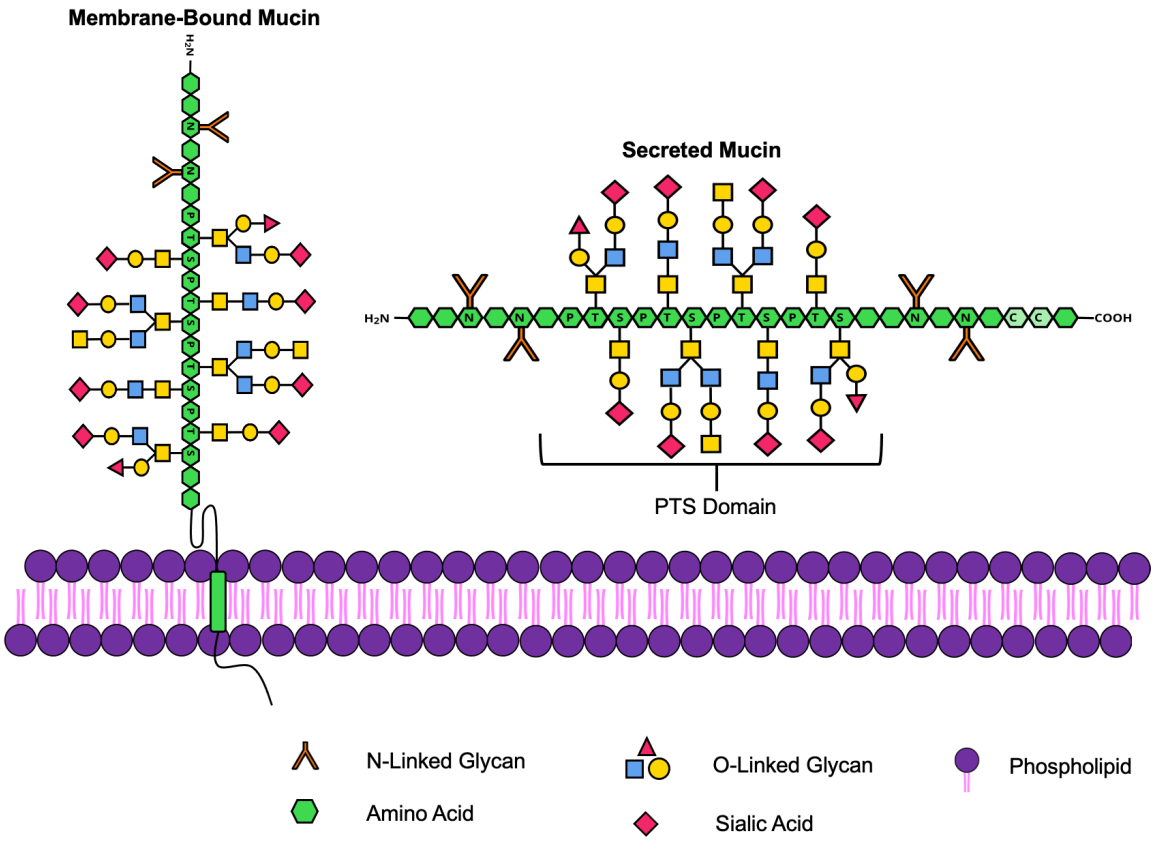

Figure 1.1 - Model of primary mucin type classifications. Membrane-bound mucins possess a transmembrane domain that anchors them to the surface of epithelial cells and allows them to form the scaffolding of the glycocalyx. Secreted mucins lack transmembrane domains, but often exhibit gel-matrix forming properties that confer mucus its viscosity and water-binding properties. Both classifications share similar molecular structuring, including a polypeptide backbone, glycan chains, and PTS domains.

Mucin-Degrading Bacteria

Mucin glycoproteins are carbon-rich macromolecules and contain most nutrients necessary for supporting bacterial growth. The abundant and diverse glycan chains offer sugars as a primary carbon source for saccharolytic bacterial species to metabolize. The amino acid rich polypeptide backbone offers a carbon source for asaccharolytic species and species with a nutritional preference for amino acids (including the canonical CF pathogens, *P. aeruginosa* and *S. aureus*). Regions rich in cystine, a sulfur-containing amino acid, regularly flank PTS domains and provide an abundant source of sulfur (Gum et al., 1992; Ho et al., 2006). While phosphorylated sugars such as glucose-6-phosphate are rare in mucin glycan chains, *in vivo* mucin gel matrices (i.e., mucus) often contain free DNA and other phosphate containing host molecules, as well as a variety of trace elements (Rouillard et al., 2022). Hydrogen, nitrogen, and oxygen are all also readily found throughout the molecular structure of mucins, readily usable as building blocks for bacterial biomass.

Despite containing the components to function as a complete nutritional source for bacteria, only a subset of microbial species has been found able to efficiently sequester and catabolize nutritional resources from mucin glycoproteins to support their growth (Flynn et al., 2016). While many bacterial species are known to produce saccharolytic and proteolytic enzymes that could facilitate catabolism of mucin components, few are able to do so successfully. This may be due, in part, to the high density and meshing of glycans that decorate mucin core proteins,

sterically and spatially impeding the function of bacterial saccharolytic enzymes. Additionally, these same glycans may shield the polypeptide core of mucins from degradation by bacterial proteases.

Of the bacterial species found to successfully degrade and utilize mucin to any extent, all express saccharolytic enzymes belonging to the general enzyme grouping known as glycosyl hydrolases (GH) (also known as glycosidases) that cleave specific sites in glycan linkages (Amin et al., 2021). Efficient mucin degradation is thought to occur in a stepwise fashion with the physically accessible outer components of the glycoprotein being utilized first, with the consequent use of the core polypeptide chain. Terminal sugar residues such as sialic acids or fucose are first cleaved via GH33 family sialidases or GH29 / GH95 family fucosidases, respectfully (Lionicanova et al., 2020). Exoglycosidase families including N-acetyl-glucosaminidases (GH84), N-acetyl-galactosaminidases (GH101), and galactosidases (GH2) are then able to sequentially cleave glycosidic linkages of terminal monosaccharides in glycan polysaccharide chains. In some instances, endoglycosidase families (GH16) cleave within a glycan chain rather than at a terminal monosaccharide, releasing glycan oligosaccharides (Kobata, 2013). Upon sufficient glycan depletion, the polypeptide protein core is left susceptible to cleavage by bacterial proteases such as elastase (Glover et al., 2022). Few bacterial species harbor a complete arsenal of relevant enzymes required to fully degrade and utilize a mucin glycoprotein monomer. Consequently, mucin degradation is considered a bacterial community effort (Wickstrom et al.,

2009; Flynn et al., 2016). Evaluation of salivary MUC5B mucin degradation via SDS-PAGE found that supragingival dental plaque bacterial communities cooperatively degrade mucin while individual community constituents were not able (Wickstrom et al., 2009).

While the healthy human respiratory system does not host dense bacterial communities like the gastrointestinal tract, impaired mucus clearance in the CF airways leads to the accumulation of abundant, non-transient bacterial communities. Cross-sectional and longitudinal studies on infants and children with CF have found the lower airways to become stably colonized with polymicrobial communities early in life (Muhlebach et al., 2018). Interestingly, these lower airway communities often share a similar composition to that of well-defined oral microbial communities, though at different cell densities (Meskini et al., 2021). This is in part due to the repeated aspiration of microbe-containing oral secretions into the lower airways, and failure of successful removal as a result of perturbed mucociliary clearance (Muhlebach et al., 2018). Colonization of the lower airways by bacterial communities is associated with increased inflammation and susceptibility to subsequent infections by canonical airway pathogens (Muhlebach et al., 2018; Huffnagle et al., 2016). Furthermore, these communities evolve over time, sharing similar microbial signatures across patient groups suggesting microbial ecological succession (Khanolkar et al., 2020).

Despite persisting in mucin-rich environments, it is unlikely that all individual bacterial species of these communities are adept at the degradation and catabolism of mucin glycoproteins. To identify the fraction of species capable of this catabolism, the fraction must be enriched for further analysis. This is accomplished by inoculation and repeated passaging of human mucus samples (i.e., saliva, sputum) in a minimal mucin medium containing only mucin as a sole carbon source. 16S rRNA gene sequencing of both saliva and CF sputum enriched anaerobically in this manner, identify four commonly cooccurring genera across samples suggesting their involvement in the degradation of mucin – *Streptococcus spp*., *Prevotella spp*., *Veillonella spp*., and *Fusobacterium spp*. (Flynn et al., 2016). Further details about each genus are provided below.

Streptococcus is a saccharolytic genus of Gram-positive cocci that is facultatively anaerobic (Patterson, 1996). *S. parasanguinus* and *S. gordonii* are two of most commonly identified species in CF airway communities (Maeda et al., 2011) and are contextually considered keystone species – colonizing the mucosal environment early and providing structure for subsequent colonization by other bacterial species (Nobbs et al., 2009). This is due, in part, to their metabolic flexibility that allows them to not only tolerate variable environmental conditions, but also produce extracellular polysaccharides that facilitate the adhesion (Steinberg et al., 1999) and cross-feeding of co-colonizing microorganisms (Schultz et al., 1979). According to the Carbohydrate-Active Enzymes (CAZY) online database (Drula et al., 2022), these species harbor several glycosyl

hydrolases suggesting they may contribute to the degradation of mucin by cleaving glycan linkages. Cleaved glycans are likely used as a carbon source in fermentation, not only leading to the production of endogenous ATP but also exogenous mixed-acid fermentation byproducts. Carbon dioxide and hydrogen gases are commonly produced in addition to a variety of organic acid byproducts dependent on environmental conditions. Lactic acid (lactate) is a highly produced organic acid, which can acidify the pH of its microenvironment, modifying growth conditions in its favor, and limiting the growth of competing bacterial species (Schultz et al., 1979; Vandenberg, 1993). Other organic acids such as acetic acid, formic acid, succinic acid, and pyruvic acid are also produced by *Streptococcus spp.* (Wang et al., 2021). *In vitro* monocultures of *S. parasanguinus* (data not shown) and *S. gordonii* (**Figure 3.3A**) have been found to grow to high densities in minimal media containing purified porcine gastric mucin as a sole carbon source.

Prevotella is an anaerobic genus of Gram-negative bacilli belonging to the phylum Bacteroidetes (Tett et al., 2021). Similar to *Streptococcus*, this genus is commonly found in bacterial communities belonging to mucosal environments of the human body – the oral cavity, respiratory system, vagina, and gastrointestinal tract. In CF, *P. melaninogenica* and *P. oris* are identified in the microbiomes of the oral cavity and lower airways (Field et al., 2010). The CAZY database bolsters the characterization of *Prevotella* as a saccharolytic genus, as it harbors many enzymes from glycosyl hydrolase, transferase, esterase, and binding module families (Drula et al., 2022). Mucin glycans degraded by these enzymes fuel

anaerobic fermentative metabolism and lead to the production of common fermentation gases as well as acetic acid, butyric acid, and propionic acid (Betancur-Murilla et al., 2023). While monocultures of *P. melaninogenica* and *P. oris* grow on minimal media containing purified porcine gastric mucin, its ability to do so is not as robust as *Streptococcus spp.* under the same conditions (**Figures 3.S1-3.S9**).

Veillonella is a Gram-negative genus of obligate anaerobes often characterized by its diminutive size (0.3μm – 0.5μm in diameter) (Rogosa et al., 1964). *Veillonella spp.*, particularly *V. parvula,* is similarly associated with human mucosal environments (Zhan et al., 2022; Pustelny et al., 2014). Interestingly, unlike the previous two genera, *Veillonella* is asaccharolytic (Rojas-Tapias et al., 2022), and harbors significantly fewer sequences associated with glycan degradation. Rather, it is known as a specialist in the fermentation of lactic acid into acetate and propionate, and the reduction of nitrate (Ng et al., 1971). Consequently, *in vitro* growth of *V. parvula* monocultures is not supported by minimal media containing mucin as a sole carbon source. However, co-culturing in the same medium with a lactic acid producing species such as *S. gordonii* results in proliferation of both species - likely a result of *Veillonella* catabolism of *Streptococcus spp* derived lactate into acetate.

Lastly, ***Fusobacterium*** is a Gram-negative genus of obligate anaerobes with a unique cell morphology regularly referred to as elongated bacilli with pointed ends

(Brennan et al., 2019). Just as the previous genera, *F. nucleatum* and *F. periodonticum* are associated with human mucosal surfaces (Strauss et al., 2008). While not as metabolically diverse as *Streptococcus spp*., *Fusobacterium* also produce extracellular polysaccharide matrices which promote the formation of polymicrobial biofilms, most notably in the oral cavity (Mohammed et al., 2013). Unlike the previous genera, *Fusobacterium* is not only asaccharolytic, but highly proteolytic (K.J. Flynn et al., 2016) – exhibiting a strong preference for the degradation and utilization of polypeptides like that of the core polypeptide backbone structure of mucins. The CAZY database supports this, listing few sequences belonging to relevant mucin degradation enzyme families (Drula et al., 2022). Amino acids cleaved from polypeptide chains are fermented by *Fusobacterium* into secondary metabolites that include common fermentation gases, acetic acid, butyric acid, propionic acid, and ammonia (Sakanaka et al., 2022; Rudin et al., 2021). Monoculture *in vitro* growth of *F. nucleatum* and *F. peridonticum* on minimal media containing mucin as a sole carbon source is limited, suggesting either a marginal capacity for some glycan degradation or limited access to the mucin polypeptide backbone.

While *in vitro* growth profiles of individual species on mucin as a sole carbon source may vary, co-culturing of two or more has a synergistic effect drastically increasing culture growth rate and final density (**Figure 4.3**)– alluding to the significant mucin metabolism of complex bacterial communities *in vivo*. Observed synergistic effects of co-culturing are likely a result of cross-feeding interactions between populations

and supports the hypothesis that efficient mucin metabolism in a mucosal environment is a microbial community effort. This observation offers explanation for the frequent co-occurrence of the described four core commensal genera in CF sputum. It also underscores their potential to impact the nutritional landscape of the CF airways, and as a consequence, potentially impact CF associated pathogens.

Pseudomonas aeruginosa

In addition to commensals, pathogens are also commonly identified in CF airway communities and are key contributors to disease pathophysiology. *Pseudomonas aeruginosa* (PA), *Staphylococcus aureus, Haemophilus influenzae, Burkholderia cepacia* complex*, Stenotrophomonas maltophila, Achromobacter xylosoxidans,* and non-tuberculosis mycobacteria are the primary pathogens associated with CF lung infections and resulting pulmonary exacerbations (Wood et al., 2019). Cohort studies have found *S. aureus* to be the most prevalent, colonizing 50% to 80% of CF patients between the approximate ages of 2 to 25 years old. However, the same studies documented a temporal change in pathogen prevalence that occurs during the mid-to-late twenties of the CF patient lifespan in which *S. aureus* is no longer dominant. Instead, its prevalence drops while the prevalence of PA increases to upwards of 80% (Pittman et al., 2011). Airway colonization by PA, happening later in a CF patient's life, is associated with increased severity and duration of pulmonary exacerbations and subsequent decreased lung function over time (Pittman et al., 2011; Crull et al., 2018). Once colonization occurs,

complete eradication of the PA population is unlikely, despite repeated rounds of antibiotic treatments – an artifact of increased prevalence of PA antibiotic resistance. Because of its burden it late-stage lung disease, association with pulmonary exacerbations (PEx), and resistance to antimicrobials, PA is considered responsible for the bulk of CF patient morbidity and mortality (Crull et al., 2018).

Pseudomonas aeruginosa *is* a Gram-negative bacillus with a preference for aerobic respiration but can respire anaerobically provided that nitrate is readily available as a terminal electron acceptor (Hernandez et al., 1991). The species is encapsulated, motile, and metabolically versatile allowing it to successfully colonize a range of environments such as soil, natural water sources, medical equipment, humans, and even more limiting environments such as hot tubs (Yu et al., 2007). While it is often implicated in human infections, it is considered an opportunistic pathogen - primarily infecting immunocompromised individuals like individuals with CF, HIV, and those with chronic wounds such as diabetic foot ulcers. PA infections are notoriously aggressive and difficult to treat. This is due to its vast arsenal of virulence factors and its intrinsic highly adaptive mechanisms of antibiotic resistance.

PA is well known as a multidrug resistant opportunistic pathogen, in part due to high genomic plasticity and ability to rapidly adapt and evolve in response to changing conditions. This is often accomplished through its high capacity for the integration of new genetic information via horizontal gene transfer (Freschi et al.,

2018). While drug resistance profiles differ between clinical strains, PA exhibits resistance to a wide range of antibiotic classes including penicillins, cephalosporins, carbapenems, aminoglycosides, and fluoroquinolones (Pang et al., 2019). PA employs a diverse set of mechanisms to drive these resistances. Many strains express membrane-bound efflux pumps capable of removing antibiotics such as beta-lactams, aminoglycosides, and fluoroquinolones from the cytoplasm (Pang et al., 2019; Westbrock-Wadman et al., 1999). Some strains also express beta-lactamases which degrade antibiotics such as penicillin and cephalosporin (Pang et al., 2019; Nordmann et al., 1993). In other cases, PA may modify antibiotic targets such as DNA topoisomerases directly, rendering fluoroquinolones ineffective by impeding their binding (Bruchmann et al., 2013). General, non-specific mechanisms such as the formation of robust biofilms containing dense polysaccharide matrices not only confer a level of blanket resistance to all antibiotics but also resistance to host immune cells by functioning as a physical barrier (Taylor et al., 2014). Together, these mechanisms make PA infections difficult to treat and solidify its status as a pathogen of enduring concern in clinical settings.

In terms of virulence, PA is equipped with type I (T1SS), type II (T2SS), type III (T3SS), and type VI (T6SS) secretion systems which facilitate the secretion of toxins, proteases, lipases, and other virulence factors into the environment or directly into the cytoplasm of competing bacterial or host cells (Bleves et al., 2010). Among its arsenal of virulence factors, phenazines are particularly cytotoxic.

Phenazines are a class of small redox-active molecules produced by PA and other bacterial species that are responsible for a host of functions including metal solubilization, biofilm stimulation, and host-cell toxicity (Briard et al., 2015; Wang et al., 2011; McGuigan et al., 2014). Phenazines engage in “redox warfare”, sequestering nutrients from host cells and generating reactive oxygen species which lead to inflammation, progressive oxidative damage, and overall necrosis of host epithelial tissue (McGuigan et al., 2014). Phenazine biosynthetic machinery is encoded by two semi-redundant operons – *phzA1-G1* (*phz1*) and phzA2-G2 (*phz2*) (Cui et al., 2016) (**Figure 1.2A**). These operons are highly regulated through a complex regulatory network that is influenced by environmental conditions as well as quorum sensing signals. In general, a quorum population density must be met for the expression of *phz1* and *phz2* (Cui et al., 2016). Additional conditions such as bioavailable iron levels may impact which of the two *phz* operons is more highly expressed (Nelson et al., 2019). In any case, these *phz1* and *phz2* are responsible for the conversion of intracellular chorismic acid into phenazine-1-carboxylic acid (PCA). PCA may then be converted into phenazine-1-carboxamide (PCN) via PhzH, Pyocyanin (PYO) via PhzM and PhzS, or 1-hydroxyphenazine (1-HP) via PhzS (Mavrodi et al., 2001). Of these molecular conversions, the conversion of the 5-methylphenazine-1-carboxylic acid betaine to pyocyanin via PhzS is the only one to require the presence of oxygen (Mavrodi et al., 2001) (**Figure 1.2A**). PCA, PCN, PYO, and 1-HP comprise the phenazines produced by PA; however, PYO is typically produced in the highest concentrations

and can be easily recognized by eye due to its characteristic blue-green pigmentation (**Figure 1.2**).

It is hypothesized that these phenazines, as well as other virulence factors, play a direct role in PA associated CF pulmonary exacerbations. As previously described, exacerbation onset results in a sharp decrease in patient lung function that typically rebounds after antibiotic therapy. In PA culture-positive patients, it is inferred that exacerbation is the result of pathogen outgrowth, subsequently corrected with the administration of an antibiotic treatment to reduce pathogen population density. However, RT-qPCR with primers specific to PA has shown that this is not always the case. Studies have shown that PA copies of the 16S rRNA gene are similar in abundance prior to the onset of the exacerbation, during its peak, and after the resolution of patient symptoms, suggesting an etiology other than changes in PA abundance (Reid et al., 2013) (**Figure 1.3**). Rather, changes in airway environmental factors (e.g., bioavailable nutrients, co-colonizing bacterial virulence factors) may increase the expression of phenazines in stable populations of PA, eliciting the onset of increased inflammation and subsequent pulmonary exacerbation state. While antibiotic treatment often results in the resolution of exacerbation symptoms, resolution without a detectable decrease in the bacterial load of PA may suggest a non-PA targeted mechanism. As established, co-colonizing bacterial communities are able to degrade mucin glycoproteins and produce diverse profiles of secondary metabolites, modifying the nutritional landscape of the airway environment. In a fashion similar to intestinal dysbiosis,

imbalances in airway bacterial community composition may spur environmental changes that elicit upregulated PA phenazine expression and subsequent exacerbation onset. In the same vein, successful exacerbation resolution via antibiotic therapy may be a result of impacting co-colonizing organisms or correcting PA antagonistic community dysbiosis, rather than efficacy against PA itself. Exact microbial community secondary metabolites that may contribute to this proposed exchange remain unknown; however, identification may offer potential novel targets for the prevention and resolution of exacerbations. Given the rapidly growing antibiotic resistance of PA, the development of novel biomarkers and therapeutic targets is critical. Better understanding of host and microbial factors that modulate PA growth and virulence *in vivo,* is the first step in these developments.

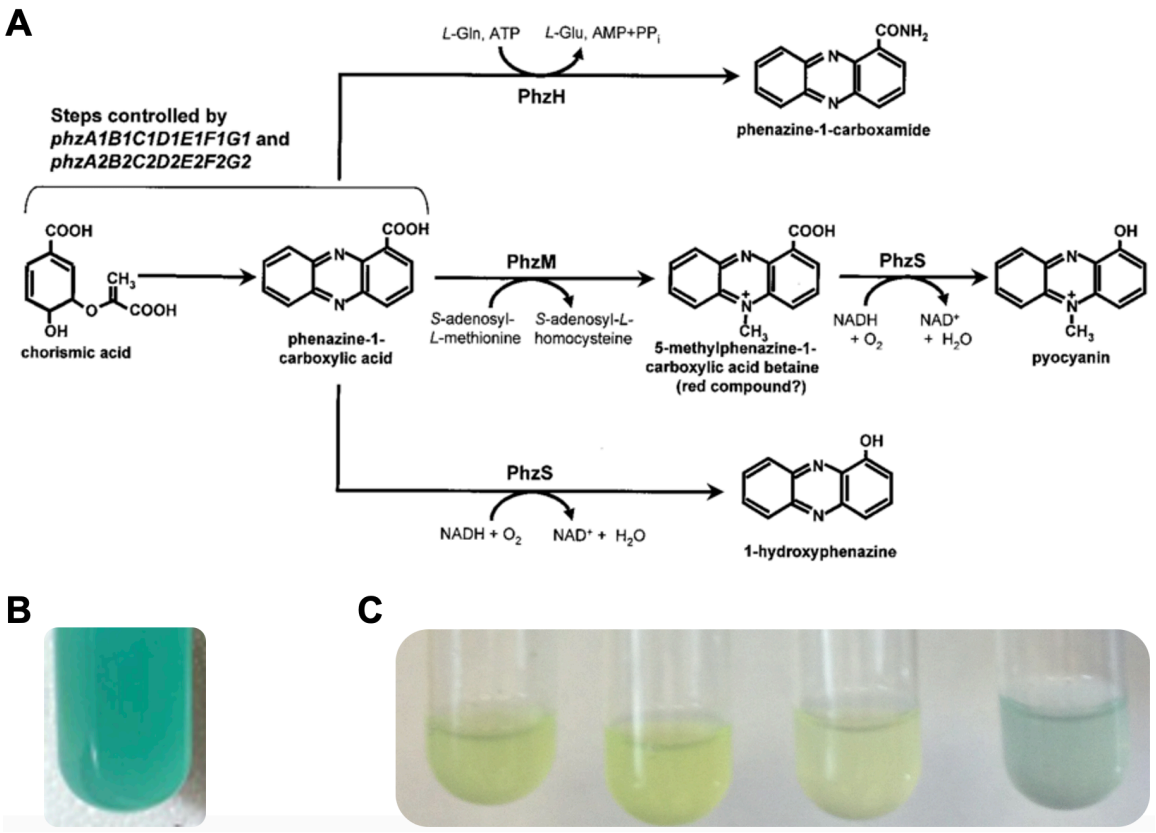

Figure 1.2 - *P. aeruginosa* produces several phenazine species as virulence factors. A) The biosynthetic pathway of phenazine expression in *P. aeruginosa.* Operons *phz1* and *phz2* drive the conversion of chorismic acid into phenazine-1-caroxylic acid (PCA), phenazine-1-carboxamide (PCN), 1-hydroxyphenazine (1HP), and pyocyanin (PYO) (Mavrodi et al., 2001). **B)** Representative photo of *P. aeruginosa* (PA14) grown in rich media. Pyocyanin in culture is visible by eye due to its distinctive blue-green coloration. **C)** *P. aeruginosa* (PA14) grown under the same conditions in the cell-free supernatants of anaerobic bacterial communities enriched from sputum derived from four unique CF patients. PYO concentrations visibly differ between cultures, independent of *P. aeruginosa* density.

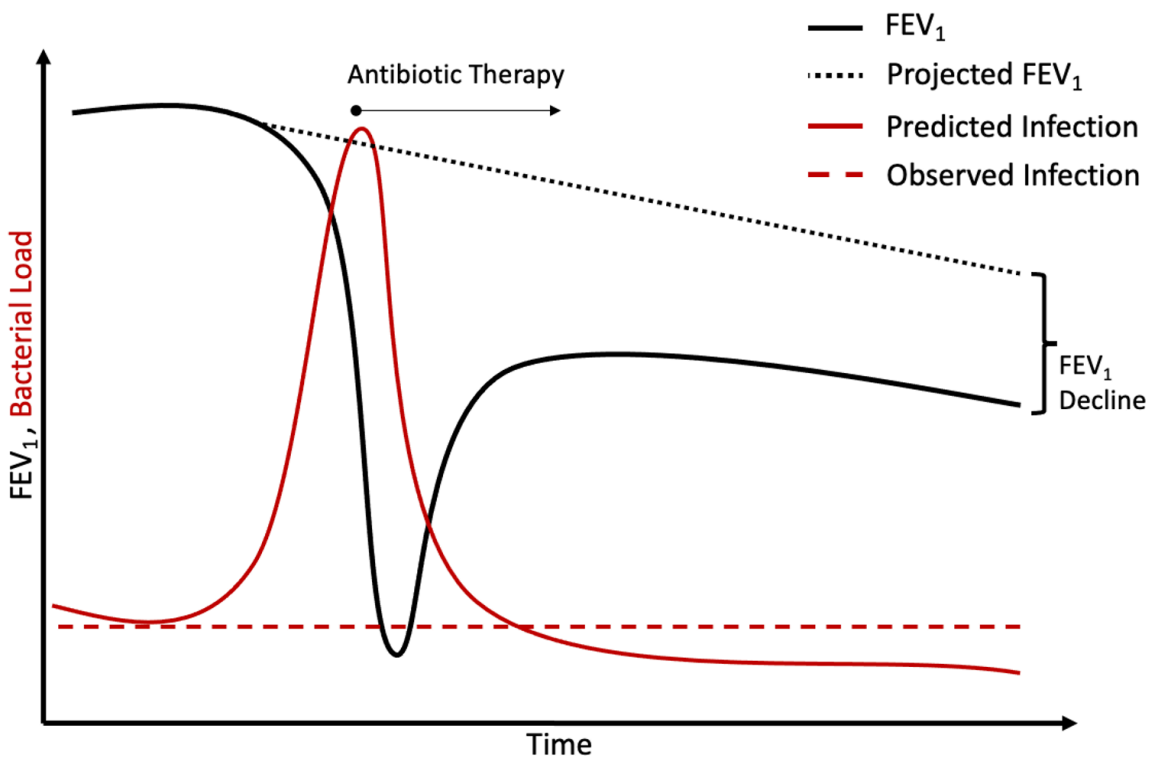

Figure 1.3 - Model of *P. aeruginosa* bacterial load throughout a CF pulmonary exacerbation event. FEV_1 (solid black line) decreases at the onset of a pulmonary exacerbation and recovers after antibiotic therapy. *P. aeruginosa* bacterial load is traditionally predicted to increase during an exacerbation and decrease following antibiotic therapy (red solid line). However, qPCR analysis suggests this is not always the case (Stokell et al., 2014). Rather, *P. aeruginosa* bacterial load remains stable before, during, and after a pulmonary exacerbation (red dotted line) suggesting an exacerbation driving force other than the simple outgrowth of the pathogen.

Mucin-Based Cross-Feeding Model

Given its high colonization rate of over 80% of CF patients over ~25 years of age, a substantial nutrient source must be present to support the high abundance of PA (Pittman et al., 2011). However, unlike the oral cavity and GI tract, externally derived dietary nutrients are not available, suggesting that bacterial growth substrates are likely host derived. While cytokines, defensins, lactoferrins, and other host factors are present as potential carbon and nitrogen sources, they are unlikely available at the high concentrations required to support the large PA bacterial loads of 10^8 to 10^{10} CFU/mL observed in patient sputum (Palmer et al., 2005). Mucin is a highly abundant biomolecule of the CF airways (Morrison et al., 2019); however, despite harboring a variety of extracellular proteases and glycosyl hydrolases (Drula et al., 2022), PA is unable to efficiently utilize it as a sole nutrient source to support its growth. Rather, it is thought to rely on the cross-feeding of degraded mucin components and secondary metabolites produced by previously described anaerobic mucin degrading bacterial species (Flynn et al., 2016). This may be due, in part, to confirmed sialidases capable of cleaving the sialic acid residues that often cap mucin O-glycans rarely being encoded (Lewis et al., 2012) – possibly inhibiting access to mucin glycans. Cleavage of terminal sialic acids or general liberation of mucin structural components by mucin degrading genera may process mucins to a state in which they are nutritionally viable for PA. However, the exact role of each cross-feeding genus (*Streptococcus, Prevotella, Veillonella,* and *Fusobacterium*) and the nature of their exchanged metabolic byproducts remain unknown.

Anaerobic mucin degraders are known to produce copious amounts of diverse organic acids, especially short-chain fatty acids, as byproducts of mucin degradation. The presence of these organic acids *in vivo* has been confirmed through analysis of CF sputum – finding mM concentrations of both acetate and propionate (**Figure 1.4A**). Origination of these organic acids from relevant bacterial sources has also been supported through the analysis of minimal mucin enrichment community supernatants – again finding mM concentrations of organic acids (Flynn et al., 2016) (**Figure 1.4B**). Organic acids not only offer a bioavailable nutrient source for PA, but these metabolites also play a role in the potentiation of antibiotic mediated PA biofilm inhibition, suggesting they may also play a larger role in the regulation of pathogen virulence (Bao et al., 2022).

When grown aerobically on a minimal mucin medium, PA strain PA14 reaches a maximum culture optical density (OD600) of ~ 0.2 - significantly lower than its maximum OD600 of ~0.8 when grown in glucose (**Figure 1.5A**). When co-cultured under aerobic conditions on top of an anoxic soft agar containing an immobilized mix of oral derived mucin degrading anaerobes (**Figure 1.5B**), growth of PA14 increases an order-of-magnitude compared to cultures in which anaerobes are omitted (**Figure 1.5C**). This suggests a cross-feeding relationship between the two populations (Flynn et al., 2016). Furthermore, PA14 produces visually variable pyocyanin concentrations when grown on the cell free supernatants of different anaerobic mucin degrading communities, independent of culture density (**Figure 1.2C**). This observation led to the main hypothesis being tested throughout this

thesis: **the specific composition of a co-colonizing community not only influences the growth of PA, but also its pathogenic potential via regulation of phenazine expression.**

If true, this hypothesis offers potential explanations for two clinically observed phenomena relating to PA and its role in CF disease progression; (i) its tendency to preferentially colonize the airways of older CF patients past their late twenties (Hewer et al., 2017), and (ii) the lack of acute population density changes of the pathogen throughout pulmonary exacerbation cycles (**Figure 1.3**). If PA is unable to degrade and utilize mucins as a sole nutrient source, it may require modification of the nutritional landscape of the airway environment by mucin degrading anaerobes. The ecological succession of that environment may be a stepwise process starting with colonization by robust mucin degrading keystone genera such as *Streptococcus* during the early years of a patient's life, followed by colonization by metabolically cooperative genera such as *Veillonella, Prevotella,* and *Fusobacterium spp.* as a patient ages. This culminates in the eventual colonization by metabolic scavengers such as PA. Scenarios in which PA bacterial load remains stable throughout the cycle of a pulmonary exacerbation (**Figure 1.3**) may be a result of unnoticed changes in co-colonizing bacterial community composition or metabolism, perturbing the cross-feeding relationship and leading to the upregulation of phenazine expression by PA - increasing airway inflammation and eliciting disease flares. It is also possible antibiotic treatment of exacerbations may alter bacterial community composition and cross-feeding

interactions rather than directly killing PA, in turn resulting in a downregulation of PA phenazine expression resulting in symptom resolution. The proposed cross-feeding model (**Figure 1.6**) offers a strong foundation for the investigation of both basic and translational scientific inquiries regarding bacterial interactions within the CF airways and the resulting clinical impacts.

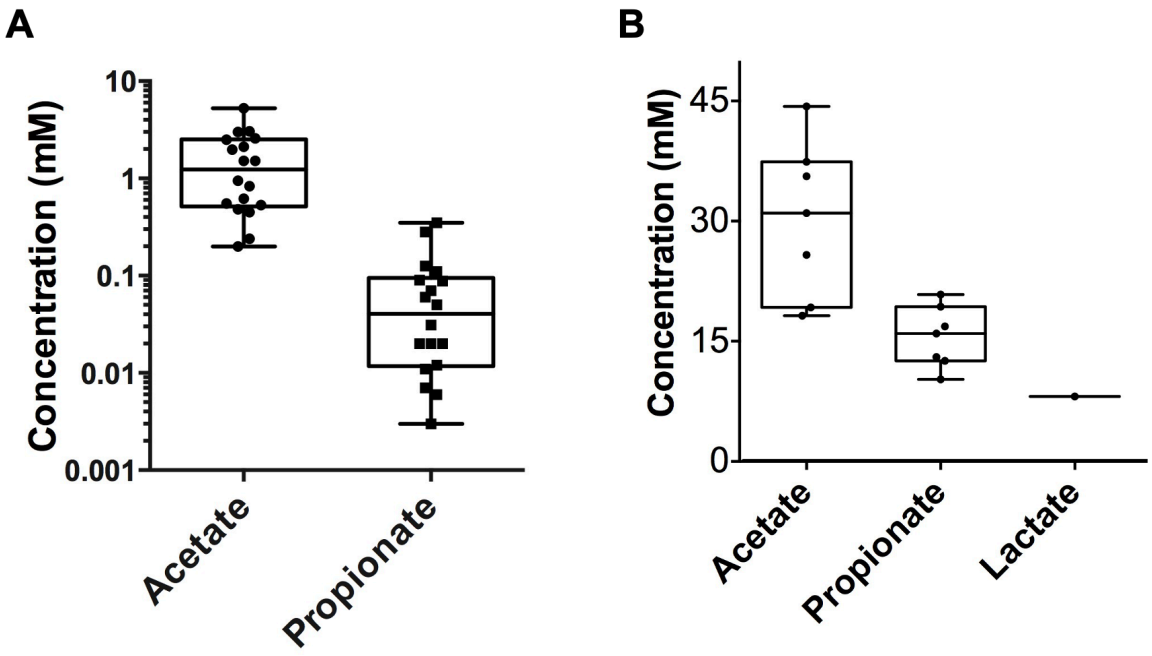

Figure 1.4 - Organic acids are present in CF sputum and subsequent mucin enrichments. A) Quantification of acetate and propionate in a CF sputum sample (Flynn et al., 2016). **B)** Quantification of acetate, propionate, and lactate in the cell free supernatant of a bacterial mucin enrichment derived from a CF sputum sample (Flynn et al., 2016).

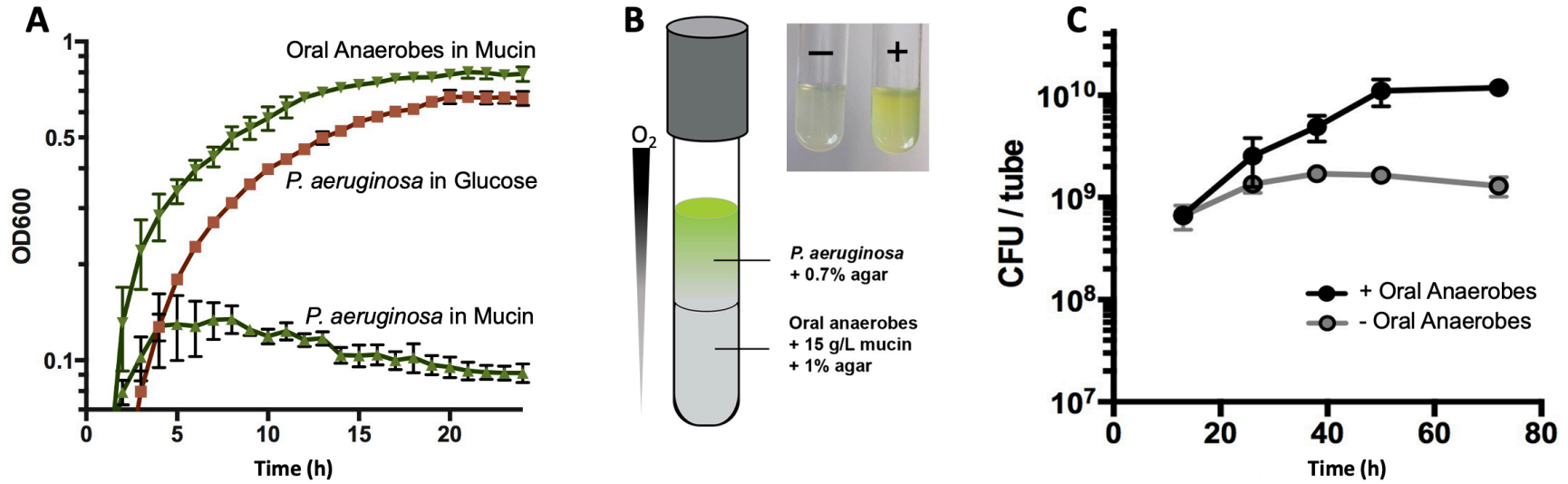

Figure 1.5 - Mucin-degrading anaerobic bacterial communities support the growth of *P. aeruginosa* on media containing mucin as a sole carbon source. A) Growth curves of *P. aeruginosa* and an oral anaerobe bacterial community with different carbon sources. *P. aeruginosa* grows to a low optical density with mucin as a sole carbon source, compared to growth with glucose. Oral derived anaerobes grow to a high density with mucin, suggesting their ability to metabolize it (Flynn et al., 2016). **B)** Co-culture cross-feeding experiment. *P. aeruginosa* was grown under aerobic conditions in a soft agar layered above thick agar anoxic layer containing an oral derived anaerobic bacterial community. Mucin was the sole carbon source (Flynn et al., 2016). **C)** Colony forming unit (CFU) counts resulting from the co-culture model with and without the inclusion of oral derived anaerobic bacteria. Inclusion of oral anaerobes resulted in an order of magnitude increase in *P. aeruginosa* growth, suggesting cross-feeding between populations (Flynn et al., 2016).

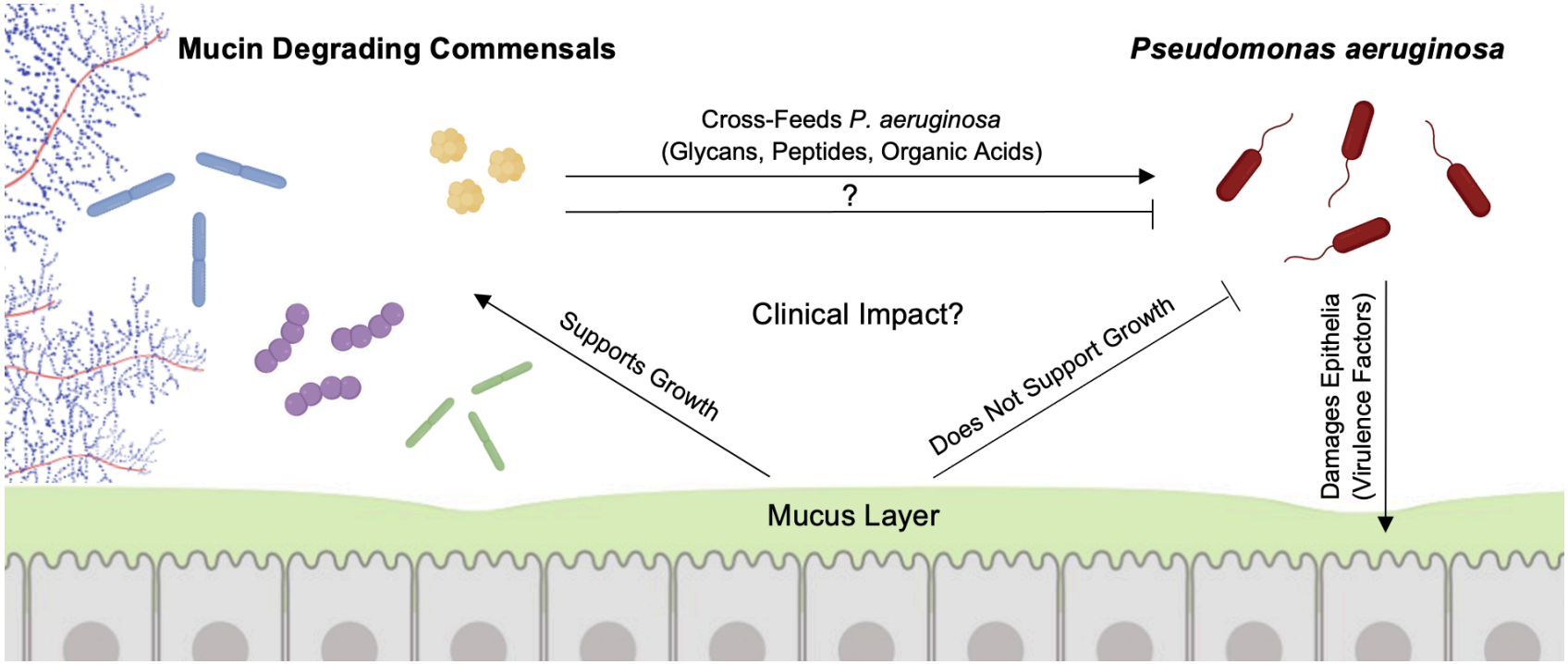

Figure 1.6 - Proposed CF cross-feeding model. Mucin support the growth of anaerobic commensal bacterial species, but poorly support the growth of *P. aeruginosa*. Data suggest the metabolism of mucin by anaerobic commensal bacterial species produces secondary metabolites that support the growth of *P. aeruginosa* and impact its expression of phenazine virulence factors. The specific commensal bacterial species, metabolic byproducts, and mechanisms of *P. aeruginosa* growth and virulence regulation remain unknown, as do the effects of these interactions on patient clinical outcomes.

Conclusion

Throughout this thesis, I employ a reductionist approach to further elucidate the intricacies of the proposed cross-feeding model (**Figure 1.6**) and identify its role in CF disease progression. In Chapter 2, I optimize the tools necessary to tease apart and evaluate the mucin, secondary metabolite, and phenazine components of the model. I describe a fast protein liquid chromatography method capable of qualitatively measuring mucin glycoprotein degradation, a method for the generation of a minimal mucin medium suitable for *in vitro* culture experiments, and two high performance liquid chromatography methods for the quantification of organic acids and phenazines. In Chapter 3, I characterize a representative oral anaerobic community adept at mucin degradation. Subsequently, I characterize individual representative bacterial species of this community and investigate the impact of their metabolic byproducts on PA growth and virulence. I further this investigation in Chapter 4, where I analyze the community composition of clinically derived CF sputum samples and the effects on PA. Together, this work offers a wealth of reference data pertaining to the metabolism of anaerobic mucin degrading bacterial species, as well novel insights into PA physiology and virulence. Additionally, this work establishes several specially optimized methodologies that provide great value in similar fields of research involving bacterial interactions and mucin glycoproteins. Ultimately, these data lay the groundwork for continued research aimed at defining predictive CF pulmonary exacerbation biomarkers and identifying novel alternative therapeutic strategies.

CHAPTER 2: Tool Development – Mucin Media and Liquid Chromatography

Summary

As described in Chapter 1, *Pseudomonas aeruginosa* (PA) is unable to efficiently degrade mucin glycoproteins. Rather, it engages in cross-feeding interactions with commensal mucin-degrading bacterial constituents of the cystic fibrosis (CF) airways that support its nutritional requirements and putatively potentiate its virulence *in vivo*. This cross-feeding model is multifaceted and requires individual characterization of pathogen, commensal, and mucin substrate components as well as interactions between each component. Several limitations impede this characterization – the lack of a biologically relevant mucin-based medium for *in vitro* experiments, the lack of a high-throughput method to measure mucin degradation, and the lack of high-throughput methods capable of measuring cross-feeding metabolites of interest (i.e., organic acids and phenazines) in mucin-rich samples. In this chapter, I overcome these limitations through the development and optimization of a minimal mucin medium (MMM) and several chromatography techniques able to quantify mucin degradation, microbially generated organic acids, and phenazines produced by PA. These tools not only offer value in the field of CF research, but any field involving microbial metabolic interactions and mucin glycoproteins.

Fast Protein Liquid Chromatography: Mucin Degradation

Introduction

Fast protein liquid chromatography (FPLC) is a method of medium pressure liquid chromatography that relies on a peristaltic pump to move samples through an analytical column for the separation and subsequent analysis of biomolecules such as DNA and proteins (Chandra et al., 1992). Columns may be packed with a variety of inert porous solid stationary phase materials (e.g., glass, silica, agarose) conducive for size-exclusion chromatography (SEC) – a technique that capitalizes on the discriminatory power of molecular size for analyte separation (Hong et al., 2012). Elution of analytes from the SEC column follows a pattern wherein species with greater molecular dimensions are more rapidly eluted, while those with smaller molecular size exhibit delayed elution due to comparatively slower transit through the stationary phase matrix. Post elution, analytes are passed through a flow cell for analysis via an ultraviolet – visible light spectrum (UV-VIS) detector which measures light absorption of eluents at key wavelengths (260 nm for nucleic acids / 280 nm for proteins) to quantify relative abundance (Manchester et al., 2018).

Despite routine implementation of this methodology in protein analysis, its applicability to mucins, while seemingly intuitive, is impeded by the innate properties of the glycoproteins (Haavik et al., 1985). Owing to their molecular weight (> 2 million kDa) and distinct gel-forming characteristics, mucins possess an increased propensity to obstruct SEC columns thereby elevating system

pressure, compromising instrument components, and ultimately hindering the separation of mucins of different molecular weights. In spite of this, utilization of FPLC SEC remains a valuable analytical tool if the aforementioned caveats are kept in mind when developing relevant separation methods. This is particularly true when compared to mucin glycoprotein analyses via alternative methods such as enzyme-linked immunosorbent assays (ELISA). While ELISA may be able to quantify mucins by employing capture antibodies specific to core mucin components (i.e., MUC5AC, MUC5B) (Kraft et al., 2008), labor required for these methods is significantly greater and they are not without their own caveats including possible hindrance of antibody binding by dense glycan chains - similar to the observed glycan protection of glycoprotein polypeptides from protease cleavage (Varki, 2016). Also, ELISAs inherently have a reduced capacity to characterize various size-based stages of glycoprotein degradation.

In the following chapter, I present an optimized FPLC SEC method for the reproducible separation of high molecular weight (HMW) and low molecular weight (LMW) mucin glycoprotein populations from mucin-rich samples. While unable to quantify absolute values of these glycoproteins, this method can be used to measure relative changes between the two, providing valuable insight into the level of HMW mucin degradation that has taken place in a sample. When combined with an FPLC fraction collector, this method also allows for collection of degraded mucin pools for further purification or downstream analysis. Development of this method has been instrumental in evaluating the mucin-degrading potential of both

individual CF-associated bacterial species and more complex communities. This approach also holds promise for wider applications beyond CF research, with potential utility in diverse fields of inquiry mucin-rich environments, such as oral, ocular, gastrointestinal, and reproductive body sites.

Materials and Methods

Media Preparation:

1X beef broth complete media was prepared with reagents as described in **Tables 2.1 - 2.2**. All reagents, with the exception of cysteine HCl, were combined and brought to a boil until full dissolution of solids into solution. Cystine HCl was added once the mixture was cooled to room temperature. Media was brought to a pH of 7.0 and degassed in an anaerobic chamber for a minimum of 6 hours prior to being dispensed into rubber crimp-top balch-type glass tubes. Media aliquots were autoclaved at 121°C for 20 minutes prior to storage in the anaerobic chamber and subsequent use.

MMM was prepared with reagents as described in **Tables 2.4 -2 .8** and following the original methodology as described Flynn et al., 2016 and on page 60.

Table 2.1 – Recipe for the preparation of complete beef broth media.

1X Beef Broth Complete Media (250 mL)	
Reagent	**Quantity**
2.25X Beef Broth*	111 mL
Trypticase	15 g
Yeast Extract	2.5 g
K_2PO_4	2.5 g
Hemin Solution (+ Vitamin K)	5 mL
DHNA	0.5 mg
$_{dd}H_2O$	111 mL
Cysteine HCl**	0.25 g
** Recipe for the preparation of 2.25X beef broth found in Table 2.* ***Combined reagents are brought to a boil for complete dissolution and cooled to room temperature prior to the addition of cysteine HCL.* *Adjusted to a pH of 7.0. Dispensed anaerobically into rubber crimp-top balch-type glass tubes. Autoclaved at 121°C for 20 minutes.*	

Table 2.2 - Recipe for the preparation of 2.25X beef broth.

2.25X Beef Broth (2000 mLs)	
Reagent	**Quantity**
Ground Beef (Organic / Low Fat)	500 g
$_{dd}H_2O$	2000 mL
NaOH	25 mL
Beef is wrapped in cheese cloth and boiled in the solution for 20 minutes followed by a 3-hour simmer. Resulting broth is collected and cool prior to subsequent filtering through cheese cloth to remove residual particulates. Final broth should be clear and brown in color.	

Salivary Mucin Preparation:

Mucins were purified from human saliva. Saliva (~25 mL) was collected in 50 mL conical tubes containing cOmplete protease inhibitor cocktail (Roche; Basel, Switzerland) and mixed to a final volume of 50 mL with a final concentration of 6 M guanidine hydrochloride (GuHCl), 100 mM Tris-HCl, 50 mM dithiothreitol (DTT), and 4 mM EDTA. Samples were incubated at 37°C for 1 hour, then centrifuged at 15,000 x g for 1 hour to remove debris. Supernatant was dialyzed against 4 L of ultrapure MilliQ water for 1 hour at room temperature twice, then dialyzed overnight at 4°C. Retentate was split into 5 mL aliquots in 50 mL conical tubes, frozen at -80°C overnight, and freeze-dried. Lyophilized samples were pooled and resuspended in 6mL of 3 M GuHCl. Samples were gently agitated for 1 hour at room temperature on an orbital shaker, centrifuged for 3 minutes at 7000 rpm to remove insoluble protein, then filtered through a 0.2 μm centrifugal filter (Thermo; Waltham, MA). Salivary mucins were then subjected to FPLC analysis.

Bacterial Strains and Culture Conditions:

Prevotella melaninogenica (ATCC 25845) was obtained from Microbiologics (St. Cloud, MN) and stored as a 50% glycerol stock at -80°C until use. This stock was used to inoculate a 3 mL culture of degassed beef broth medium anaerobically within an anaerobic chamber (Coy Laboratory Products, Michigan, USA) containing a gas mixture of 90% N_2, 5% CO_2, and 5% H_2. After 48 hours of anaerobic incubation at 37°C, cells were spun down at 8,000 x g for 2 minutes, washed with fresh media, and then passaged into a fresh 3 mL culture of 1:1 BB:MMM. After another 48-hour incubation under the same conditions, cells were

again spun and washed before a final passage into a fresh 3 mL culture of 100% MMM. 1 mL aliquots were collected from this culture at 12, 24, 36, 48, and 72 hours post anaerobic incubation at 37°C for downstream analysis.

Sample Preparation Method Testing:

In all sample preparation methods, 700 μL aliquots of the sample were subjected to filtration through a 0.22 μm polyethersulfone (PES) centrifuge filter at some point in processing to fully remove bacterial cells or other non-soluble components prior to injection into the FPLC instrument. A subset of samples underwent centrifugation at 8,000 x g for 10 minutes prior to this filtration. Other sample subsets were subjected to mucin concentration via a Pierce™ PES 3K MWCO 0.5 mL protein concentrator (Thermo Scientific, Massachusetts, USA) centrifuged at 15,000 x g for 45 minutes. This was followed by reconstitution of the mucin concentrate in 1 mL of $_{dd}H_2O$ prior to injection into the FPLC. The result was four distinct sample preparation methods that were tested: filtration only (F), cell pelleting + filtration (P+F), filtration + concentration (F+C), and cell pelleting + filtration + concentration (P+F+C).

Column Length Testing:

A 10/200mm Tricorn column and 10/300mm Tricorn column were packed with Sepharose CL-2B agarose gel filtration base matrix (Cytiva; Massachusetts, USA) in identical fashion and individually equipped on a ÄKTA Pure FPLC instrument. MMM aliquots derived from the same stock were filtered through a 0.22 μm PES

centrifuge filter prior being subjected to the finalized FPLC protocol detailed below – once using each column length. Data collected from the use of each column size was processed and directly compared.

Filter Pore Size and Material Testing (FPLC):

1 mL MMM aliquots of the same stock were filtered through 0.22 μm and 0.45 μm PES and PVDF (polyvinylidene fluoride) 0.5 mL centrifuge spin filters at 12,000 x g for 1 minute each. 700 μLs of each filtrate was collected and subjected to the finalized FPLC protocol detailed below on an instrument equipped with a 10/200 mm Tricorn column. Collected data were processed and directly compared.

Sample Preparation:

Bacterial culture aliquots were subjected to centrifugation at 8,000 x g for 10 minutes. Supernatant was collected, with care not to disturb the cell pellet, and filtered through a 0.22 μm PES centrifuge filter. A minimum of 700 μLs of filtrate from each sample was collected and transferred into 2 mL crimp top glass vials with pierceable septa (Thermo Scientific) which were then loaded into the FPLC autosampler for subsequent analysis.

Column Stationary Phase Packing:

Tricorn column end cap filters were soaked in 70% EtOH for 20 minutes prior to column assembly as specified by the product manual. The column was immobilized at a 45° angle via the use of a laboratory support stand and flask

clamp. Sepharose CL-2B agarose beads were diluted with 70% EtOH until the viscosity of H_2O was achieved. This solution was then sonicated at maximum settings for 15 minutes to degas the solution and prevent the formation of bubbles in the column post-packing. A 25 mL serological was used to slowly trickle the degassed stationary phase solution into the angled column, taking care not to generate turbulence and gas bubbles. EtOH was allowed to drain from the bottom of the filter capped column until the stationary phase became compacted. This was repeated until the column was fully packed, never allowing the level of EtOH to drop below the line of compacted stationary phase. The fully packed column was then loaded onto the FPLC instrument and subjected to a 2 hour 70% EtOH flush to ensure complete elimination of all trapped air. The column was then equilibrated with method specific running buffer.

Fast Protein Liquid Chromatography:

FPLC analysis was performed on a ÄKTA Pure instrument with compatible ALIAS autosampler equipped with a 10/200 mm Tricorn column packed with Sepharose CL-2B agarose gel filtration base matrix. 500 μLs of each sample filtrate was injected via the autosampler and subjected to a 48-minute isocratic run method at a flow rate of 0.4 mL/min with a mobile phase consisting of 50 mM phosphate buffer and 150 mM NaCl brought to a pH of 7.2 using 1N HCl (**Table 2.3**). Conductance and absorbance at a wavelength of 280 nm (protein specific) were monitored throughout each sample run. Protein standards from the Cytiva

(Massachusetts, USA) HMW gel filtration calibration kit were used as general size markers for sample analysis.

Table 2.3 - Recipe for FPLC running buffer.

150mM NaCl 50mM Na_2HPO_4 FPLC Running Buffer (1000 mLs)	
Reagent	**Quantity**
NaCl	8.76 g
Na_2HPO_4	7.098 g
$_{dd}H_2O$	1000 mL
Adjust the solution to a final pH of 7.2 using HCL.	

Data Analysis:

FPLC run protocol creation and subsequent data analysis were completed using ÄKTA Pure instrument compatible Unicorn™ 7.0 software. Raw chromatograms resulting from completed sample runs were first evaluated for appropriate conductance values and peak retention time (RT), intensity, and shape. Area under the curve (AUC) values were recorded from appropriately gated peaks prior to data export as CSV files. Exported CSV files were then imported into GraphPad Prism™ 9.0 for final processing.

Results and Discussion

Fast Protein Liquid Chromatography Method Optimization:

The proposed FPLC-based methodology leverages SEC (**Figure 2.1A)** to effectively segregate mucin glycoproteins into HMW and LMW populations, facilitating the relative quantification of global mucin degradation in a given sample via the ratio between these two populations (**Figure 2.1B**). On chromatograms generated using this methodology, absorbance value (mAU) on the y-axis indicates the relative abundance of a mucin population, while the RT (min) along the x-axis indicates relative size of a mucin population. Based on the analysis of molecular weight standards, absorbance peaks occurring between the RT of approximately 0 to 12 minutes are considered HMW mucins (> ~50 kDa), while peaks occurring between the RT of approximately 12 to 20 minutes are considered LMW mucin components (< ~50 kDa) (**Figure 2.1B**) – likely glycopeptides. Alterations in peak characteristics observed across samples subjected to varying

conditions serve as indicators of mucin degradation variation. This is evident in the comparison of MMM and salivary mucin, where source and processing steps (i.e., during manufacturing of porcine gastric mucin) likely contribute to the significant disparity between the HMW (peak 1) glycoprotein fractions between groups (**Figure 2.1B**). Nevertheless, minor variations in column attributes, such as column length, may also impinge upon peak properties and should be considered during method development.

To investigate the effect of column length on sample resolution, I compared the analysis of identical samples using the same workflow but implementing two different column lengths – 200 mm and 300 mm, both packed with the same Sepharose CL-2B agarose stationary phase. Resulting chromatograms displayed changes in peak RT, but no significant change in peak resolution between the two columns (**Figure 2.2A**). Consequently, the shorter 200 mm column was chosen for use in the finalized method for its reduced consumption of stationary phase materials and comparative ease of packing.

Another variable to consider was the type of filter used for sample preparation prior to FPLC analysis. Filtration of all injected samples is required to remove bacterial cells and other insoluble contaminants prior to FPLC analysis, regardless of sample sterility. However, filter pore size and material have the potential to impact the amount of mucin recovered in the flowthrough, and subsequently affect final peak properties. Identical MMM aliquots were subjected to filtration through 0.22 μm and 0.45 μm pore size centrifugation filtration with filters composed of PES

(polyethersulfone) or PVDF (polyvinylidene difluoride) material. Final FPLC analysis of filtrate confirmed that filtration through PES filters, even of a smaller pore size of 0.22 μm, resulted in a higher yield of mucin glycoproteins when compared to filtration through a larger pore size 0.45 μm PVDF filter (**Figure 2.2B**). This may be due, in part, to the asymmetric filter structure of PES filter material which allows gradient separation of variably sized mucin degradation species, reducing filter clogging. PVDF filter structure is symmetric, promoting accumulation of mucins across a uniform filter depth and subsequently clogging filter pores (**Figure 2.2C**). As a result, the final optimized FPLC workflow relies on the use of 0.22 μm PES filters for any sample preparation steps.

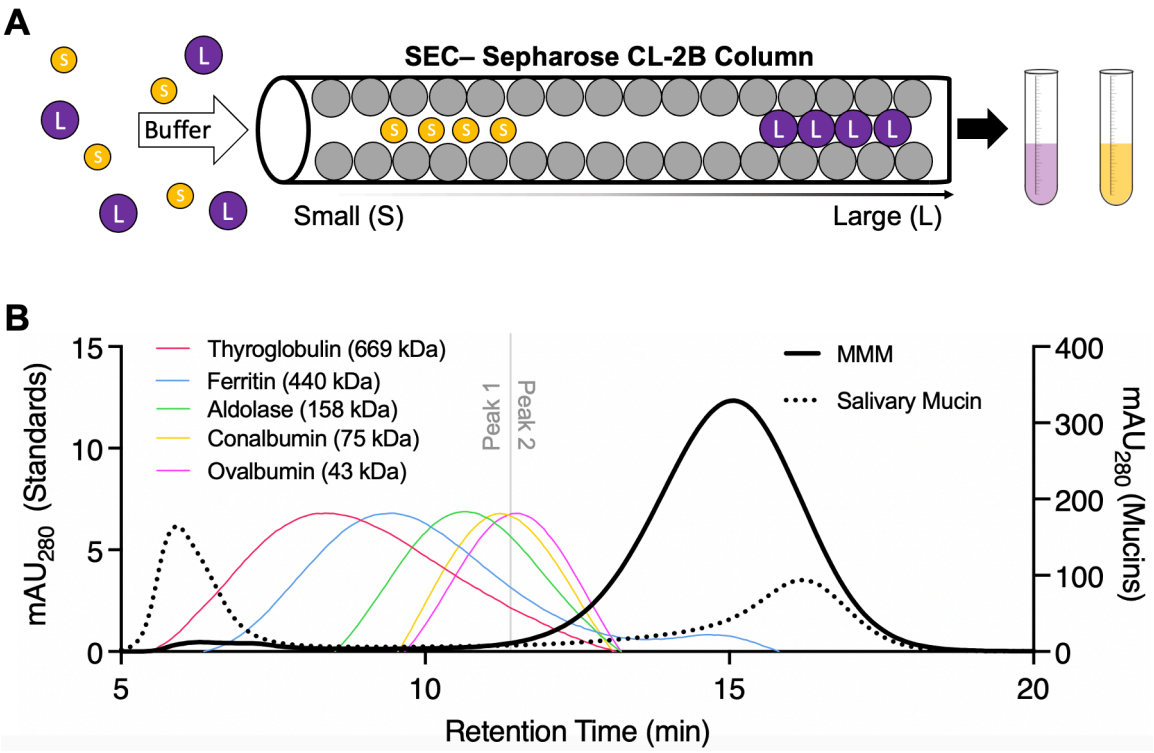

Figure 2.1 – FPLC can be used to quantify relative mucin degradation. A) Schematic describing FPLC size exclusion chromatography (SEC. A stationary phase matrix is used to separate glycoprotein analytes based on size. Larger analytes pass through the matrix more quickly resulting in a shorter retention time (RT), while the opposite is true for smaller analytes. **B)** Composite chromatogram from the finalized (FPLC) method displaying the absorbance values (y-axis) and RTs (x-axis) for several protein standards (left y-axis) and two mucin media types (right y-axis) – minimal mucin media (MMM) and salivary mucin. Analyte absorbances are gated into peak 1 (high molecular weight) and peak 2 (low molecular weight) by a RT of < 12 minutes or > 12 minutes respectively.

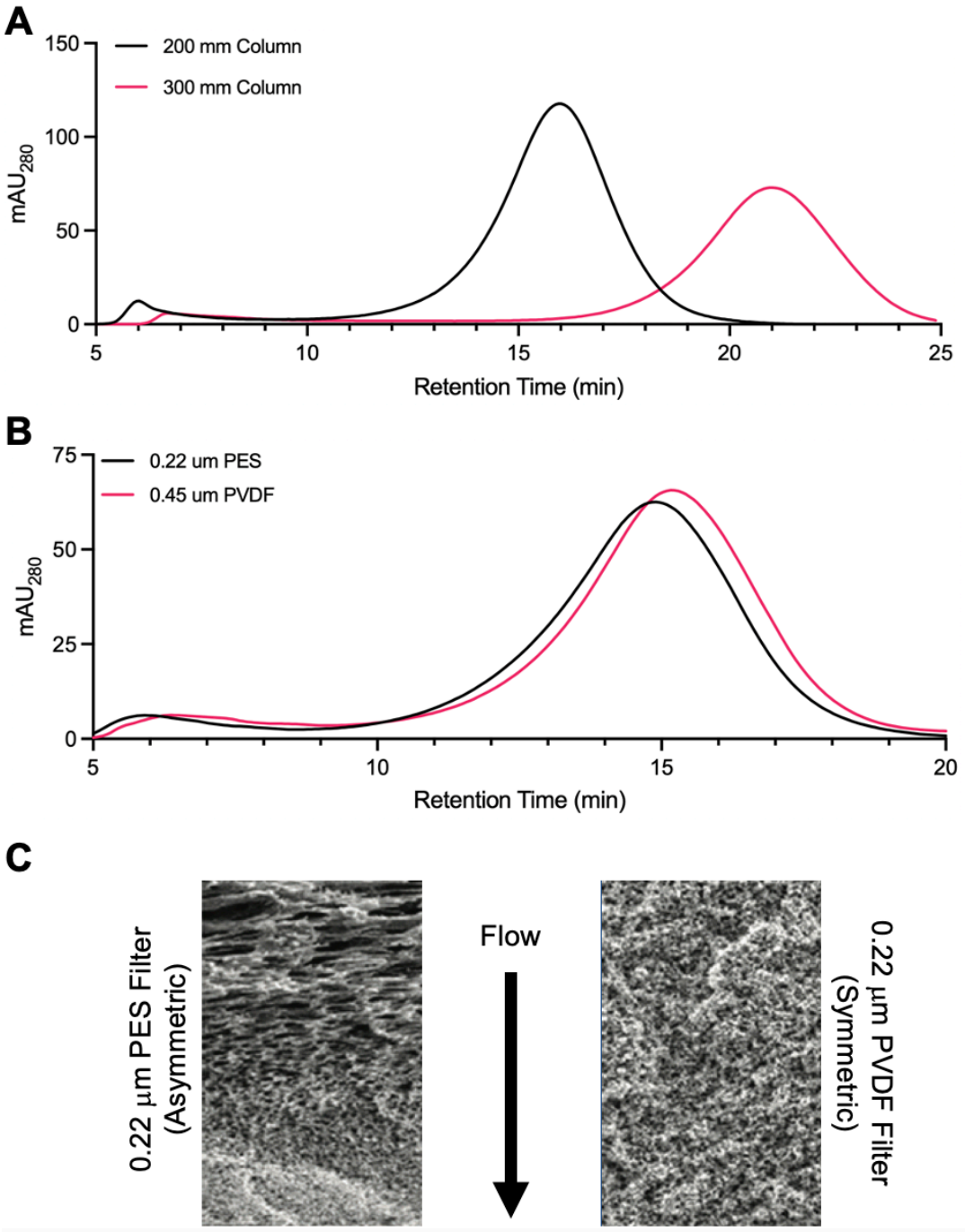

Figure 2.2 – The impact of column length and filter material on peak properties. A) Fast protein liquid chromatography (FPLC) chromatogram comparing the traces of identical minimal mucin media (MMM) aliquots run on a 200 mm column vs a 300 mm with the same stationary phase and run method. **B)** Chromatogram comparing the traces of identical MMM aliquots filtered through filter membranes of different pore size and material and subjected to the same run method. **C)** Scanning electron microscopy (SEM) imaging of a filter material cross sections highlighting the differences in material symmetry (Steffen, 2018).

Sample Preparation Method Optimization:

While sterile control samples of MMM or salivary mucin only require filtration through a 0.22 μm PES centrifuge filter prior to FPLC analysis, this minimal sample preparation is not suitable for all sample types. Viscous samples run the risk of clogging the FPLC column. To identify the optimal sample preparation method prior to FPLC injection, several methodologies were tested on the 72-hour MMM supernatant of *Prevotella melaninogenica*. When aliquots of this culture were only filtered in a fashion similar to that of control MMM, a significant reduction in all absorbance values were observed, suggesting clogging of the filter membrane resulting in decreased mucin yield in the flowthrough. This was remedied by simply pelleting the bacterial cells via centrifugation prior to filtration (**Figure 2.3**). To reduce the risk of FPLC column damage and clogging from high sample viscosity, a 3K MWCO protein concentrator was used to concentrate sample mucins for reconstitution in a larger volume of H_2O prior to FPLC injection. While this processing method resulted in a less viscous sample and notable absorbance peaks, mucin integrity appeared to be affected (**Figure 2.3**). Ultimately, this concentration-based sample preparation was found to be unnecessary for applications using MMM. However, it still may prove useful in applications involving more viscous mucin samples such as salivary mucin or clinical sputum samples.

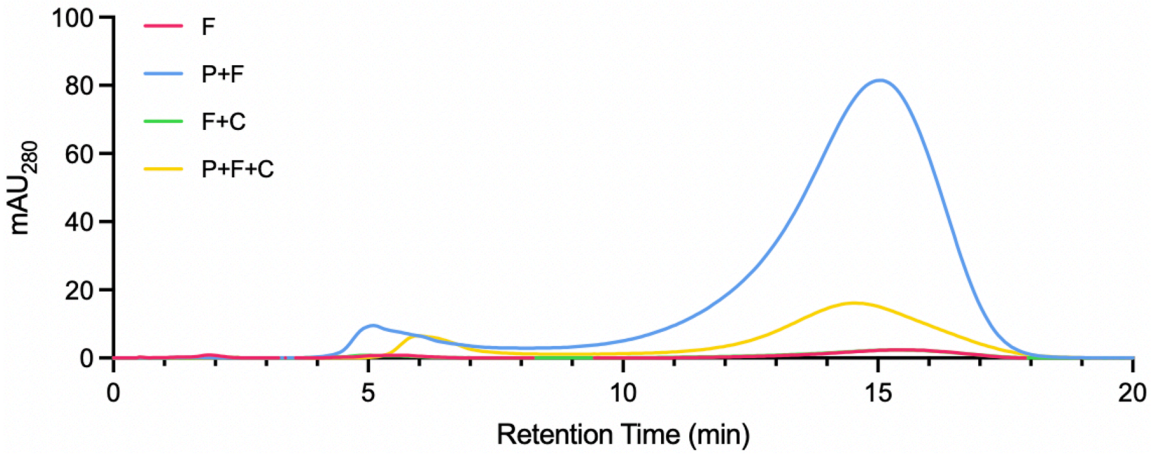

Figure 2.3 – Comparison of sample preparation methodologies. FPLC chromatogram comparing identical aliquots of *P. melaninogenica* minimal mucin media (MMM) culture supernatant post 72 hours of incubation at 37°C. Aliquots were processed prior to analysis using a combination of different methodologies - filtration through a 0.22 μm PES centrifuge filter (F), cell pelleting via centrifugation prior to filtration (P), and mucin concentration and reconstitution via a 3k MWCO protein concentrator (C).

In vitro Method Validation:

Following optimization of the FPLC and sample preparation methods, I sought to validate the workflow and demonstrate its utility through the analysis of *in vitro* mucin degradation over time by a representative mucin degrading species. Using the described workflow, I analyzed the mucin degradation profile of *Prevotella melaninogenica,* a species commonly identified in the CF airways, in MMM over 48 hours. The resulting composite chromatogram displayed two distinct peaks gated in the HMW (peak 1) and LMW (peak 2) RTs, as expected (**Figure 2.4A**). Closer inspection of the HMW peak (peak 1) confirms a gradual decrease in absorbance value over time when compared to the MMM control (**Figure 2.4B**). Conversely, the opposite trend is observed in the LMW peak (peak 2). Not only do the AUC values increase over time but the median RT increases over time as well (**Figure 2.4C**) – both suggesting the degradation of mucin into smaller species. Together, these data validate the use of the proposed optimized FPLC workflow.

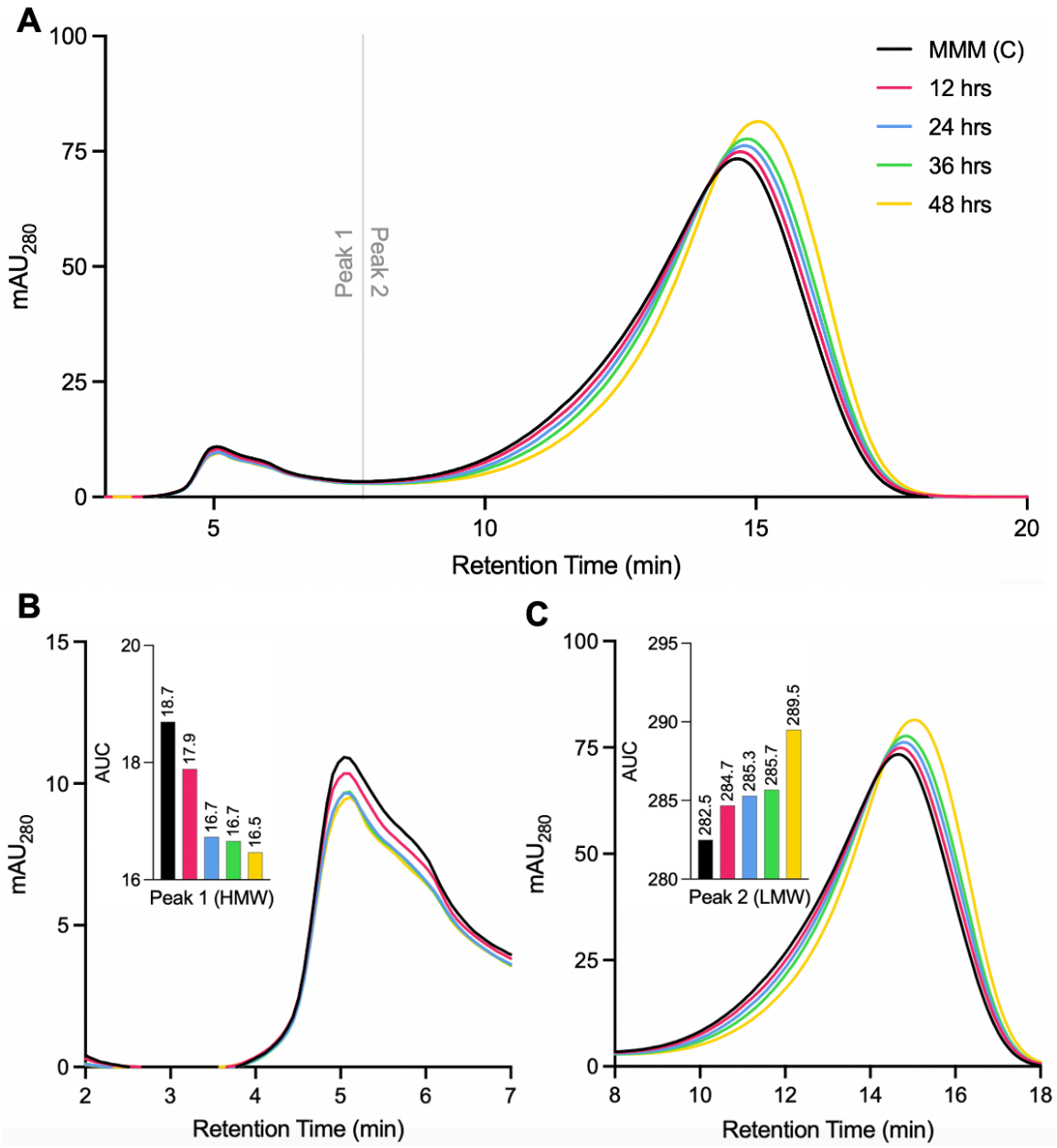

Figure 2.4 – Mucin degradation profile of *Prevotella melaninogenica*. A) Composite FPLC chromatogram of a minimal mucin medium (MMM) control and *P. melaninogenica* MMM culture supernatants derived from different incubation time points. **B)** Chromatogram focusing on the high molecular weight (HMW) peak (peak 1) of the composite chromatogram. Inset bar graph displayed the calculated area under the curve (AUC) values for each peak. **C)** Chromatogram focusing on the low molecular weight (LMW) peak (peak 2) of the composite chromatogram. Inset bar graph displayed the calculated AUC values for each peak.

Conclusion

In this section, I have presented an optimized FPLC SEC method that enables the reproducible separation of HMW and LMW mucin glycoprotein populations from mucin-rich samples – excluding many non-mucin LMW bacterial products that are too small to be captured by the column . This method overcomes the limitations inherent in conventional methods for analyzing mucin glycoproteins, which have been impeded by mucin size and its unique gelling properties. This method not only measures relative mucin size but can also be used to collect mucins of a desired size for further purification or downstream analysis.

This optimized method has potential for evaluating the mucin-degrading capacity of both individual CF-associated commensal bacterial species and the diverse communities they comprise. This information not only offers basic insights into microbial physiology but is of critical importance in understanding the impact of airway microbial communities on canonical CF pathogens (i.e., *PA*) *in vivo* - a necessary step in better understanding the pathogenesis of CF and developing new therapeutic strategies that target these interactions.

Moreover, the approach has broader implications beyond CF research. Use of FPLC SEC for analyzing mucins has applications in diverse fields of inquiry that involve mucin glycoproteins, such as oral, ocular, gastrointestinal, and reproductive research. The described method provides a powerful tool for studying bacterial-mucin interactions and will enable more precise investigations of these complex relationships in controlled *in vitro* experiments.

Minimal Mucin Medium Optimization

Introduction

As previously described, mucins are large glycoproteins and the primary components of mucus which plays a critical role in the healthy function of mucosal epithelial surfaces of the body including the respiratory, digestive, and reproductive tracts. As more is learned about this class of molecules, it has become apparent that their interactions with bacteria *in vivo* may play a role in the progression of certain diseases such as CF and may directly impact patient clinical outcomes (Granchelli et al., 2018). Despite recent findings (Jean-Pierre et al., 2023) that have expanded our knowledge on the subject, many of the underlying mechanisms of these bacterial-mucin interactions remain largely uncharacterized. This, in part, is due to several inherent challenges mucin biology imposes on successful study of these interactions.

In vitro models of bacterial-mucin interactions are valuable tools for uncovering these underlying mechanisms; however, it remains difficult to recapitulate the *in vivo* nutritional landscape of a mucus environment. Several mucin-based media for *in vitro* culturing experiments, such as artificial sputum media (ASM) exist (Sriramulu et al., 2005), but are very rich and nutritionally undefined making them a poor choice for reductionist experiments that require tight regulation of nutritional variables. MMM has also been described in literature by our laboratory (Flynn et al., 2016) and has been utilized as a medium for the cultivation of bacteria on mucin as a sole carbon source – minimizing other nutritional variables.

MMM is created with the use of porcine gastric mucin (PGM) which is primarily composed of the mucin species MUC5AC (Sigma-Aldrich, Missouri, USA). This is one of the primary mucin species of the human respiratory system (MUC5B is the other) (Okuda et al., 2019), making this mucin source a cheap, abundantly available, and biologically relevant alternative to human-derived mucin. However, recent characterization data of MMM has shown that commercially available PGM is primarily composed of LMW mucins (**Figure 2.1B**) – likely a result of the manufacturing process. While still a useful tool for *in vitro* experiments, the lack of substantial HMW mucin differs from what is observed *in vivo* and presents a challenge when trying to best recapitulate bacterial-mucin interactions.

To address this challenge, I built upon our conventional MMM generation method in an effort to increase HMW mucins and decrease contaminants. To accomplish this, PGM mucin was first characterized via FPLC to better understand the factors contributing to its degradation and contamination. Data from this characterization subsequently informed the optimization preparation of MMM.

In this subsection, I present the findings of our PGM characterization as well as an optimized approach for the generation of MMM which results in a final medium consisting of a significantly higher fraction of HMW mucins and reduction of contaminants (i.e., organic acids) from PGM. Throughout this work, I demonstrate that this optimized MMM can support the growth of diverse bacterial species and

allows us to better investigate how individual bacteria and bacterial communities interact with and metabolize mucin glycoproteins.

Materials and Methods

Original Minimal Mucin Media Preparation:

MMM was prepared as previously described (Flynn et al., 2016) (**Tables 2.4 - 2.8**) (**Figure 2.5A**). Type III PGM (Sigma-Aldrich, Missouri, USA) was added to ddH_2O at a concentration of 30 g/L prior to autoclaving at 121°C for 30 minutes. Autoclaved PGM was transferred into 20 μm regenerated cellulose (RC) dialysis tubing (Fisher Scientific) for two, 2-hour incubations in ddH_2O at room temperature, followed by overnight incubation at 4°C. ddH_2O was replaced between each incubation. This was followed by transfer into 50 mL centrifuge bottles and subsequent centrifugation at 30,000 *x* g for 1 hour. Supernatant was carefully removed, avoiding solids, and ddH_2O was added to the mucin solution at a 1:1 ratio, and buffered with 50 mM KH_2PO_4 (**Tables 2.5 - 2.6**) and 150 mM NaCl. 1 mM $MgSO_4$ and a vitamin and mineral mix (**Tables 2.7 - 2.8**) were then added to the buffered mucin solution. The final solution was filtered through 30 mL capacity 0.22 μm PVDF syringe filters. Mucin content was determined using FPLC as described below. Complete medium was stored at -20°C for immediate use (< 2 weeks) or -80°C for long-term storage (> 2 weeks).

Optimized Minimal Mucin Media Preparation:

MMM was prepared in a fashion generally similar to what was previously described, but with modifications (**Table 2.4 – 2.8**) (**Figure 2.5B**). Type III PGM

was added to ddH_2O at a concentration of 30 g/L prior to autoclaving at 121°C for 15 minutes and transfer to 250 mL centrifuge bottles for centrifugation at 15,000 *x* g for 1 hour. Supernatant was carefully removed, avoiding solids, and sequentially filtered through PES membranes (3 μm,1 μm, 0.45 μm, 0.22 μm) (Merck Millipore, Massachusetts, USA) using a peristaltic pump. Filtrate was transferred into 20 μm RC dialysis tubing for two, 2-hour incubations in ddH_2O at room temperature, followed by overnight incubation at 4°C. ddH_2O was replaced between each incubation. Post dialysis, ddH_2O was added to the mucin solution at a 1:1 ratio and was buffered with 50 mM KH_2PO_4 (**Tables 2.5 - 2.6**) and 150 mM NaCl. 1 mM $MgSO_4$ and a vitamin and mineral mix (**Tables 2.7 - 2.8**) were then added to the buffered mucin solution and filtered through a 0.22 μm bottle top PES filter (Foxx Life Science, New Hampshire, USA). Mucin content was determined using FPLC as described below. Complete medium was stored at -20°C for immediate use (< 2 weeks) or -80°C for long-term storage (> 2 weeks).

Table 2.4 - Recipe for 1X minimal mucin media.

1X Minimal Mucin Media (500 mL)	
Reagent	**Quantity**
Pre-Autoclaving	
Porcine Gastric Mucin (Type III)	7.5 g
$_{dd}H_2O$ (Prior to Autoclaving)	250 mL
Post-Autoclaving, Dialysis, and Centrifugation	
$_{dd}H_2O$	250 mL
Mineral and Vitamin Salts Mix*	36 mL
** Recipe for the preparation of mineral and vitamin salt mix found in Table 5.*	

Table 2.5 - Recipe for mineral and vitamin salts mix.

Mineral and Vitamin Salts Mix (36 mL)	
Reagent	**Quantity**
NaCl (1.7M)	25 mL
$MgSO_4$ (1M)	0.5 mL
NCN (Phosphate Buffer) *	10 mL
Trace Minerals and Vitamins **	0.5 mL
** Recipe for the preparation NCN phosphate buffer found in Table 6.* *** Recipe for the preparation of trace minerals is found on Table 7 and trace vitamins on Table 8. Addition of final 0.5 mL volume to this solution is from a 1:1 ratio mix of the individual mineral and vitamin stocks.*	

Table 2.6 - Recipe for NCN phosphate buffer.

NCN Phosphate Buffer (100 mL)	
Reagent	**Quantity**
KH_2PO_4	19.7 g
$K_2HPO_4 \cdot 3H_2O$	32.3 g
$_{dd}H_2O$	100 mL
Adjust the solution to a final pH of 7.4 using HCL.	

Table 2.7 - Recipe for trace minerals.

Trace Minerals (1000 mL)	
Reagent	**Quantity**
Nitrilotriacetic acid	~1.5 mL
$MnCl_2 \cdot 4H_2O$	0.1 g
$FeSO_4 \cdot 7H_2O$	0.5 g
$CoCl_2 \cdot 6H_2O$	0.17 g
$ZnCl_2$	0.1 g
$CuSO_4 \cdot 5H_2O$	0.03 g
$AlK(SO_4)_2 \cdot 12H_2O$	0.005 g
H_3BO_3	0.005 g
Na_2MoO_4	0.09 g
$NiCl_2$	0.05 g
$Na_2WO_4 \cdot 2H_2O$	0.02 g
Na_2SeO_4	0.1 g
$CaCl_2 \cdot 2H_2O$	0.04 g
Adjust the solution to a final pH of 6.5 using nitrilotriacetic acid.	

Table 2.8 – Recipe for trace vitamins

Trace Vitamins (1000 mL)	
Reagent	**Quantity**
Biotin	0.002 g
Folic Acid	0.002 g
Pyridoxine-HCl	0.01 g
Thiamine	0.005 g
Riboflavin	0.005 g
Nicotinic acid	0.005 g
Pantothenic acid	0.005 g
Vitamin B12	0.0001 g
p-Aminobenzoic acid	0.005 g
Thioctic acid	0.005 g
Adjust the solution to a final pH of 8.0 using NaOH.	

Baseline Mucin Degradation Testing:

Sterile MMM was incubated anaerobically at 37°C for a total of 72 hours. Aliquots were collected at hours 0, 24, 48, and 72. These aliquots were subjected to FPLC analysis.

Freeze Thaw Cycle Mucin Degradation Testing:

Sterile MMM was subjected to FPLC analysis to measure mucin degradation pre-freeze thaw cycling. The same stock of MMM was subjected to two repeated freeze thaw cycles at -80°C for 24 hours each cycle. Aliquots were collected following each freeze thaw cycle and analyzed via FPLC.

Mucin Molecular Size Testing:

700 μL aliquots of sterile MMM from the same stock were subjected to concentration via PES centrifuge protein concentrators with 3, 5, 10, and 100 kDa molecular weight cut offs (MWCO). Concentration occurred via centrifugation at 15,000 *x* g for 1 hour. Concentrated mucin was reconstituted in 700 μL of ddH_2O prior to FPLC analysis.

Fast Protein Liquid Chromatography:

FPLC analysis of mucin degradations accomplished using the reagents in **Table 2.3** and the methodology previously described on page 46.

Data Analysis:

Analysis of FPLC data was accomplished using Unicorn™ 7.0 and Prism™ 9.0 software as previously described on page 48.

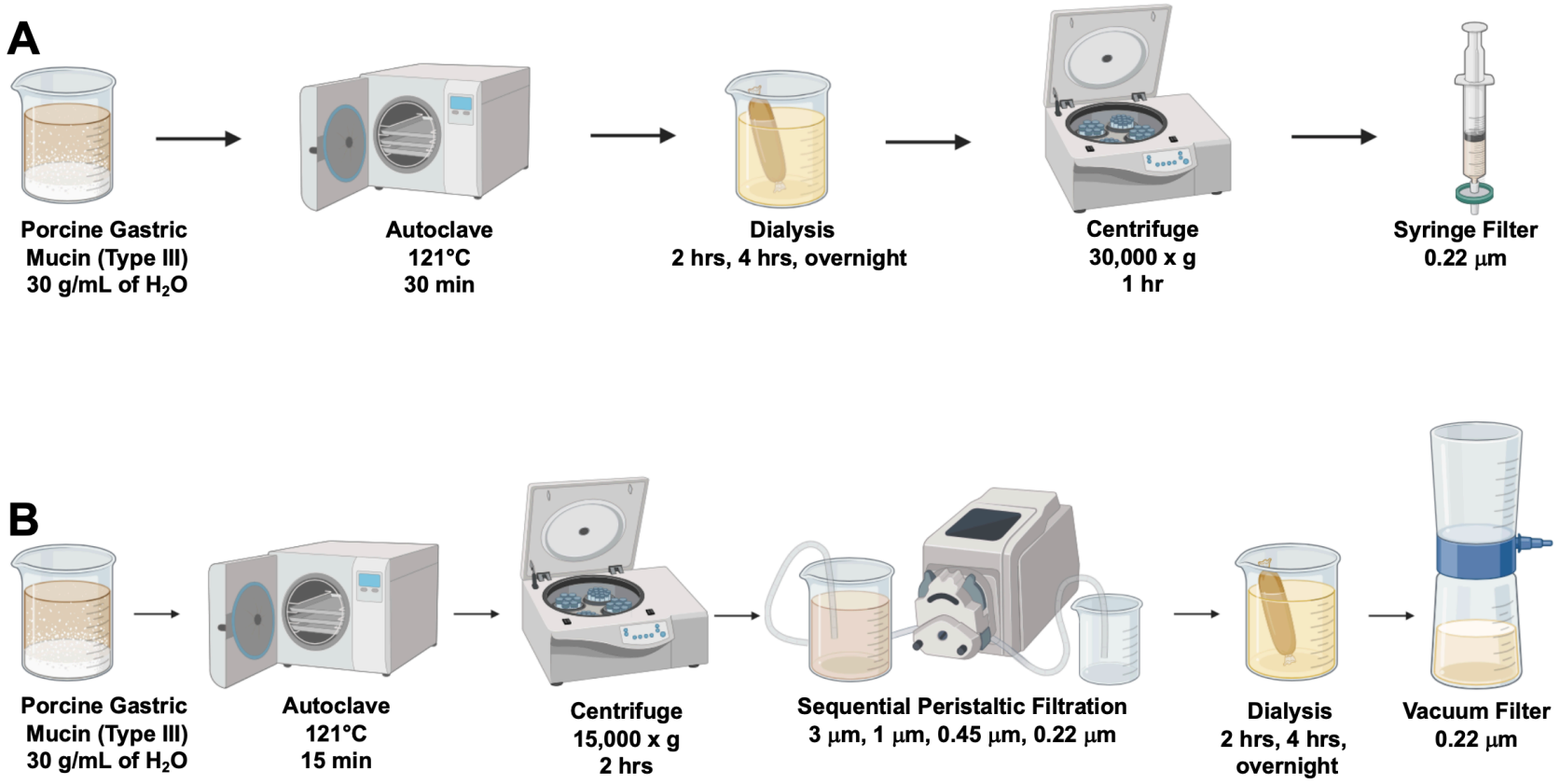

Figure 2.5 – Workflow used to generate minimal mucin medium (MMM). A) Illustration of the **A)** original workflow and **B)** optimized method.

Results and Discussion

Minimal Mucin Media Characterization:

To better understand what factors impact the ratio of HMW and LMW mucins in MMM, I investigated the effects of heat and freeze thaw cycles on MMM mucin degradation. As most culture experiments utilizing MMM undergo anaerobic incubation at 37°C, I sought to establish an understanding of the baseline mucin degradation that occurs at this temperature without the addition of microbes. Over the course of a 72-hour incubation, I observed a marginal and gradual decrease in the AUC values of the HMW peak conversely corresponding to an increase in the AUC values of the LMW peak (**Figure 2.6A**). This suggests that while minimal, some baseline level of MMM mucin degradation occurs due to incubation at elevated temperatures. This should be kept in mind, particularly when evaluating the chromatograms of bacterial species for mucin degradation.

MMM generation is a time consuming and laborious process. As such, large batches are often made at once, and frozen at -80°C for long term storage. Additionally, partially used aliquots of MMM are commonly placed back into storage, subjecting them to multiple freeze-thaw cycles. As established, any changes in FPLC chromatogram traces can impact the accurate evaluation of mucin degradation for a bacterial species or community of interest. Accordingly, I sought out to elucidate the impact of freeze-thaw cycles on MMM mucin integrity. While one freeze-thaw cycle at -80°C for 24 hours resulted in no significant change in mucin ratios compared to MMM that was never frozen, an additional cycle

resulted in mucin degradation. This was observable not only by an increase in LMW peak AUC values but also an increase in LMW peak RT (**Figure 2.6B**). Given these data, I recommend against the use of MMM that has been frozen more than one time at -80°C. Aliquoting freshly generated MMM into smaller volumes for storage may aid in the reduction of unused media.

While the use of HMW protein standards has informed us of the correlation between molecular size and RT of HMW (RT < 12 min) glycoproteins, the molecular size range of LMW (RT > 12 min) glycoproteins remained uncharacterized. In lieu of LMW standards, I employed a series of PES protein concentrators with sequential LMW MWCO values (3, 5, 10, 100 kDa). Resulting MMM mucin concentrates were reconstituted in water prior to FPLC analysis to observe the traces generated by isolated mucin species populations of various sizes. As expected, all traces maintained the presence of a HMW peak, confirming the contents of that peak are well over 100 kDa. All observed differences between conditions occurred in the LMW peak suggesting the molecular size range of glycoproteins composing it includes species between 3 to 100 kDa. As MWCO values increased, the AUC and median RT of the LMW peak decreased, suggesting loss of smaller mucin species from the sample (**Figure 2.6C**). These findings allow us to assign a general estimated molecular size range for glycoproteins that contribute to the LMW peak observed in FPLC traces – providing further context to our experimental results.

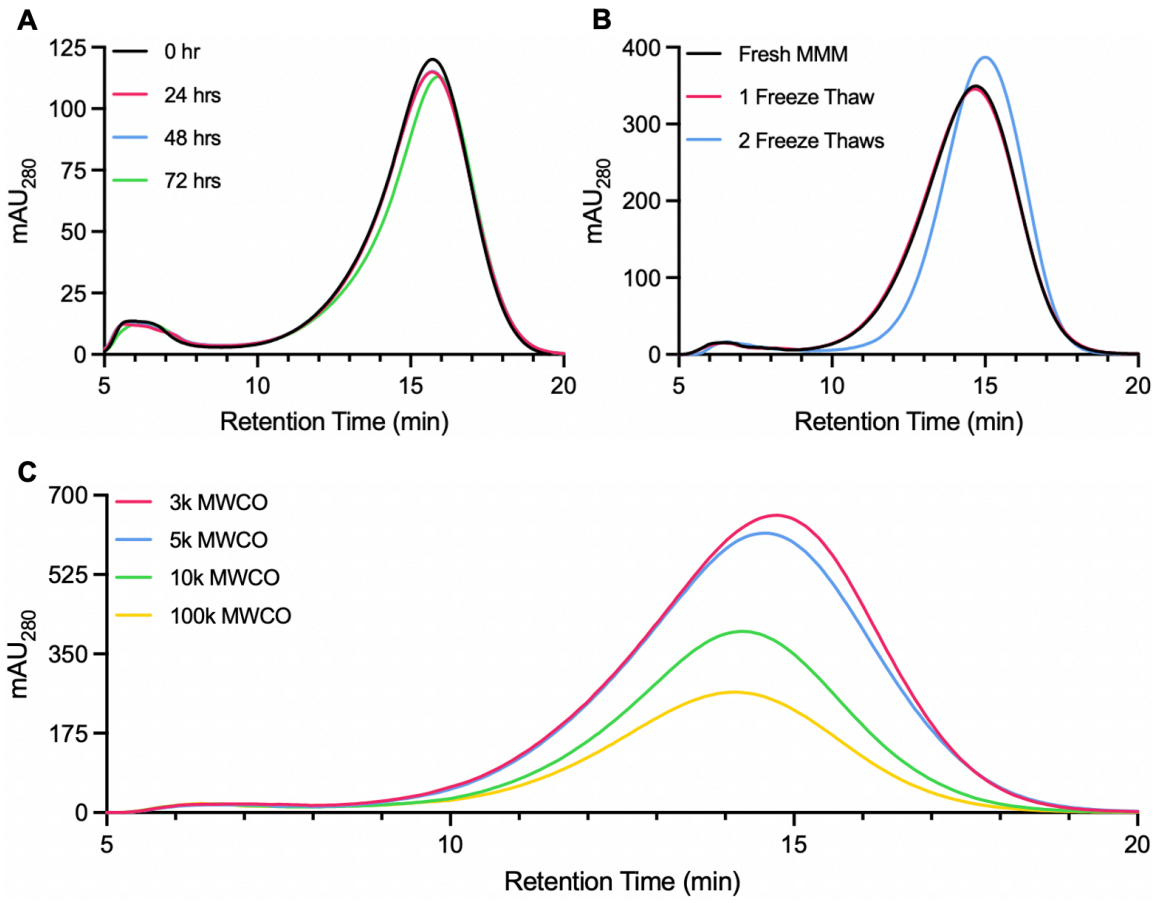

Figure 2.6 – Characterization of basic mucin properties in MMM. A) FPLC chromatogram comparing the traces of sterile MMM incubated anaerobically at 37°C for 0, 24, 48, and 72 hours. **B)** Chromatogram comparing the traces of sterile freshly generated MMM to sterile MMM that was frozen at -80°C for 24 hours one time or two times. **C)** Chromatogram comparing the traces of the reconstituted mucin concentrate generated from concentration of MMM through PES protein concentrators with different molecular weight cut-offs.

Validation of Improved Minimal Mucin Media:

Characterization of MMM aided in the identification of several modifications that could be made to the original MMM generation protocol to increase the ratio of HMW mucins. First, autoclave time was decreased from 30 minutes to 15 minutes (**Figure 2.5B**) – greatly increasing the final ratio of HMW mucins. Autoclaving, unsurprisingly, greatly contributes to mucin degradation – an effect that can be observed when autoclave time is reduced or removed from the protocol altogether (**Figure 2.7**). I explored alternative methods such as UV irradiation; however, I deemed the inclusion of an autoclave step necessary to prevent microbial growth and degradation of mucins by bacterial enzymes.

I also modified the ordering of the original protocol steps to prioritize removal of large insoluble components prior to dialysis (**Figure 2.5B**) – increasing dialysis efficiency. MMM contains very low levels (<0.1 mM) of organic acids contaminants (i.e., acetate, propionate, lactate) that vary between batches. This is a consequence of the source environment of PGM – the organic acid rich gastrointestinal tract. Preliminary HPLC analysis of organic acids in MMM suggests the optimized generation method results in a final medium with less organic acid contamination (data not shown).

Another pitfall of MMM generated using the original methodology was a high rate of stock contamination. Initially thought to be a result of user error, final sterilization of the media via 0.22 μm PVDF syringe filtration was identified as the issue.

Filtration using this method requires high pressure due to the viscosity of the medium. This likely not only resulted in membrane blockages which decreased mucin yields, but also membrane breakages which compromised sterilization. To overcome this, I implemented a sequential filtration method utilizing a peristaltic pump that ceases function at high pressures. This was followed by a final filtration through a 0.22 μm PES vacuum filter. This approach resulted in less membrane blockages, a significantly more transparent final medium, and reduced contamination.

Together, these protocol modifications (**Figure 2.5**) represent a refined process that minimized sources of error. MMM generated using both the original and optimized methods were directly compared via FPLC analysis. The result was a significant reduction in RT for both the HMW and LMW mucin peaks of the optimized MMM, suggesting a decrease in global mucin degradation and an increase in the average size (kDa) of mucin species in the medium compared to the original (**Figure 2.7A**). Additionally, the AUC values for each respective peak increased in the optimized MMM suggesting a higher concentration of mucin glycoproteins in each compared to the original – the result of notably improved mucin yield throughout the processing steps (**Figure 2.7B-C**).

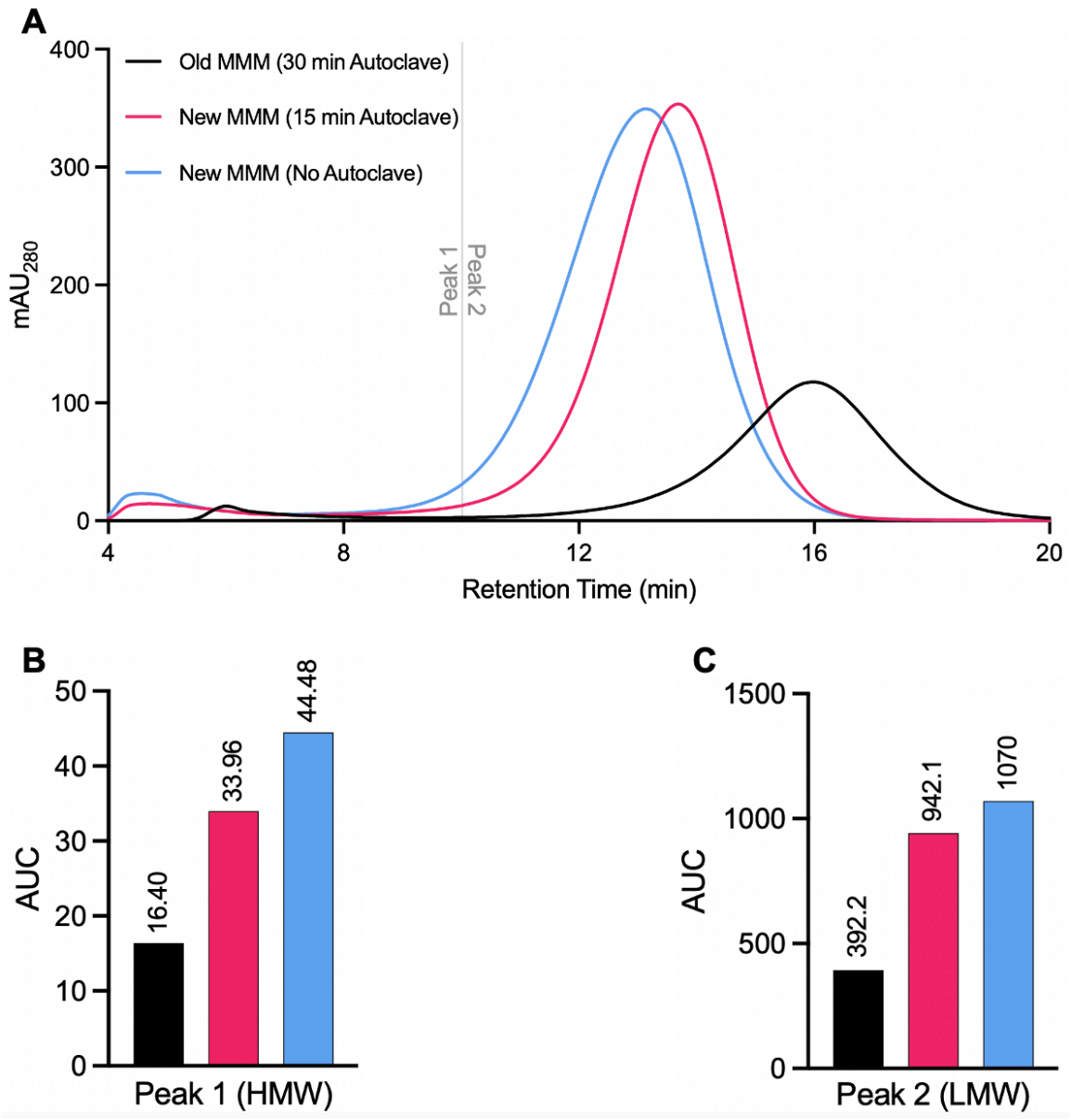

Figure 2.7 – FPLC comparison of MMM preparation methodologies. A) Composite FPLC chromatogram comparing the traces of MMM generated using the original method, the optimized method, and the optimized method without an autoclaving step. **B)** Area under the curve (AUC) values of peak 1 (high molecular weight) mucins. **C)** AUC values of peak 2 (low molecular weight) mucins.

Conclusion

In this section, I not only optimize MMM for the study of microbial-mucin interactions but also provide new insights into the impact of environmental variables, such as temperature, on the integrity of our mucin medium. Deeper understanding of how variations in experimental conditions can affect the integrity of mucin has important implications for experimental design and reproducibility.

I further validated the efficacy of our optimized MMM by directly comparing it to the original media generation method via FPLC. Through this validation process, I observed a significant increase in the abundance of HMW mucins in the optimized MMM, indicating improved preservation and representation of the MUC5AC mucin population. This reinforces the reliability and relevance of our optimized medium in more accurately capturing an *in vivo* mucin profile and facilitating the study of mucin degradation by various microbial species.

High Performance Liquid Chromatography: Phenazine Analysis

Introduction

As described above, CF is characterized by the accumulation of viscous mucus in the airways, providing an ideal environment for the colonization of opportunistic pathogens (Blanchard et al., 2022). Among them, PA is considered the major contributor to the morbidity and mortality associated with disease progression (Crull et al., 2018). PA is notorious for its adaptability and ability to establish chronic airway infections, leading to a decline in lung function in individuals with CF (Crull et al., 2018).

The production of phenazines, a class of redox-active secondary metabolites, contribute to the ability of PA to colonize and persist in the airways. Phenazine-1-carboxylic acid (PCA), phenazine-1-carboxamide (PCN), 1-hydroxyphenazine (1HP), and the notably visually blue pyocyanin (PYO) are the primary phenazines produced (**Figure 2.8**). These compounds exhibit diverse biological activities, such as electron transfer, redox cycling, cytotoxicity, modulation of host immune responses, and antibiotic resistance (Briard et al., 2015; Wang et al., 2011; McGuigan et al., 2014) - ultimately driving the pathogenicity of PA in the airway environment.

Due to their potential impact on CF clinical outcomes, the function and regulation of PA phenazines is of ongoing interest in research. Accordingly, accurate quantification of phenazine derivatives, both *in vivo* and *in vitro*, is essential for

better understanding their roles in CF respiratory infections. This is also essential in evaluating the efficacy of novel therapeutic interventions targeting phenazine production – a much needed alternative to antibiotic therapies that are growing ineffective against multi-drug resistant PA strains. Historically, liquid-liquid organic extraction of pyocyanin followed by acidification and spectrophotometric colorimetric measurement has been a widely employed method for phenazine quantification (Essar et al., 1990; Ozdal, 2019; Najafi et al., 2021; Gupte et al., 2021). Extraction of phenazines and subsequent acidification changes the color of pyocyanin from blue to red (**Figure 2.8**), allowing it to be measured at an absorbance of 520 nm. While useful, this approach suffers from several limitations that can affect its accuracy and reliability. For example, this method is limited to the quantification of PYO, excluding other phenazines of interest. It is susceptible to interference from co-extracted compounds, such as pigments and other molecules, which can lead to erroneous determinations of PYO concentrations. Liquid-liquid extraction of PYO aims to reduce this interference; however, inherent loss of target compound yield associated with this method further obfuscates the accuracy of final calculated values. Furthermore, colorimetric measurement at a single wavelength may lack specificity and can be influenced by background absorbance.

To overcome these limitations and enhance the accuracy of phenazine quantification, there is a need for more reliable methods – particularly compatible with mucin-rich sample types. High performance liquid chromatography (HPLC)

coupled with appropriate detection techniques, such as ultraviolet-visible (UV-Vis) spectroscopy or mass spectrometry (MS), offers a powerful alternative as it provides superior separation, specificity, and the ability to resolve multiple phenazine derivatives.

Here, I describe novel sample preparation and HPLC methods for the quantification of phenazines in mucin-rich PA *in vitro* cultures. I demonstrate the advantages of HPLC over the conventional organic extraction and colorimetric approaches, highlighting its improved accuracy, sensitivity, and ability to detect a wider range of phenazines. Method performance is validated through the quantification of known phenazine standard concentrations and those produced by PA under two different culture conditions.

By offering a more accurate and comprehensive quantification of relevant phenazines, this HPLC method significantly contributes to our understanding of the roles these compounds play in PA infections.

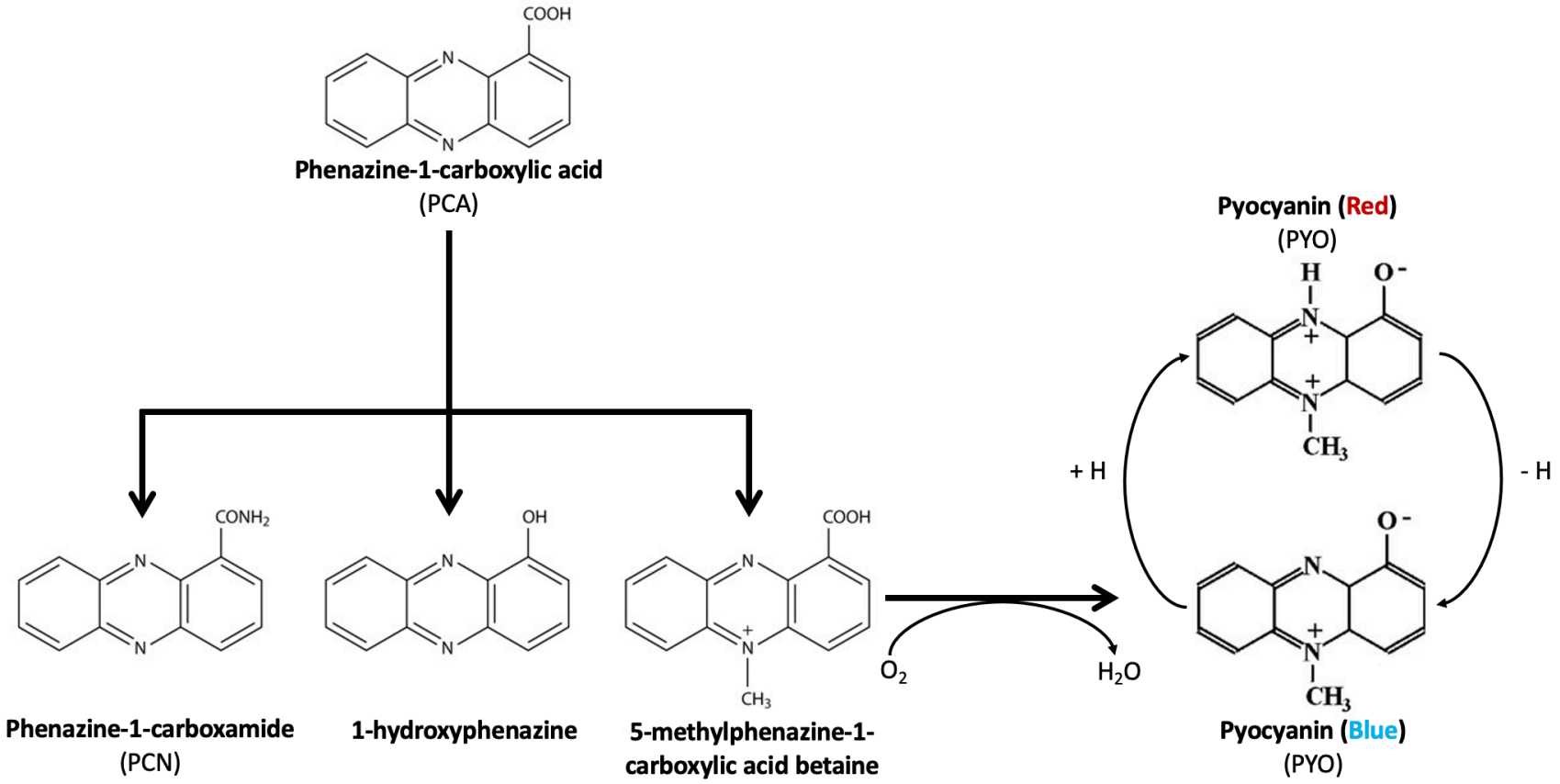

Figure 2.8 – Schematic of *P. aeruginosa* phenazine biosynthesis. *P. aeruginosa* converts chorismic acid into phenazine-1-carboxylic acid (PCA) which is a precursor for phenazine-1-carboxamide (PCN), 1-hydroxyphenazine (1HP), 5-methylphenazine-1-carboxylic acid betaine, and pyocyanin (PYO). Under aerobic conditions, PYO is blue in color. Acidification of PYO in solution results in a color change of the molecule to a bright red or pink.

Materials and Methods

Media Preparation:

MMM was prepared with reagents as described in **Tables 2.4 - 2.8**. Similarly, steps for preparation of the media follow the optimized method described on pages 60.

Bacterial Culturing:

The representative anaerobic oral community (AOC), described in Chapter 3 (page 127) was used to inoculate a 5 mL culture of MMM and was incubated anaerobically at 37°C for 72 hours. Cells were pelleted via centrifugation at 8,000 x g for 10 minutes. Supernatant was collected and stored for use in downstream culture experiments.

Overnight cultures of PA laboratory reference strain PA14 (Obtained from Marvin Whiteley Laboratory, Georgia Tech) in LB Miller Broth (LB) (IBI Scientific, IA, USA) were washed two times with $_{dd}H_2O$ and used to inoculate 200 μLs of fresh MMM or AOC MMM supernatant in a 96-well plate format to a calculated starting OD600 of 0.01. Plates were then incubated at 37°C with continuous shaking at 210rpm in a Synergy H-1 Plate Reader (BioTek). After 72 hours, photos were taken of the cultures and cultures were subjected to the sample preparation methods detailed below.

Colorimetric PYO Quantification:

PYO extraction and colorimetric quantification was completed as described in Essar et al., 1990, with modifications. Briefly, PA14 cultures to be analyzed were pelleted via centrifugation at 15,000 x g for 1 minute and supernatants were filtered through a 0.22 μm PES centrifuge filter. 600μL of chloroform was added to 1 mL aliquots of pooled filtrate from respective media conditions and vortexed for 5 minutes. Samples were then centrifuged at 15,000 x g for 10 minutes resulting in the formation of two distinct layers. 300 μL of the lower chloroform layer, blue in color from extracted PYO, was transferred into a new microfuge tube and 150 μL of 0.2 M HCl was added to acidify the solution which resulted in a change in sample color from blue to red (**Figure 2.8**). Samples were then vortexed for 5 minutes and again centrifuged at 15,000 x g for 10 minutes resulting in two distinct layers. 100 μL of the red upper layer was transferred into a 96-well plate for absorbance reading at 520 nm with 100 μL of 0.2 M HCl used as a blank. Final PYO concentration was calculated via the following formula including the molar attenuation coefficient of PYO (Najafi et al., 2021):

$$\text{PYO (mg/L)} = A_{520} \times 17.072$$

Average yield was evaluated using pure pyocyanin standards ranging from 5 μg/mL to 25 μg/mL and comparing the final calculated concentrations to those of acidified pure standards of matching concentrations that did not undergo the extraction protocol. The difference in final measured concentrations between

samples of matching starting concentrations was used to calculate the percentage of PYO recovery.

High Performance Liquid Chromatography Sample Preparation:

PA14 MMM culture aliquots were pelleted via centrifugation at 15,000 x g for 1 minute. Supernatant was collected and subjected to filtration through a 0.22 μm PES centrifuge filter. Filtrate was transferred to a 0.5 mL capacity RC 3 kDa MWCO protein concentrator (MiliQ) and centrifuged for 45 minutes at 15,000 x g to remove mucins from the flowthrough. Filtrate was transferred to 200 μL capacity poly-spring inserts placed within 2 mL HPLC vials with pierceable septa tops. Vials were sealed prior to loading into the HPLC autosampler instrument module.

Reverse Phase High Performance Liquid Chromatography:

HPLC was used to quantify concentrations of phenazines (**Table 2.9**). Prepared samples were analyzed using a Dionex UltiMate 3000 HPLC system operated by Chromeleon software (v.7.0, Thermo Fisher) comprised of compatible RS pump, autosampler, column oven, FLD detector, RS diode array, and fraction collector (Thermo Fisher). This instrument was equipped with an Acclaim C18 3 μm 120A° 3.0 x 1500 mm column and accompanying guard column (Thermo Fisher). Analyte separation was achieved using a 30-minute gradient run method including a 5-minute equilibration and consisting of 0.1% trifluoroacetic acid (TFA) and 99.9% CH_3CN mobile phases (**Table 2.10**) at a steady flow rate of 1 mL/min. A total of 8 μL of sample was used per run and injected into the system via the autosampler, with a brief washing of the injection needle with 10% CH_3OH before and after each

injection. Column oven temperature was maintained at 40°C. The RS diode array was configured to collect UV readings at the wavelengths of 370 nm with default frequency. Pure stocks of PYO, PCA, and PCN were used to generate standard curves for accurate quantification of phenazines in experimental samples.

Data Analysis:

Analysis of HPLC chromatograms was completed as described on page 101.

Table 2.9 - Phenazines and their respective HPLC detection parameters.

Phenazine	Abbreviation	Average Retention Time (min)	Standard Range (mM)	R^2
Phenazine - 1 - Carboxamide	PCN	12.75	0.1-100	0.99
Phenazine - 1 - Carboxylic Acid	PCA	14.75	0.1-100	1
Pyocyanin	PYO	5.5	0.1-100	1

Table 2.10 - HPLC mobile phase gradient for phenazine detection.

Time (min)	Flow (mL/min)	CH_3CN	0.1% TFA	Curve
Equilibration				
0.0	1.0	100%	0%	5
Start Run				
5.0	1.0	100%	0%	
11.0	1.0	90%	10%	5
23.0	1.0	60%	40%	5
25.0	1.0	5%	95%	5
28.0	1.0	5%	95%	5
28.0	1.0	100%	0%	5
30.0	**Stop Run**			

Results and Discussion

Colorimetric Pyocyanin Quantification:

To better understand the limitations of the conventional colorimetric method of PYO quantification, I sought to evaluate the accuracy of it in the measurement of PYO standards of known concentration. While co-occurring pigmented molecules in chemically complex bacterial supernatants can cause interference in the analysis of PYO at 520 nm, necessitating the use of an organic extraction protocol, this is not a factor in the measurement of pure standards. This allowed us to forego organic extraction and obtain absorbance values for PYO at concentrations of 5, 10, 15, 20, and 25 μg/mL. These were compared to absorbance values obtained from standards of matching concentrations, that did undergo organic extraction, to calculate the average yield of the extraction protocol (**Figure 2.9**) – a contributing factor to overall method accuracy.

Final calculated values for the standards subjected to extraction were less than half of the true starting concentration. Additionally, standard deviations between replicates were high, confirming high variability in extraction yield (**Figure 2.9**). Together with the limitation of this method to only quantify one phenazine species of interest, these data confirm that the conventional colorimetric approach is a poor option for experimental quantification of PA produced phenazines.

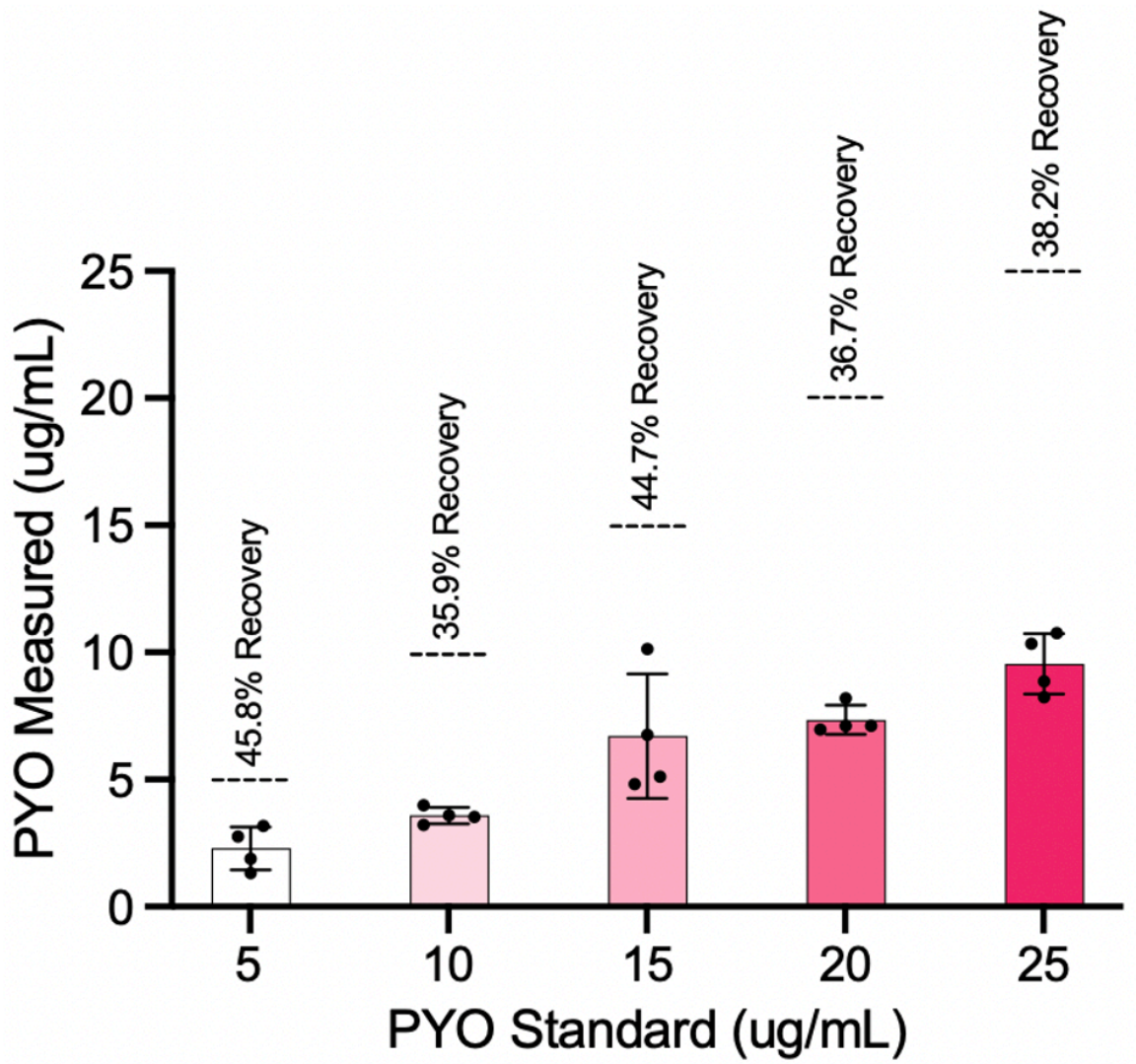

Figure 2.9 – Yield of pyocyanin (PYO) standards using conventional extraction and colorimetric quantification. Concentrations of PYO measured via liquid-liquid extraction and colorimetric quantification (y-axis), compared to the known standard concentrations prior to extraction (x-axis and dotted black lines). PYO yield was calculated using the difference between values as percentage of recovery (dotted black lines).

High Performance Liquid Chromatography Phenazine Quantification:

HPLC quantification of phenazines was accomplished using an Acclaim C18 column with a non-polar stationary phase matrix capable of separating phenazine analytes based on polarity (**Figure 2.10A**). The use of PYO, PCN, and PCA standards generated in first $_{dd}H_2O$ and then MMM were used to optimize the HPLC run method parameters and validate the ability of the method to detect phenazines. 1HP standards were also tested at various concentrations and wavelengths, but no peaks were identified. As a result, 1HP was excluded from subsequent analyses. The final HPLC method resulted in chromatograms with clean and defined analyte peaks and virtually no background signal (**Figure 2.10B**) – properties conducive for accurate and reproducible quantification. Analyte peak properties can be found in **Table 2.9**.

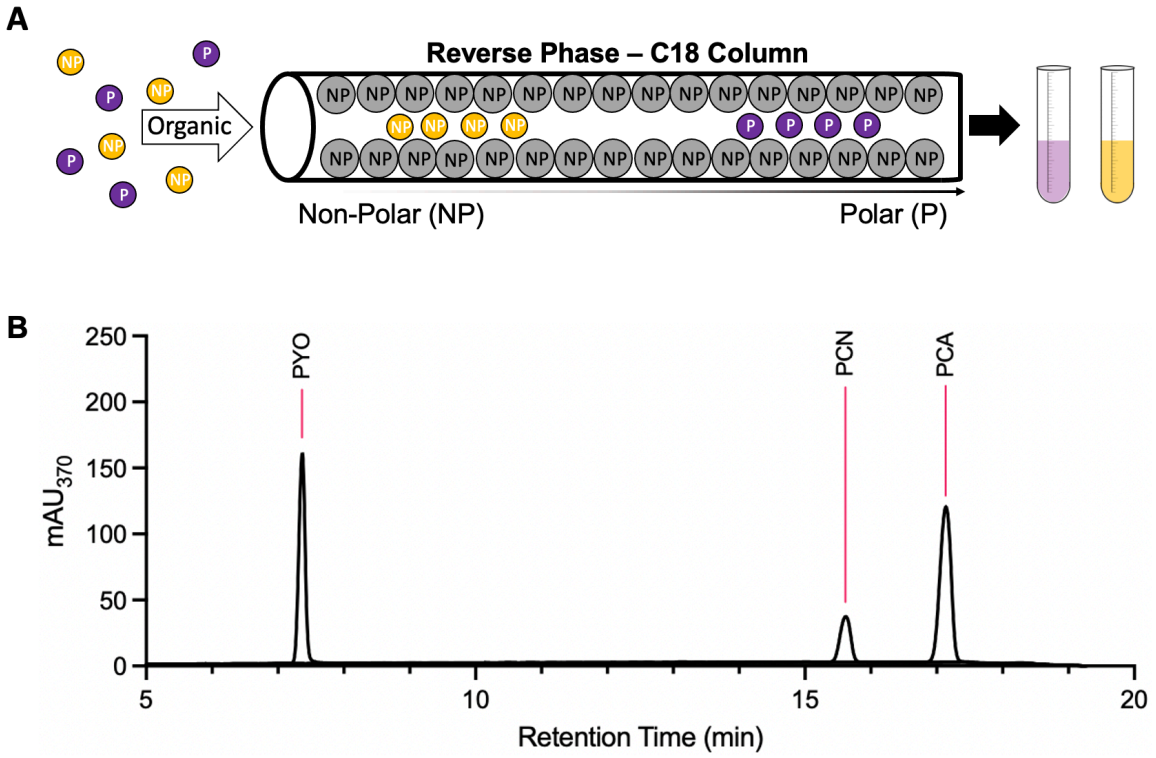

Figure 2.10 – Reverse phase HPLC can be used to successfully quantify phenazines. A) Schematic describing the basic theory behind the HPLC method employed. A C18 column with a non-polar stationary phase is used to separate phenazine analytes based on polarity. More polar analytes are eluted first resulting in a shorter retention time (RT), while the opposite is true for less polar analytes. **B)** Composite chromatogram from finalized HPLC phenazine quantification method displaying absorbance values (y-axis) and RTs (x-axis) of 5mM standards of phenazine-1-carboxylic acid (PCA), phenazine-1-carboxamide (PCN), and pyocyanin (PYO) in mucin-depleted minimal mucin media (MMM).

In Vitro Method Validation:

While the results of the HPLC based phenazine standard detection and quantification were promising, I sought to validate the method with experimental samples to ensure that more complex solutions with co-occurring pigments would not interfere with analyte peak properties. To do so, I measured phenazine profiles of PA14 grown on MMM and the cell free supernatant of AOC. Post incubation, clear differences in color between cultures were observed (**Figure 2.11**). The MMM condition resulted in a blue culture indicative of high pyocyanin concentration (**Figure 2.11A**), while the AOC condition resulted in a green culture (**Figure 2.11B**) indicative of high pyoverdine concentration - a yellow-green pigment (Meyer, 2000). Presence of this pigment would likely interfere with pyocyanin quantification via colorimetric assay. This observable difference in color provided a loose reference for the results of HPLC quantification, as levels of pyocyanin would be expected to be quantified in the blue MMM culture compared to the green AOC culture.

The pooled MMM condition sample contained 358 μM of pyocyanin (**Figure 2.12B**) compared to 244 μM in the pooled AOC supernatant condition sample (**Figure 2.12D**). Levels of PCA were likewise higher in the MMM condition (**Figure 2.12B,D**).

While largely successful, this HPLC analysis carries two caveats. First, PCN levels were below the measurable concentration range – impeding its quantification

(**Figure 2.12A,C**). Second, minor peak splitting of the PCA peak was observed, likely due to an improperly maintained and conditioned column (**Figure 2.12A,C**). Moving forward, both caveats can be addressed by extending the standard curve range for the analytes and cleaning the column prior to sample runs, respectively.

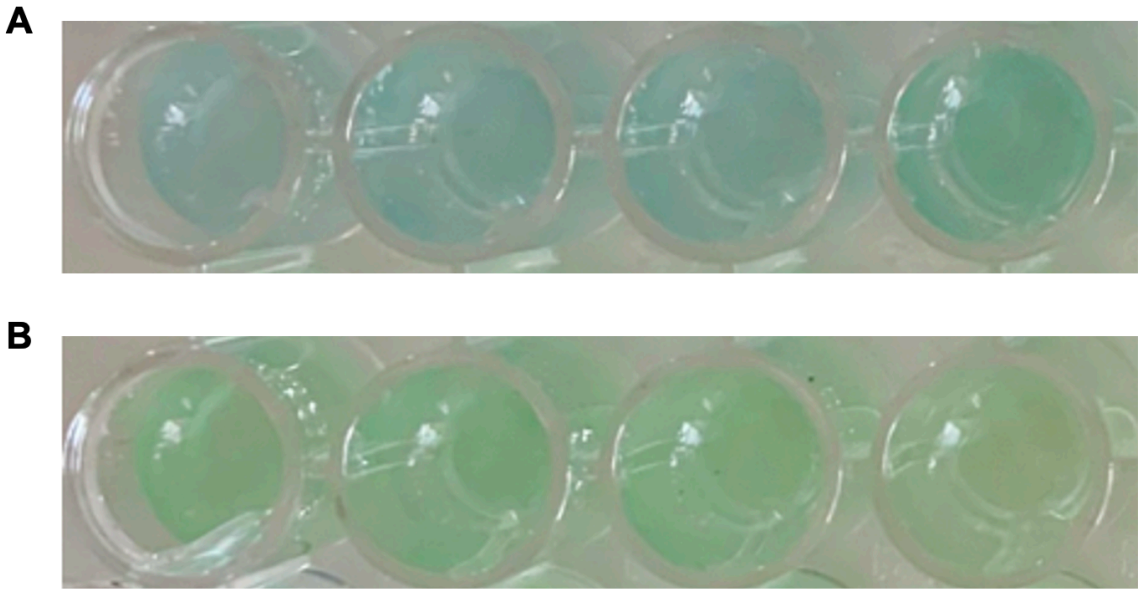

Figure 2.11 – Comparison of visual PYO profiles generated by *P. aeruginosa* in two different culture media. A) Photo of replicate cultures of *P. aeruginosa* laboratory strain PA14 grown aerobically in 200μL of minimal mucin medium (MMM). **B)** Photo of replicate cultures of PA14 grown in the 72-hour MMM supernatant of a representative anaerobic oral community (AOC) under the same conditions.

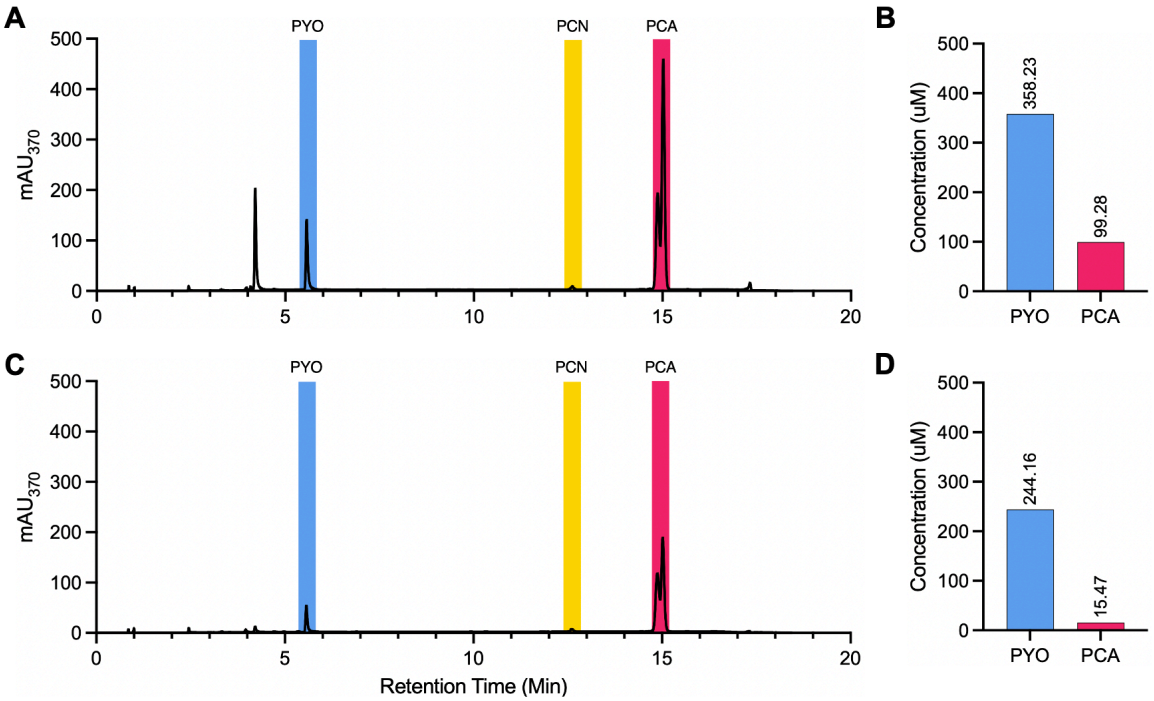

Figure 2.12 – HPLC quantification of phenazines produced by *P. aeruginosa* in different culture media. A) HPLC chromatogram of phenazine profile produced by *P. aeruginosa* strain PA14 when cultured in MMM (**Figure 2.11A**). **B)** Area under the curve (AUC) values for each detectable phenazine corresponding to the previous chromatogram. **C)** HPLC chromatogram of phenazine profile produced by PA14 when cultured in the 72-hour MMM supernatant of a representative anaerobic oral community (AOC) (**Figure 2.11B**). **D)** AUC values for each detectable phenazine corresponding to the previous chromatogram.

Conclusion

In this section, I presented an HPLC based method for the quantification of PA sourced phenazine compounds in complex bacterial supernatants. While HPLC based phenazine analysis is not novel, this method offers a cost effective and high-throughput alternative to other HPLC methods that require subsequent MS analysis of LC separated analytes. This method also offers a significant improvement in both labor expenditure and accuracy compared to the conventional colorimetric based quantification requiring upstream organic extraction of PYO.

Our HPLC based method was optimized through the use of pure standards and validated through the analysis of phenazine profiles generated by PA14 under two growth conditions. While some caveats were identified, they have since been addressed. While only carried out for the purposes of method validation, results of this experiment already provide insight into the regulation of PA phenazines which are generally considered to be mediated by quorum sensing and thus regulated in a growth dependent manner. However, in this validation experiment, PA14 grew to a significantly higher optical density (OD600 = 1.036) after 72 hours of growth in AOC supernatant compared to MMM (OD600 = 0.372) while producing a much lower concentration of phenazines (**Figure 2.12**). This suggests a growth phase-independent mechanism of phenazine regulation.

High-Throughput Quantification of Microbial-Derived Organic Acids in Mucin-Rich Samples via Reverse Phase High Performance Liquid Chromatography.

Alex R. Villarreal[1], Sarah K. Lucas[1], Joshua R. Fletcher[1], Ryan C. Hunter[1*]

[1] Department of Microbiology & Immunology, University of Minnesota, 689 23rd Avenue SE, Minneapolis, MN 55455

† Reprinted with modifications from *Journal of Medical Microbiology*. **Alex R. Villarreal**, Sarah K. Lucas, Josh Fletcher, Ryan C. Hunter. "High-throughput quantification of microbial-derived organic acids in mucin-rich samples via reverse phase high performance liquid chromatography." *In press.*

Abstract

Organic acids (short chain fatty acids, amino acids, etc.) are common metabolic byproducts of commensal bacteria of the gut and oral cavity in addition to microbiota associated with chronic infections of the airways, skin, and soft tissues. A ubiquitous characteristic of these body sites in which mucus-rich secretions often accumulate in excess, is the presence of mucins; HMW glycosylated proteins that decorate the surfaces of non-keratinized epithelia. Owing to their size, mucins complicate quantification of microbial-derived metabolites as these large glycoproteins preclude use of 1D and 2D gel approaches and can obstruct analytical chromatography columns. Standard approaches for quantification of organic acids in mucin-rich samples typically rely on laborious extractions or outsourcing to laboratories specializing in targeted metabolomics. Here we report a high-throughput sample preparation process that reduces mucin abundance and an accompanying isocratic reverse phase high performance liquid chromatography (HPLC) method that enables quantification of microbial-derived organic acids. This approach allows for accurate quantification of compounds of interest (0.01 mM – 100 mM) with minimal sample preparation, a moderate HPLC method run time, and preservation of both guard and analytical column integrity. This approach paves the way for further analyses of microbial-derived metabolites in complex clinical samples.

Key Words: Reverse Phase Liquid Chromatography, High Performance Liquid Chromatography, Mucin, Glycoproteins, Organic Acids, Amino Acids, Targeted Metabolomics

Introduction

Mucin glycoproteins, the primary macromolecular constituent of mucus, range from 1 to 20 megadaltons in size and consist of a threonine-, serine-, proline-, and cysteine-rich polypeptide backbone extensively decorated by O-linked glycans (Kim, et al., 1996; Hang et al., 2005; Cornfield et al., 2015) secreted by mucosal epithelial cells, (Kim et al., 1997) mucins aggregate through the formation of disulfide bonds and non-covalent interactions to form a hydrogel that lends mucus its characteristic viscosity and structure (Kim et al., 1997; Sellers et al., 1989). Mucins line all non-keratinized epithelial surfaces and are vital in the maintenance of the ocular, oral, respiratory, gastrointestinal (GI), and reproductive systems (Andrianifahanana et al., 2006), as they serve a variety of barrier and innate immunity functions (Andrianifahanana et al., 2006; Song et al., 2020). Conversely, disruptions, modifications, or aberrant production of the mucus layer can lead to chronic infection (e.g., CF, chronic rhinosinusitis) or dysbiotic bacterial community assembly (e.g., in the large intestine) (McGuckin et al., 2011).

In the case of CF (CF), mutations in the gene encoding the CF transmembrane regulator (CFTR) protein lead to ionic imbalance and accumulation of viscous, dehydrated mucus in the airways (Ehre et al., 2014; Whelan et al., 2015). Mucus accretion not only impairs respiratory function through physical obstruction and eliciting inflammation, but also impairs mucociliary clearance – a vital function of innate immunity that removes exogenous microbiota (Kurbatova et al., 2015; Wanner et al., 1996). Ultimately, this results in the development of chronic bacterial infection by *PA, Staphylococcus aureus*, and other airway pathogens, which

further deteriorate respiratory function over time (Razvi et al., 2009; Flynn et al., 2016). Interestingly, unlike many GI microbiota, canonical airway pathogens inefficiently utilize mucins as a nutrient source (Flynn et al., 2016). Instead, their growth is thought to be supported by other host-derived nutrients and/or secondary metabolites produced via degradation and mixed-acid fermentation of mucins by co-colonizing bacteria (Flynn et al., 2016). Among these metabolites, organic acids (e.g., short chain fatty acids, amino acids) are most abundant (Flynn et al., 2016; Mirkovic et al., 2015) and are known to shape the growth, physiology, and antibiotic susceptibility of airway pathogens (Flynn et al., 2016; Mirkovic et al., 2015; Bao et al., 2022).

Quantification of organic acids in clinical samples and bacterial culture supernatants is commonly accomplished by analyte separation via liquid or gas chromatography followed by via mass spectrometry (Flynn et al., 2016; Heyen et al., 2020). However, these workflows can be problematic for quantification of organic acids in mucus-rich samples due to the HMW and gelling properties of mucins. Their intrinsic properties leave mucins incompatible with many chromatography methods as they preclude the use of 1D and 2D gel approaches and can obstruct analytical separation columns and chromatography instruments (Kesimer et al., 2012; Kesimer 2009). To overcome these complications, mucins can be depleted via acid hydrolysis (Cornfield et al., 2000; Goso et al., 2017) or organic acids can be extracted from mucin-rich samples via liquid-liquid or solid phase extraction prior to analysis (Flynn et al., 2016; Schoemig et al., 2017). However, extraction methods inherently result in variable reduction of target

analyte concentrations which must be accounted for in final quantification, introducing the potential for error and reduced accuracy. Samples can also be outsourced to laboratories specializing in metabolomics (Moros et al., 2017), but this approach can be low-throughput, time consuming, and cost-prohibitive.

We sought to overcome these challenges by developing a high-throughput sample preparation approach capable of depleting mucin content with minimal impact on organic acid concentrations. We then sought to develop a compatible HPLC method able to separate and quantify organic acids of interest without the need for subsequent mass spectrometry validation. Here we describe the validation of our workflow that accomplishes these objectives and offers a high-throughput, cost-effective method for the quantification of microbial-derived metabolites across a range of mucin-rich environments.

Materials and Methods

Chemicals:

L-isoleucine, L-leucine, L-phenylalanine, and L-valine were purchased from Alfa Aesar (Massachusetts, USA). L-lysine and L-proline were purchased from Sigma-Aldrich (Missouri, USA). L-methionine and L-threonine were purchased form Arcos Organics (New Jersey, USA). Sodium acetate, sodium pyruvate, and citric acid were purchased from Fisher Scientific (Massachusetts, USA). Anhydrous sodium sulfate, sodium butyrate, sodium propionate, sodium L-lactate, sodium formate, sodium hexanoate, and methanesulfonic acid were purchased from Sigma-Aldrich (Missouri, USA). Sodium succinate was purchased from Fluka (Neu-Ulm,

Germany). Anhydrous acetonitrile was purchased from VWR (Pennsylvania, USA).

All standards were prepared using the filtrate of a minimal mucin medium (see below) run through a Pierce PES 3K MWCO 0.5 mL protein concentrator (Thermo Scientific, Massachusetts, USA). 10 mM or 1 M stock solutions of all organic acids were used to produce a range of standards (0.01 mM-100 mM). All standards were filtered through a 0.22 µm PES centrifuge filter (Thermo Scientific) prior to analysis.

Media Preparation:

A minimal mucin medium (MMM) was prepared as previously described (Flynn et al., 2016) with modifications. Briefly, type III porcine gastric mucin (PGM) (Sigma-Aldrich) was added to ddH_2O at a concentration of 30 g/L prior to autoclaving at 121°C for 15 minutes and centrifugation at 15,000 *x* g for 1 h. Supernatant was carefully removed, avoiding solids, and sequentially filtered through PES membranes (3 μm,1 μm, 0.45 μm, 0.22 μm) (Merck Millipore, Massachusetts, USA) using a peristaltic pump. Filtrate was transferred into 20 μm regenerated cellulose (RC) dialysis tubing (Fisher Scientific) for two, 2-hour incubations in ddH_2O at room temperature, followed by overnight incubation at 4°C. ddH_2O was replaced between each incubation. Post dialysis, ddH_2O was added to the mucin solution at a 1:1 ratio and was buffered with 50 mM KH_2PO_4 and150 mM NaCl. 1 mM $MgSO_4$ and a vitamin and mineral mix (**Tables 2.4 - 2.8**) were then added to the buffered mucin solution and filtered through a 0.22 μm bottle top PES filter

(Foxx Life Science, New Hampshire, USA). Mucin content was determined using FPLC as described below. Complete medium was stored at -20°C for immediate use (< 2 weeks) or -80°C for long-term storage (> 2 weeks).

Fast Protein Liquid Chromatography:

FPLC analysis was performed on a ÄKTA Pure instrument with compatible ALIAS autosampler equipped with a 10/200 mm Tricorn column packed with Sepharose CL-2B agarose gel filtration base matrix (Cytiva; Massachusetts, USA). A minimum of 700 μLs per sample was filtered through 0.22 μm PES centrifuge filters before transfer into 2 mL crimp top glass vials with pierceable septa (Thermo Scientific). 500 μLs of each sample filtrate was injected via the autosampler and subjected to a 48-minute isocratic run method at a flow rate of 0.4 mL/min with a mobile phase consisting of 50 mM phosphate buffer and 150 mM NaCl brought to a pH of 7.2 using 1 N HCl (**Table 2.3**).

Clinical Sample Collection:

Expectorated mucus was collected from adult subjects with CF at the University of Minnesota Adult CF Center as previously described (Flynn et al., 2016). Studies were approved by the Institutional Review Board at UMN (IRB 1401M47262). All subjects provided informed consent prior to sample collection.

Cultivation of Microorganisms:

Bacterial cultivation was performed in an anaerobic chamber (Coy Laboratory Products, Michigan, USA) containing a gas mixture of 90% N_2, 5% H_2, and 5% CO_2. All media was allowed to de-gas and equilibrate in the chamber for more than 12 hours before use. *Streptococcus gordonii*, *Prevotella melaninogenica, Veillonella parvula,* and *Fusobacterium nucleatum* were each maintained on Brain Heart Infusion (BHI) agar containing hemin and vitamin K and used to inoculate 3 mL of BHI broth containing hemin and vitamin K and MMM at a 1:1 ratio. Following a 48-hour incubation at 37°C, cultures were passaged into 3 mL of MMM and incubated at 37°C for another 48 h before centrifugation at 10,000 x *g* for 2 minutes. Pellets were washed twice with MMM and used to inoculate experimental cultures for downstream HPLC analysis. Likewise, an anaerobic microbial community was enriched from CF mucus. To do so, 1 mL of PBS was added to a clinical sample, mechanically homogenized, and was used to inoculate 3 mL culture of 1:1 BHI:MMM. Following a 48-hour incubation, the culture was passaged into 3 mL of MMM and incubated at 37°C for another 48-hour**.** This was repeated for a total of four passages before the final culture was used to generate a 20% glycerol stock and supernatant for downstream HPLC analysis.

Reverse Phase High Performance Liquid Chromatography:

HPLC was used to quantify concentrations of organic acids (**Table 2.11**) and amino acids (**Table 2.12**). Bacterial cultures grown in MMM were first centrifuged at 4,000 x *g* for 10 minutes. Supernatants were then filtered through 0.22 µm PES

centrifuge filters. Supernatants were then filtered through a 0.5 mL 3,000 MWCO PES protein concentrator (Thermo Scientific) to remove HMW mucins. For analysis of raw samples, 1 mL of PBS was added to sputum before homogenization. A 1 mL aliquot was then removed and subjected to the sample preparation method described above.

Filtrates were analyzed using a Dionex UltiMate 3000 HPLC system operated by Chromeleon software (v.7.0, Thermo Fisher) comprised of compatible RS pump, autosampler, column oven, FLD detector, RS diode array, and fraction collector (Thermo Fisher). This instrument was equipped with an Acclaim organic acid 5 µm 120A° 4.0 x 250 mm column and accompanying guard column (Thermo Fisher). Analyte separation was achieved using an isocratic run method with a mobile phase of 100 mM $NaSO_4$ (pH adjusted to pH 2.6 using CH_3SO_3H). This method consisted of an 8-minute equilibration step and subsequent 24-minute static flow at a rate of 1 mL/min. A total of 6 µL of sample was used per run and injected into the system via the autosampler, with a brief washing of the injection needle with 10% CH_3OH before and after each injection. Column oven temperature was maintained at 30°C. The RS diode array was configured to collect UV readings at the wavelengths of 210 nm with default frequency.

Data Analysis:

Chromeleon software (v.7.0) was used to view and process raw data. Raw chromatograms were stacked and offsets removed to compare standard runs and

perform an initial quality control of each run sequence. Quantitative processing methods were created for each target analyte. The integrated Cobra Wizard was used to gate and smooth peaks of interest on a single standard of intermediate concentration (1-10 mM) for a given analyte. To ensure gating accuracy, each sample was manually checked and the AUC recorded for later processing in Prism 9.0 (GraphPad). Cobra wizard was run with default settings.

Concentrator Analyte Recovery:

MMM was filtered through a 3,000 MWCO PES protein concentrator to remove HMW mucins. The mucin-depleted flow-through was then used to prepare 10 mM standards of organic acids (Table 1) and 1 mM standards of amino acids (Table 2) – preventing the analytes from coming in direct contact with the filter. Identical standards were then prepared in unfiltered MMM before being filtered through 3,000 MWCO PES protein concentrators – exposing the analytes to the filter. Paired standards of each analyte were then run back-to-back on the HPLC using methods described above. Chromeleon 7.0 and Prism 9.0 (GraphPad) were used to calculate concentrations of analyte in each sample. Analyte recovery was determined by comparison of change in analyte concentration between the two methods of preparation. To compare filter-based analyte recovery to a more common extraction approach, 10 mM standards of acetate, butyrate, lactate, and propionate were first prepared in MMM before undergoing a liquid-liquid extraction as previously described (De Baere et al., 2013).

Analytical Column Wear:

A 10 mM standard of acetate was run on a new Acclaim organic acid (OA) analytical column to measure analyte peak properties under ideal column conditions. The same analytical column was then subjected to a total of 145 runs consisting of standards, bacterial supernatants, and clinical sample supernatants, prior to a final run of the same 10 mM acetate standard. A column cleaning protocol was performed as recommended by the manufacturer (Thermo Fischer Scientific, 2009), consisting of flushing the column with 10 column volumes of 0.22 μm filtered ddH_2O, then 20 column volumes of 100% acetonitrile, then another 10 column volumes of 0.22 μm filtered ddH2O, before a final equilibration of the column with 15 column volumes of 100 mM Na^2SO_4 (pH=2.65). Following this, the same 10 mM acetate standard was run again. The accompanying guard column was not replaced prior to cleaning. Data were processed and compared as described above.

Table 2.11 - Organic acids and their respective detection parameters corresponding to pure standards in minimal mucin media (MMM) as determined by (HPLC).

Metabolite	Classification	Average Retention Time (min)	Standard Range (mM)	R^2	PES Filter Yield (%)
Acetate	Short-chain fatty acid	3.60	0.1-100	1	99.94
Butyrate	Short-chain fatty acid	17.75	0.1-100	1	96.43
Citrate	Tricarboxylic acid	4.60	0.1-100	0.99	82.35
Formate	Monocarboxylic acid	2.65	1-100	0.99	102.00
Lactate	Alpha-hydroxy acid	3.4	0.1-100	0.99	93.61
Propionate	Short-chain fatty acid	7.30	0.1-100	0.99	91.93
Pyruvate	Keto acid	2.80	0.1-100	0.99	83.94
Succinate	Dicarboxylic acid	5.35	0.1-100	0.99	115.82

Table 2.12 - Amino acids and their respective detection parameters corresponding to pure standards in minimal mucin media (MMM) as determined by HPLC.

Metabolite	Classification	Average Retention Time (min)	Standard Range (mM)	R^2	PES Filter Yield (%)
Isoleucine	Branched-chain, nonpolar, aliphatic amino acid	5.70	0.01 - 10	0.99	97.70%
Leucine	Branched-chain, nonpolar, aliphatic amino acid	6.15	0.01 - 10	0.99	105.57%
Lysine	Polar, positively charged amino acid	2.00	0.01 - 10	0.99	116.15%
Methionine	Nonpolar, aliphatic amino acid	3.90	0.01 - 10	0.99	79.94%
Phenylalanine	Nonpolar, aromatic amino acid	14.45	0.01 - 10	1	86.35%
Proline	Polar, uncharged amino acid	2.35	0.01 - 10	0.99	125.00%
Threonine	Polar, uncharged amino acid	2.15	0.01 - 10	0.99	78.56%
Valine	Branched-chained, nonpolar, aliphatic amino acid	3.10	0.01 - 10	0.99	100.87%

Results and Discussion

Depletion of High Molecular Weight Mucins:

The size and intrinsic properties of mucin (**Figure 2.13A**) can interfere with most analytical chromatography methods. Thus, we sought to develop an approach to deplete mucins from bacterial cultures and human-derived clinical samples without reducing concentrations of organic acids of interest. To do so, MMM was filtered through 3k MWCO PES and RC protein concentrators and analyzed via FPLC. Unfiltered MMM and a series of HMW protein standards (Cytiva) were used to establish the relation between protein size (kDa) and column RT (**Figure 2.13B-C**). Chromatograms shown demonstrate that full depletion of HMW mucins (peak 1, RT 5-12 min) was achieved using both filtration methods. As determined by peak area under curve (AUC), LMW mucins (peak 2, RT 12-20 min) were reduced by ~97% and 86% by PES and RC filtration, respectively, demonstrating the efficacy of our protocol. We then determined analyte recovery post-filtration to ensure no significant loss of metabolite concentrations (**Tables 2.11- 2.12**)**.** 10 mM solutions of four representative analytes (acetate, butyrate, propionate, and lactate) were also subjected to a more conventionally used liquid-liquid extraction approach for comparison (**Figure 2.13D**). In each case, PES filtration resulted in analyte recovery percentages near 100%, demonstrating improvement over standard liquid extraction approaches.

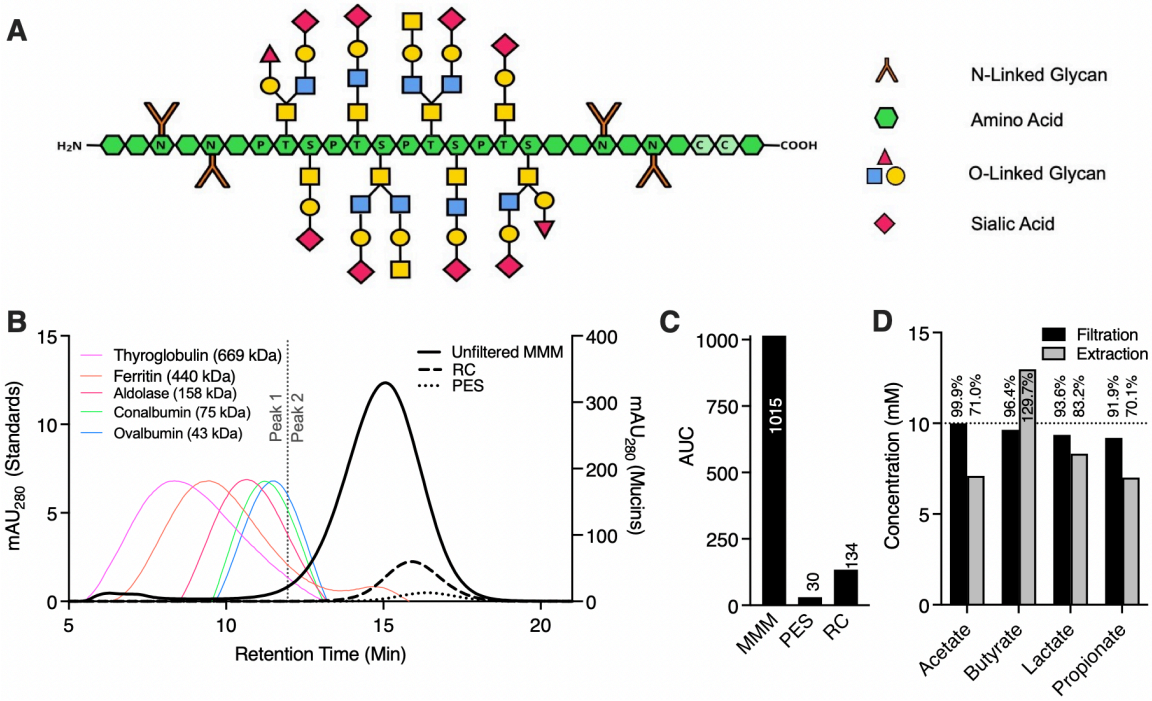

Figure 2.13 - Mucin glycoproteins can be efficiently depleted from mucin-rich samples via filtration. A) Chemical structure of a mucin glycoprotein. **B)** Fast protein liquid chromatography (FPLC) chromatogram conveying relative protein size and concentration of Cytiva protein standards (left y-axis) and minimal mucin media (MMM) (right y-axis) subjected to mucin depletion using 3k MWCO regenerated cellulose (RC) or 3k MWCO polyethersulfone (PES) protein concentrators. Ovalbumin (43 kDa) RT = 11.55, conalbumin (75 kDa) RT 11.22, aldolase (158 kDa) RT = 10.60, ferritin (440 kDa) RT = 9.17, and thyroglbulin (669 kDa) RT = 8.17. **C)** Area under the curve (AUC) values, conveying relative protein concentration, calculated from the MMM peaks of the FPLC chromatogram. **D)** Yield (mM) of 10 mM standards of acetate, butyrate, lactate, and propionate in MMM after mucin depletion and liquid-liquid extraction.

Quantification of Organic Acids in Mucin-Rich Specimens:

To further demonstrate the efficacy of filtration-based sample preparation, 5 mM standards of representative organic acids (acetate, butyrate, lactate, and propionate) in MMM were prepared and were either left untreated or depleted of mucin via filtration through 3k MWCO protein concentrators prior to analysis via reverse-phase HPLC. For untreated mucin rich standards, unstable baseline readings, peak shouldering, missing peaks, and other chromatogram anomalies were observed (**Figure 2.14A**), underscoring how mucins obfuscate analyte quantification via HPLC. In contrast, resulting chromatograms of mucin depleted standards were free from previously observed aberrations (**Figure 2.14B**), indicating mucin depletion via PES filtration is sufficient sample preparation for HPLC organic acid profiling. To further demonstrate the efficacy this sample preparation method, a panel of 8 organic acids (3.125 mM, **Table 2.11**) and 8 amino acids (0.938 mM, **Table 2.12**) were prepared as mixed standards in mucin-rich MMM and subjected to the full HPLC workflow (**Figure 2.15A**) to provide a chromatogram containing peaks of all analytes of interest (**Figure 2.15B**). These analytes were chosen based on their known generation by fermentative bacteria of the CF airways and for their associated carboxylic acid functional groups that enable detection at λ = 210 nm. These data confirm analyte RTs and adequate peak separation. While there is evidence of minor peak overlap in some instances, peaks are clearly distinguishable from one another. Subsequent analysis of biological samples (**Figure 2.16A,C,E**) suggest peak overlap is less prevalent in

practice, as biological samples are less likely to contain the high concentration of analytes as in the artificial mixed standard (**Figure 2.15B**).

Further validation of the workflow was performed by analysis of various biological samples of higher complexity than standards in a minimal medium; (i) cell-free supernatants of CF associated bacteria (*Streptococcus gordonii*, *Prevotella melaninogenica, Veillonella parvula,* and *Fusobacterium nucleatum*) grown in MMM (**Figure 2.16A,B; Figure 2.S1**), (ii) cell-free supernatant of a mixed anaerobic bacterial community isolated from CF sputum (**Figure 2.16C,D**), and (iii) a mucus-rich clinical CF sputum sample from which the enrichment was derived (**Figure 2.16E,F**). Each sample was analyzed using the described workflow, including PES filtration, and concentrations (mM) of select organic acids (**Table 2.11**) were calculated from the chromatograms. While several amino acids were detectable, PES filtration yields of this analyte group (**Table 2.12**) were variable and over 100% in some instances. Because of this, this workflow may be better suited for detection and relative quantification of amino acids rather than absolute quantification. Consequently, we elected not to include amino acid analytes in the metabolite profiles (**Figure 2.16B,D,F**). Data presented demonstrate the ability of this workflow to not only quantify complex biologically derived organic acid profiles from minimal defined medium, but also directly from bacterial cultures and complex human-derived material.

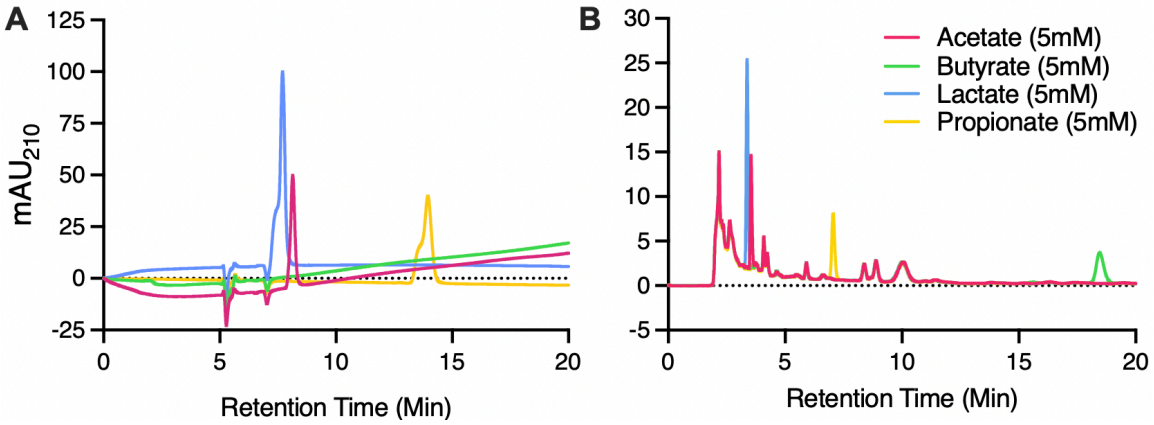

Figure 2.14 - Sample mucin depletion improves organic acid analyte resolution and eliminates peak aberrations. A) High performance liquid chromatography (HPLC) chromatogram of 5 mM standards of acetate, butyrate, lactate, and propionate in minimal mucin media (MMM) without a mucin depletion step included. **B)** HPLC chromatogram of 5 mM standards of acetate, butyrate, lactate, and propionate in MMM generated using the same run method, but with the inclusion of a mucin depletion step using a 3k MWCO PES protein concentrator. Each standard was run separately.

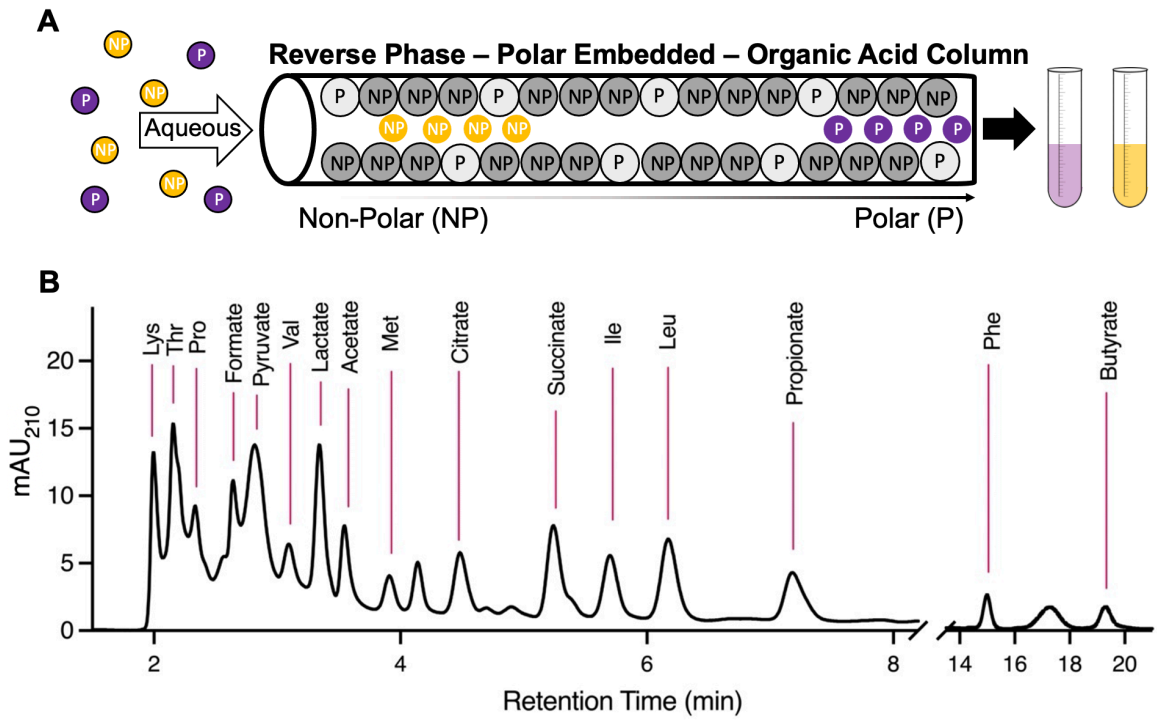

Figure 2.15 - Reverse phase high performance liquid chromatography (HPLC) can quantify organic acids and amino acids in mucin-rich samples. A) Schematic of Acclaim Organic Acid (OA) column used to quantify organic acids and amino acids in samples. The largely non-polar stationary phase matrix possesses polar inclusions that aid in the separation of analytes based on polarity. More polar analytes are eluted more quickly resulting in a shorter retention time (RT), while the opposite is true for non-polar analytes. **B)** HPLC chromatogram of a mixed standard solution of amino acids (0.938 mM, Table 2.12) and other organic acids (3.125 mM, Table 2.11).

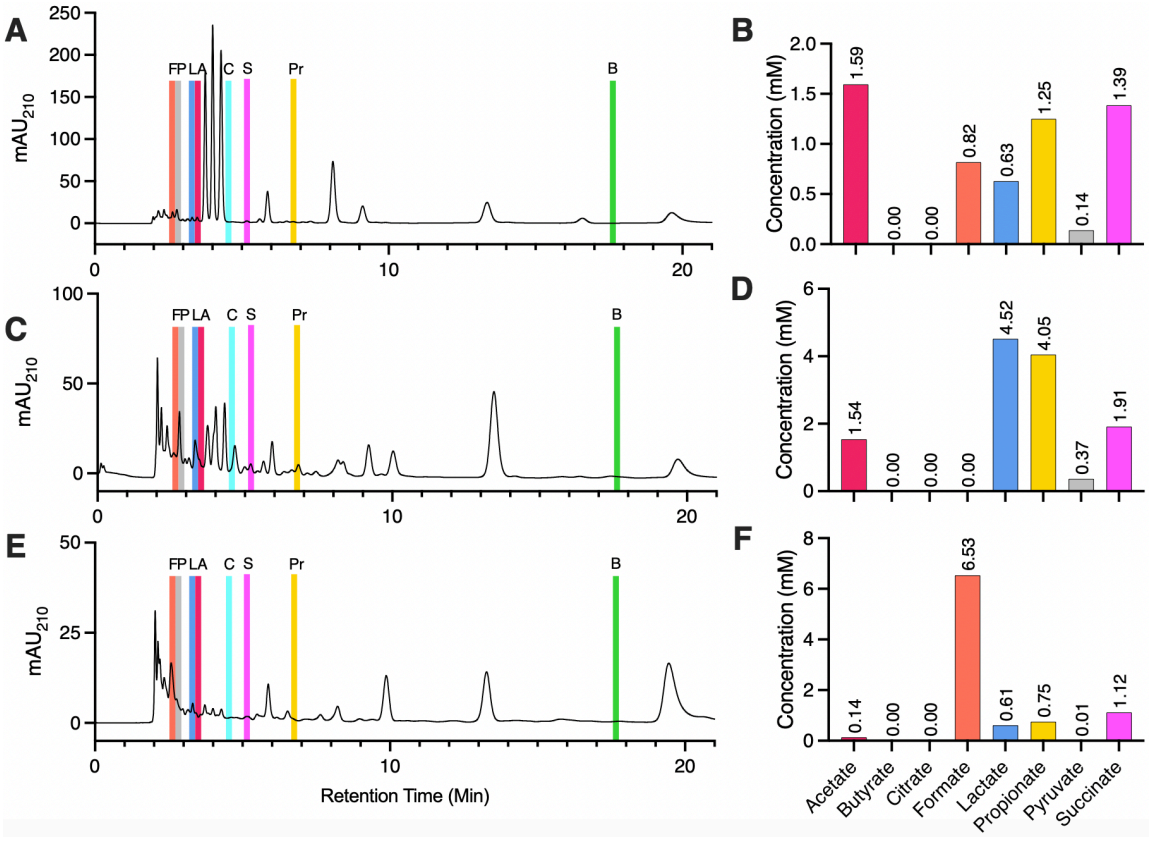

Figure 2.16 - HPLC workflow allows for the quantification of organic acids in a variety of mucin-rich sample types. A) HPLC chromatogram of supernatant generated by *Streptococcus gordonii* grown anaerobically in MMM for 48 hours. **B**) Corresponding organic acid profile of *Streptococcus gordonii*. **C**) HPLC chromatogram of supernatant generated by a clinical CF sputum sample mucin enrichment grown anaerobically in MMM for 48 hours. **D**) Corresponding organic acid profile of the clinical CF sputum sample mucin enrichment. **E**) HPLC chromatogram of raw clinical CF sputum sample that was used to generate mucin enrichment. **F**) Corresponding organic acid profile of raw clinical CF sputum sample.

Column Integrity:

While the data demonstrate the efficacy of our sample preparation and HPLC methods for metabolite quantification, we questioned its long-term use. More specifically, we asked whether repeated analysis of mucin-rich samples would lead to analytical column performance decline and/or damage over time. To ensure that low levels of residual LMW mucins that remain after sample preparation (**Figure 2.13B,C**) do not significantly impact the lifespan of the column, a 10 mM standard of acetate was measured multiple times across a run of ~150 mucin-rich samples and standards of various types. As shown in **Figure 2.17A**, deterioration of peak properties (i.e., baseline, peak width, peak height) for the acetate standard were observed after 146 consecutive runs. However, peak properties were restored after a completing a standard acetonitrile-based column cleaning protocol and subsequent equilibration. AUC values of the peaks corroborate restoration of peak resolution and area after column cleaning (**Figure 2.17B**).

Degradation of column retention and resolution with use is expected with any method as HPLC analytical columns are generally consumable products. However, data shown here affirm the sustainability of our optimized HPLC workflow, provided the column is properly maintained. For optimal column performance, we recommend a column wash protocol be completed after the analysis of each individual sample set. Replacement of the guard cartridge between sample sets of different origins (i.e., clinical samples, MMM) is also ideal. Analysis of freshly prepared standards prior to analysis of new sample set is

recommended to ensure accurate peak identification and concentration calculation over the lifespan of the column. Once peak resolution is reduced and the lower range of analyte concentrations are no longer detectable, it is recommended that a new column be used.

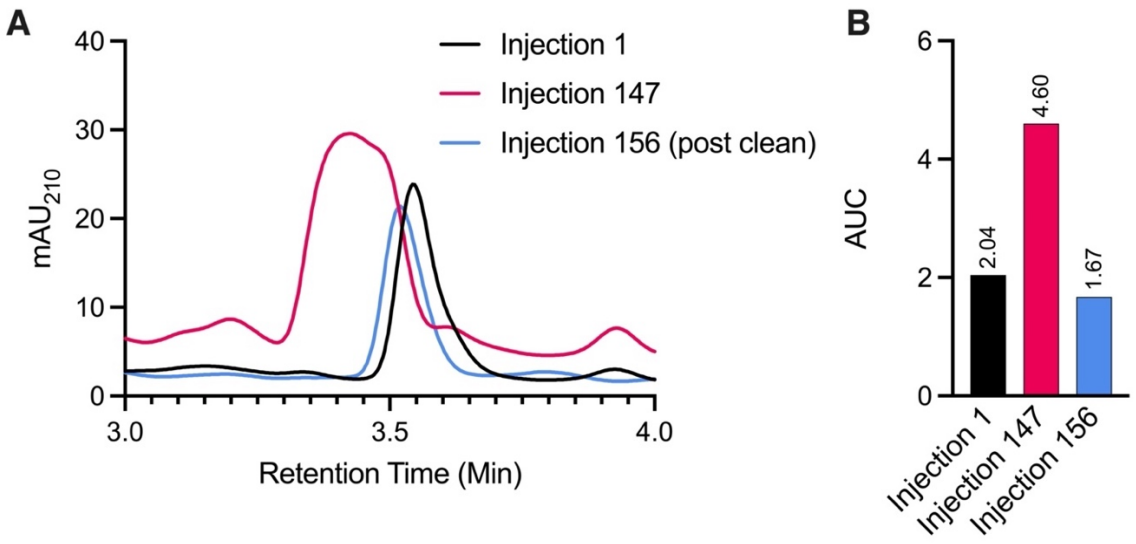

Figure 2.17 - Analytical column integrity is preserved with regular maintenance. A) HPLC chromatogram of the same 10 mM standard of acetate prepared in mucin depleted MMM and run using the same method as the 1st, 147th, and 156th injection on a new analytical column. A column cleaning protocol was completed after the 155th injection before the final acetate analysis. **B)** AUC values calculated from the peaks in the HPLC chromatogram.

Conclusion

We describe a filter-based method for depletion of mucins in clinical and laboratory samples and an accompanying single-step reverse-phase HPLC method capable of organic acid quantification without the need for subsequent mass spectrometry analysis. Our data demonstrate the depletion of HMW glycoproteins, while greatly reducing the concentration of LMW mucins. This filter-based sample preparation method was also shown to reduce the loss of acetate (filter = 0.06% loss / extraction = 29.0% loss), butyrate (filter = 3.6% loss / extraction = 29.4% gain), lactate (filter = 6.4% loss / extraction = 16.8% loss), and propionate (filter = 8.07% loss / extraction = 29.9% loss) yield when directly compared to conventional liquid-liquid extraction techniques (**Figure 2.13D**). Additionally, our sample preparation method was found to preserve integrity of the analytical column and HPLC instrument (**Figure 2.17**). Using this workflow, we demonstrate the successful quantification of organic acids derived from individual anaerobic bacteria (*Streptococcus gordonii*, *Prevotella melaninogenica, Veillonella parvula,* and *Fusobacterium nucleatum*) (**Figure 2.16A,B; Figure 2.S1**), a complex mucin enrichment community derived from a clinical CF sputum sample (**Figure 2.16C,D**), as well as the paired raw clinical sample itself (**Figure 2.16E,F**).

This approach paves the way for future studies of mucin-rich samples (e.g., CF sputum, sinus mucus) in which anaerobic microbiota are widely appreciated to comprise a significant component of the microbiota, yet their contributions to disease pathogenesis are poorly understood. Through mucin depletion and

accurate quantification of their mixed acid fermentation metabolites, our approach promises to generate greater insights into how they shape the host chemical environment. This method has already been widely implemented within our lab and has contributed to several manuscripts in preparation and publication. This HPLC approach has been used to evaluate the utilization of acetate and propionate by *PA* (**Figure 2.S2**), profile the organic acids generated from clinical sinus sample mucin enrichments (**Figure 2.S3**) and investigate the impact of *F. nucleatum* organic acids on *S. aureus* growth (**Figure 2.S4**). While we use the respiratory tract as our model system, this workflow represents a high-throughput and cost-effective method for quantification of microbial organic acids across a wide array of mucin-rich host environments.

Acknowledgments

The authors thank Adam Gilbertsen for technical support and reagent acquisition, Nicholas Glogowski of Thermo Fisher for instrument support and training, and Richard Martinez and the staff at the UMN CF Center for clinical sample acquisition.

Author Contributions:

Alex Villarreal: Conceptualization, Methodology, Validation, Visualization, Writing – original draft. **Jeffrey Flynn**: Methodology**. Sarah Lucas**: Resources, Visualization. **Josh Fletcher**: Resources. **Ryan Hunter**: Conceptualization,

Funding Acquisition, Supervision, Resources, Visualization, and Writing – review & editing.

Funding:

This work was supported by a National Heart, Blood, Lung Institute (NHLBI) Research Project Grant (1R01HL136919) awarded to RCH, an Administrative Research Supplement (HL136919-03S1) to ARV, a NHLBI T32 fellowship (2T32HL007741-21) to ARV, and a National Institute of Dental and Craniofacial T32 Fellowship (#T90DE0227232) to SKL. The funders had no role in study design, data collection or interpretation, or the decision to submit the work for publication.

Declaration of Competing Interest:

The authors declare that they have no known competing interests that may have influenced the data reported in this publication.

Supplemental

High-Throughput Quantification of Microbial-Derived Organic Acids in Mucin-Rich Samples via Reverse Phase High Performance Liquid Chromatography.

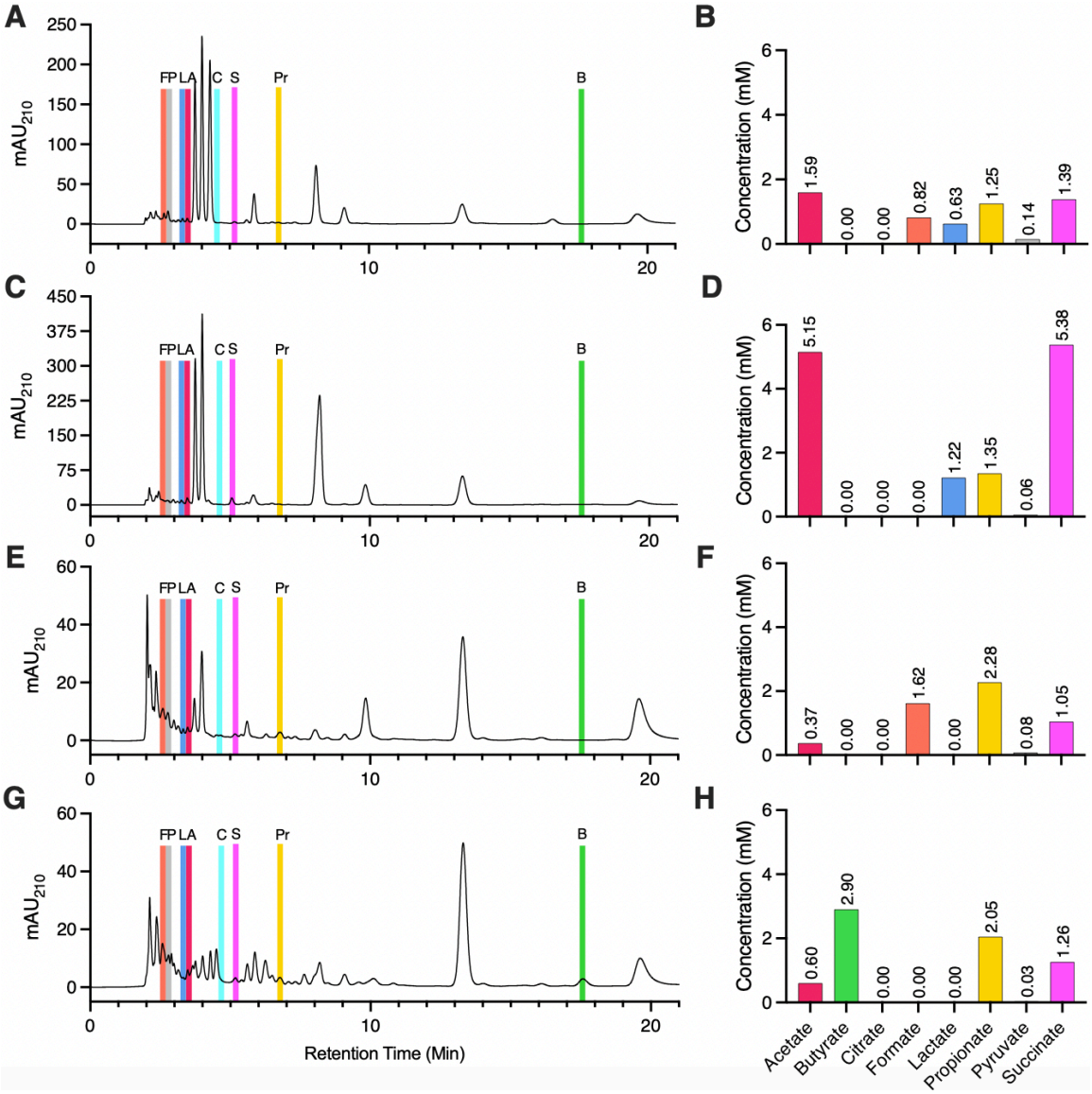

Figure 2.S1 - HPLC-based quantification of organic acids in mucin-rich cell free supernatants derived from CF associated microbiota. HPLC chromatogram and corresponding organic acid profile of supernatants generated by **A,B)** *Streptococcus gordonii,* **C,D**) *Prevotella melaninogenica*, **E,F)** *Veillonella parvula*, and **G,H)** *Fusobacterium nucleatum*.

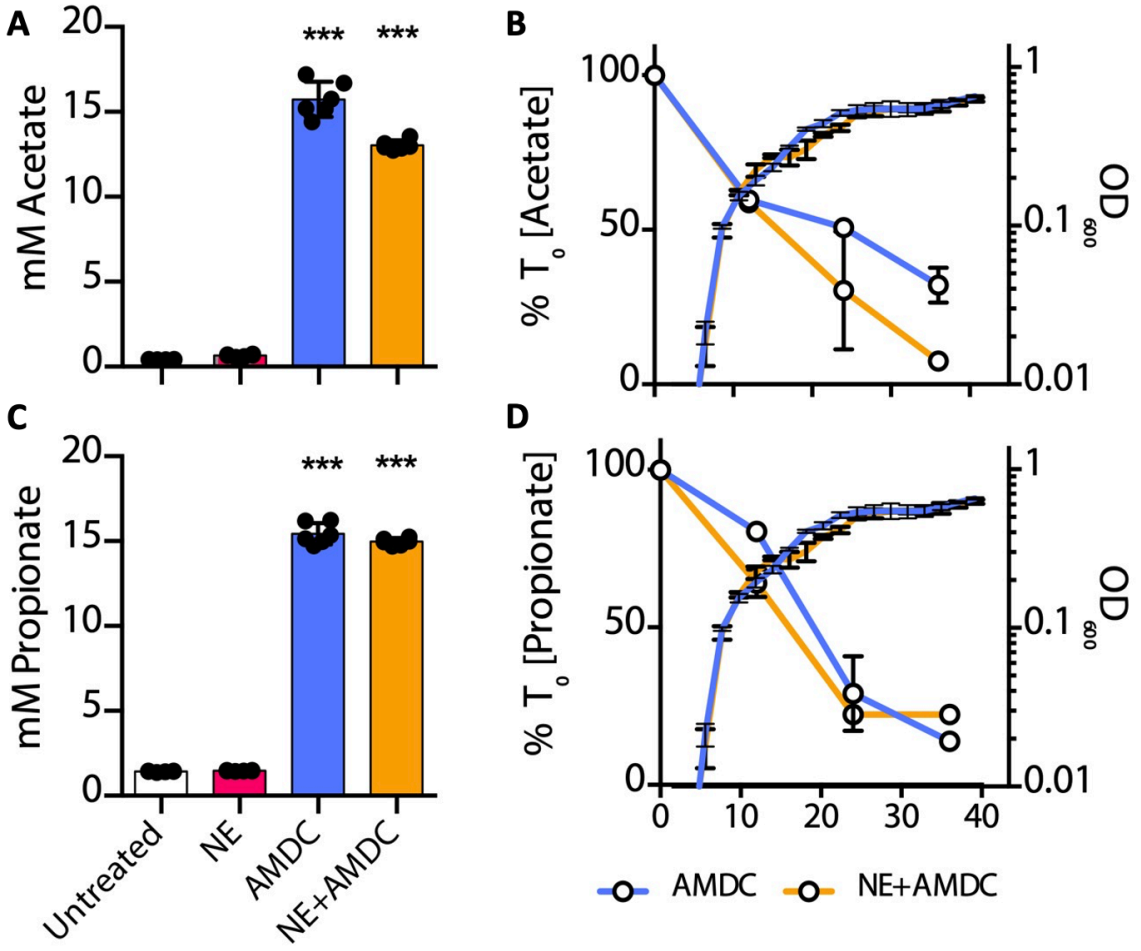

Figure 2.S2 - Increased growth of *P. aeruginosa* on anaerobe-derived supernatants is mediated by acetate and propionate. A) Acetate and **B)** propionate concentrations generated via mucin degradation by neutrophil elastase (NE) and an anaerobic mucin degrading consortium (AMDC). **C)** Acetate and **D)** propionate utilization (open circles) is concomitant with an increase in *P. aeruginosa* growth (OD_{600}). Bars represent the mean and standard deviation of three biological replicates.

† Reprinted from Sabrina Arif, Jeffrey Flynn, Talia Wiggen, Sarah Lucas, **Alex Villarreal**, Jordan Dunitz, Ryan Hunter. Contributions of host and bacterial mucinase activity in support of *P. aeruginosa* growth in the CF airways. Manuscript in preparation.

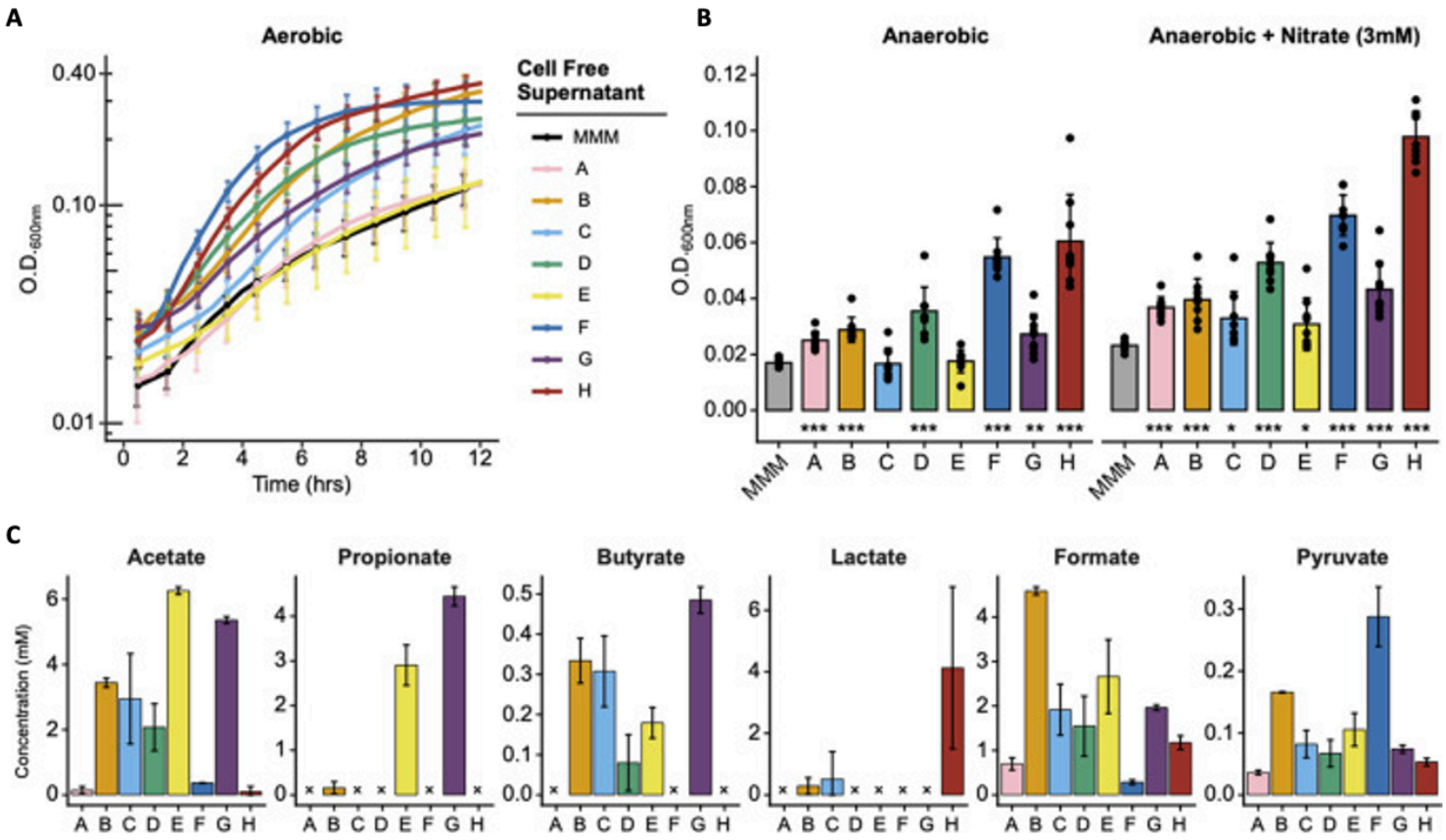

Figure 2.S3 - S. aureus growth on cell-free supernatants from chronic rhinosinusitis (CRS) mucin-degrading communities. A) S. aureus USA300 LAC aerobic growth on cell-free supernatant (CFS) from CRS-derived mucin-degrading communities relative to intact mucin alone (MMM [black]). **B)** S. aureus anaerobic growth on CFS with and without sodium nitrate (3 mM). **C)** HPLC quantification of mixed-acid fermentation metabolite concentrations (mM) in CFS. x, not detectable; ***, $P < 0.001$; **, $P < 0.01$; *, $P < 0.05$.

† Reprinted from Lucas SK, **Villarreal AR**, Ahmad M, Itabiyi A, Feddema E, Boyer HC, Hunter RC. 2021. Anaerobic microbiota derived from the upper airways impact *Staphylococcus aureus* physiology. *Infect Immun* 89:e00153-21. DOI: 10.1128/IAI.00153-21

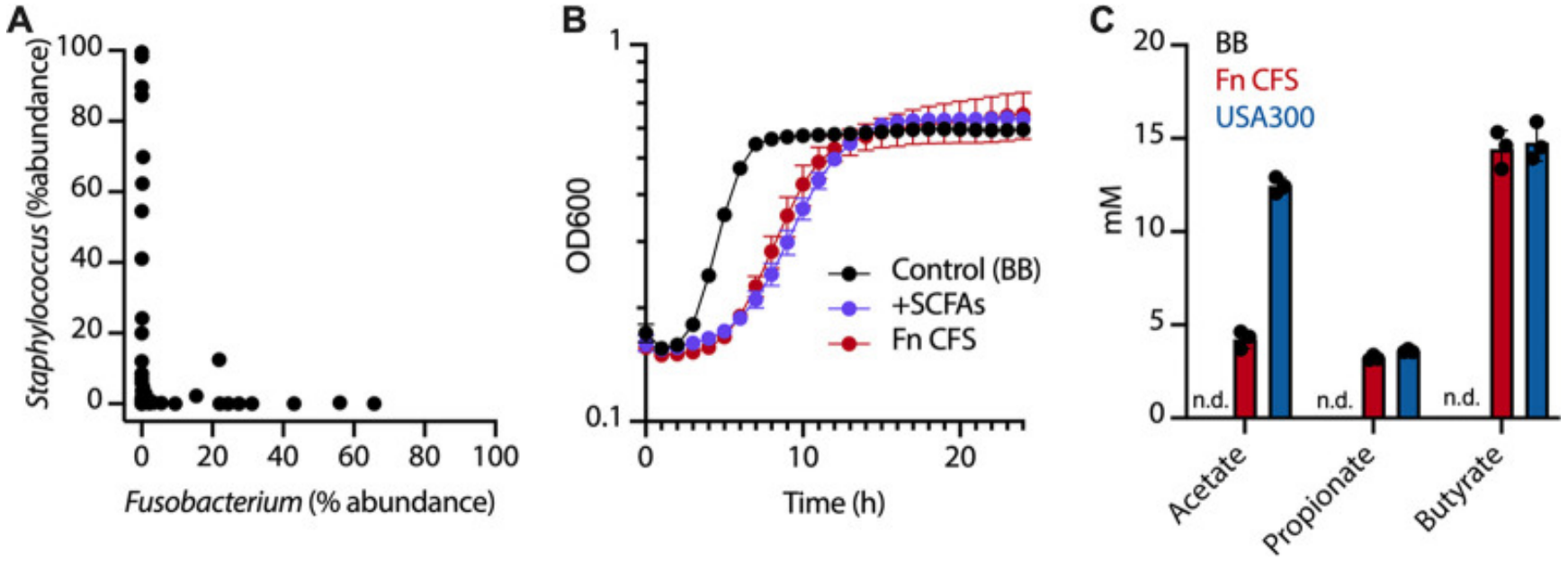

Figure 2.S4 - *S. aureus* growth is impaired in *F. nucleatum* supernatants. A) Relative abundances of *Fusobacterium* and Staphylococcus in sinus mucus from patients with chronic rhinosinusitis are inversely correlated. **B)** Representative growth curve of S. aureus USA300 in Brucella broth (BB; control); BB supplemented with 5 mM acetate, 5 mM propionate, and 15 mM butyrate; and cell-free supernatants from F. nucleatum (Fn CFS). **C)** Production of SCFAs by F. nucleatum after 48 h (Fn CFS) and their levels after S. aureus (USA300) growth in Fn CFS. SCFAs were below the limit of detection in sterile BB. All data shown in B and C are the mean ± standard deviation of three biological replicates.

† Reprinted from Fletcher JR, **Villarreal AR**, Penningroth MR, Hunter RC. 2022. *Staphylococcus aureus* overcomes anaerobe-derived short-chain fatty acid stress via FadX and the CodY Regulon. *J Bacteriology* 204(5):e0006422 DOI: 10.1128/jb.00064-22

CHAPTER 3: *In vitro* Characterization of Anaerobic Bacterial Mucin Degradation and its Impact on *Pseudomonas aeruginosa*

Summary

Tools developed in Chapter 2 overcome several technical limitations and allow for the effective characterization of individual components of the proposed cross-feeding model – pathogen, commensals, mucins, secondary metabolites, and interactions between them. In this chapter, I first use metagenomic sequencing to define the species level composition of a representative anaerobic oral community (AOC) adept at growth on mucin as a sole carbon source and able to consistently support the growth of PA through cross-feeding. Informed by this data, I select representative anaerobic species and characterize their growth on mucin, ability to degrade mucin, and ability to generate organic acid byproducts. Additionally, I investigate the effects of both individual anaerobic species cell free supernatants on the PA growth. While this chapter focuses on *in vitro* reductionist experiments driven by putative mucin degrading anaerobic bacterial species found in the oral cavity, its findings are relevant to my broader thesis as many of the same genera and species identified are also found in the CF airways.

Individual Anaerobe Metabolic Profiles and Effects of Organic Acids on *Pseudomonas aeruginosa* Physiology.

Introduction

PA is a canonical pathogen of the CF airways. As previously described, it reaches densities as high as 10^{10} CFU/mL in patient sputum (Palmer et al., 2005) and is considered responsible for the bulk of patient morbidity and mortality. While it may seem to thrive in the dehydrated mucin rich mucus that lines the CF airways, its ability to successfully colonize, proliferate, and induce pathogenesis is reliant on interactions between the pathogen and complex communities of co-colonizing microbiota. As an example, PA is unable to efficiently utilize mucins as a sole carbon source. Rather, it depends on a cross-feeding relationship with co-colonizing anaerobic bacterial genera that are adept at the catabolism of mucin glycoproteins (Flynn et al., 2016). This catabolism results in liberated mucin glycans and polypeptides as well as fermentation byproducts such as organic acids. These byproducts are not only hypothesized to support the growth of PA, but also potentiate its virulence through regulation of biofilm formation and phenazine production.

Of the bacterial genera associated with the mucin-based cross-feeding model, *Streptococcus, Prevotella, Veillonella,* and *Fusobacterium* are the most commonly identified among CF microbiota (Flynn et al., 2016; Francoise et al., 2020; Tony-Odigie et al., 2022). Interestingly, these four genera are also abundant in the oral cavity (Flynn et al., 2016; Caselli et al., 2020). This underscores the remarkable

interplay, particularly in CF patients, between the oral cavity and lower airway microbial communities. Microaspiration of oral secretions into the lower airways is a common occurrence that affects even healthy adults but is more prevalent in infants and children (Ficke et al., 2022). Healthy non-CF airways do not suffer from the accumulation of viscous mucus, and consequently are able to remove aspirated foreign bodies, such as bacterial cells, from the lower airways via mucociliary clearance and innate immunity. These processes are disrupted in the CF airways, leading to the accumulation of aspirated foreign bodies rather than their removal (Kurbatova et al., 2015). This lack of successful clearance is thought to dynamically link the oral cavity to the CF airways – with the oral cavity functioning as an influential gateway dictating the microbial composition of the latter. This relationship is considered to be a driving force in the initial acquisition and succession of the CF airway microbiome in pediatric patients, conditioning nutritional landscape and promoting subsequent colonization by CF associated pathogens – such as PA (Muhlebach et al., 2018; Clarke et al., 2018).

The four described genera (*Streptococcus, Prevotella, Veillonella,* and *Fusobacterium*) may also fill similar niches across environments. *Streptococcus*, a prominent member of the oral microbiome (Baty et al., 2022), is most known for its ability to degrade oral mucins (Hoeven et al., 1991; Glover et al., 2022), contribute to dental caries, and initialize colonization of oral surfaces (Hillman et al., 1987). High abundances of *Streptococcus* in CF airways also correlate with CF PEx (Scott et al., 2019), suggesting a similar ecological role in the airways. Its ability to

initialize colonization of surfaces and degrade mucins may support PA growth and pathogenicity, contributing to CF PEx.

Considering its distinct linkage and similarity to CF airway bacterial communities, oral derived microbiota offer an easily accessible and relevant sample source for the study of anaerobic mucin degradation and cross-feeding interactions. Here, I capitalized on this by characterizing the bacterial composition of a representative anaerobic oral community (AOC). Informed by these data, I selected several representative strains of identified species to further evaluate through *in vitro* growth experiments. These strains and their associated metabolites were also studied for their ability to impact the physiology of PA. Resulting data support the linkage between the oral and CF airway environments lend new insights into specific bacterial interactions occurring withing the proposed cross-feeding model.

Materials and Methods

Chemicals:

A full description of organic acids used in growth experiments can be found on page 97.

Bacterial Strains & Growth Conditions:

Anaerobic species are listed in **Table 3.1**. All representative species were first cultured in 1X complete beef broth medium for 48 hours prior to being passaged into MMM for another 48-hour incubation. Cell free supernatants of individual

anaerobic cultures were obtained by centrifugation at 12,000 *x* g for 1 min followed by filtration through a 0.22 μm PES centrifuge filter. All culturing occurred at 37°C within an anaerobic chamber (Coy Laboratory Products, Michigan, USA) containing a gas mixture of 90% N_2, 5% CO_2, and 5% H_2. AOC culturing was conducted in the same chamber and described below.

Pseudomonas aeruginosa PA14 (obtained from Marvin Whiteley, Georgia Tech) was used in these experiments. All PA14 growth experiments were completed aerobically in a 96-well plate format. Plates were incubated in a BioTek Synergy H1 plate reader at 37°C, with shaking at 240 rpm, and OD600 reading being collected each hour.

Media Preparation:

Complete beef broth medium was prepared with reagents as described in **Tables 2.1 - 2.2**. MMM was prepared with reagents as described in **Tables 2.4 - 2.8**. Similarly, steps for preparation of MMM follow the optimized method described on pages 60.

Representative Anaerobic Oral Community Enrichment Generation:

AOC mucin enrichment was previously described in Flynn et al, 2016. This original community was used to generate several 0.5 mL frozen stocks stored at -80°C. Each individual stock can be used to inoculate up to 5 mL of MMM under anaerobic

conditions. These cultures are used to generate more frozen stocks as needed and may explain variability over time.

Metagenomic Sequencing & Analysis:

AOC was grown for 72 hours at 37°C under anaerobic conditions before genomic DNA was extracted from an 800 μL aliquot using a DNeasy Powersoil kit (Qiagen, Carlsbad, CA). Genomic DNA was submitted to the University of Minnesota Genomics Center (UMGC) for library preparation and sequencing using Illumina MiSeq TruSeq 2x300. A negative control sample of fresh MMM was also included.

Sequence analysis was conducted via terminal linked to Minnesota Supercomputing Institute (MSI) servers. The KneadData (Pereira-Marques et al., 2019) pipeline, containing Trimmomatic (Bolger et al., 2014) and Bowtie2 (Langmead et al., 2012), was used to perform initial sequence read quality control. Trimmomatic first removed library adapters and low-quality reads. Bowtie2 then paired reads and removed contaminating host sequences by aligning sequences against reference host genomes. Human and porcine genomes were used as references for sequence removal, given the origins of the microbial community and MMM, respectively. Quality controlled reads were input to MetaPhLAn 2.0 (Truong et al., 2015) – a computational tool for profiling of microbial metagenomes. MetaPhlAn 2.0 utilizes over 1 million clade specific marker genes and over 17,000 reference genomes across several databases to profile microbial communities to the species level. Default settings were used to generate an ASV table used as

input for GraPlAn (Asnicar et al., 2015) to generate a phylogenetic tree. ASV values were also used to generate a taxa plot using GraphPad Prism 9.0.

16S rRNA Gene Sequencing & Analysis:

Genomic DNA was extracted from AOC cultures using a DNeasy Powersoil kit and subjected to next generation 16S rRNA sequencing by the UMGC. This and subsequent analyses were performed as described on page 167.

Fast Protein Liquid Chromatography:

FPLC characterization of mucin degradation was accomplished using the methodology previously described on pages 46 - 48.

High Performance Liquid Chromatography:

HPLC quantification of organic acids (**Table 2.11**) and phenazines (**Table 2.9**) was accomplished using the methodology described on pages 101 and 81, respectively.

Results and Discussion

Sequencing of a Representative Anaerobic Oral Community:

A mucin enrichment community was generated from a human saliva sample in Flynn et al., 2016, sequenced, and subsequently used in our laboratory as a representative anaerobic mucin degrading control. AOC has consistently exhibited robust growth on MMM (**Figure 4.2B**), mucin degradation abilities (**Figure 4.2C-**

D), and generation of diverse organic acids (**Figure 4.4B**). As a result, I sought to define the composition of this microbial community in greater detail and investigate the putative roles of its individual constituents in mucin catabolism and cross-feeding of PA. To accomplish this, I first sequenced the metagenome of the community to obtain species level resolution of its bacterial composition. Quality control steps of sequence analysis resulted in no alignment to human or porcine genomes – supporting the effectiveness of our methods at reducing host DNA contamination from both sample and mucin host sources. Post-processing, a final ASV table was used to generate a taxa plot of relative species abundance (**Figure 3.1A**) and an accompanying cladogram to visualize bacterial diversity (**Figure 3.1B**). Consistent with the initial 16S rRNA gene amplicon sequencing of AOC in Flynn et al., 2016, *Streptococcus, Prevotella, Veillonella,* and *Fusobacterium* were found to be prevalent genera in the community– solidifying their putative classification as core components of anaerobic mucin degrading microbiota of the CF airways.

Metagenomic sequencing allowed for species level resolution (**Figure 3.1A-B**), and highlighted the presence of several other genera previously undetected. For example, *Solobacterium moorei* is a Gram-positive obligately anaerobic bacillus associated with human feces, dental caries, and halitosis (Barrak et al., 2020; Pedersen et al., 2011). Irrespective of its high abundance in AOC, little is known of the metabolism or mucin degradation abilities of this species. Conversely, the well-characterized *Bifidobacterium dentium* was also identified at a low abundance

in AOC. This species is a Gram-positive anaerobe associated with oral infections and colonization of the intestinal mucosal lining (Ventura et al., 2009; Engevik et al., 2019). It is highly associated with mucins and possesses the genetic repertoire for saccharide degradation and the generation of acetate and lactate (Ventura et al., 2009). As a result, species were studied in further detail.

Despite exhibiting mucin catabolism and robust cross-feeding abilities, we have observed instances of AOC cultures growing poorly on MMM, failing to degrade mucins, and even seemingly inhibiting the growth of PA (data not shown). To better understand the cause of this, I inoculated four individual AOC cultures from the same frozen stock and incubated them at the same time under the same conditions. Genomic DNA was extracted from each community and subjected to 16S rRNA gene sequencing for bacterial composition profiling. The resulting taxa plots (**Figure 3.2**) displayed drastic differences in the relative abundances of bacterial genera between each culture – despite employing identical culturing techniques and time frames. Many of the same genera are identified across all sequenced cultures, including the metagenomic sequenced culture; however, abundances of each varied greatly.

While these data further support the classification of the four previously described genera (*Streptococcus, Prevotella, Veillonella,* and *Fusobacterium*) as core mucin degraders, they also highlight caveats to consider when using a stock community (i.e. AOC) as a mucin-degrading community control. It's bacterial composition,

despite yielding consistent results, is subject to change between each culture. As a result, each AOC culture should be treated as a unique community and subjected to its own sequencing and characterization. While not explored further in this thesis, this representative community serves as unique model for the study of colonization, ecological succession, and polymicrobial interactions within the CF airways.

Informed by these sequencing data, representative strains of species identified in AOC were chosen for individual evaluation of growth on mucin, mucin degradation, and organic acids generation. Prior to characterization, each strain was analyzed for the presence of carbohydrate-active enzyme (CAZy) sequences via the CAZy online database (**Table 3.1**). While not an absolute measure of the ability of a species to degrade mucins, species with higher counts of CAZy sequences (**Table 3.1**) appear to exhibit an increased capacity for mucin degradation (**Figure 3.3B**). As an example, *Bifidobacterium dentium* is associated with mucosal layers and is known to degrade polysaccharides. It also has over 171 sequences across 24 sub-families belonging to the glycosyl hydrolase family of enzymes – a high number of sequence counts compared to other species (**Table 3.1**). *B. dentium* also exhibited the most relative degradation of HMW mucins compared to those same species (**Figure 3.3B**).

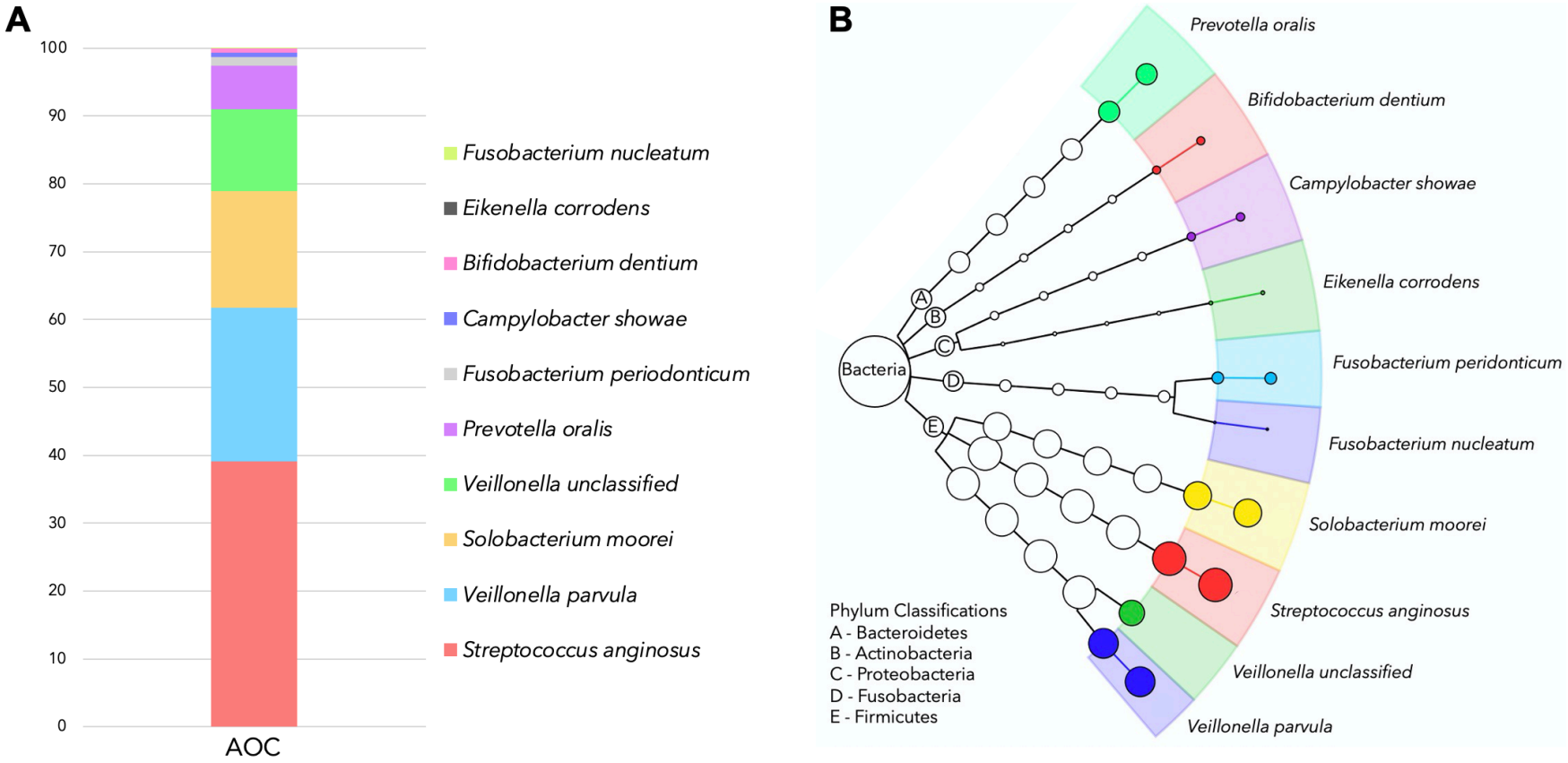

Figure 3.1 – Metagenomic profiling of a representative anaerobic oral community. A) Taxa plot displaying species level relative abundance from ASV table of community bacterial composition. **B)** GraPhlAn generated cladogram of the same taxonomic data. Base letters indicate phylum classification, circle size indicates relative abundance, and circle color indicates species.

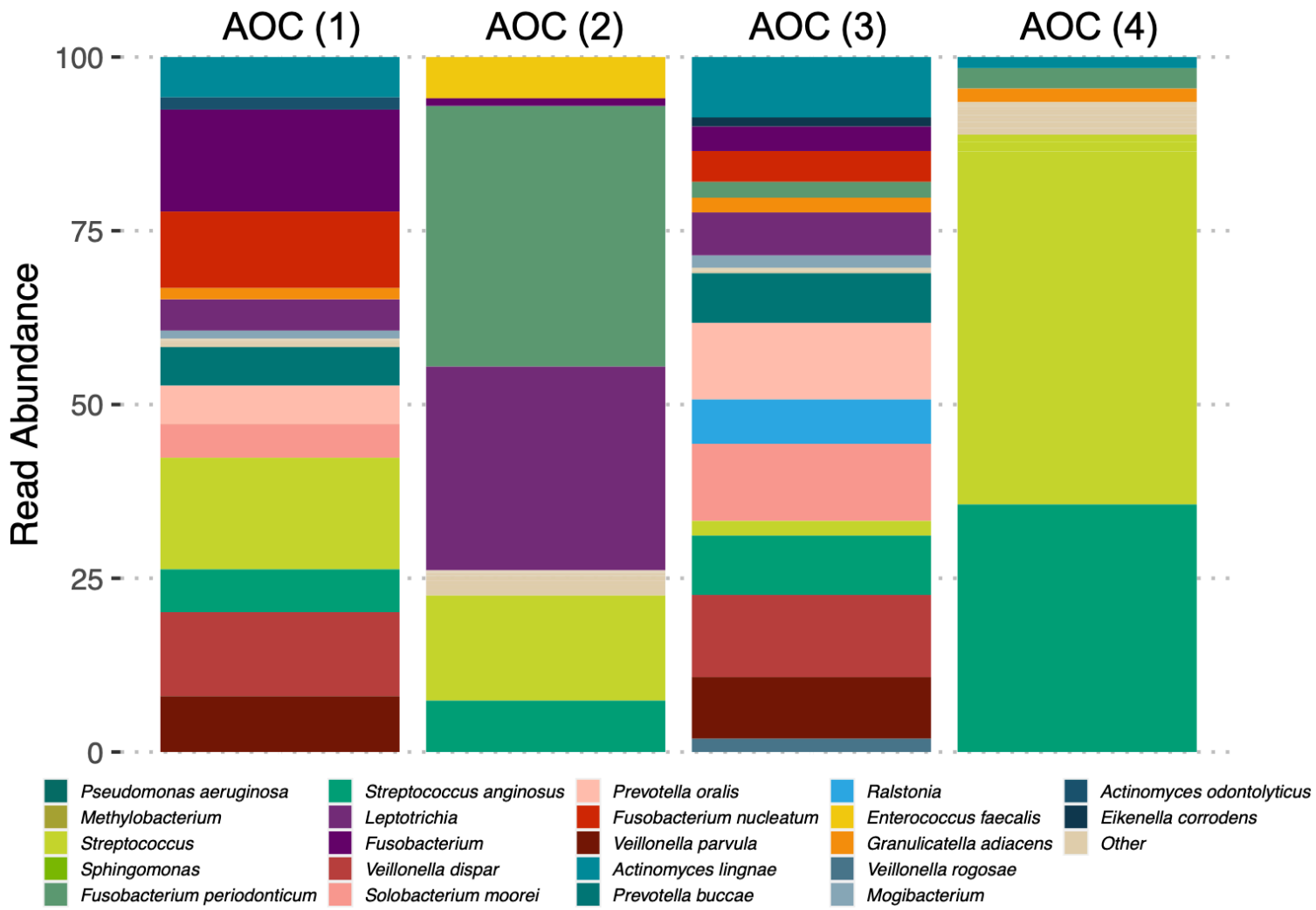

Figure 3.2 – Repeated 16S rRNA gene amplicon profiling of a representative anaerobic community. Taxa plots of species level relative abundances in four separate AOC cultures derived from the same set of frozen stocks and cultured under the same conditions at the same time.

Table 3.1 – List of representative bacterial species selected from AOC sequencing data for characterization. Counts of total carbohydrate-active enzymes sequences and subfamilies for each species are also listed.

Carbohydrate-Active Enzyme (CAZy Database) Families and Sequence Counts											
Species	**Strain**	**Glycoside Hydrolase**		**Glycosyl Transferase**		**Polysaccharide Lyase**		**Carbohydrate Esterase**		**Carbohydrate-Binding Module**	
		# of sequences	*# of families*	*# of sequences*	*# of families*	*# of sequences*	*# of families*	*# of sequences*	*# of families*	*# of sequences*	*# of families*
Bifidobacterium dentium	**ATCC 27534	171	24	24	10	0	0	2	2	10	7
Bifidobacterium longum	**ATCC 15707	171	24	24	10	0	0	2	2	10	7
Fusobacterium nucleatum	ATCC 25586	6	4	23	11	0	0	5	3	4	2
Prevotella melaninogenica	ATCC 25845	57	30	39	13	0	0	4	3	4	4
* *Prevotella oralis*	ATCC 33269	N/A	N/A	N/A	N/A	N/A	N/A	N/A	N/A	N/A	N/A
* *Solobacterium moorei*	CCUG 39336	N/A	N/A	N/A	N/A	N/A	N/A	N/A	N/A	N/A	N/A
Streptococcus gordonii	DL1 Challis CH1	32	17	24	9	0	0	2	2	12	8
Streptococcus parasanguinis	ATCC 15912	36	20	29	11	0	0	3	3	6	5
Veillonella parvula	**ATCC 10790	4	3	18	10	0	0	1	1	0	0

** No representative strain genomes for the species available on the CAZy database.*

*** Genome of strain used in experiments not available on the CAZy database. Data from closely related representative strain included in table. (Bifidobacterium dentium Bd1; Bifidobacterium longum 105-A; Veillonella parvula NCT11810)*

Anaerobe Growth on Mucin:

Informed by AOC sequencing data, representative species were chosen from identified genera for *in vitro* characterization on MMM. MMM cultures were incubated anaerobically at 37°C with OD600 readings collected at 24-hour time points (**Figure 3.3A**). *Streptococcus gordonii* exhibited the most robust growth with a final OD600 reading of 0.473 – consistent with the high CAZy sequence counts (**Table 3.1**) and high relative abundance of this genus across sequenced samples (**Figure 3.1-3.2**). Conversely, *Veillonella parvula* exhibited the least robust growth with a final OD600 reading of just 0.04 – consistent with its nutritional preference for amino acids and lactate rather than saccharides (Bjorkroth et al., 2020).

Post 72-hour incubation, cell free supernatants (CFS) were collected from each culture and subjected to mucin degradation analysis via FPLC (**Figure 3.3B**). Consistent with its robust growth, *S. gordonii* exhibited the highest mucin degradation – followed by *P. oralis*. Not only did it generate a decrease in the area under the curve (AUC) values of the high molecular weight (HMW) and low molecular weight (LMW) peaks, but it also yielded an increase in median retention time (RT) of the LMW peak – suggesting a measurable degrease in the average molecular size of mucins comprising that peak. While growth data (**Figure 3.3A**) predicted *V. parvula* to exhibit the least mucin degradation, it exhibited more degradation of both HMW and LMW mucins compared to the better growing *S. moorei.* The cause of this remains unknown, but one plausible explanation could be ability of *S. moorei* to cleave and catabolize terminal sugar residues from mucin

glycans, such as sialic acids. This ability would allow *S. moorei* to sustain its nutritional requirements while reducing the impact on overall mucin species molecular size. This ability may also provide advantages for other microbiota – leaving glycans vulnerable to further degradation by other community constituents. Unfortunately, little supporting data exists for this species in the literature, underscored by its lack of CAZy database entries (**Table 3.1**).

Organic acid profiles generated from the same CFSs via HPLC revealed metabolic diversity between species (**Figure 3.3C**). All findings appeared to be consistent with current published literature. S. *gordonii,* was one of the few species to produce detectable levels of lactate (Egland et al., 2004). While no organic acid data exist for *P. oralis,* its high production of acetate and formate are consistent with what is observed in the related *P. copri* (Huang et al., 2021). *V. parvula*, characterized by its nutritional preference of lactate and production of propionate (Wicaksono et al., 2020), produced no lactate but high levels of propionate. *F. nucleatum,* known to produce butyrate (Wang et al., 2021), was the only species to do so. *B. dentium* produced detectable levels of acetate and lactate, consistent with its pyruvate fermentation metabolic pathways (Ventura et al., 2009). It was also the only species to generate detectable levels of citrate. Lastly, *S. moorei* produced a diverse and unique organic acid profile with high levels of propionate, lactate, and formate. No literature currently exists on the organic acids generated by *S. morrei*, making these data the first of its kind.

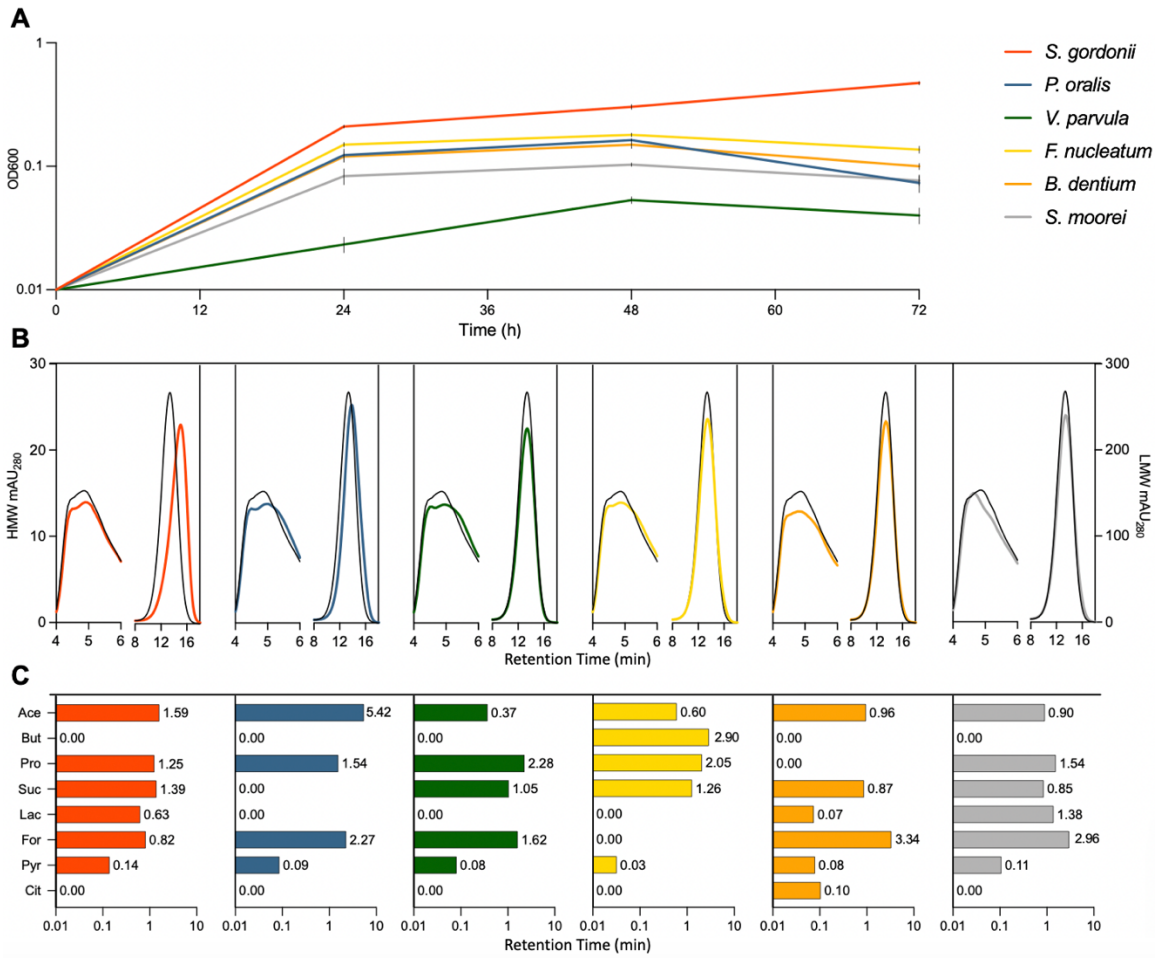

Figure 3.3 – Characterization of representative mucin-degrading anaerobes. A) 72-hour growth curves of representative strains grown anaerobically at 37°C in MMM. Endpoint OD600 readings: *S. gordonii* (0.473)*; P. oralis* (0.073)*; V. parvula* (0.04)*; F. nucleatum* (0.136)*; B. dentium* (0.100)*; S. morreii (*0.077). **B)** FPLC chromatograms displaying the high molecular weight peaks (left partition and y-axis) and low molecular weight peaks (right partition and y-axis) of the same representative strains (colored lines) post 72-hour incubation compared to a MMM non-incubated control (black line). **C)** HPLC generated organic acid profiles of the same 72-hour representative strain cultures.

Effects of Anaerobe Cell Free Supernatants on P. aeruginosa Physiology:

Characterization of individual species grown on MMM allowed for the evaluation of their various effects PA14 physiology – growth, mucin degradation ability, and organic acid generation. PA14 was grown under aerobic conditions for 72-hours in the CFSs of each anaerobic species, as well as a MMM control (**Figure 3.4A**). All CFS resulted in improved growth of PA14, compared to growth in the MMM control which resulted in an extended lag phase. *S. gordonii* CFS resulted in the most robust PA14 growth, consistent with its rich organic acid profile (**Figure 3.3C**). Interestingly, PA14 growth on MMM, *V. parvula,* and *S. moorei* CFSs resulted in growth resembling a bi-phasic or diauxic growth patten. Diauxie is most commonly observed when a bacterial culture depletes its preferred nutrient source and must modify its metabolism to utilize a present secondary nutrient source (Chu et al., 2016). Without further analysis or PA14 organic acid utilization, the exact nutrients contributing to this growth phenotype remain unknown. It is worth noting that the MMM control, lacking microbial derived organic acids, elicits the same growth phenotype.

The impact of each CFS on biofilm formation of PA14 was evaluated via a crystal violet microtiter assay (**Figure 3.4B**). The CFS of *V. parvula* was the only condition to elicit a significant effect on PA14 biofilm formation – resulting in a two-fold increase in biofilm production after normalization to culture final optical density. Despite this striking increase, no observed patters in mucin degradation or organic acid production by *V. parvula* appear to correlate with this effect. However, this

effect is well documented in the literature, as *V. parvula* was previously found to promote the development of robust PA14 aggregates and biofilm structures when co-cultured (Pustelny et al., 2015). These data not only support that finding, but also suggest that the observed promotion of PA14 biofilm formation by *V. parvula* is not contact dependent and can be replicated by growth on *V. parvula* CFS. This indicates that a signaling molecule, other than the organic acids analyzed in this study, may play a role in this phenomenon. While not significant, growth on *F. nucleatum* CFS resulted in lower PA14 biofilm formation. Butyrate has been shown to inhibit biofilm formation in other bacterial species (Liu et al., 2022; Zhu et al., 2022), and may play a role in this context as well.

Phenazines produced by PA14 during growth in different CFS were measured via HPLC (**Figure 3.4C**). Unfortunately, due to supply chain issues imposed by the COVID-19 pandemic, samples were pooled to ration remaining supplies – eliminating the ability to perform statistical analysis. Nevertheless, several interesting patterns warrant follow up experiments. For example, PA14 growth in *V. parvula* and *S. morrei* CFSs resulted in slightly higher concentrations of all phenazines. These were the same species that grew poorly on MMM and elicited a bi-phasic growth pattern by PA14. Interestingly, growth on *B. dentium* CFS resulted in moderate levels of PCA, but no PYO or PCN. This same phenomenon is observed in Chapter 4 of this work – elicited by a sputum mucin enrichment community containing low levels of *Bifidobacterium.* In that same dataset, expression of *phzS* transcripts, responsible for final conversion of intermediates to

PYO, was paradoxically elevated. Although no such transcript expression data exist for this data set, the observed pattern mirrors that of what is documented in Chapter 4 – suggesting a possible growth-independent mechanism of PA14 phenazine suppression by co-colonizing anaerobic microbiota via regulation of *phzS* or the protein it encodes.

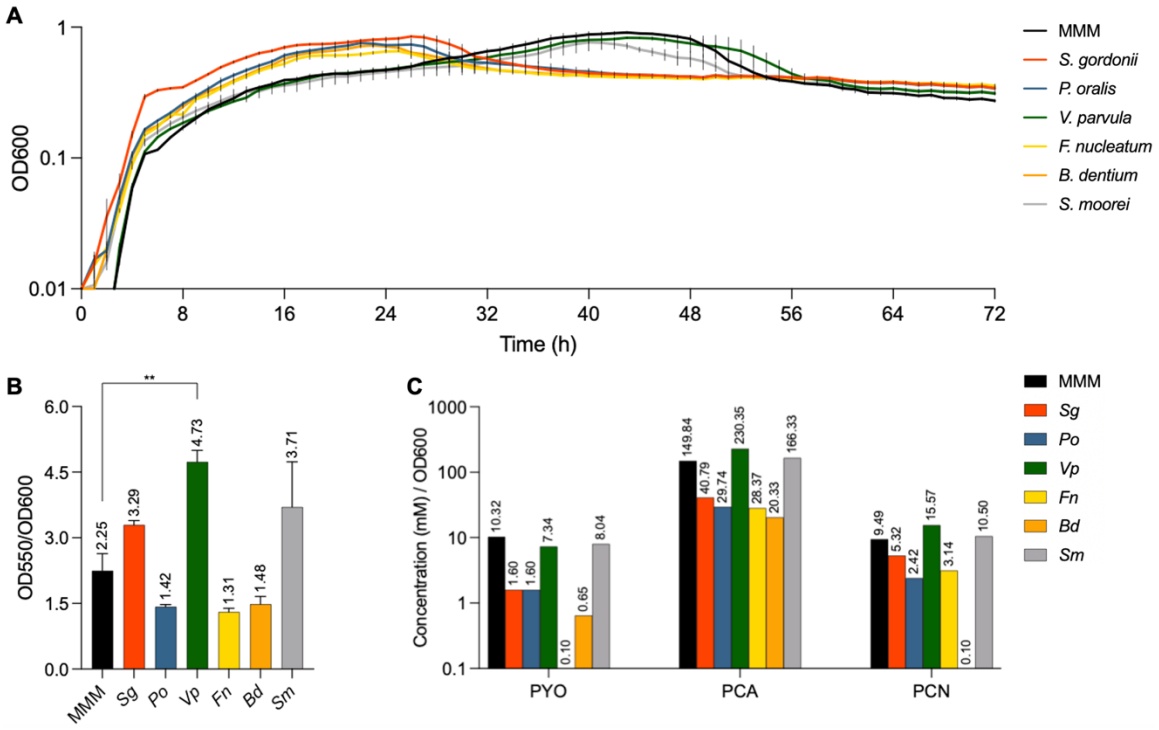

Figure 3.4 – Characterization of PA14 grown on anaerobe cell free supernatants. A) Growth curves of PA14 grown in anaerobe-derived cell free supernatants and a minimal mucin media (MMM) control. Endpoint OD600 readings: MMM (0.274); *S. gordonii* (0.343)*; P. oralis (*0.340)*; V. parvula* (0.313)*; F. nucleatum* (0.355)*; B. dentium* (0.353)*; S. morreii (*0.314). **B)** Biofilm production of the same PA14 cultures at 72 hours as measured by a crystal violet biofilm assay and normalized to average end point optical density values (OD600) (*n* = 3; Kruskal-Wallis with uncorrected Dunn's multiple comparisons; * = $P < 0.05$; ** = $P < 0.005$). **C)** Phenazine production of the same PA14 cultures as measured by HPLC.

Effects of Individual Organic Acids on P. aeruginosa Physiology:

To further investigate the role of microbially generated organic acids on PA14 physiology, follow up growth experiments including supplementation of MMM with pure stocks of organic acids were implemented. The addition of organic acids (6.25 mM – 50 mM) resulted in striking differences in visual culture profiles (**Figure 3.5**) – in part due to difference in pyocyanin concentrations. Other colored pigments, such as pyoverdine, may have also contributed to these visual differences.

Aerobic growth of PA14 at 37°C over 48 hours in MMM supplemented with 50mM of organic acids resulted in differential phenotypes (**Figure 3.6A**). All conditions with organic acid supplementation resulted in longer exponential growth phases and higher final OD600 readings compared to the non-supplemented control. This supports the claim that PA is able to catabolize microbially produced organic acids in our proposed cross-feeding model. Consistent with the literature, PA14 exhibited the most robust growth when cultured in MMM supplemented with 50 mM of its preferred carbon source – succinate (Yung et al., 2019). Interestingly, PA14 appeared to perform better in acetate supplemented MMM compared to MMM supplemented with lactate, at odds with the claim that PA preferentially uses lactate over acetate (McGill et al., 2021). Of the organic acids tested, supplementation with butyrate and propionate resulted in the least robust growth profiles, excluding that of growth in un-supplemented MMM. Again, this is consistent with literature as neither of these organic acids are nutritionally preferred by PA14 (McGill et al., 2021).

Evaluation of biofilm formation of the same PA14 cultures resulted in one statistically significant observation. As described in the previous section, butyrate has been found to inhibit biofilm formation in other bacterial species such as *Salmonella typhimurium* (Liu et al., 2022) and *Vibrio parahaemolyticus* (Zhu et al., 2022). The data suggest the same may be true for PA, as growth in MMM supplemented with 50 mM of butyrate resulted in a significant decrease in biofilm formation. This finding carries implications in the development of novel treatments targeting PA biofilm formation.

PA14 phenazine production in response to growth on organic acids was quantified via HPLC. Again, COVID-19 imposed supply chain shortages required the pooling of samples – preventing statistical analysis. However, supplementation with butyrate resulted in moderate PCA production but decreased PYO and PCN production. While not as drastic as the similar pattern observed in the individual anaerobic CFS and clinical enrichment CFS (Chapter 4), this observation still indicates the involvement of PhzS. Interestingly, growth on MMM supplemented with formate was the only condition that elicited a notably low level of PCA. While PYO and PCN levels are also lower, the lack of PCA suggests a causative mechanism other than *phzS* regulation. PCA is upstream in the biosynthetic pathway of PYO and PCN generation. Possible explanations for this observed phenomenon include direct degradation of PCA or regulation of the transcription, translation, or final products of genes upstream in its biosynthetic pathway –

phzA1-G1 and *phzA2-G2*. Further. Transcriptional analyses would help to elucidate the underlying mechanisms.

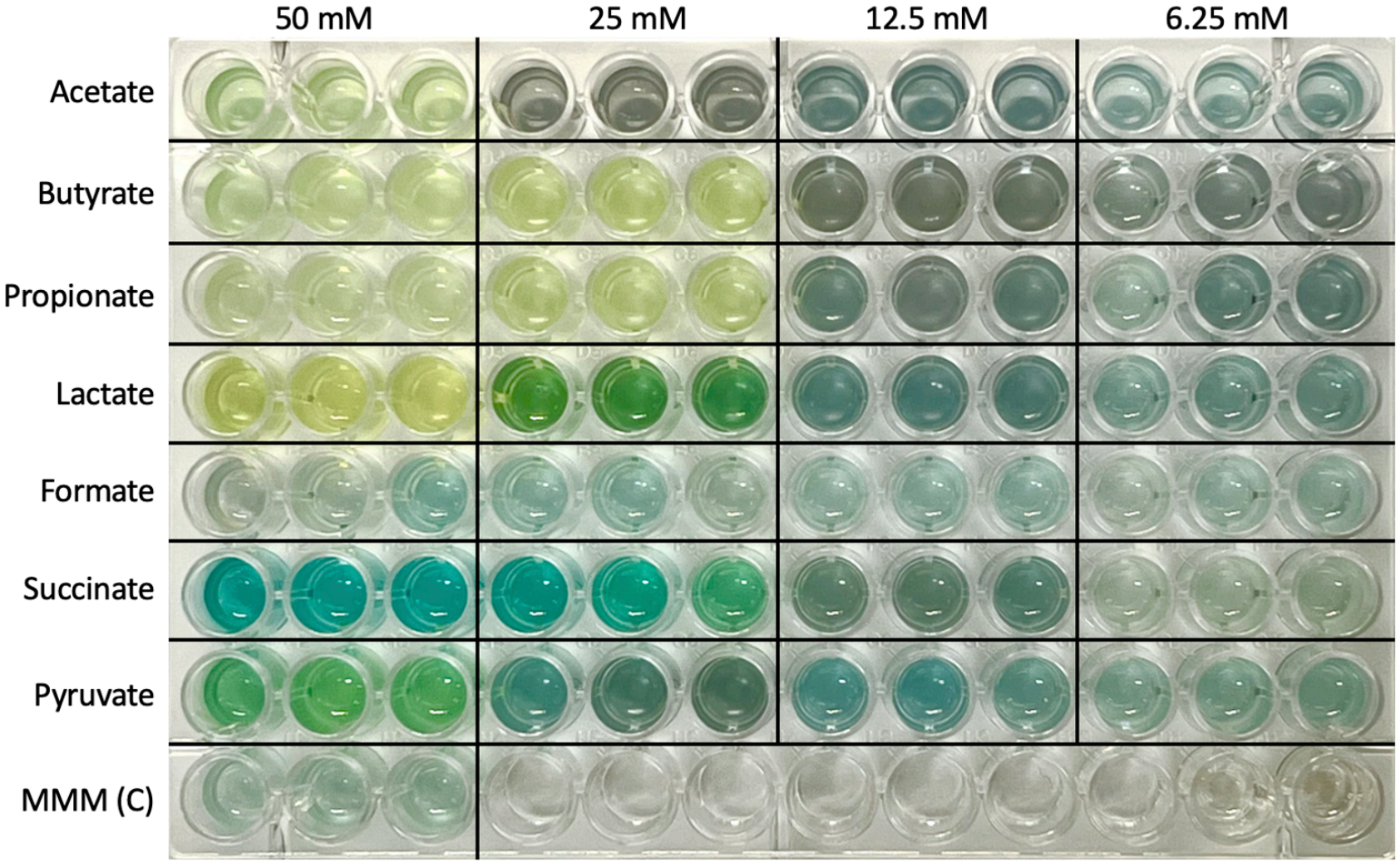

Figure 3.5 –PA14 grown in MMM supplemented with organic acids. PA14 grown in replicates (4) of MMM supplemented with various concentrations of organic acids.

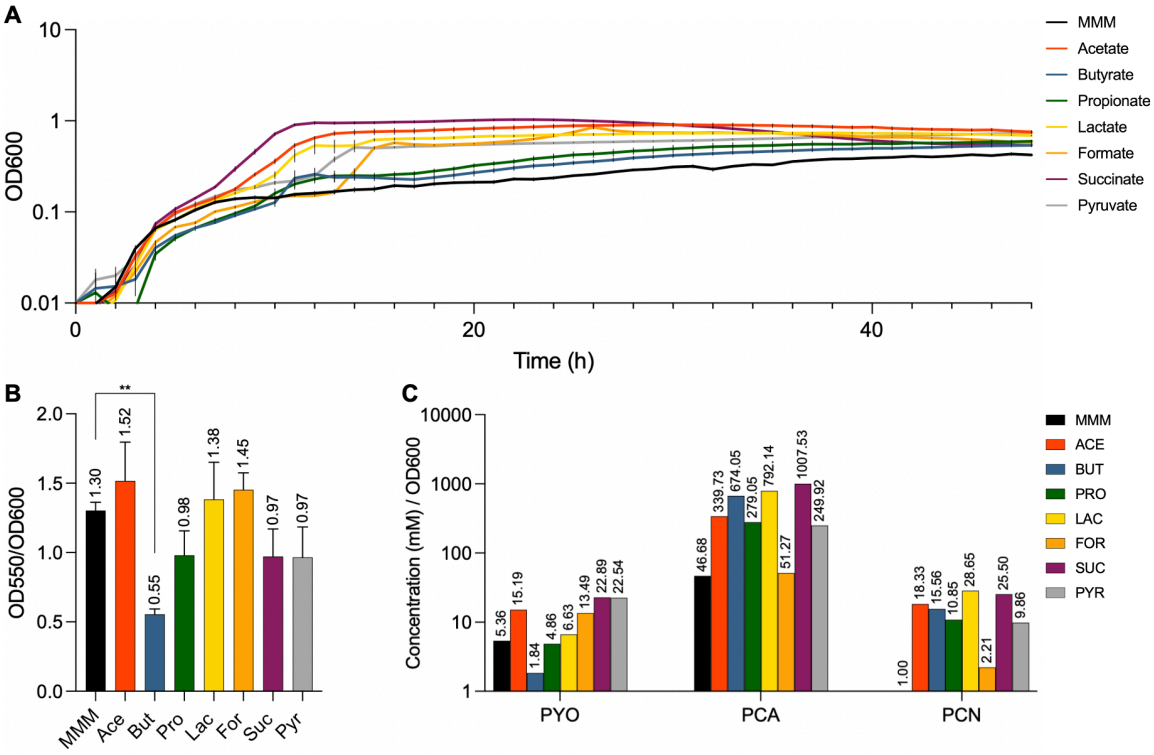

Figure 3.6 - Characterization of PA14 grown in MMM supplemented with organic acids. A) Growth curves of PA14 grown in MMM supplemented with 50 mM of various organic acids, as well as a MMM control condition. Endpoint OD600 readings: MMM (0.423); Acetate (0.757)*;* Butyrate *(*0.539)*;* Propionate (0.596)*;* Lactate (0.689)*;* Formate (0.569)*;* Succinate *(*0.556); Pyruvate (0.737). **B)** Biofilm production of the same PA14 cultures at 48 hours as measured by a crystal violet biofilm assay and normalized to average end point optical density values (OD600) (*n* = 4; Kruskal-Wallis with uncorrected Dunn's multiple comparisons; * = $P < 0.05$; ** = $P < 0.005$). **C)** Phenazine production of the same PA14 cultures post at the 48-hour time point as measured by HPLC.

Conclusion

In this chapter, I define the bacterial composition of a representative AOC mucin enrichment that was found to perform well when grown on MMM with mucin as a sole carbon source. Metagenomic sequencing reinforced the classification of several genera as core anaerobic mucin degrading community components. 16S rRNA gene sequencing of the same AOC supported this finding, but also highlighted instability in the relative abundances of taxa across samples, despite sharing the same culturing conditions. The wealth of sequencing data was used to inform selection of several representative strains for further *in vitro* characterization. Growth on mucin, mucin degradation abilities, and generation of organic acids were evaluated for each strain, as were the effects of each strain CFS on the physiology of PA14. To further minimize variables, pure stocks of organic acids identified in bacterial CFSs were used to supplement MMM prior to PA14 inoculation. Effects of each organic acid on PA14 growth, biofilm formation, and phenazine production were evaluated.

Both individual anaerobe CFS and organic acid supplementation resulted in the improved growth of PA14 compared to growth in MMM alone. *V. parvula* was found to significantly increase PA14 biofilm formation, while butyrate (50 mM) was found to significantly decrease it. The power of the phenazine findings was reduced due to a small *n* of 1 resulting from the required pooling of samples. However, a seemingly *phzS* dependent reduction of PYO was observed in PA14 grown on *B. dentium* CFS, similar to what was observed in PA14 growth on an enrichment CFS

in Chapter 4. Growth on formate (50 mM) was the only condition to result in a comparatively lower concentration of PCA. Additionally, data collected from these experiments have been used to generate detailed physiological profiles for key species grown on mucin glycoproteins as a sole carbon source. This provides researchers across several fields a valuable, and in many cases novel, resource to reference when considering the interactions between mucin and their organism of interest.

Individually, these data offer several novel avenues of research to further investigate the regulation of PA physiology. Together, they strongly support the overarching hypothesis of this dissertation – co-colonizing microbiota of the CF airways impact the growth and virulence of PA via cross-feeding *in vivo*. Further characterization of the proposed cross-feeding model promises future identification of clinically relevant bacterial interactions and metabolic byproducts. This could be an important step towards the development of novel CF PEx treatment strategies that achieve symptom resolution indirectly by target co-colonizing microbiota rather than PA directly – an apparent need in the field as clinical PA strains rapidly develop multidrug resistance.

Supplemental

In vitro Characterization of Anaerobic Bacterial Mucin Degradation its Impact on *Pseudomonas aeruginosa.*

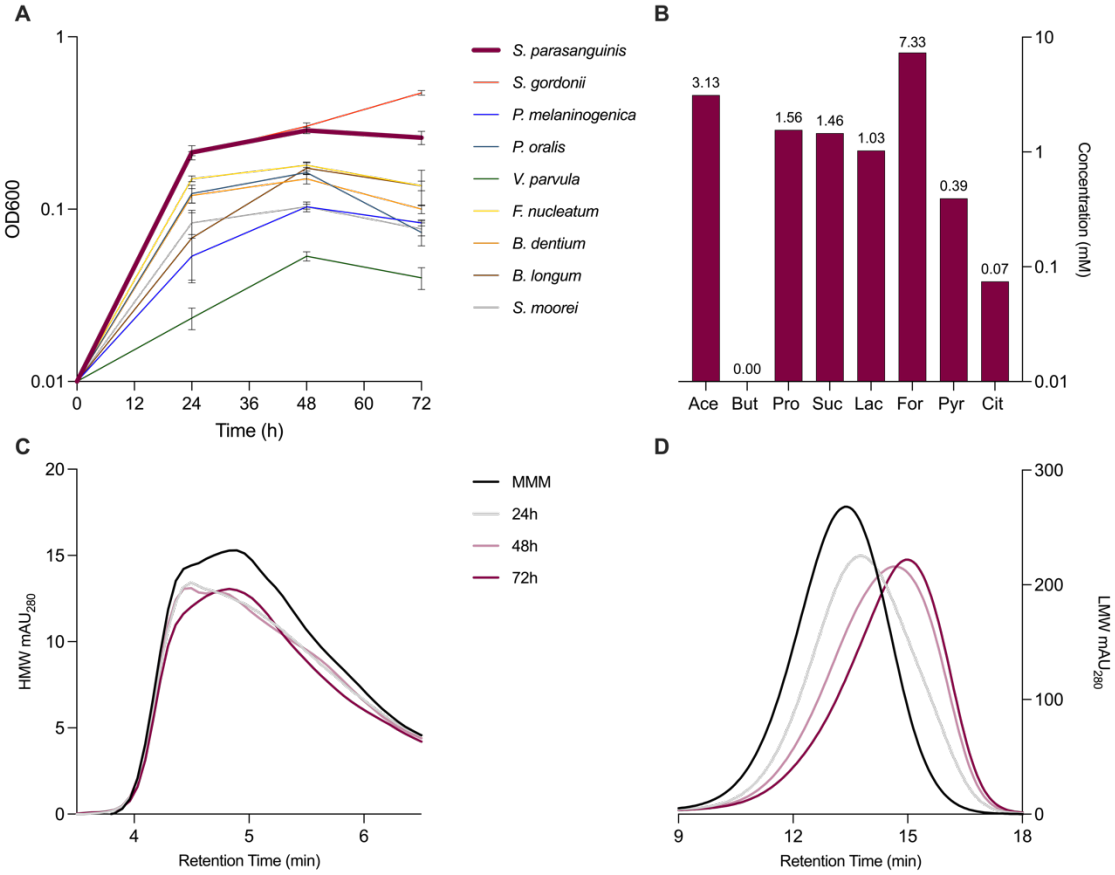

Figure 3.S1 – Characterization of *S. parasanguinis* grown on MMM. A) 72-hour growth curves of *S. parasanguinis* compared to representative strains. All were grown anaerobically at 37°C in MMM. **B)** HPLC generated organic acid profile of 72-hour *S. parasanguinis* culture. **C)** FPLC chromatogram displaying the relative degradation of high molecular weight mucins in MMM by *S. parasanguinis* over time. **D)** FPLC chromatogram displaying the relative degradation of low molecular weight mucins in MMM by *S. parasanguinis* over time.

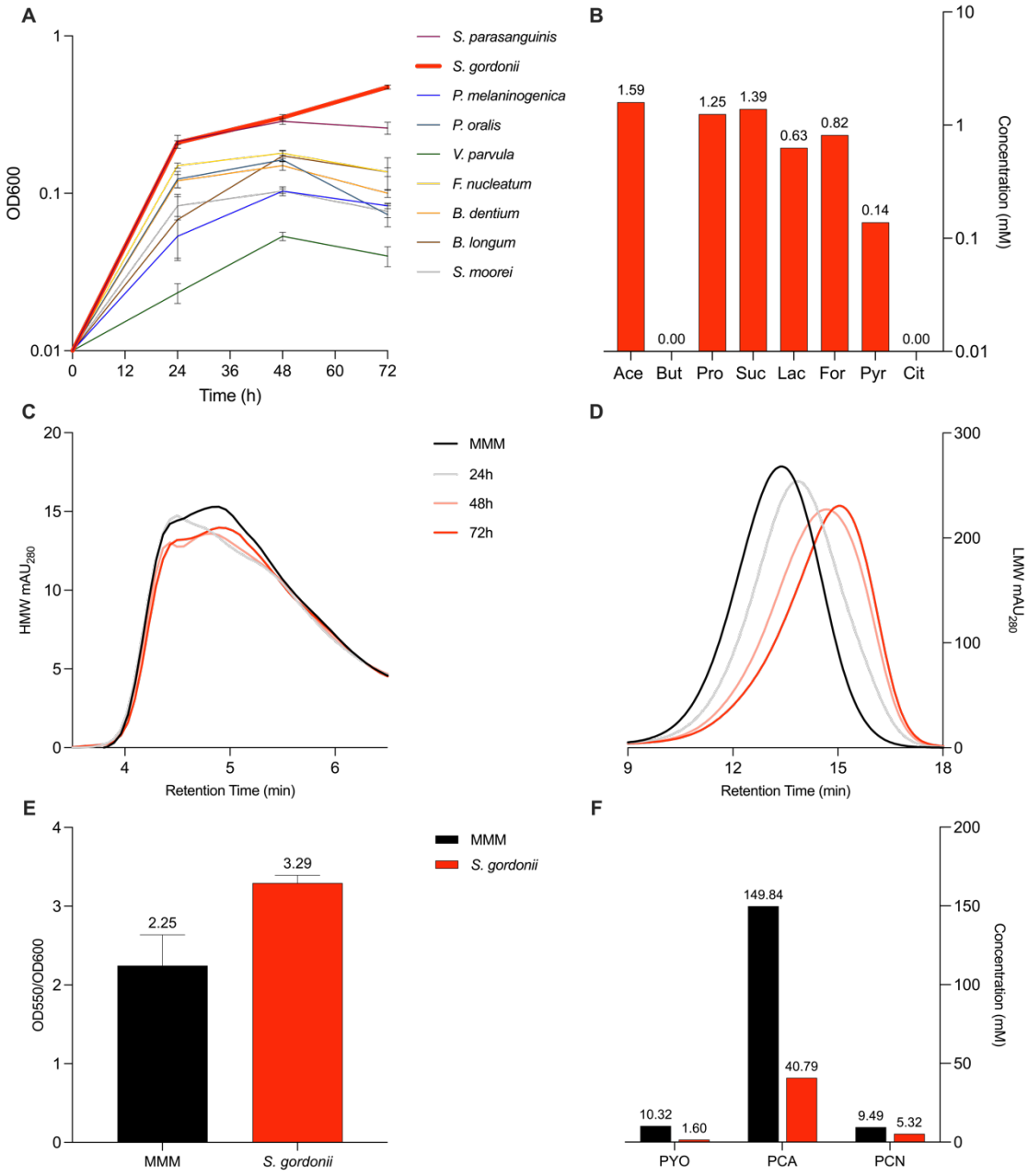

Figure 3.S2 – Characterization of *S. gordonii* grown on MMM. A) 72-hour growth curves of *S. gordonii* compared to representative strains. All were grown anaerobically at 37°C in MMM. **B)** HPLC generated organic acid profile of 72-hour *S. gordonii* culture. **C)** FPLC chromatogram displaying the relative degradation of high molecular weight mucins in MMM by *S. gordonii* over time. **D)** FPLC chromatogram displaying the relative degradation of low molecular weight mucins in MMM by *S. gordonii* over time. **E)** Biofilm formation of PA14 grown on *S. gordonii* CFS for 72 hours. **F)** Phenazine production of the same PA14 cultures as measured by HPLC.

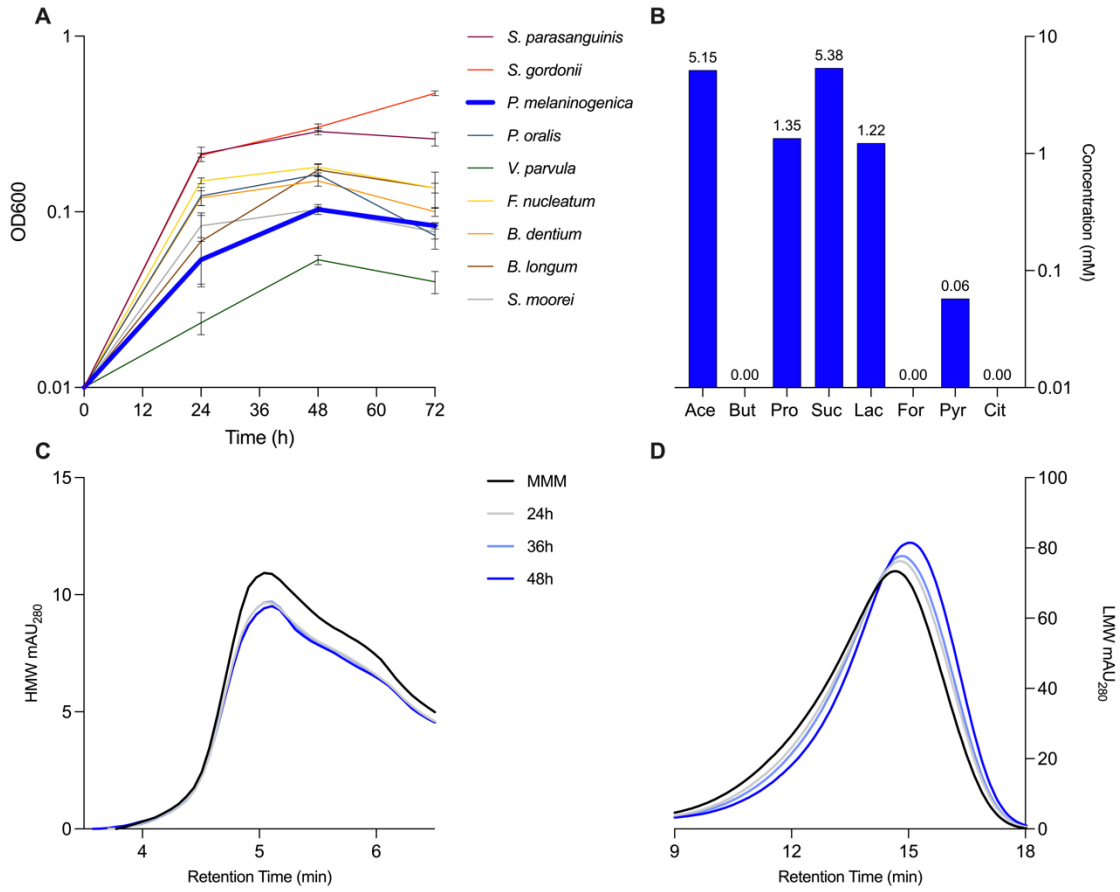

Figure 3.S3 – Characterization of *P. melaninogenica* grown on MMM. A) 72-hour growth curves of *P. melaninogenica* compared to representative strains. All were grown anaerobically at 37°C in MMM. **B)** HPLC generated organic acid profile of 72-hour *P. melaninogenica* culture. **C)** FPLC chromatogram displaying the relative degradation of high molecular weight mucins in MMM by *P. melaninogenica* over time. **D)** FPLC chromatogram displaying the relative degradation of low molecular weight mucins in MMM by *P. melaninogenica* over time.

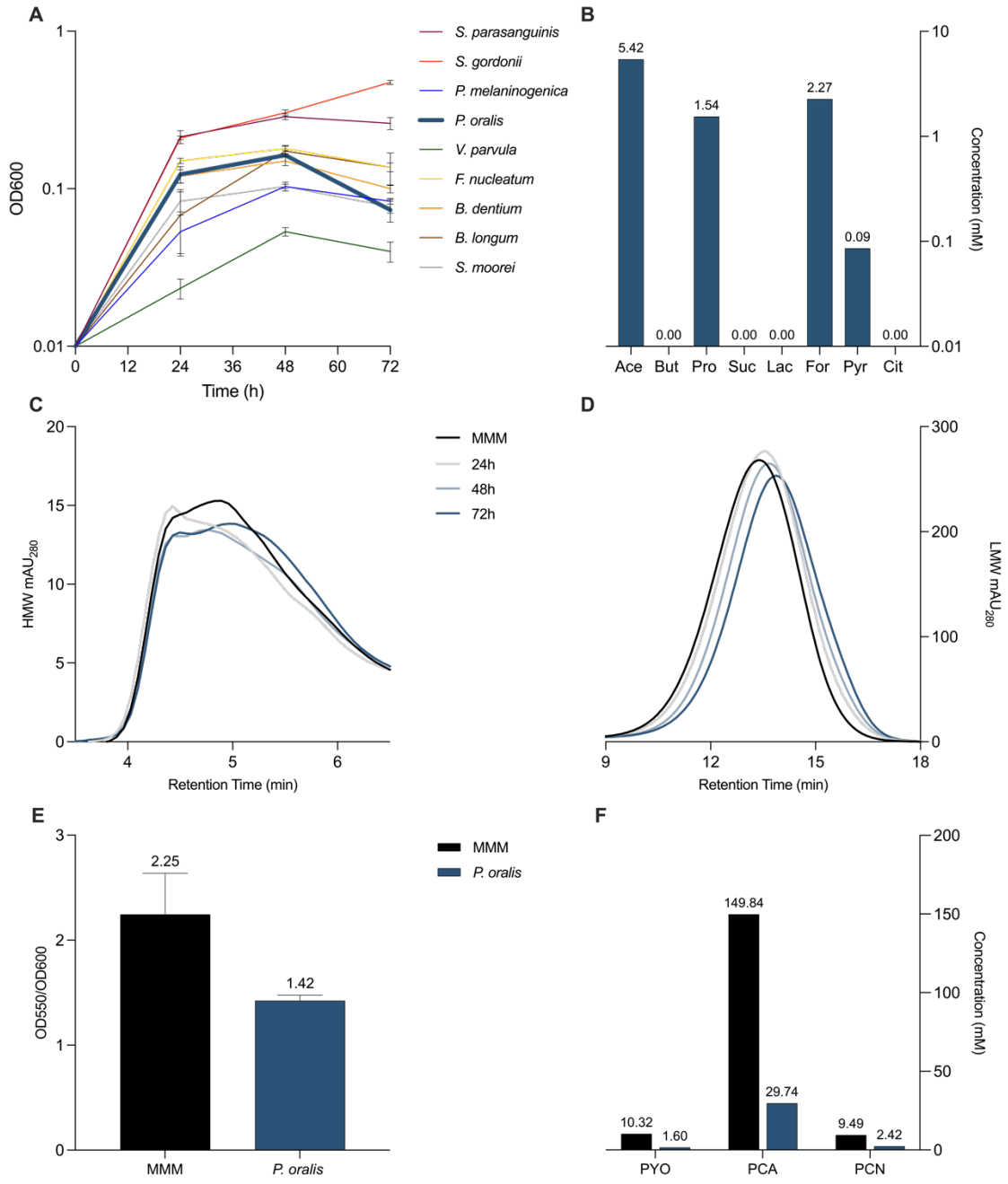

Figure 3.S4 – Characterization of *P. oralis* grown on MMM. A) 72-hour growth curves of *P. oralis* compared to representative strains. All were grown anaerobically at 37°C in MMM. **B)** HPLC generated organic acid profile of 72-hour *P. oralis* culture. **C)** FPLC chromatogram displaying the relative degradation of high molecular weight mucins in MMM by *P. oralis* over time. **D)** FPLC chromatogram displaying the relative degradation of low molecular weight mucins in MMM by *P. oralis* over time. **E)** Biofilm formation of PA14 grown on *P. oralis* CFS for 72 hours. **F)** Phenazine production of the same PA14 cultures as measured by HPLC.

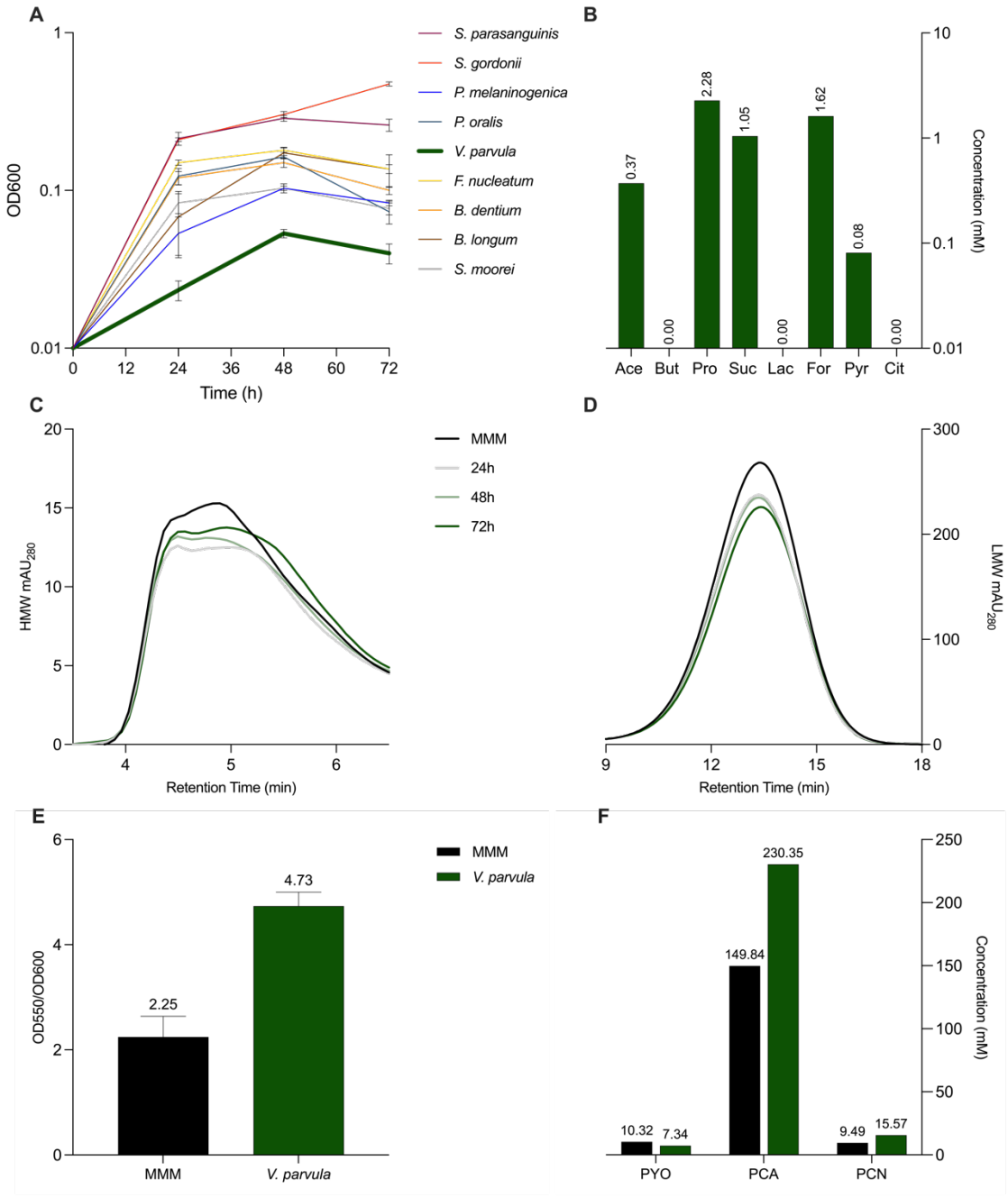

Figure 3.S5 – Characterization of *V. parvula* grown on MMM. A) 72-hour growth curves of *V. parvula* compared to representative strains. All were grown anaerobically at 37°C in MMM. **B)** HPLC generated organic acid profile of 72-hour *V. parvula* culture. **C)** FPLC chromatogram displaying the relative degradation of high molecular weight mucins in MMM by *V. parvula* over time. **D)** FPLC chromatogram displaying the relative degradation of low molecular weight mucins in MMM by *V. parvula* over time. **E)** Biofilm formation of PA14 grown on *V. parvula* CFS for 72 hours. **F)** Phenazine production of the same PA14 cultures as measured by HPLC.

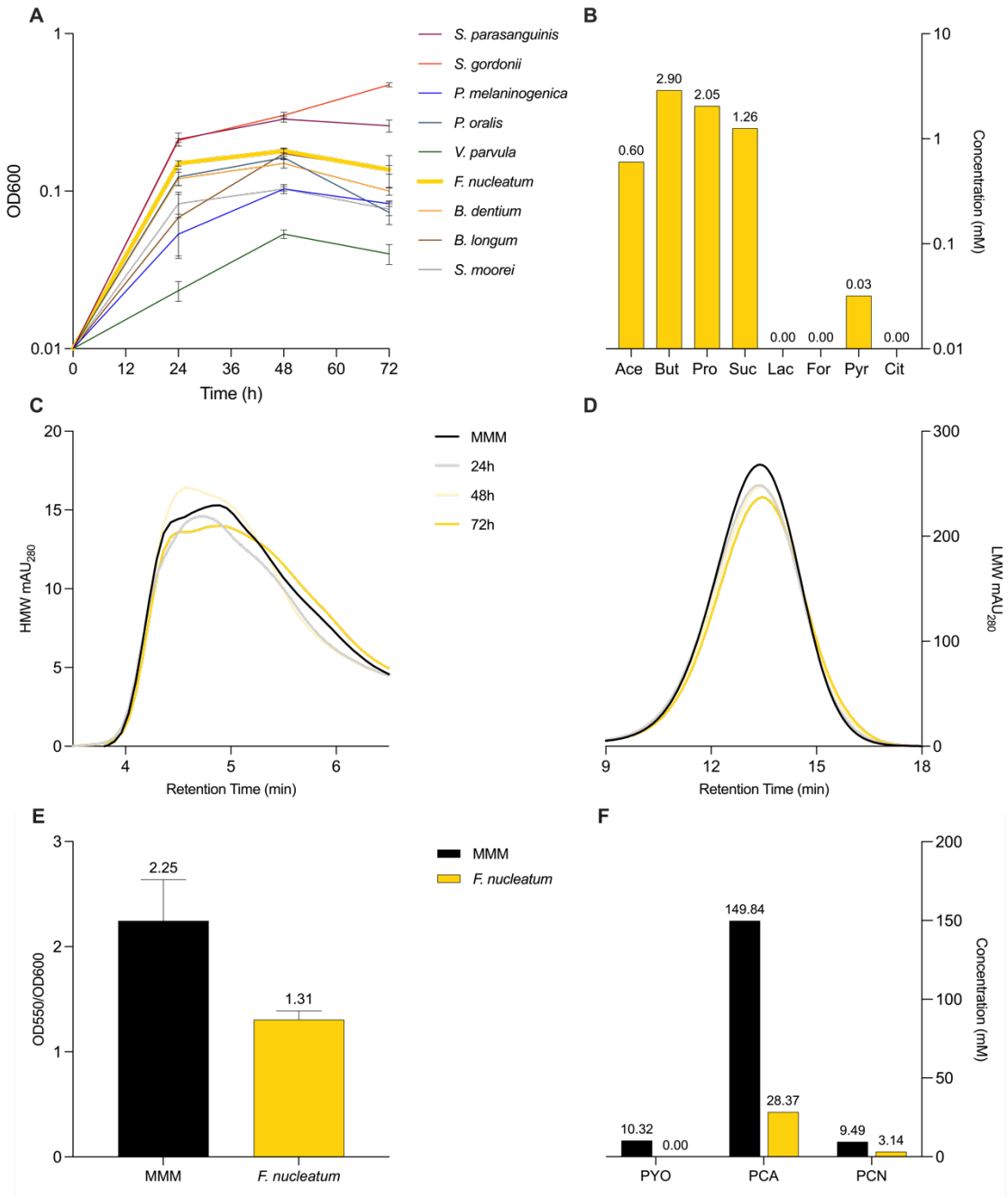

Figure 3.S6 – Characterization of *F. nucleatum* grown on MMM. A) 72-hour growth curves of *F. nucleatum* compared to representative strains. All were grown anaerobically at 37°C in MMM. **B)** HPLC generated organic acid profile of 72-hour *F. nucleatum* culture. **C)** FPLC chromatogram displaying the relative degradation of high molecular weight mucins in MMM by *F. nucleatum* over time. **D)** FPLC chromatogram displaying the relative degradation of low molecular weight mucins in MMM by *F. nucleatum* over time. **E)** Biofilm formation of PA14 grown on *F. nucleatum* CFS for 72 hours. **F)** Phenazine production of the same PA14 cultures as measured by HPLC.

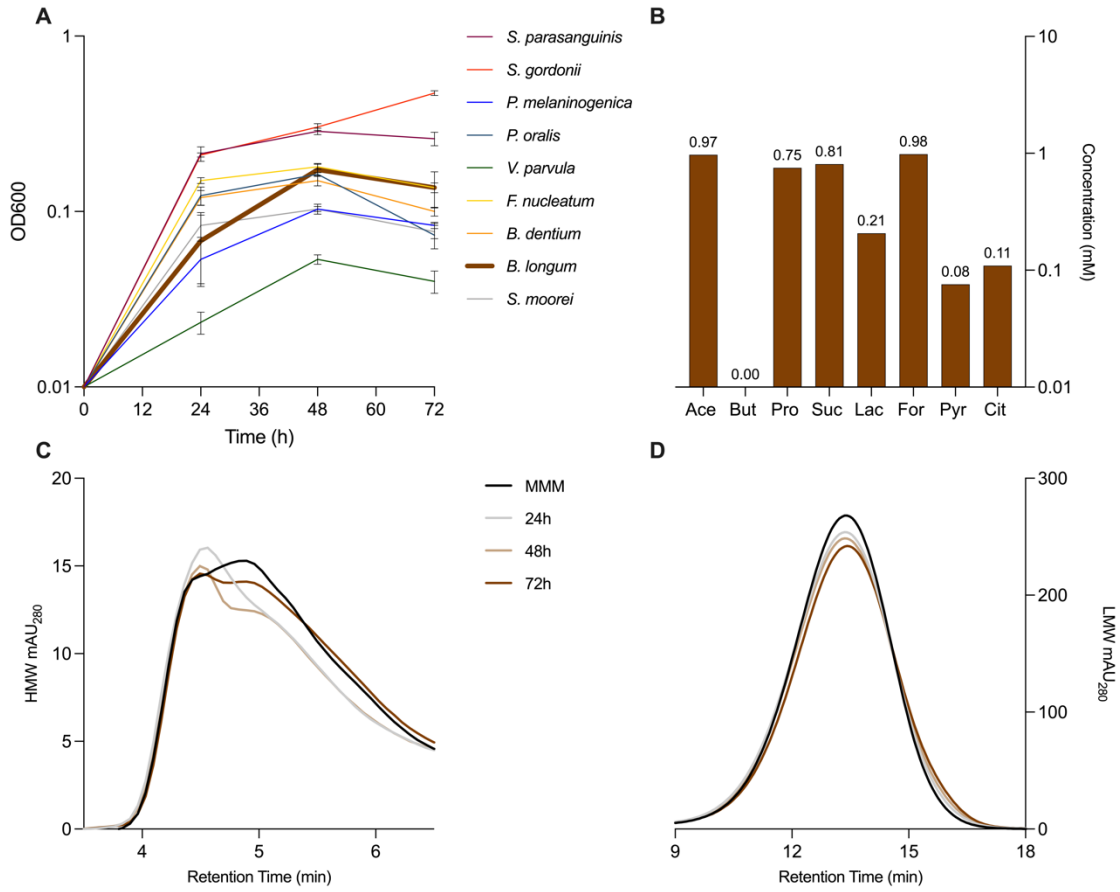

Figure 3.S7 – Characterization of *B. longum* grown on MMM. A) 72-hour growth curves of *B. longum* compared to representative strains. All were grown anaerobically at 37°C in MMM. **B)** HPLC generated organic acid profile of 72-hour *B. longum* culture. **C)** FPLC chromatogram displaying the relative degradation of high molecular weight mucins in MMM by *B. longum* over time. **D)** FPLC chromatogram displaying the relative degradation of low molecular weight mucins in MMM by *B. longum* over time.

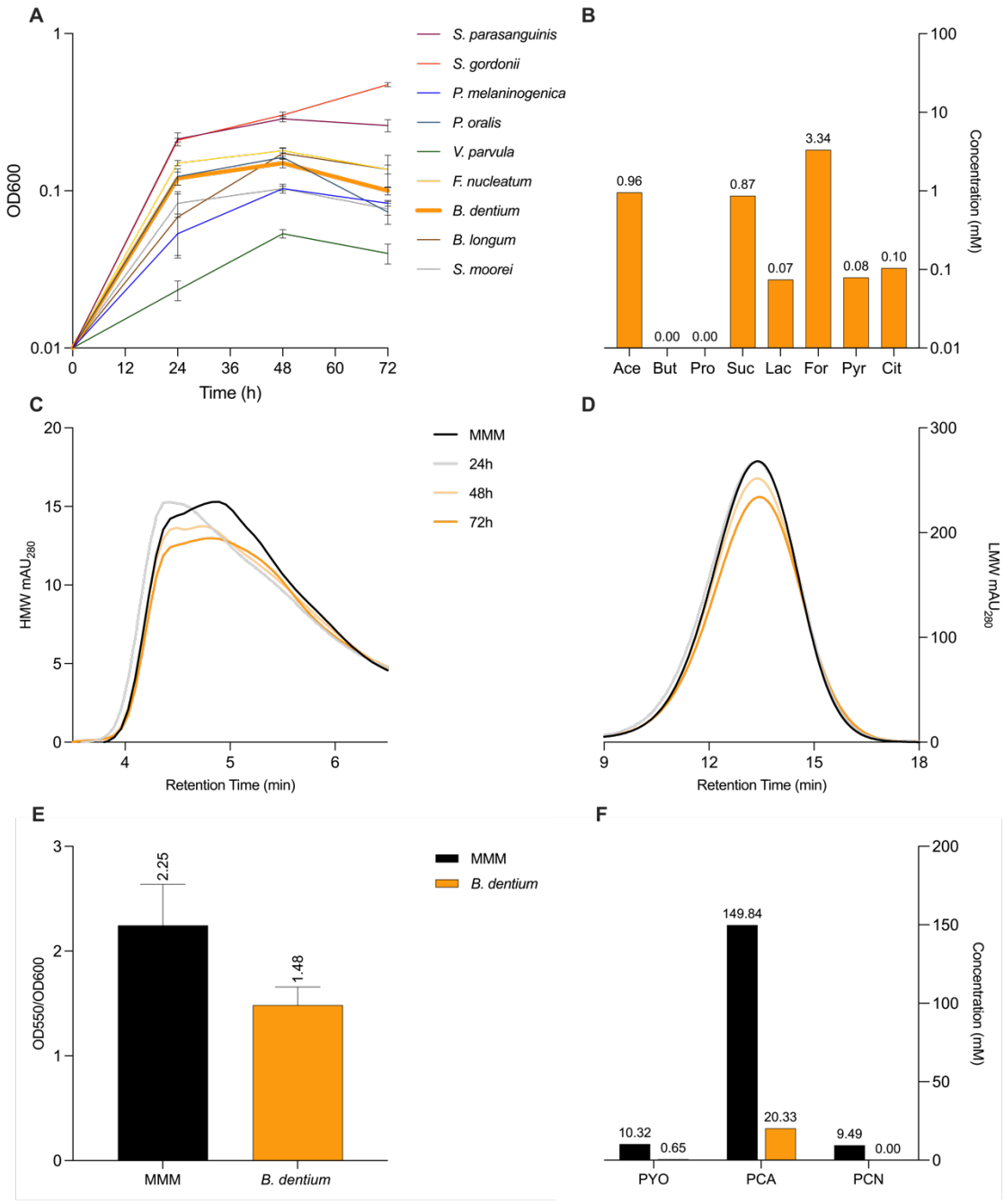

Figure 3.S8 – Characterization of *B. dentium* grown on MMM. A) 72-hour growth curves of *B. dentium* compared to representative strains. All were grown anaerobically at 37°C in MMM. **B)** HPLC generated organic acid profile of 72-hour *B. dentium* culture. **C)** FPLC chromatogram displaying the relative degradation of high molecular weight mucins in MMM by *B. dentium* over time. **D)** FPLC chromatogram displaying the relative degradation of low molecular weight mucins in MMM by *B. dentium* over time. **E)** Biofilm formation of PA14 grown on *B. dentium* CFS for 72 hours. **F)** Phenazine production of the same PA14 cultures as measured by HPLC.

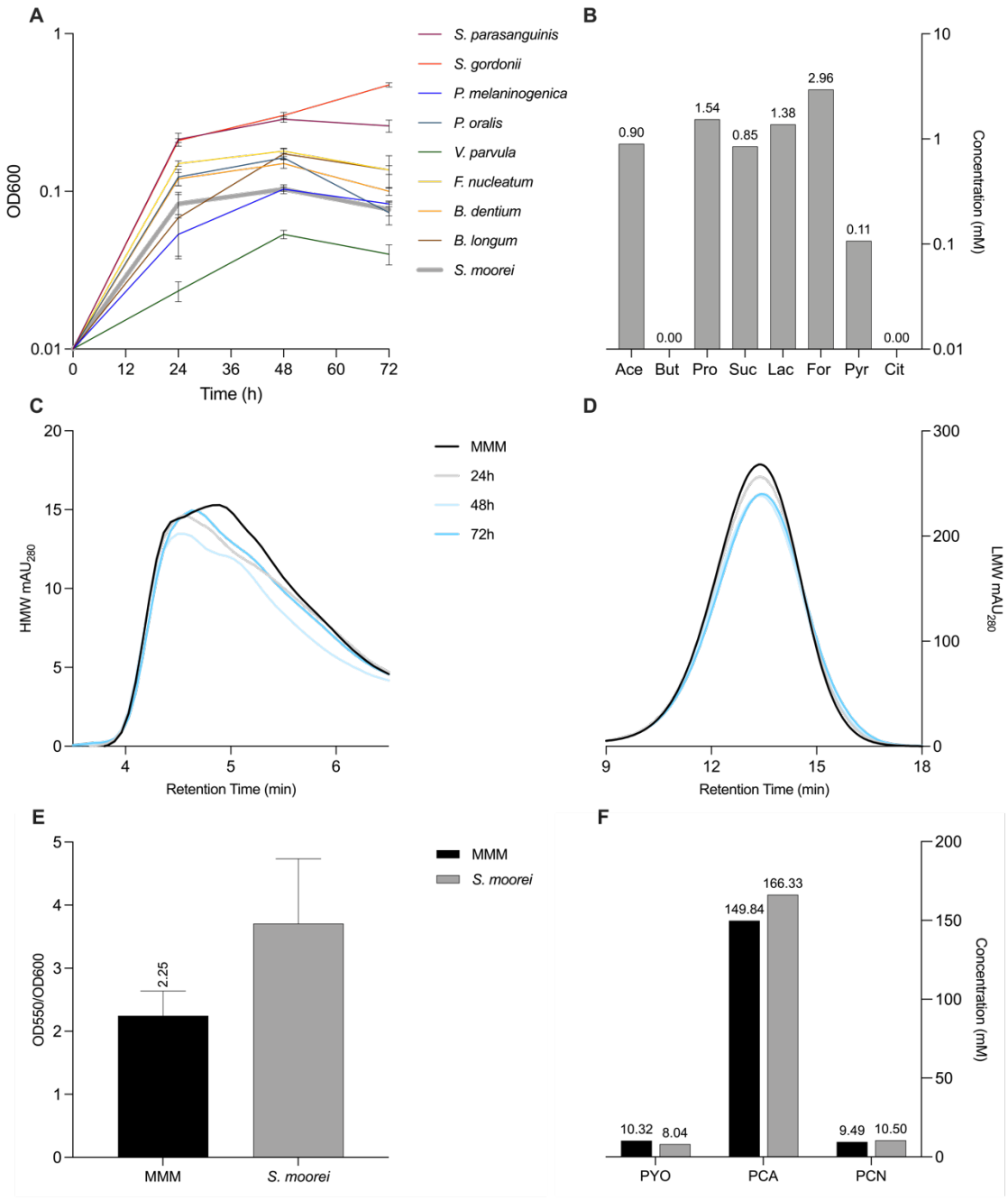

Figure 3.S9 – Characterization of *S. moorei* grown on MMM. A) 72-hour growth curves of *S. moorei* compared to representative strains. All were grown anaerobically at 37°C in MMM. **B)** HPLC generated organic acid profile of 72-hour *S. moorei* culture. **C)** FPLC chromatogram displaying the relative degradation of high molecular weight mucins in MMM by *S. moorei* over time. **D)** FPLC chromatogram displaying the relative degradation of low molecular weight mucins in MMM by *S. moorei* over time. **E)** Biofilm formation of PA14 grown on *S. moorei* CFS for 72 hours. **F)** Phenazine production of the same PA14 cultures as measured by HPLC.

CHAPTER 4: The Impact of Clinical Bacterial Community Composition on *Pseudomonas aeruginosa* physiology

Summary

In Chapter 3, I took a reductionist approach to investigate the roles of individual bacterial species and a more complex anaerobic oral community in the degradation of mucin. Some species were found to potentially effectuate the virulence of *P. aeruginosa* in a growth-independent manner, and follow-up experiments suggested that organic acids may play a role. While insightful, these data are limited in their value to elucidate the broader cross-feeding interactions at play within the complex bacterial airway communities of the CF airways. In this chapter, I address this limitation this by collecting clinical CF sputum samples, characterizing their bacterial compositions, and enriching for the fractions of those compositions capable of growth on mucin as a sole nutrient source. Utilizing many of the previously described methods, I characterize these enrichments and their effects on the physiology of *P. aeruginosa.*

Mucin-Degrading Microbiota Present in the Cystic Fibrosis Airways Alter *Pseudomonas aeruginosa* Growth and Virulence.

Alex R. Villarreal[1], Sabrina Arif[1], Kayla Hoffman[1], Talia Wiggen[1], Ryan C. Hunter[1*]

[1] Department of Microbiology & Immunology, University of Minnesota, 689 23rd Avenue SE, Minneapolis, MN 55455

† Reprinted from manuscript in preparation. Alex R. Villarreal, Sabrina Arif, Kayla Hoffman, Talia Wiggen, and Ryan C. Hunter. "Mucin-Degrading Microbiota Present in the Cystic Fibrosis Airways Alter *Pseudomonas Aeruginosa* Growth and Virulence." *In prep.*

Abstract

Cystic Fibrosis (CF) is a condition hallmarked by the accumulation of mucin glycoproteins in the airways, supporting the establishment of stable complex microbial communities, and resulting in chronic infections by *Pseudomonas aeruginosa* (PA). Despite its high rate of colonization and dense bacterial load *in vivo*, PA is unable to efficiently utilize mucin, a primary biomolecule of the CF airways, as a sole nutrient source. Rather, PA requires the presence of mucin-degrading bacteria, also common in airways, to process mucins into more bioavailable metabolites (i.e., organic acids). This cross-feeding relationship may also impact the expression of PA virulence factors (i.e., phenazines and biofilm formation), though which of these bacterial community constituents and respective mucin degradation products impact PA growth and virulence remains unclear.

To investigate this, 16S rRNA gene sequencing was used to identify bacterial communities of clinical CF sputum samples and their resident microbiota isolated through mucin enrichments. An experimental pipeline comprised of growth assays and liquid chromatography analyses was then employed to further characterize these enrichments and their effects on PA physiology. Growth, biofilm production, and phenazine expression of PA in response to these supernatants differed significantly between patient samples, suggesting that airway community composition may influence PA virulence *in vivo* – specifically through post-transcriptional regulation of *phz*S. These data may offer potential alternative targets for treatment of chronic CF lung infections.

Introduction

CF is a genetic disease affecting approximately 100,000 people worldwide, with more than 1,000 new cases being diagnosed annually (Shteinberg et al., 2021). It is characterized by the loss of function of CF transmembrane conductance regulator (CFTR) proteins responsible for transporting chloride ions across the membranes of the airway epithelium and maintaining homeostasis (D'Amore et al., 2022). Loss of chloride ion transport leads to the accretion of a viscous dehydrated mucus layer, impairing mucocilliary clearance and ultimately leading to chronic inflammation and bacterial infections (Robinson et al., 2002). These chronic bacterial infections punctuate repeated periods of decreased patient lung function known as pulmonary exacerbations (PEx), resulting in the deterioration of lung function over a patient's lifetime and decreased life expectancy (Carmody et al., 2015).

Culture-dependent techniques often identify *Staphylococcus aureus* and PA as pathogens associated with chronic PEx – with *S.* aureus being more prevalent in younger patients and PA becoming dominant in the late twenties of CF patients (Hahn et al., 2021). Colonization by PA post-adolescence is associated with an increase in the frequency and severity of PExs, making it the canonical CF pathogen responsible for a majority of CF patient morbidity and mortality (Crull et al., 2018). Notwithstanding, the nutrients that support the colonization and persistence of PA remain poorly understood. Despite reaching densities of 10^9 cells per gram of mucus (Palmer et al., 2005), PA is unable to efficiently utilize

mucins, the primary biomolecule of the CF airways, as a sole nutrient source. Rather, PA growth is supported via a cross-feeding relationship with anaerobic mucin-degrading bacteria generally considered commensal microbiota of the oral cavity (Flynn et al., 2016). *In vitro*, PA exhibits significantly increased growth on cell free supernatants (CFS) of mucin-degrading bacterial communities compared to on mucin alone, suggesting that liberation of mucin glycans and/or peptides, or the production of secondary metabolites by mucin-degraders support the growth of PA (Flynn et al., 2016). Organic acids (e.g., acetate, butyrate, propionate, and lactate) are produced by anaerobic mucin-degrading bacteria via mixed-acid fermentation and are thought to contribute to this cross-feeding relationship as they are detected in both clinical sputum samples and the *in vitro* cultures of their constituent microbiota (Flynn et al., 2016).

Phenazine-1-carboxylic acid (PCA), phenazine-1-carboxamide (PCN), and pyocyanin (PYO) are the three primary phenazines produced by PA and are responsible for a host of functions such as metal solubilization (Briard et al., 2015), biofilm stimulation (Wang et al., 2011), and host-cell cytotoxicity (McGuigan et al., 2014). They are expressed via two redundant quorum sensing regulated operons – *phzA1-G1* and *phzA2-G2* (Cui et al., 2016). Interestingly, phenazine production by PA may impacted in a growth-independent manner by their co-colonizers, as strain PA14 produces variable levels of PYO when grown on different CF sputum sample mucin enrichment CFS. This suggests that in addition to supporting the growth of PA, mucin byproducts derived from co-colonizing microbiota may play a

key role in the virulence of PA *in vivo*. The mechanisms underlying this regulation remain unknown.

In this chapter, I further characterize mucin-based cross-feeding and identify potential mechanisms behind growth and virulence regulation of PA by co-colonizing microbiota. To do so, I first evaluated clinical sputum samples by mucin enrichment and 16S rRNA gene sequencing to isolate and define the bacterial community members capable of growth on mucin as a sole nutrient source. Growth assays and liquid chromatography were then used to evaluate the ability of each community to metabolize mucins and the metabolites they produce. CFS generated by these enrichment communities were used as growth media for *P. aeruginosa* strain PA14 so that effects on growth, organic acid utilization, phenazine expression, and biofilm formation could be determined. Finally, the expression of key PA virulence genes was quantified by qRT-PCR the evaluate the transcriptional response of PA to co-colonizing bacterial communities. The resulting insights offer putative identification of novel regulation pathways of PA and lay the groundwork for a better understanding of how PA behavior is shaped by its growth environment *in vivo.*

Materials and Methods

Bacterial Strains & Growth Conditions:

Strain PA14 of *Pseudomonas aeruginosa* (Obtained from Marvin Whiteley, Georgia Tech) was used throughout the described experimental pipeline. Prior to

use, a glycerol stock of PA14 stored at -80°C was streaked on Luria-Bertani (LB) (IBI Scientific, IA, USA) agar plates and incubated aerobically at 37°C for 24 hours. Colonies from this plate were used for up to 2 weeks to inoculate overnight LB liquid cultures for use in experiments. All PA14 growth experiments were completed aerobically, shaking at 240 rpm at 37°C unless otherwise stated.

Media Preparation:

MMM was prepared with reagents as described in **Tables 2.4 - 2.8**. Similarly, steps for preparation of the media follow the optimized method described on page 60. Brain heart infusion (BHI) liquid media (Becton, Dickinson, and Company (BD), NJ, USA), was used for anaerobic starter cultures.

Clinical Sample Collection & Processing:

Expectorated sputum was collected from adult subjects with cystic fibrosis at the University of Minnesota Adult CF Center as previously described (Flynn et al., 2016). Upon acquisition, clinical CF sputum samples were labeled, weighed, diluted with 1.5 mLs of sterile phosphate buffered saline, and mechanically homogenized using a 10-gauge syringe and repeated vortexing. A 1,000 μL aliquot was collected for downstream 16S rRNA gene sequencing, a 300 μL aliquot was collected for organic acid profiling, and a 200 μL aliquot was collected for mucin enrichment. Remaining sample volumes were stored at -80°C. These studies were approved by the Institutional Review Board at UMN (IRB 1401M47262). All subjects provided informed consent prior to sample collection.

Mucin-Degrading Community Enrichment Generation:

Directly following acquisition and processing of a CF sputum sample, 200uL of the homogenized sample was rapidly moved into an anerobic chamber (Coy Laboratory Products, Michigan, USA) containing a gas mixture of 90% N_2, 5% H_2, and 5% CO_2. The aliquot was used to inoculate 3 mL of 1:1 BHI:MMM culture that was degassed and equilibrated in the chamber for ~12 hours prior to inoculation. Following a 48-hour incubation at 37°C, the culture was passaged into 3 mL of MMM and incubated at 37°C for another 48 hours. This process was repeated for a total of four passages before inoculating a 15 mL MMM culture that was incubated at 37°C for 72 hours. A 1 mL aliquot of this culture was collected for downstream 16S rRNA gene sequencing, a 500 μL aliquot was used to generate a 25% glycerol stock, a 300 μL aliquot was collected for organic acid profiling, and the remainder was subjected to cell pelleting and filtration through a 0.22 μm PES filter to generate a cell-free supernatant (CFS) for downstream experiments. CFS were stored at -80°C until use.

16S rRNA Gene Sequencing & Analysis:

Genomic DNA was extracted from 800 μL sputum aliquots and their respective mucin-degrading community enrichments using a DNeasy Powersoil kit (Qiagen, Carlsbad, CA). Genomic DNA was submitted to the University of Minnesota Genomics Center (UMGC) for 16S rRNA gene library preparation and subsequent sequencing of the V4 region using Illumina MiSeq TruSeq 2x300 paired-end sequencing. Sterile MMM was also included as a control.

Sequence analysis was conducted on 8 CF sputum samples, their subsequent mucin enrichments, and an uninoculated MMM control. Sequence analyses, statistical analysis, and data visualizations were performed in R Studio. Cutadapt/4.2 (Martin, 2011) was used to remove primer sequences, with size filtering set to 215 bp at minimum and 285 bp at maximum. DADA2/1.26 (Callahan, 2016) was used to trim sequences and filter for quality. DADA2 inferred a parametric error model used to identify and correct sequencing errors. Reads were dereplicated, paired ends merged, and chimeric reads removed using default options. Genus-level taxonomy was assigned using the RDP Bayesian classifier (Wang, 2007) and SILVA-132 taxonomy training set (Quast, 2012). Species-level taxonomy was assigned only if an ASV unambiguously matched a sequence from at least two of the following four databases: SILVA-132, *e*HOMD (Escapa, 2018), RefSeq+RDP, and GTDB (Alishum, 2022). Species were manually assigned if two or more databases assigned the same species. If there was an even split, where different databases assign different species, "not applicable" was manually placed. If there was an uneven split, the majority species assigned by the databases was manually assigned. A phylogenetic tree was approximated by first performing a multiple alignment using DECIPHER/2.26.0 (Wright, 2012). Phangorn/2.11.1 (Schliep, 2011) was used to construct a phylogenetic tree. Sequences without classification at the phylum level, phyla with a total feature prevalence of less than 10, or a mean feature prevalence of 1 were removed; as were ASVs with a mean relative abundance below 1×10^{-4}, or at or below a prevalence threshold set to 1. As a result of filtering, three samples and their corresponding enrichments were

removed prior to data visualization. Of the final processed samples there were 70 ASVs of which 19 were assigned to the species level.

Fast Protein Liquid Chromatography:

FPLC analysis of mucin degradations accomplished using the reagents in **Table 2.3** and the methodology previously described on pages 46 - 48.

High Performance Liquid Chromatography:

HPLC quantification of 8 organic acids (**Table 2.11**) was accomplished using the methodology previously described on page 101. HPLC analysis of three phenazines (**Table 2.9**) in PA14 cultures was accomplished using the methodology previously described on page 81.

Quantitative Reverse Transcriptase Polymerase Chain Reaction:

Triplicate 0.5 mL aliquots of mucin enrichment CFS were loaded into a non-coated 48-well plate (Corning, New York, USA) and inoculated with PA14 to a starting OD600 of 0.01. The plate was covered with a gas permeable seal (Bio-Rad, California, USA) and incubated in a BioTek Synergy H1 plate reader for approximately 18 hours at 37°C with orbital shaking at 240rpm. A final time point optical density reading (OD600) was taken for each well at 18 hours. Cultures were pipetted from each well into separate 1 mL microfuge tubes and centrifuged at 10,000 x g for one minute. Supernatants were collected for downstream organic acid and phenazine HPLC analysis.

Cell pellets were washed twice with PBS before RNA was extracted via phenol-chloroform liquid-liquid extraction, as previously described (Fletcher et al., 2022). Extracted RNA was purified and concentrated using a Clean and Concentrator - 5' Kit (Zymo Research, California, USA) following manufacturer guidelines. Final RNA samples were used as templates to generate cDNA via reverse transcription using a NEB M0253S Murine Moloney Leukemia Virus Reverse Transcriptase (New England Biolabs, Massachusetts, USA). cDNA was quantified using a Nanodrop 3000 (Thermo Fischer Scientific, Massachusetts, USA) and stored at -80°C until use.

cDNA was diluted 1:15 with molecular grade PCR water and used for qRT-PCR with primers specific to virulence related target genes (**Table 4.2**). SsoAdvanced Universal Sybr green Supermix (Bio-Rad, California, USA) was used to prepare qRT-PCR reactions according to manufacturer guidelines. Amplifications were performed in biological triplicate and technical duplicate. Target gene expression relative to the MMM control group was calculated using the $\Delta\Delta$Ct method (Livak et al., 2001) with *clpX* used as a housekeeping gene.

Microtiter Dish Biofilm Assay:

Following the methods described in O'Toole et al., 2011, 96-well plates used in PA14 48-hour growth assays were washed, stained with crystal violet dye for 12 minutes, and decolorized with acetic acid for 12 minutes. The contents of each well

were then transferred to a fresh 96-well plate and read at an absorbance at 520 nm in a BioTek Synergy H1 plate reader to quantify pigment intensity.

Results and Discussion

Sequencing of Sputum Samples and Mucin Enrichments:

Following the described mucin enrichment protocol, a total of eight clinical CF sputum samples (CSS) were collected, processed, and repeatedly passaged on MMM to enrich for the bacterial taxa adept at survival on mucin as a sole nutrient source. Both CSSs and their respective enrichments were subjected to 16S rRNA gene sequencing. After filtering for sequence quality, five of eight CSSs and their respective mucin enrichments were evaluated for global differences in bacterial composition. Principal coordinate analysis (PCoA) of the sequencing data, revealed distinct clustering between groups, suggesting significant differences in the bacterial community compositions (**Figure 4.1A**). This was further supported by the separation of these respective clusters on the PCoA plot, underscoring the magnitude of the bacterial diversity and distribution disparity between the two groups.

Further analysis using a double principal coordinate analysis (DPCoA) (**Figure 4.1A**) revealed associations of specific bacterial taxa with each sample group (**Figure 4.1B**). Particularly, the Actinobacteriota phylum was observed to cluster more closely with CSSs, while Firmicutes clustering was found to be in closer proximity with that of the enrichments. Other taxa formed a distinct and separate

cluster - indicating less pronounced associations with either sample group. Changes in the absolute abundance of genera between CSSs and their respective enrichments (**Table 4.1**) confirmed this observation in greater detail – showing a 6.9% increase in *Streptococcus* (Firmicutes) and a 14.5% increase in *Actinomyces* (Actinobacteriota) across enrichments compared to the CSSs.

Together, these data support the effectiveness of our mucin enrichment approach that yields distinct bacterial populations differing from the original community. This difference in population suggests those populations identified in enrichments, are better suited for catabolism of mucin, and may play a role in the proposed cross-feeding model. Additionally, the increase of *Streptococcus* and *Actinomyces* abundances in the enrichments suggest these genera are adept at the direct utilization of mucin as a sole nutrient source, or that they play a pivotal role in the cross-feeding interactions of mucin-degrading bacterial communities. This is consistent with prior work that identified *Streptococcus spp.* in mucin enrichments and confirmed the ability of this genus to degrade mucin glycoproteins (Flynn et al., 2016).

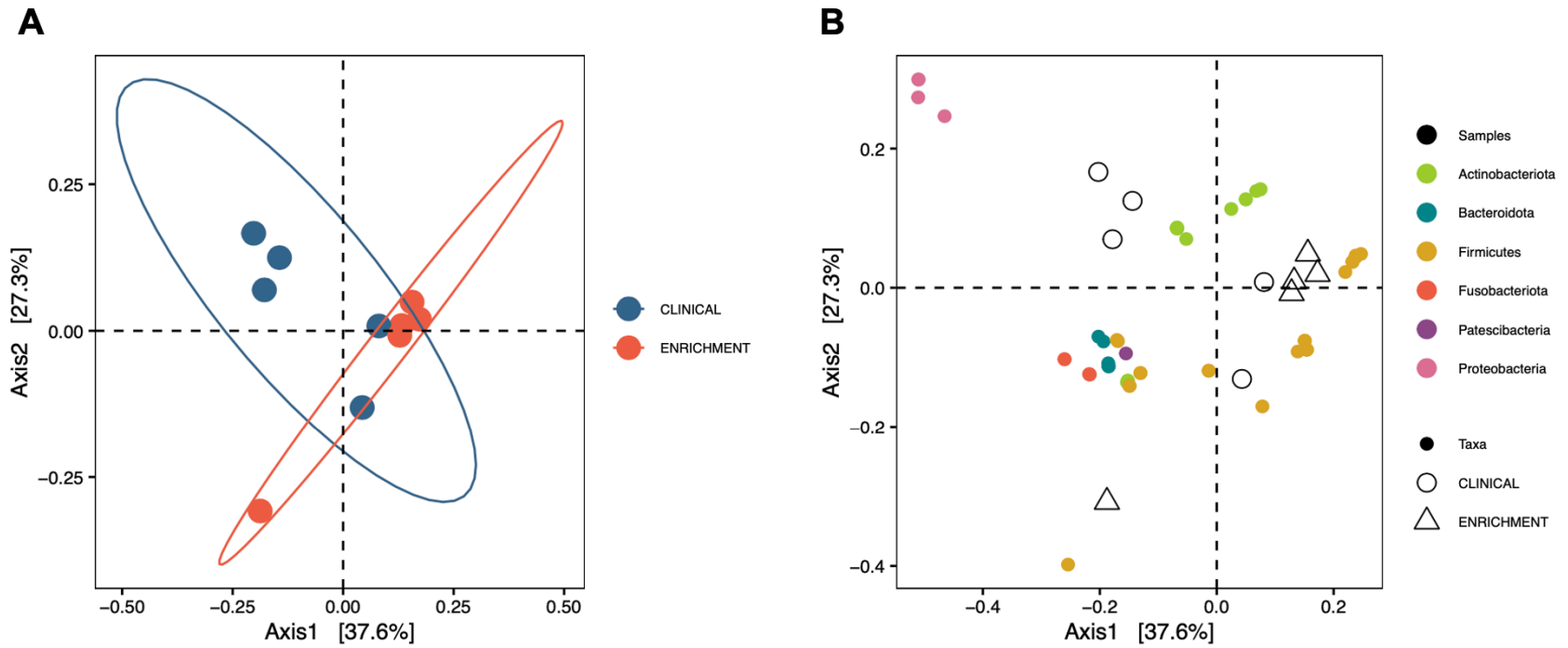

Figure 4.1 – 16S rRNA gene sequencing bacterial abundance between clinical sputum samples and mucin enrichments. A) Principal coordinates analysis comparing proportional bacterial abundance data from clinical sputum samples and respective mucin enrichment cultures. **B)** Double principal coordinate analysis comparing proportional bacterial abundance data from clinical sputum samples and respective mucin enrichment cultures with associated phyla.

Table 4.1 – Comparison of 16S rRNA gene sequencing genera read abundance percentages between clinical sputum samples and respective mucin enrichments.

Percentage of Genera Read Abundance		
Genus	**Clinical**	**Enrichment**
Streptococcus	19.1	26
Actinomyces	7.7	22.2
Granulicatella	5.3	18.2
Staphylococcus	15.5	2.6
Pseudomonas	15.6	0
Parvimonas	0.1	12.8
Rothia	11	0
Atopoobium	0.4	7.4
Haemophilus	7.2	0
Enterococcus	0	5.8
Lacticaseibacillus	0.1	5
Gemella	5.2	0
Leptotrichia	2.4	0
Prevotella_7	1.6	0
Fusobacterium	1.6	0
Bifidobacterium	1.5	0
Veillonella	1.5	0
Neisseria	1.1	0
TM7x	0.7	0
Porphyromonas	0.5	0
Capnocytophaga	0.5	0
Prevotella	0.3	0
Stromatobaculum	0.3	0
Mogibacterium	0.3	0
Solobacterium	0.3	0
Lachnoanaerobaculum	0.2	0

Characterization of Mucin Enrichment Communities:

Final taxa plots of mucin enrichment community relative abundances did differ significantly from their respective CSS (**Figure 4.2A**); however, they also differed from what has been previously observed in our laboratory and current literature. *Streptococcus, Fusobacterium, Prevotella,* and *Veillonella* are consistently the most enriched genera on MMM (**Figures 3.1-3.2**) (Flynn et al., 2016). Despite these genera being present in the CSSs, all but *Streptococcus* were absent in the mucin Es (**Table 4.1; Figure 4.2A**). As a result of initial media contamination and the need to repeat the enrichment protocol, this could possibly be explained as an artifact of CSS integrity. Age of the sample, repeated freeze thaw cycles, and prolonged exposure to oxygen may have negatively impacted the viability of facultative and obligately anaerobic genera.

All mucin enrichment communities grew to a detectable optical density (OD600) over 72 hours on MMM (**Figure 4.2B**). Notably, Enrichment 2 was found to grow to the lowest optical density (0.44) while Enrichment 4 was found to grow to the highest (1.56). This may be partly due to Enrichment 4 having the highest relative abundances of *Streptococcus* and *Actinomyces*, and Enrichment 2 having neither of these mucin-degrading associated genera present (**Figure 4.2A**). This is supported by FPLC analysis of relative mucin degradation by the enrichment communities (**Figure 4.2C,D**). While Enrichment 2 exhibits a decrease in the area under the curve (AUC) of the high molecular weight (HMW) peak (**Figure 4.2C**), it is the only enrichment to not cause a significant increase in the median retention

time (RT) of the low molecular weight (LMW) peak (**Figure 4.2D**). This indicates that LMW mucins are not decreasing in molecular size and suggests Enrichment 2 is comparatively less adept at mucin degradation– consistent with its poor growth on MMM (**Figure 4.2B**). Conversely, Enrichment 4 exhibited the greatest impact on both peaks (**Figure 4.2C,D**) - consistent with its robust growth (**Figure 4.2B**). Other enrichments exhibited less reduction in the AUC of the HMW peak (**Figure 4.2C**) compared to Enrichment 2, but greater impacts on the AUC and RT of the LMW peak (**Figure 4.2D**). This may suggest that while Enrichment 2 may be adept at the degradation of HMW mucins, it lacks key community constituents (i.e., *Streptococcus*) that allow for subsequent degradation of LMW mucins – a process that may be required for efficient community cross-feeding and robust growth of a community on MMM.

Together, these five mucin enrichment communities span a wide range of bacterial composition and performance in growth on MMM and mucin degradation. As a result, these data led to the central hypothesis being tested: *P. aeruginosa* physiology is driven by the bacterial community composition of the CF airways.

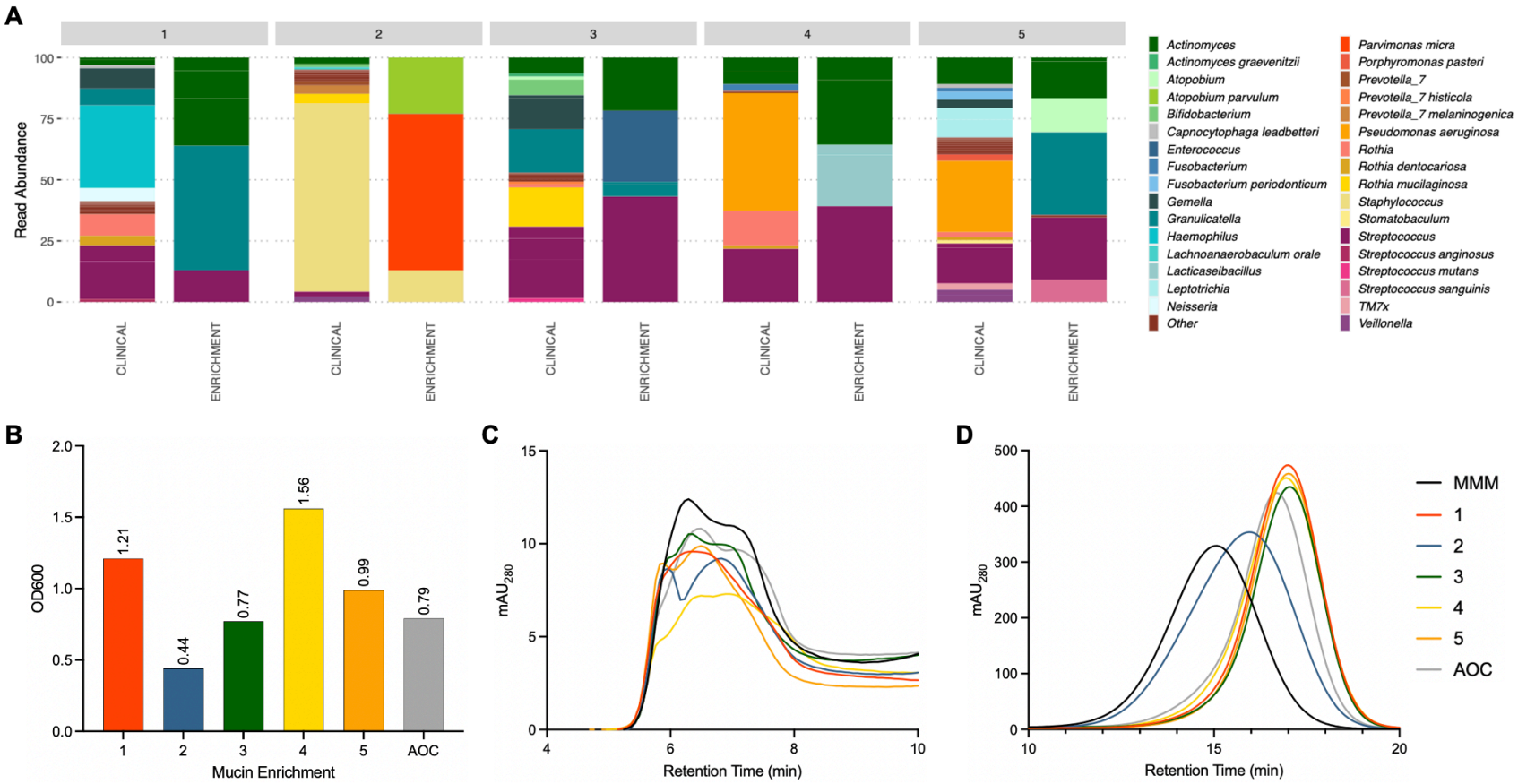

Figure 4.2 – Characterization of mucin enrichment communities. A) 16S rRNA gene sequencing taxa plots displaying relative abundances of phyla in clinical sputum samples and respective mucin enrichments. **B)** 72-hour end point optical density (OD600) values for final mucin enrichment cultures incubated anaerobically at 37°C on MMM. **C)** High molecular weight peak (1) inset of FPLC chromatogram measuring relative mucin degradation of the same enrichment cultures. **D)** Low molecular weight peak (2) inset of FPLC chromatogram measuring relative mucin degradation of the same enrichment cultures.

Characterization of PA14 Growth and Virulence in Response to Enrichments:

Strain PA14 was grown on the 72-hour time point enrichment cell free supernatants (ECFS), as well as MMM and representative anaerobic oral community (AOC) CFS controls (**Figure 4.3A**). PA14 grew to the highest density in the AOC CFS control and as expected, lowest in the MMM control. Of the ECFSs, PA14 grew the most rapidly and to the highest density on ECFS4, which exhibited the best growth performance in MMM (**Figure 4.2B**) and the most mucin degradation (**Figure 4.2C,D**). Notably, PA14 exhibited a prolonged lag growth phase when grown on AOC CFS, ECFS3, and ECFS4, even when compared to growth on ECFS2 which exhibited poor growth performance in MMM (**Figure 4.2B**) and reduced LMW mucin degradation (**Figure 4.2D**). These data suggest either an inhibitory effect or a less robust nutrient pool for cross-feeding.

Interestingly, the three lag phase promoting ECFSs also resulted in a significant reduction of biofilm formation by PA14, as measured by a crystal violent microtiter biofilm assay (**Figure 4.3B**). An increase in the lag growth phase of a bacterial culture can be caused by a variety of culture conditions, such as pH and salinity, but is most associated with stress from suboptimal nutrient availability (Rolfe et al., 2012; Hamill et al., 2020). However, suboptimal nutrient availability is also known to promote biofilm formation in many bacteria, including PA, as a long-term survival strategy (Salgar-Chaparro et al., 2020; Petrova et al., 2012). Consequently, an increase in biofilm formation by PA14 cultures with increased lag phases would be expected, rather than the significant reduction observed. One potential explanation

for this observed phenomenon is dependent on the concentration of HMW mucins rather than general nutrient availability. HMW intact intestinal mucins have been show to attenuate PA biofilm formation *in vitro* (Wheeler et al., 2020). While the three lag phase promoting enrichments exhibit adept degradation of LMW mucins (**Figure 4.2D**), they also exhibit the least degradation of HMW, even when compared to the poorly performing Enrichment 2 (**Figure 4.2B,C**). Conversely, Enrichment 4 exhibited the greatest degradation of HMW mucins (**Figure 4.2C**) and resulted in the highest level of biofilm formation by PA14 (**Figure 4.3B**). Increased concentration of HMW mucins in ECFSs may play a role in the observed increased lag growth phase and suppressed biofilm production of PA14.

In addition to affecting biofilm formation, PA14 growth on AOC CFS, ECFS3, and ECFS5 also significantly impacted phenazine production (**Figure 4.3C**). Growth on AOC CFS resulted in a significant increase in PCA, growth on ECFS3 resulted in a significant decrease in PYO, and growth on ECFS5 resulted in highly significant decreases in both PYO and PCN. PA phenazine production is generally considered to be regulated by the LasR, RhlR, and PqsR quorum sensing systems (Tuon et al., 2022; Venturi et al., 2006). However, recent findings suggest that mucins and mucin-derived monosaccharides can also regulate the production of phenazines (Hoffman et al., 2020). Despite growth to a high optical density (**Figure 4.3A**), two of these ECFSs resulted in suppressed PYO and PCN production. While the underlying mechanisms of this suppression remain unclear, these data

demonstrate a clear growth-independent regulation of PA phenazine production by CF airway microbiota.

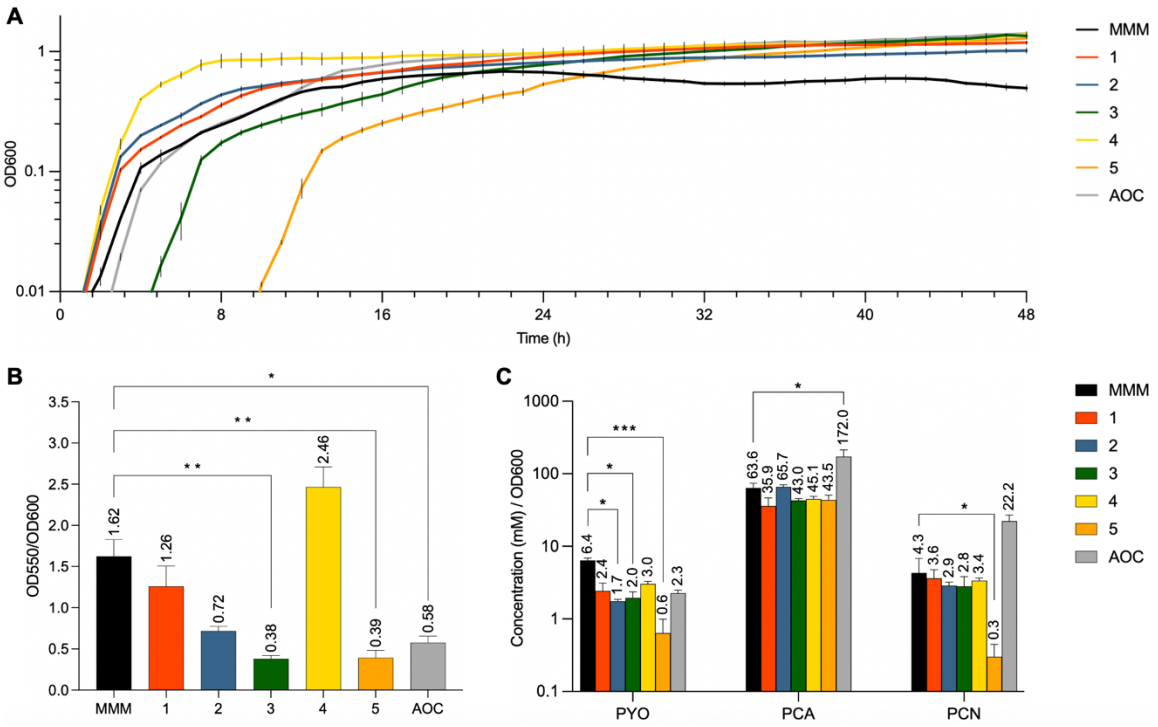

Figure 4.3 – Characterization of PA14 growth, biofilm production, and phenazine expression in cell free supernatants of mucin enrichments. A) 48-hour growth curves of PA14 in cell free supernatants of mucin enrichments and a minimal mucin media (MMM) control condition. Endpoint OD600 readings: MMM (0.496); 1 (1.188); 2 (1.022); 3 (1.355); 4 (1.405); 5 (1.296); AOC (1.415). **B)** Biofilm production of the same PA14 cultures at 48 hours as measured by a crystal violet biofilm assay and normalized to average end point optical density values (OD600) (n = 3; Kruskal-Wallis with uncorrected Dunn's multiple comparisons; * = P < 0.05; ** = P < 0.005). **C)** Phenazine production of PA14 cultures post 18 hours of incubation (RT-qPCR cultures) as measured by HPLC (n = 3; Kruskal-Wallis with uncorrected Dunn's multiple comparisons; * = P < 0.05; ** = P < 0.005; *** = P < 0.0005).

Organic Acid Profiles and Utilization by PA14:

HPLC was used to generate organic acid profiles for CSS (**Figure 4.4A**) and their respective mucin enrichments before (**Figure 4.4B**) and after (**Figure 4.4C**) PA14 growth. CSS exhibited high levels of formate, but relatively low concentrations of other organic acids (**Figure 4.4A**). Enrfichments exhibited more robust yet variable organic acids profiles (**Figure 4.4B**). It is known that the nutritional preferences of PA prioritize catabolism of amino acids, followed by organic acids, and finally glucose (McGill et al., 2021; Dolan et al., 2020). This is accomplished via carbon catabolite repression (CCR), which is a metabolic strategy used to enhance microbial fitness (Yung et al., 2019). Classic CCR (cCCR) is common in most model organisms and drives a nutritional preference for glucose over organic acids. However, in the case of PA, its nutritional preference is reversed, and accomplished by a specific CCR strategy termed reverse diauxie (or rCCR) (Yung et al., 2019). Of the organic acids, PA sequentially prefers succinate, lactate, and acetate under aerobic conditions (McGill et al., 2021). This is also evident in the organic acid profile data, as the concentrations of succinate and acetate are reduced post PA14 growth (**Figure 4.4C**). Additionally, Enrichment 4 contained the highest concentration of succinate (1.96 mM) (**Figure 4.4B**), which resulted in the most robust growth of PA14 (**Figure 4.3A**) – likely a result of the high concentration of its preferred carbon source.

Interestingly, while succinate and acetate concentrations were depleted across all PA14 cultures, this was not the case for lactate (**Figure 4.4C**). Lactate was

previously shown to be preferred over acetate by PA (McGill et al., 2021), and consequently, its concentration in media would be expected to be preferentially depleted prior to acetate. However, in several ECFS (1, 4, and 5), lactate concentrations increased following PA14 growth, suggesting the production of lactate by PA14 rather than its catabolism (**Figure 4.4C**). The production of organic acids such lactate is traditionally associated with anaerobic fermentation (Moestedt et al., 2020); however, PA14 does not have a strong preference for glucose and was grown aerobically. Lactate can also be produced as a biproduct of overflow metabolism - a process by which partially oxidized secondary metabolites (i.e., acetate and lactate) are secreted during the catabolism of glucose as a means to maintain redox homeostasis (Dolan et al., 2020); however, this phenomenon is associated with cCCR and has yet to be observed in rCCR employed by PA (Yung et al., 2019; McGill et al., 2021). While glucose fermentation and overflow metabolism are unlikely explanations for the observed production of lactate, PA14 has been known to ferment pyruvate into lactate via lactate dehydrogenase LdhA (Goldberg et al., 2018), for its long-term survival in anaerobic conditions. However, this fermentation was only observed under anaerobic conditions without the availability of nitrate respiration (Eschbach et al., 2004). Pyruvate was measured at higher concentrations in ECFSs found to elicit lactate production by PA14 (**Figure 4.4B**), confirming the substrate for this type of fermentation was available.

Despite this being a likely avenue for lactate production by PA14, all PA14 cultures were grown on the same 96-well plate under aerobic conditions with vigorous and continuous shaking – likely supporting aerobic respiration rather than less energetically favorable pyruvate fermentation. One explanation for this observed phenomenon could be poor aeration of cultures and depletion of nitrate, resulting in microaerophilic conditions and spurring pyruvate fermentation. Another possible explanation may be the detection of anaerobic community molecular signals (e.g., quorum sensing molecules) by PA14, signaling the potential for impending anaerobic conditions and eliciting the preparation for those conditions via preemptive metabolism modification. Within the context of CF, this signaling would prove to be advantageous as the oxygen content of the CF airways is highly variable and transient – as a result of mucus plugs and clearing events (Cowley et al., 2015; Worlitzsch et al., 2002)

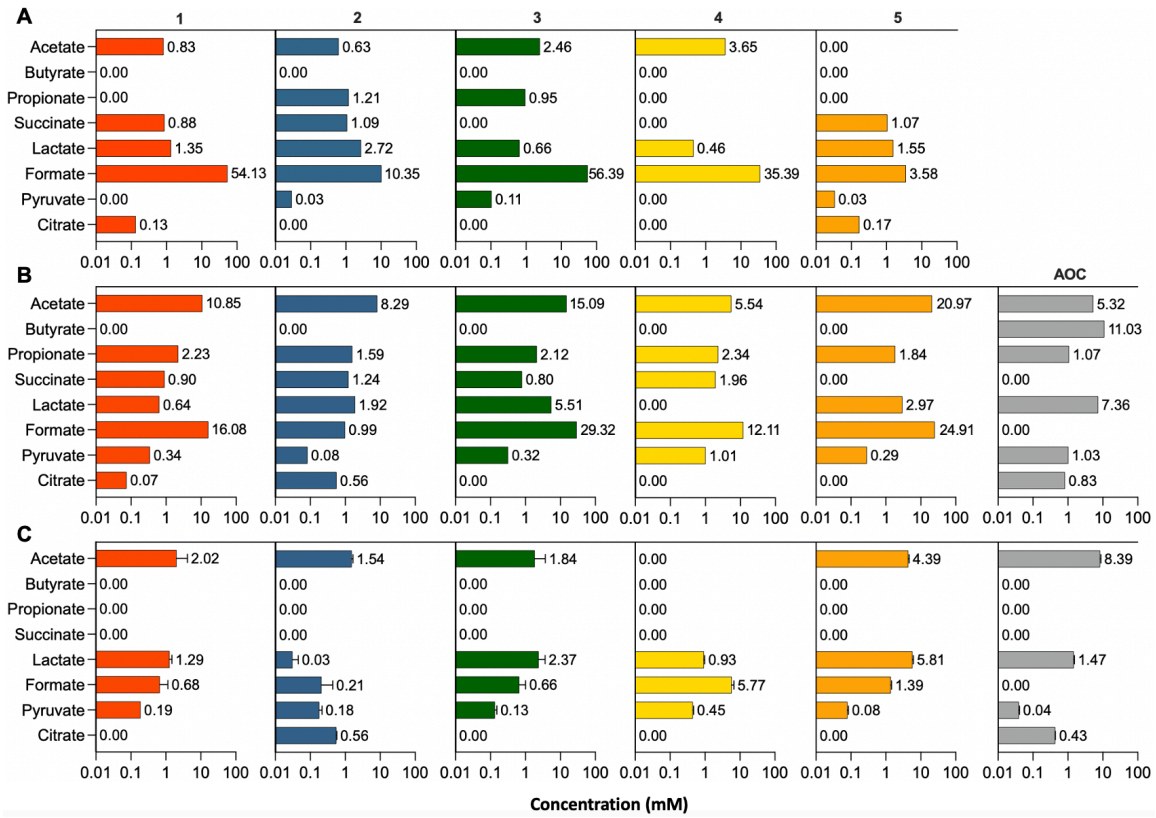

Figure 4.4 – HPLC generated organic acid profiles of clinical sputum samples, mucin enrichments, and PA14 cultures. A) Organic acid profiles of clinical sputum samples, **B)** respective mucin enrichments (72-hour incubation), and **C)** PA14 cultured in the cell free supernatants of the same clinical sputum mucin enrichments (18-hour incubation).

RT-qPCR of PA14 Virulence Associated Genes:

RT-qPCR was performed on the same PA14 cultures previously characterized to validate phenazine quantification data, to identify underlying mechanisms contributing to changes in phenazine production, and to investigate the overall effects on PA14 virulence. A panel of eight virulence associated genes were targeted for analysis (**Table 4.2**) and differential gene expression was determined relative to PA14 grown in a MMM control (**Figure 4.5**). Of the noteworthy results, PA14 grown in ECFS4 was found to have lower expression of *rhlI* compared to the control (**Figure 4.5**). *rhlI* is a component of the PA LasR quorum sensing system, which is known to regulate virulence factors such as biofilm formation (Mukherjee et al., 2017). The significant reduction in expression of this gene may be associated with the drastic increase of biofilm formation observed (**Figure 4.3B**).

Strikingly, a significant increase in the expression of both *phzG1* and *phzS* was observed in PA14 grown in ECFS5 (**Figure 4.5**). *phzG1* encodes the enzyme for the final conversion of chorismic acid into PCA (Blankenfeldt et al., 2004). *phzS* encodes an enzyme that catalyzes the conversion of intermediates into either PYO or 1-HP (Mavrodi et al., 2001). Observing a significant increase in these transcripts would suggest an increase in the end product of PYO; however, the opposite was observed. PA14 grown in ECFS5 was found to produce significantly lower concentrations of the phenazine compared to the MMM control (**Figure 4.3C**). Additionally, while *phzM* expression was found to also be slightly raised by this ECFS, it's increase did not match that of *phzS.* This is notable, as PhzS is

hypothesized to directly interact with PhzM in the production of PYO (Greenhagen et al., 2008).

Post-transcriptional regulation, translational regulation, gene product (enzyme) degradation, and mRNA negative feedback loops are all possible explanations for this observed result. However, it is also notable that conversion of intermediates to PYO by PhzS requires the presence of oxygen (Mavrodi et al., 2001). A lack of available oxygen would impede the production of PYO, as observed in the phenazine quantification of PA14 grown in ECFS5 (**Figure 4.3C**). As a result, this may elicit the upregulation of *phzS* in an effort to produce the phenazines, or it may lead to the accumulation of *phzS* transcripts due to downregulated translation. Future work will be required to determine the underlying mechanism of this observation.

Table 4.2 – *Pseudomonas aeruginosa* virulence associated gene information and respective primer sequences used in RT-qPCR.

RT-qPCR Virulence Gene Targets				
Gene	**Locus Tag**	**Predicted Product**	**Virulence Function**	**Primer Sequences**
phzG1	PA4216	pyridoxamine 5'-phosphate oxidase	phenazine biosynthesis (PCA)	**F**: 5'-AAACCCTCGCCGACATC-3' **R**: 5'-ACAGTTCGAACAGGCAGTAG-3'
phzG2	PA1905	pyridoxamine 5'-phosphate oxidase	phenazine biosynthesis (PCA)	**F**: 5'-AAACCCTCGCCGACATC-3' **R**: 5'-ACAGTTCGAACAGGCAGTAG-3'
lasI	PA1432	autoinducer synthesis protein LasI	N-(3-oxo-dodecanoyl)-L-homoserine lactone quorum sensing system	**F:** 5'-TGACGCACTCAGTCCTTATTAC-3' **R**: 5'-AGGTGTTCTTCAGCATGTAGG-3'
rhlI	PA3476	autoinducer synthesis protein RhlI	N-(butanoyl)-L-homoserine lactone quorum sensing system	**F**; 5'-GCAGCTGGCGATGAAGATA-3' **R**: 5'-GCCGTTGCGAACGAAATAG-3'
phzM	PA4209	phenazine-specific methyltransferase	phenazine biosynthesis (intermediate)	**F**: 5'-GCGACATGGTGCTGTTCTA-3' **R**: 5'-GCTTCAGGTAGCTGTAHAAGTC-3'
phzS	PA4217	flavin-containing monooxygenase	phenazine biosynthesis (PYO & 1HP)	**F**: 5'-CGAACCCATCGATATCCTCATT-3' **R**: 5'-TATCTCGCTGCTGCTTTCC-3'
qscR	PA1898	quorum-sensing control repressor	quorum sensing system regulation	**F**: 5'-CTGACCGCGCCTAAATATCA-3' **R**: 5'-GGTCGATGGATGTGTAGTCTTC-3'
ptsP	PA0337	phosphoenolpyruvate-protein phosphotransferase PtsP	quorum sensing system regulation	**F**: 5'-CGTCAGGTCGACTTCCTTTC-3' **R**: 5'-ATGCAGGTAGTCGTAGAGGT-3'

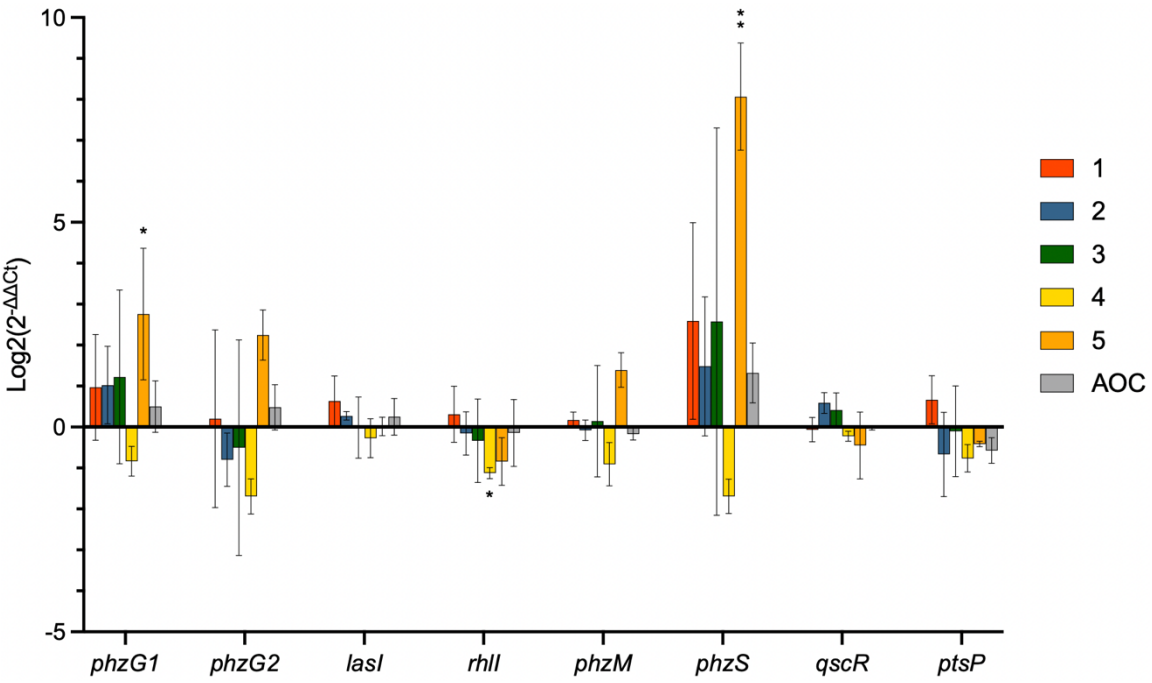

Figure 4.5 – Differential expression of PA14 virulence associated genes in response to mucin enrichment supernatants. RT-qPCR Log2 transformed $2^{-\Delta\Delta Ct}$ values of PA14 virulence associated genes normalized to the values of the minimal mucin media (MMM) control condition. (*n* = 3; Kruskal-Wallis with uncorrected Dunn's multiple comparisons; * = $P < 0.05$; ** = $P < 0.005$)

Conclusion

In this chapter, I first defined the bacterial composition of CSSs and respective mucin enrichments (**Figure 4.1; Figure 4.2A; Table 4.1**) – finding Actinobacteriota and Firmicutes to be highly associated with mucin enrichments, suggesting key roles for these taxa in the cross-feeding dynamics of mucin-degrading bacterial communities. Next, I characterized each enrichment by evaluating its growth performance on MMM and its mucin degradation abilities (**Figure 4.2 B-D**). Following this, I investigated the effect of each ECFS on the growth, biofilm formation, and phenazine production of PA14 (**Figure 4.3**). I identified three ECFSs (AOC, 3, and 5) that elicited a prolonged lag growth phase by PA14. ECFS5 also suppressed the production of PYO and PCN by PA14, despite supporting its growth to a high final density. Subsequent RT-qPCR analysis of the genes responsible for PA phenazine production (**Figure 4.5; Table 4.2**) paradoxically revealed a significant increase in *phzG1* and *phzS* in PA14 grown in ECFS5, despite decreased levels of quantified phenazines. The organic acid profiles of the CSSs and respective enrichments before and after PA14 growth were analyzed via HPLC (**Figure 4.4**). ECFSs with high levels of succinate best supported the growth of PA14. However, several ECFSs rich in pyruvate (1, 4, and 5) elicited the production of lactate under aerobic conditions.

Of all the ECFSs, ECFS5 had the most notable impact on PA14 physiology, as it was found to produce a high concentration of lactate, most likely via pyruvate fermentation – a pathway that is only active under anaerobic conditions without

nitrate. It was also found to produce decreased levels of PYO and PCN, in contrast to high expression of *phzS* – encoding an enzyme that requires oxygen to catalyze the production of PYO. Considered together, these data suggest that PA14 was potentially exposed to an oxygen-limiting environment, despite being grown under aerobic conditions with vigorous continuous shaking. One other possible explanation is that detection of anaerobic bacterial community constituent molecular signals by PA, may signal impending anaerobic conditions and spur preemptive metabolic shifts accordingly – providing a fitness advantage. This remains to be explored and the mechanisms underlying this potential phenomenon remain unknown. Follow-up experiments measuring the expression of lactate dehydrogenase LdhA in relation to aerobic lactate production, and Western blots quantifying PhzS in relation to increased *phzS* transcripts may help better explain the observed results.

Together, these data support the initial hypothesis that the composition of co-colonizing microbiota can impact the growth and virulence of PA via growth-independent mechanisms. While this work was completed *in vitro*, its support of this hypothesis has many *in vivo* implications on the current paradigms surrounding chronic bacterial infections and PExs of CF patients. These results lay the groundwork for follow-up studies aimed at identification of the underlying mechanisms of phenazine suppression in PA – a promising pathway to the identification of CF PEx biomarkers and alternative treatment targets.

CHAPTER 5: Conclusion

Summary of Research

The primary objective of this thesis was to further investigate the general cross-feeding model proposed by Flynn et al., 2016, in which *P. aeruginosa* (PA) growth and virulence within the cystic fibrosis (CF) airways is potentiated through cross-feeding interactions with co-colonizing, anaerobic, mucin-degrading bacteria. To do so, I employed a combination of experimental approaches relying on sequencing, liquid chromatography, and classical microbiology techniques. Altogether, data generated throughout this thesis revealed new insights into the putative niches of individual bacterial genera in both the proposed cross-feeding model and the larger context of the CF airways.

In Chapter 1, I provided background on the epidemiology, etiology, and pathophysiology of CF. I defined mucin glycoproteins as a major macromolecular component of airway mucus and expounded on the role of mucus in the promotion of airway blockages and chronic bacterial infections in the CF airways. I continued by describing several bacterial genera (*Streptococcus, Prevotella, Veillonella,* and *Fusobacterium*) commonly identified in CF sputum samples and associated with mucosal environments – suggesting their capacity for mucin catabolism. I conveyed the significance of these genera by describing the canonical CF airway pathogen PA and providing evidence for its reliance on their mucin degradation byproducts (i.e., organic acids) for growth. Considering this information, I described a modified cross-feeding model (Flynn et al., 2016) in which the pristine airways of infants and young children with CF are colonized by aspirated oral

bacteria, ultimately developing into complex communities that modify the nutritional landscape of the airway environment over time. I propose that niche modification by these communities prime the airways for subsequent colonization of PA. I concluded this section by suggesting impacts on PA virulence (i.e., biofilms, phenazines) *in vivo* by this cross-feeding model and reiterating the importance of its continued study.

In Chapter 2, I described several experimental limitations that impede the characterization of individual cross-feeding model components. The first being the lack of a standardized high-throughput method for the evaluation of mucin glycoprotein degradation. While enzyme-linked immunosorbent assays (ELISA) can be used to quantify core mucin components, this method has many caveats. Building upon current fast protein liquid chromatography (FPLC) protocols in our laboratory, I optimized and validated a high-throughput method for the relative quantification of high molecular weight (HMW) and low molecular weight (LMW) mucins.

A second limitation is the lack of a pure defined minimal mucin medium (MMM) to evaluate bacterial mucin catabolism *in vivo*. While our laboratory already used one formulation of this medium, it was found to contain variable traces of organic acids and was prone to contamination as an artifact of its generation protocol. Using this protocol as a starting point, I developed an optimized approach which resulted in an improved MMM – exhibiting reduced batch effects, increased HMW mucin

concentration, increased average mucin molecular size, and elimination of trace organic acids.

The last limitation addressed was the lack of accurate, affordable, and high-throughput methods for the quantification of organic acid derived from bacterial mucin fermentation, and phenazines produced by PA. Conventional organic acid quantification is accomplished through liquid-liquid extraction of analytes and subsequent liquid chromatography – mass spectrometry. This is a laborious and costly multi-step methodology. Conventional phenazine quantification is accomplished through liquid-liquid extraction of analyte and subsequent analysis via colorimetry. This method is laborious, inaccurate, and limited to the quantification of only one phenazine species – PYO. In both cases, methodologies are further complicated by the inclusion of large mucin glycoproteins. I address these limitations first by describing a filter-based sample preparation method capable of depletion of over 97% of mucins in a sample. I then present two independent high performance liquid chromatography (HPLC) methods for the accurate, cost effective, and high-throughput quantification of organic acids and phenazines, respectably. Method optimization data were also presented to support the effectiveness of each method, and finalized methods were validated through the analysis of experimental *in vitro* bacterial cell free supernatants (CFS).

Using tools developed in the previous chapter, in Chapter 3 I identify key bacterial species of the cross-feeding model, characterize their physiology when grown on

mucins and evaluate the impact of their CFSs and respective individual organic acids on PA growth and virulence. Metagenomic and 16S amplicon sequencing were used to define the bacterial composition of a representative anaerobic oral community (AOC). Several genera were identified (*Streptococcus, Prevotella, Veillonella, Fusobacterium, Bifidobacterium,* and *Solobacterium*) and representative species of each were selected for characterization on MMM. *Bifidobacterium* was found to best degrade HMW mucins, support the growth of PA, and suppress its production of PYO and PCN – suggesting a role as an initial colonizer and primary mucin degrader in the cross-feeding model (**Figure 5.1**). *Streptococcus* was found to best degrade LMW mucins and support the growth of PA – suggesting a role as a secondary mucin degrader (**Figure 5.1**). *Veillonella* and *Solobacterium* were found to lack robust mucin degradation abilities and poorly support the growth of PA, while also eliciting increased biofilm and phenazine production. Together, these data detail several specific cross-feeding interactions that may commonly occur and underscore their stepwise fashion (**Figure 5.1**).

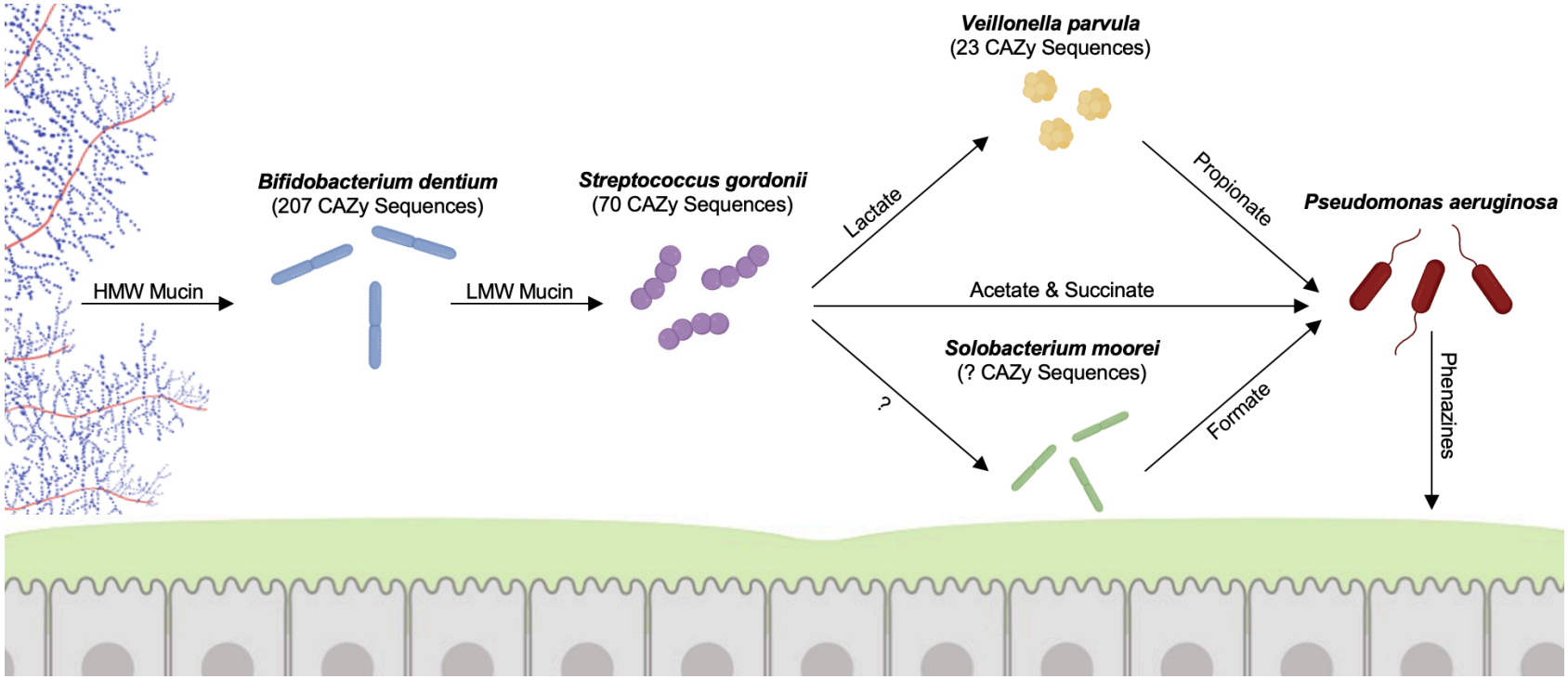

Figure 5.1 – Simplified model of predicted cross-feeding interactions. Simplified cross-feeding model depicting *P. aeruginosa* as well as four anaerobes and their respective carbohydrate-active enzyme (CAZy) sequence repertoire. Arrows represent predicted metabolic inputs and outputs of each species. (?) indicates that no inference could be made from collected data or current literature.

Follow up experiments evaluated the effects of individual microbially produced organic acids on PA growth and virulence. PA growth on MMM supplemented with 50 mM of each organic acid resulted in variable culture coloration. Succinate, lactate, and acetate, respectively, were found to best support the growth of PA – consistent with the reverse diauxie carbon catabolic repression strategy of PA (McGill et al., 2021). Of all the organic acids, supplementation with butyrate resulted in the largest impact on PA virulence – drastically suppressing biofilm and pyocyanin production.

In Chapter 4, I evaluated the impact of clinically derived mucin-degrading bacterial communities on PA physiology. Sputum samples and mucin enrichments were subjected to 16S amplicon sequencing to define their bacterial community compositions. FPLC analysis of mucin degradation confirmed a wide range of mucin degrading abilities across enrichment cultures. HPLC analysis of organic acids confirmed the same, identifying diverse organic acids profiles. Interestingly, when grown aerobically on enrichment cell free supernatants (ECFS), some PA cultures produced high concentrations of lactate indicative of pyruvate fermentation. All community CFSs supported the growth of PA compared to growth on MMM alone; however, ECFS5 profoundly impacted PA virulence through the suppression of biofilm, PYO, and PCN production. Follow up analysis found a significant increase in *phzS* transcripts suggesting potential post-transcriptional regulation, translational regulation, or gene product degradation.

Future Directions

The tools and techniques developed in Chapter 2 offer great value not only to the future directions of the presented work, but also to the CF field at-large. As conveyed in the Chapter 2 Supplement, my HPLC organic acid quantification method has already been used to generate data for multiple projects within our own laboratory and external collaborators (*in press*; data not shown).

Cumulative results of Chapters 3 and 4 identified several novel avenues of research moving forward, the first being continued characterization of cross-feeding interactions between anaerobic bacterial community constituents. While data generated in Chapter 3 profiled organic acids generated by individual species of airway microbiota grown on mucin, there was no experimental characterization of interactions between each of these species. Informed by the organic acid profiles and current literature, specific cross-feeding interactions between species could be inferred (**Figure 5.1**); however, greater resolution will be required. My HPLC organic acid detection method can be paired with *in vitro* co-culturing, sequential culturing, and CFS culturing of these individual species to achieve increased resolution of their metabolic interactions. The outcome would directly address the current gap in knowledge pertaining to bacterial community metabolism in mucin associated environments such as the oral cavity, gastrointestinal tract, and airways.

In Chapter 4, PA14 was observed to produce considerable concentrations of lactate when grown under aerobic conditions in ECFSs with high levels of acetate and pyruvate. While PA14 is known to produce lactate, it is only known to do so through the fermentation of pyruvate by LdhA (Goldberg et al., 2018) under fully anaerobic conditions and without the presence of nitrate for anaerobic respiration (Eschbach et al., 2004). Data suggest this may be a strategy for long-term survival in anaerobic environments or environments with turbulent rapidly shifting oxygen gradients (Eschbach et al., 2004) – like the CF airways (Cowley et al., 2015). Considering the current literature, PA14 producing lactate under aerobic conditions is unusual. As described, one possible explanation is the detection of anaerobe-derived metabolites (e.g., quorum sensing molecules) by PA that may signal the potential for impending anaerobic conditions and elicit the preparation for those conditions via preemptive metabolism modification by PA. Follow up experiments using CFS and similar concentrations of pure organic acids to replicate the observed lactate generation phenotype would be the next logical step towards investigating this phenomenon. Differential expression analysis of PA genes associated with general metabolism regulation and lactate metabolism (i.e., *ldhA, lldA, lldD, lldE*) (Goldberg et al., 2018) under lactate producing conditions may shed light on underlying mechanisms responsible for lactate production under seemingly aerobic conditions. Further research on this topic promises the potential for novel insights into co-colonizing community regulation of PA within CF airways.

A final avenue of future research focuses on the regulation of phenazine production by PA14. In both Chapter 3 and Chapter 4, microbially generated CFSs were found to elicit a significant suppression of PYO and PCN production by PA14. In both cases, PCA production remained unaffected, and the observed phenotype could not be recreated by growth of PA14 on MMM supplemented with organic acids. Subsequent analysis of differentially expressed PA virulence genes, in one of the two PA14 cultures exhibiting this phenotype, identified a significant increase in *phzS* transcripts. The product of *phzS* catalyzes the final conversion of intermediates in PYO and 1-HP, and requires oxygen to do so. Observing an increase in its transcripts would suggest an increase in final PYO concentrations, rather than the significant decrease observed. Similar to the previously described observation of PA14 production of lactate, this phenomenon would also be more easily explained if PA14 had been grown under anaerobic conditions as the lack of oxygen would inhibit the enzymatic activity of PhzS. Follow-up experiments aimed at replicating the observed phenotype and quantifying PhzS via Western blot, in addition to quantification of its transcripts via RT-qPCR, are the next steps in elucidating the underlying mechanisms of this putative PA phenazine regulation by co-colonizing microbiota. Confirmation of such regulation would provide an invaluable alternative target for the development of novel CF therapeutic strategies.

Concluding Remarks

While highly effective modulator therapies like Trikafta have led to monumental improvements in CF patient lung function, quality of life, and life expectancy, chronic infections by rapidly developing multi-drug resistant bacterial strains remain an ever-present challenge. As the efficacy of our front-line antibiotics diminish, identification of novel therapeutic targets through both basic and translational research strategies remains paramount. CF and similar conditions resulting in polymicrobial infections are complex and difficult to impactfully study with even the most stringent reductionist strategies. The polymicrobial cross-feeding model proposed by Flynn et al., 2016, and further characterized in this thesis, offers a valuable tool for the study of complex bacterial community interactions applicable across a variety of research fields. It is my hope that the tools developed, and the conclusions inferred in this thesis, also provide value across such fields.

BIBLIOGRAPHY

Alfonso-Sánchez, M. A., Pérez-Miranda, A. M., García-Obregón, S., & Peña, J. A. (2010). An evolutionary approach to the high frequency of the Delta F508 CFTR mutation in European populations. *Medical Hypotheses*, *74*(6), 989–992. https://doi.org/10.1016/j.mehy.2009.12.018

Ali Mohammed, M. M., Nerland, A. H., Al-Haroni, M., & Bakken, V. (2013). Characterization of extracellular polymeric matrix, and treatment of Fusobacterium nucleatum and Porphyromonas gingivalis biofilms with DNase I and proteinase K. *Journal of Oral Microbiology*, *5*, 10.3402/jom.v5i0.20015. https://doi.org/10.3402/jom.v5i0.20015

Amin, K., Tranchimand, S., Benvegnu, T., Abdel-Razzak, Z., & Chamieh, H. (2021). Glycoside Hydrolases and Glycosyltransferases from Hyperthermophilic Archaea: Insights on Their Characteristics and Applications in Biotechnology. *Biomolecules*, *11*(11), 1557. https://doi.org/10.3390/biom11111557

Andrianifahanana, M., Moniaux, N., & Batra, S. K. (2006). Regulation of mucin expression: Mechanistic aspects and implications for cancer and inflammatory diseases. *Biochimica Et Biophysica Acta*, *1765*(2), 189–222. https://doi.org/10.1016/j.bbcan.2006.01.002

Asnicar, F., Weingart, G., Tickle, T. L., Huttenhower, C., & Segata, N. (2015). Compact graphical representation of phylogenetic data and metadata with GraPhlAn. *PeerJ*, *3*, e1029. https://doi.org/10.7717/peerj.1029

Audie, J. P., Janin, A., Porchet, N., Copin, M. C., Gosselin, B., & Aubert, J. P. (1993). Expression of human mucin genes in respiratory, digestive, and reproductive tracts ascertained by in situ hybridization. *Journal of Histochemistry & Cytochemistry*, *41*(10), 1479–1485. https://doi.org/10.1177/41.10.8245407

Bao, X., Bové, M., & Coenye, T. (2022). Organic Acids and Their Salts Potentiate the Activity of Selected Antibiotics against Pseudomonas aeruginosa Biofilms Grown in a Synthetic Cystic Fibrosis Sputum Medium. *Antimicrobial Agents and Chemotherapy*, *66*(1), e0187521. https://doi.org/10.1128/AAC.01875-21

Barrak, I., Stájer, A., Gajdács, M., & Urbán, E. (2020). Small, but smelly: The importance of Solobacterium moorei in halitosis and other human infections. *Heliyon*, *6*(10), e05371. https://doi.org/10.1016/j.heliyon.2020.e05371

Bar-Shira, E., Cohen, I., Elad, O., & Friedman, A. (2014). Role of goblet cells and mucin layer in protecting maternal IgA in precocious birds. *Developmental & Comparative Immunology*, *44*(1), 186–194. https://doi.org/10.1016/j.dci.2013.12.010

Baty, J. J., Stoner, S. N., & Scoffield, J. A. (2022). Oral Commensal Streptococci: Gatekeepers of the Oral Cavity. *Journal of Bacteriology*, *204*(11), e00257-22. https://doi.org/10.1128/jb.00257-22

Bear, C. E. (2020). A Therapy for Most with Cystic Fibrosis. *Cell*, *180*(2), 211. https://doi.org/10.1016/j.cell.2019.12.032

Betancur-Murillo, C. L., Aguilar-Marín, S. B., & Jovel, J. (2022). Prevotella: A Key Player in Ruminal Metabolism. *Microorganisms*, *11*(1), 1. https://doi.org/10.3390/microorganisms11010001

Bhatt, J. M. (2013). Treatment of pulmonary exacerbations in cystic fibrosis. *European Respiratory Review*, *22*(129), 205–216. https://doi.org/10.1183/09059180.00006512

Blanchard, A. C., & Waters, V. J. (2022). Opportunistic Pathogens in Cystic Fibrosis: Epidemiology and Pathogenesis of Lung Infection. *Journal of the Pediatric Infectious Diseases Society*, *11*(Supplement_2), S3–S12. https://doi.org/10.1093/jpids/piac052

Blankenfeldt, W., Kuzin, A. P., Skarina, T., Korniyenko, Y., Tong, L., Bayer, P., Janning, P., Thomashow, L. S., & Mavrodi, D. V. (2004). Structure and function of the phenazine biosynthetic protein PhzF from Pseudomonas fluorescens. *Proceedings of the National Academy of Sciences*, *101*(47), 16431–16436. https://doi.org/10.1073/pnas.0407371101

Bleves, S., Viarre, V., Salacha, R., Michel, G. P. F., Filloux, A., & Voulhoux, R. (2010). Protein secretion systems in Pseudomonas aeruginosa: A wealth of pathogenic weapons. *International Journal of Medical Microbiology*, *300*(8), 534–543. https://doi.org/10.1016/j.ijmm.2010.08.005

Bolger, A. M., Lohse, M., & Usadel, B. (2014). Trimmomatic: A flexible trimmer for Illumina sequence data. *Bioinformatics*, *30*(15), 2114–2120. https://doi.org/10.1093/bioinformatics/btu170

Brennan, C. A., & Garrett, W. S. (2019). Fusobacterium nucleatum—Symbiont, opportunist and oncobacterium. *Nature Reviews Microbiology*, *17*(3), Article 3. https://doi.org/10.1038/s41579-018-0129-6

Briard, B., Bomme, P., Lechner, B. E., Mislin, G. L. A., Lair, V., Prévost, M.-C., Latgé, J.-P., Haas, H., & Beauvais, A. (2015). Pseudomonas aeruginosa manipulates redox and iron homeostasis of its microbiota partner Aspergillus fumigatus via phenazines. *Scientific Reports*, *5*(1), Article 1. https://doi.org/10.1038/srep08220

Brockhausen, I., Schachter, H., & Stanley, P. (2009). O-GalNAc Glycans. In A. Varki, R. D. Cummings, J. D. Esko, H. H. Freeze, P. Stanley, C. R. Bertozzi, G. W. Hart, & M. E. Etzler (Eds.), *Essentials of Glycobiology* (2nd ed.). Cold Spring Harbor Laboratory Press. http://www.ncbi.nlm.nih.gov/books/NBK1896/

Bruchmann, S., Dötsch, A., Nouri, B., Chaberny, I. F., & Häussler, S. (2013). Quantitative Contributions of Target Alteration and Decreased Drug Accumulation to Pseudomonas aeruginosa Fluoroquinolone Resistance. *Antimicrobial Agents and Chemotherapy*, *57*(3), 1361–1368. https://doi.org/10.1128/aac.01581-12

Bustamante-Marin, X. M., & Ostrowski, L. E. (2017). Cilia and Mucociliary Clearance. *Cold Spring Harbor Perspectives in Biology*, *9*(4), a028241. https://doi.org/10.1101/cshperspect.a028241

Carmody, L. A., Zhao, J., Kalikin, L. M., LeBar, W., Simon, R. H., Venkataraman, A., Schmidt, T. M., Abdo, Z., Schloss, P. D., & LiPuma, J. J. (2015). The daily dynamics of cystic fibrosis airway microbiota during clinical stability and at exacerbation. *Microbiome*, *3*(1), 12. https://doi.org/10.1186/s40168-015-0074-9

Caselli, E., Fabbri, C., D'Accolti, M., Soffritti, I., Bassi, C., Mazzacane, S., & Franchi, M. (2020). Defining the oral microbiome by whole-genome sequencing and resistome analysis: The complexity of the healthy picture. *BMC Microbiology*, *20*(1), 120. https://doi.org/10.1186/s12866-020-01801-y

Chaaban, M. R., Kejner, A., Rowe, S. M., & Woodworth, B. A. (2013). Cystic Fibrosis Chronic Rhinosinusitis: A Comprehensive Review. *American Journal of Rhinology & Allergy*, *27*(5), 387–395. https://doi.org/10.2500/ajra.2013.27.3919

Chandra, G., Patel, P., Kost, T. A., & Gray, J. G. (1992). Large-scale purification of plasmid DNA by fast protein liquid chromatography using a Hi-Load Q Sepharose column. *Analytical Biochemistry*, *203*(1), 169–172. https://doi.org/10.1016/0003-2697(92)90060-K

Chu, D., & Barnes, D. J. (2016). The lag-phase during diauxic growth is a trade-off between fast adaptation and high growth rate. *Scientific Reports*, *6*(1), Article 1. https://doi.org/10.1038/srep25191

Clarke, D., Gorman, I., Ringholz, F., McDermott, M., Cox, DW., Greally, P., Linnane, B., & Mc Nally, P. (2018). Pulmonary aspiration in preschool children with cystic fibrosis. *RESPIRATORY RESEARCH*, *19*(1), 255. https://doi.org/10.1186/s12931-018-0954-1

Conway, S. P., Brownlee, K. G., Denton, M., & Peckham, D. G. (2003). Antibiotic Treatment of Multidrug-Resistant Organisms in Cystic Fibrosis. *American Journal of Respiratory Medicine*, *2*(4), 321–332. https://doi.org/10.1007/BF03256660

Corfield, A. P. (2000). *Glycoprotein Methods and Protocols The Mucins* (1st ed. 2000.). Humana Press. https://doi.org/10.1385/1592590489

Corfield, A. P. (2015). Mucins: A biologically relevant glycan barrier in mucosal protection. *Biochimica Et Biophysica Acta*, *1850*(1), 236–252. https://doi.org/10.1016/j.bbagen.2014.05.003

Cowley, E. S., Kopf, S. H., LaRiviere, A., Ziebis, W., & Newman, D. K. (2015). Pediatric Cystic Fibrosis Sputum Can Be Chemically Dynamic, Anoxic, and Extremely Reduced Due to Hydrogen Sulfide Formation. *MBio*, *6*(4), e00767. https://doi.org/10.1128/mBio.00767-15

Crull, M. R., Somayaji, R., Ramos, K. J., Caldwell, E., Mayer-Hamblett, N., Aitken, M. L., Nichols, D. P., Rowhani-Rahbar, A., & Goss, C. H. (2018). Changing Rates of Chronic Pseudomonas aeruginosa Infections in Cystic Fibrosis: A Population-Based Cohort Study. *Clinical Infectious Diseases: An Official Publication of the Infectious Diseases Society of America*, *67*(7), 1089–1095. https://doi.org/10.1093/cid/ciy215

Cui, Q., Lv, H., Qi, Z., Jiang, B., Xiao, B., Liu, L., Ge, Y., & Hu, X. (2016). Cross-Regulation between the phz1 and phz2 Operons Maintain a Balanced Level of Phenazine Biosynthesis in Pseudomonas aeruginosa PAO1. *PloS One*, *11*(1), e0144447. https://doi.org/10.1371/journal.pone.0144447

Dahlstrand Rudin, A., Khamzeh, A., Venkatakrishnan, V., Basic, A., Christenson, K., & Bylund, J. (2021). Short chain fatty acids released by Fusobacterium nucleatum are neutrophil chemoattractants acting via free fatty acid receptor 2 (FFAR2). *Cellular Microbiology*, *23*(8), e13348. https://doi.org/10.1111/cmi.13348

D'Amore, C., Borgo, C., Bosello Travain, V., & Salvi, M. (2022). KDM2A and KDM3B as Potential Targets for the Rescue of F508del-CFTR. *International Journal of Molecular Sciences*, *23*(17), Article 17. https://doi.org/10.3390/ijms23179612

De Baere, S., Eeckhaut, V., Steppe, M., De Maesschalck, C., De Backer, P., Van Immerseel, F., & Croubels, S. (2013). Development of a HPLC-UV method for the quantitative determination of four short-chain fatty acids and lactic acid produced by intestinal bacteria during in vitro fermentation. *Journal of Pharmaceutical and Biomedical Analysis*, *80*, 107–115. https://doi.org/10.1016/j.jpba.2013.02.032

Demouveaux, B., Gouyer, V., Gottrand, F., Narita, T., & Desseyn, J.-L. (2018). Gel-forming mucin interactome drives mucus viscoelasticity. *Advances in Colloid and Interface Science*, *252*, 69–82. https://doi.org/10.1016/j.cis.2017.12.005

Derrien, M., van Passel, M. W., van de Bovenkamp, J. H., Schipper, R. G., de Vos, W. M., & Dekker, J. (2010). Mucin-bacterial interactions in the human oral cavity and digestive tract. *Gut Microbes*, *1*(4), 254–268. https://doi.org/10.4161/gmic.1.4.12778

Dolan, S. K., Kohlstedt, M., Trigg, S., Vallejo Ramirez, P., Kaminski, C. F., Wittmann, C., & Welch, M. (2020). Contextual Flexibility in Pseudomonas aeruginosa Central Carbon Metabolism during Growth in Single Carbon Sources. *MBio*, *11*(2), e02684-19. https://doi.org/10.1128/mBio.02684-19

Drula, E., Garron, M.-L., Dogan, S., Lombard, V., Henrissat, B., & Terrapon, N. (2022). The carbohydrate-active enzyme database: Functions and literature. *Nucleic Acids Research*, *50*(D1), D571–D577. https://doi.org/10.1093/nar/gkab1045

Egland, P. G., Palmer, R. J., & Kolenbrander, P. E. (2004). Interspecies communication in Streptococcus gordonii–Veillonella atypica biofilms: Signaling in flow conditions requires juxtaposition. *Proceedings of the National Academy of Sciences of the United States of America*, *101*(48), 16917–16922. https://doi.org/10.1073/pnas.0407457101

Ehre, C., Ridley, C., & Thornton, D. J. (2014). Cystic fibrosis: An inherited disease affecting mucin-producing organs. *The International Journal of Biochemistry & Cell Biology*, *52*, 136–145. https://doi.org/10.1016/j.biocel.2014.03.011

Engevik, M. A., Luk, B., Chang-Graham, A. L., Hall, A., Herrmann, B., Ruan, W., Endres, B. T., Shi, Z., Garey, K. W., Hyser, J. M., & Versalovic, J. (2019). Bifidobacterium dentium Fortifies the Intestinal Mucus Layer via Autophagy and Calcium Signaling Pathways. *MBio*, *10*(3), e01087-19. https://doi.org/10.1128/mBio.01087-19

Eschbach, M., Schreiber, K., Trunk, K., Buer, J., Jahn, D., & Schobert, M. (2004). Long-Term Anaerobic Survival of the Opportunistic Pathogen Pseudomonas aeruginosa via Pyruvate Fermentation. *Journal of Bacteriology*, *186*(14), 4596–4604. https://doi.org/10.1128/JB.186.14.4596-4604.2004

Essar, D. W., Eberly, L., Hadero, A., & Crawford, I. P. (1990). Identification and characterization of genes for a second anthranilate synthase in Pseudomonas aeruginosa: Interchangeability of the two anthranilate synthases and evolutionary implications. *Journal of Bacteriology*, *172*(2), 884–900. https://doi.org/10.1128/jb.172.2.884-900.1990

Ficke, B., Rajasurya, V., Sanghavi, D., & Cascella, M. (2023). Chronic Aspiration. In *StatPearls*. StatPearls Publishing. http://www.ncbi.nlm.nih.gov/books/NBK560734/

Field, T. R., Sibley, C. D., Parkins, M. D., Rabin, H. R., & Surette, M. G. (2010). The genus Prevotella in cystic fibrosis airways. *Anaerobe*, *16*(4), 337–344. https://doi.org/10.1016/j.anaerobe.2010.04.002

Fletcher, J. R., Villareal, A. R., Penningroth, M. R., & Hunter, R. C. (n.d.). Staphylococcus aureus Overcomes Anaerobe-Derived Short-Chain Fatty Acid Stress via FadX and the CodY Regulon. *Journal of Bacteriology*, *204*(5), e00064-22. https://doi.org/10.1128/jb.00064-22

Flynn, J. M., Cameron, L. C., Wiggen, T. D., Dunitz, J. M., Harcombe, W. R., & Hunter, R. C. (2020). Disruption of Cross-Feeding Inhibits Pathogen Growth in the Sputa of Patients with Cystic Fibrosis. *MSphere*, *5*(2), e00343-20. https://doi.org/10.1128/mSphere.00343-20

Flynn, J. M., Niccum, D., Dunitz, J. M., & Hunter, R. C. (2016). Evidence and Role for Bacterial Mucin Degradation in Cystic Fibrosis Airway Disease. *PLoS Pathogens*, *12*(8), e1005846. https://doi.org/10.1371/journal.ppat.1005846

Flynn, K. J., Baxter, N. T., & Schloss, P. D. (2016). Metabolic and Community Synergy of Oral Bacteria in Colorectal Cancer. *MSphere*, *1*(3), e00102-16. https://doi.org/10.1128/mSphere.00102-16

Force, S. D., Kilgo, P., Neujahr, D. C., Pelaez, A., Pickens, A., Fernandez, F. G., Miller, D. L., & Lawrence, C. (2011). Bilateral Lung Transplantation Offers Better Long-Term Survival, Compared With Single-Lung Transplantation, for Younger Patients With Idiopathic Pulmonary Fibrosis. *The Annals of Thoracic Surgery*, *91*(1), 244–249. https://doi.org/10.1016/j.athoracsur.2010.08.055

Françoise, A., & Héry-Arnaud, G. (2020). The Microbiome in Cystic Fibrosis Pulmonary Disease. *Genes*, *11*(5), 536. https://doi.org/10.3390/genes11050536

Freschi, L., Vincent, A. T., Jeukens, J., Emond-Rheault, J.-G., Kukavica-Ibrulj, I., Dupont, M.-J., Charette, S. J., Boyle, B., & Levesque, R. C. (2019). The Pseudomonas aeruginosa Pan-Genome Provides New Insights on Its Population Structure, Horizontal Gene Transfer, and Pathogenicity. *Genome Biology and Evolution*, *11*(1), 109–120. https://doi.org/10.1093/gbe/evy259

Gipson, I. K., & Argüeso, P. (2003). Role of mucins in the function of the corneal and conjunctival epithelia. *International Review of Cytology*, *231*, 1–49. https://doi.org/10.1016/s0074-7696(03)31001-0

Glen, K. A., & Lamont, I. L. (2021). β-lactam Resistance in Pseudomonas aeruginosa: Current Status, Future Prospects. *Pathogens*, *10*(12), 1638. https://doi.org/10.3390/pathogens10121638

Glover, J. S., Ticer, T. D., & Engevik, M. A. (2022). Characterizing the mucin-degrading capacity of the human gut microbiota. *Scientific Reports*, *12*(1), Article 1. https://doi.org/10.1038/s41598-022-11819-z

Goso, Y., Sugaya, T., Ishihara, K., & Kurihara, M. (2017). Comparison of Methods to Release Mucin-Type O-Glycans for Glycomic Analysis. *Analytical Chemistry*, *89*(17), 8870–8876. https://doi.org/10.1021/acs.analchem.7b01346

Goss, C. H., Newsom, S. A., Schildcrout, J. S., Sheppard, L., & Kaufman, J. D. (2004). Effect of Ambient Air Pollution on Pulmonary Exacerbations and Lung Function in Cystic Fibrosis. *American Journal of Respiratory and Critical Care Medicine*, *169*(7), 816–821. https://doi.org/10.1164/rccm.200306-779OC

Granchelli, A. M., Adler, F. R., Keogh, R. H., Kartsonaki, C., Cox, D. R., & Liou, T. G. (2018). Microbial Interactions in the Cystic Fibrosis Airway. *Journal of Clinical Microbiology*, *56*(8), e00354-18. https://doi.org/10.1128/JCM.00354-18

Grossman, R. F., Frost, A., Zamel, N., Patterson, G. A., Cooper, J. D., Myron, P. R., Dear, C. L., & Maurer, J. (1990). Results of Single-Lung Transplantation for Bilateral Pulmonary Fibrosis. *New England Journal of Medicine*, *322*(11), 727–733. https://doi.org/10.1056/NEJM199003153221104

Gum, J. R., Hicks, J. W., Toribara, N. W., Rothe, E. M., Lagace, R. E., & Kim, Y. S. (1992). The human MUC2 intestinal mucin has cysteine-rich subdomains located both upstream and downstream of its central repetitive region. *Journal of Biological Chemistry*, *267*(30), 21375–21383. https://doi.org/10.1016/S0021-9258(19)36620-7

Gupte, A., Jyot, J., Ravi, M., & Ramphal, R. (2021). High pyocyanin production and non-motility of Pseudomonas aeruginosa isolates are correlated with septic shock or death in bacteremic patients. *PLoS ONE*, *16*(6), e0253259. https://doi.org/10.1371/journal.pone.0253259

Haavik, S., Paulsen, B. S., & Wold, J. K. (1985). Purification of a basic glycoprotein allergen from pollen of timothy by high-performance liquid chromatography. *Journal of Chromatography A*, *321*, 199–208. https://doi.org/10.1016/S0021-9673(01)90436-4

Hahn, A., Burrell, A., Chaney, H., Sami, I., Koumbourlis, A. C., Freishtat, R. J., Zemanick, E. T., Louie, S., & Crandall, K. A. (2021). Importance of beta-lactam pharmacokinetics and pharmacodynamics on the recovery of microbial diversity in the airway of persons with cystic fibrosis. *Journal of Investigative Medicine*, *69*(7), 1350–1359. https://doi.org/10.1136/jim-2021-001824

Hamill, P. G., Stevenson, A., McMullan, P. E., Williams, J. P., Lewis, A. D. R., S, S., Stevenson, K. E., Farnsworth, K. D., Khroustalyova, G., Takemoto, J. Y., Quinn, J. P., Rapoport, A., & Hallsworth, J. E. (2020). Microbial lag phase can be indicative of, or independent from, cellular stress. *Scientific Reports*, *10*(1), Article 1. https://doi.org/10.1038/s41598-020-62552-4

Hang, H. C., & Bertozzi, C. R. (2005). The chemistry and biology of mucin-type O-linked glycosylation. *Bioorganic & Medicinal Chemistry*, *13*(17), 5021–5034. https://doi.org/10.1016/j.bmc.2005.04.085

Hanssens, L. S., Duchateau, J., & Casimir, G. J. (2021). CFTR Protein: Not Just a Chloride Channel? *Cells*, *10*(11), Article 11. https://doi.org/10.3390/cells10112844

Hansson, G. C. (2019). Mucus and mucins in diseases of the intestinal and respiratory tracts. *Journal of Internal Medicine*, *285*(5), 479–490. https://doi.org/10.1111/joim.12910

Herath, M., Hosie, S., Bornstein, J. C., Franks, A. E., & Hill-Yardin, E. L. (2020). The Role of the Gastrointestinal Mucus System in Intestinal Homeostasis: Implications for Neurological Disorders. *Frontiers in Cellular and Infection Microbiology*, *10*. https://www.frontiersin.org/articles/10.3389/fcimb.2020.00248

Hernandez, D., Dias, F. M., & Rowe, J. J. (1991). Nitrate transport and its regulation by O2 in Pseudomonas aeruginosa. *Archives of Biochemistry and Biophysics*, *286*(1), 159–163. https://doi.org/10.1016/0003-9861(91)90022-B

Heyen, S., Scholz-Böttcher, B. M., Rabus, R., & Wilkes, H. (2020). Method development and validation for the quantification of organic acids in microbial samples using anionic exchange solid-phase extraction and gas chromatography-mass spectrometry. *Analytical and Bioanalytical Chemistry*, *412*(27), 7491–7503. https://doi.org/10.1007/s00216-020-02883-3

Hillman, J. D., Dzuback, A. L., & Andrews, S. W. (1987). Colonization of the human oral cavity by a Streptococcus mutans mutant producing increased bacteriocin. *Journal of Dental Research*, *66*(6), 1092–1094. https://doi.org/10.1177/00220345870660060101

Ho, S. B., Dvorak, L. A., Moor, R. E., Jacobson, A. C., Frey, M. R., Corredor, J., Polk, D. B., & Shekels, L. L. (2006). Cysteine-rich domains of muc3 intestinal mucin promote cell migration, inhibit apoptosis, and accelerate wound healing. *Gastroenterology*, *131*(5), 1501–1517. https://doi.org/10.1053/j.gastro.2006.09.006

Hoffman, C. L., Lalsiamthara, J., & Aballay, A. (2020). Host Mucin Is Exploited by Pseudomonas aeruginosa To Provide Monosaccharides Required for a Successful Infection. *MBio*, *11*(2), e00060-20. https://doi.org/10.1128/mBio.00060-20

Hong, P., Koza, S., & Bouvier, E. S. P. (2012). A Review Size-Exclusion Chromatography for the Analysis of Protein Biotherapeutics and Their Aggregates. *Journal of Liquid Chromatography & Related Technologies*, *35*(20), 2923–2950. https://doi.org/10.1080/10826076.2012.743724

Huang, F., Sardari, R. R. R., Jasilionis, A., Böök, O., Öste, R., Rascón, A., Heyman-Lindén, L., Holst, O., & Karlsson, E. N. (2021). Cultivation of the gut bacterium Prevotella copri DSM 18205T using glucose and xylose as carbon sources. *MicrobiologyOpen*, *10*(3), e1213. https://doi.org/10.1002/mbo3.1213

Huffnagle, G. B., Dickson, R. P., & Lukacs, N. W. (2017). The respiratory tract microbiome and lung inflammation: A two-way street. *Mucosal Immunology*, *10*(2), Article 2. https://doi.org/10.1038/mi.2016.108

Hurley, M. N., Ariff, A. H. A., Bertenshaw, C., Bhatt, J., & Smyth, A. R. (2012). Results of antibiotic susceptibility testing do not influence clinical outcome in children with cystic fibrosis. *Journal of Cystic Fibrosis: Official Journal of the European Cystic Fibrosis Society*, *11*(4), 288–292. https://doi.org/10.1016/j.jcf.2012.02.006

Jaggi, K. S., & Gangal, S. V. (1987). Purification and characterization of allergens from Xanthium strumarium pollen. *Molecular and Cellular Biochemistry*, *78*(2), 177–190. https://doi.org/10.1007/BF00229692

Jean-Pierre, F., Hampton, T. H., Schultz, D., Hogan, D. A., Groleau, M.-C., Déziel, E., & O'Toole, G. A. (2023). Community composition shapes microbial-specific phenotypes in a cystic fibrosis polymicrobial model system. *ELife*, *12*, e81604. https://doi.org/10.7554/eLife.81604

Kavanaugh, N. L., Zhang, A. Q., Nobile, C. J., Johnson, A. D., & Ribbeck, K. (2014). Mucins suppress virulence traits of Candida albicans. *MBio*, *5*(6), e01911. https://doi.org/10.1128/mBio.01911-14

Kesimer, M., Kirkham, S., Pickles, R. J., Henderson, A. G., Alexis, N. E., Demaria, G., Knight, D., Thornton, D. J., & Sheehan, J. K. (2009). Tracheobronchial air-liquid interface cell culture: A model for innate mucosal defense of the upper airways? *American Journal of Physiology. Lung Cellular and Molecular Physiology*, *296*(1), L92–L100. https://doi.org/10.1152/ajplung.90388.2008

Kesimer, M., & Sheehan, J. K. (2012). Mass Spectrometric Analysis of Mucin Core Proteins. *Methods in Molecular Biology (Clifton, N.J.)*, *842*, 67–79. https://doi.org/10.1007/978-1-61779-513-8_4

Khanolkar, R. A., Clark, S. T., Wang, P. W., Hwang, D. M., Yau, Y. C. W., Waters, V. J., & Guttman, D. S. (2020). Ecological Succession of Polymicrobial Communities in the Cystic Fibrosis Airways. *MSystems*, *5*(6), e00809-20. https://doi.org/10.1128/mSystems.00809-20

Kim, K. C., McCracken, K., Lee, B. C., Shin, C. Y., Jo, M. J., Lee, C. J., & Ko, K. H. (1997). Airway goblet cell mucin: Its structure and regulation of secretion. *The European Respiratory Journal*, *10*(11), 2644–2649. https://doi.org/10.1183/09031936.97.10112644

Kim, Y. S., Gum, J., & Brockhausen, I. (1996). Mucin glycoproteins in neoplasia. *Glycoconjugate Journal*, *13*(5), 693–707. https://doi.org/10.1007/BF0070233

KOBATA, A. (2013). Exo- and endoglycosidases revisited. *Proceedings of the Japan Academy. Series B, Physical and Biological Sciences*, *89*(3), 97–117. https://doi.org/10.2183/pjab.89.97

König, P., Gayer, D., Barbero, G. J., & Shaffer, J. (1995). Short-term and long-term effects of albuterol aerosol therapy in cystic fibrosis: A preliminary report. *Pediatric Pulmonology*, *20*(4), 205–214. https://doi.org/10.1002/ppul.1950200402

Konstan, M. W., & Ratjen, F. (2012). Effect of dornase alfa on inflammation and lung function: Potential role in the early treatment of cystic fibrosis. *Journal of Cystic Fibrosis*, *11*(2), 78–83. https://doi.org/10.1016/j.jcf.2011.10.003

Kraft, M., Adler, K. B., Ingram, J. L., Crews, A. L., Atkinson, T. P., Cairns, C. B., Krause, D. C., & Chu, H. W. (2008). Mycoplasma pneumoniae induces airway epithelial cell expression of MUC5AC in asthma. *European Respiratory Journal*, *31*(1), 43–46. https://doi.org/10.1183/09031936.00103307

Kurbatova, P., Bessonov, N., Volpert, V., Tiddens, H. a. W. M., Cornu, C., Nony, P., Caudri, D., & CRESim Working Group. (2015). Model of mucociliary clearance in cystic fibrosis lungs. *Journal of Theoretical Biology*, *372*, 81–88. https://doi.org/10.1016/j.jtbi.2015.02.023

Lagow, E., DeSouza, M., & Carson, D. (1999). Mammalian reproductive tract mucins. *Human Reproduction Update*, *5*(4), 280–292. https://doi.org/10.1093/humupd/5.4.280

Landry, R. M., An, D., Hupp, J. T., Singh, P. K., & Parsek, M. R. (2006). Mucin-Pseudomonas aeruginosa interactions promote biofilm formation and antibiotic resistance. *Molecular Microbiology*, *59*(1), 142–151. https://doi.org/10.1111/j.1365-2958.2005.04941.x

Langmead, B., & Salzberg, S. L. (2012). Fast gapped-read alignment with Bowtie 2. *Nature Methods*, *9*(4), 357–359. https://doi.org/10.1038/nmeth.1923

Langton Hewer, S. C., & Smyth, A. R. (2017). Antibiotic strategies for eradicating Pseudomonas aeruginosa in people with cystic fibrosis. *The Cochrane Database of Systematic Reviews*, *2017*(4), CD004197. https://doi.org/10.1002/14651858.CD004197.pub5

Lewis, A. L., & Lewis, W. G. (2012). Host sialoglycans and bacterial sialidases: A mucosal perspective. *Cellular Microbiology*, *14*(8), 1174–1182. https://doi.org/10.1111/j.1462-5822.2012.01807.x

Liessi, N., Pesce, E., Braccia, C., Bertozzi, S. M., Giraudo, A., Bandiera, T., Pedemonte, N., & Armirotti, A. (n.d.). Distinctive lipid signatures of bronchial epithelial cells associated with cystic fibrosis drugs, including Trikafta. *JCI Insight*, *5*(16), e138722. https://doi.org/10.1172/jci.insight.138722

Lin, Y.-C., Cornell, W. C., Jo, J., Price-Whelan, A., & Dietrich, L. E. P. (2018). The Pseudomonas aeruginosa Complement of Lactate Dehydrogenases Enables Use of d- and l-Lactate and Metabolic Cross-Feeding. *MBio*, *9*(5), e00961-18. https://doi.org/10.1128/mBio.00961-18

Lipničanová, S., Chmelová, D., Ondrejovič, M., Frecer, V., & Miertuš, S. (2020). Diversity of sialidases found in the human body – A review. *International Journal of Biological Macromolecules*, *148*, 857–868. https://doi.org/10.1016/j.ijbiomac.2020.01.123

Liu, J., Zhu, W., Qin, N., Ren, X., & Xia, X. (2022). Propionate and Butyrate Inhibit Biofilm Formation of Salmonella Typhimurium Grown in Laboratory Media and Food Models. *Foods*, *11*(21), 3493. https://doi.org/10.3390/foods11213493

Livak, K. J., & Schmittgen, T. D. (2001). Analysis of relative gene expression data using real-time quantitative PCR and the 2(-Delta Delta C(T)) Method. *Methods (San Diego, Calif.)*, *25*(4), 402–408. https://doi.org/10.1006/meth.2001.1262

Lyon, A., & Bilton, D. (2002). Fertility issues in cystic fibrosis. *Paediatric Respiratory Reviews*, *3*(3), 236–240. https://doi.org/10.1016/S1526-0542(02)00184-7

Ma, Y.-X., Wang, C.-Y., Li, Y.-Y., Li, J., Wan, Q.-Q., Chen, J.-H., Tay, F. R., & Niu, L.-N. (2020). Considerations and Caveats in Combating ESKAPE Pathogens against Nosocomial Infections. *Advanced Science*, *7*(1), 1901872. https://doi.org/10.1002/advs.201901872

Madrid, J. F., Ballesta, J., Pastor, L. M., Perez-Tomas, R., & Hernandez, F. (1989). Distribution of mucins in the mucosa of the digestive tract of reptiles: A histochemical study. *Acta Histochemica*, *85*(2), 117-IN1. https://doi.org/10.1016/S0065-1281(89)80053-4

Maeda, Y., Elborn, J. S., Parkins, M. D., Reihill, J., Goldsmith, C. E., Coulter, W. A., Mason, C., Millar, B. C., Dooley, J. S. G., Lowery, C. J., Ennis, M., Rendall, J. C., & Moore, J. E. (2011). Population structure and characterization of viridans group streptococci (VGS) including Streptococcus pneumoniae isolated from adult patients with cystic fibrosis (CF). *Journal of Cystic Fibrosis*, *10*(2), 133–139. https://doi.org/10.1016/j.jcf.2010.11.003

Manchester, K. L. (1996). Use of UV Methods for Measurement of Protein and Nucleic Acid Concentrations. *BioTechniques*, *20*(6), 968–970. https://doi.org/10.2144/96206bm05

Marshall, B. C., Butler, S. M., Stoddard, M., Moran, A. M., Liou, T. G., & Morgan, W. J. (2005). Epidemiology of cystic fibrosis-related diabetes. *The Journal of Pediatrics*, *146*(5), 681–687. https://doi.org/10.1016/j.jpeds.2004.12.039

Marson, F. A. L., Bertuzzo, C. S., & Ribeiro, J. D. (2016). Classification of CFTR mutation classes. *The Lancet Respiratory Medicine*, *4*(8), e37–e38. https://doi.org/10.1016/S2213-2600(16)30188-6

Mavrodi, D. V., Bonsall, R. F., Delaney, S. M., Soule, M. J., Phillips, G., & Thomashow, L. S. (2001). Functional Analysis of Genes for Biosynthesis of Pyocyanin and Phenazine-1-Carboxamide from Pseudomonas aeruginosa PAO1. *Journal of Bacteriology*, *183*(21), 6454–6465. https://doi.org/10.1128/JB.183.21.6454-6465.2001

McCormack, J., Bell, S., Senini, S., Walmsley, K., Patel, K., Wainwright, C., Serisier, D., Harris, M., & Bowler, S. (2007). Daily versus weekly azithromycin in cystic fibrosis patients. *European Respiratory Journal*, *30*(3), 487–495. https://doi.org/10.1183/09031936.00163306

McDermott, M., Cerullo, A. R., Parziale, J., Achrak, E., Sultana, S., Ferd, J., Samad, S., Deng, W., Braunschweig, A. B., & Holford, M. (2021). Advancing Discovery of Snail Mucins Function and Application. *Frontiers in Bioengineering and Biotechnology*, *9*. https://www.frontiersin.org/articles/10.3389/fbioe.2021.734023

McGill, S. L., Yung, Y., Hunt, K. A., Henson, M. A., Hanley, L., & Carlson, R. P. (2021). Pseudomonas aeruginosa reverse diauxie is a multidimensional, optimized, resource utilization strategy. *Scientific Reports*, *11*, 1457. https://doi.org/10.1038/s41598-020-80522-8

McGuckin, M. A., Lindén, S. K., Sutton, P., & Florin, T. H. (2011). Mucin dynamics and enteric pathogens. *Nature Reviews. Microbiology*, *9*(4), 265–278. https://doi.org/10.1038/nrmicro2538

McGuigan, C. F., & Li, X.-F. (2014). Cytotoxicity and genotoxicity of phenazine in two human cell lines. *Toxicology in Vitro: An International Journal Published in Association with BIBRA*, *28*(4), 607–615. https://doi.org/10.1016/j.tiv.2013.12.007

Meskini, M., Siadat, S. D., Seifi, S., Movafagh, A., & Sheikhpour, M. (2021). An Overview on the Upper and Lower Airway Microbiome in Cystic Fibrosis Patients. *Tanaffos*, *20*(2), 86–98.

Meyer, J. M. (2000). Pyoverdines: Pigments, siderophores and potential taxonomic markers of fluorescent Pseudomonas species. *Archives of Microbiology*, *174*(3), 135–142. https://doi.org/10.1007/s002030000188

Mirković, B., Murray, M. A., Lavelle, G. M., Molloy, K., Azim, A. A., Gunaratnam, C., Healy, F., Slattery, D., McNally, P., Hatch, J., Wolfgang, M., Tunney, M. M., Muhlebach, M. S., Devery, R., Greene, C. M., & McElvaney, N. G. (2015). The Role of Short-Chain Fatty Acids, Produced by Anaerobic Bacteria, in the Cystic Fibrosis Airway. *American Journal of Respiratory and Critical Care Medicine*, *192*(11), 1314–1324. https://doi.org/10.1164/rccm.201505-0943OC

Moestedt, J., Müller, B., Nagavara Nagaraj, Y., & Schnürer, A. (2020). Acetate and Lactate Production During Two-Stage Anaerobic Digestion of Food Waste Driven by Lactobacillus and Aeriscardovia. *Frontiers in Energy Research*, *8*. https://www.frontiersin.org/articles/10.3389/fenrg.2020.00105

Moros, G., Chatziioannou, A. C., Gika, H. G., Raikos, N., & Theodoridis, G. (2017). Investigation of the derivatization conditions for GC-MS metabolomics of biological samples. *Bioanalysis*, *9*(1), 53–65. https://doi.org/10.4155/bio-2016-0224

Morrison, C. B., Markovetz, M. R., & Ehre, C. (2019). Mucus, Mucins and Cystic Fibrosis. *Pediatric Pulmonology*, *54*(Suppl 3), S84–S96. https://doi.org/10.1002/ppul.24530

Morrison, L., & Milroy, S. (2020). Oscillating devices for airway clearance in people with cystic fibrosis. *Cochrane Database of Systematic Reviews*, *4*. https://doi.org/10.1002/14651858.CD006842.pub5

Munkholm, M., & Mortensen, J. (2014). Mucociliary clearance: Pathophysiological aspects. *Clinical Physiology and Functional Imaging*, *34*(3), 171–177. https://doi.org/10.1111/cpf.12085

Najafi, M., Nakhaei Moghaddam, M., & Yousefi, E. (2021). The Effect of Silver Nanoparticles on Pyocyanin Production of Pseudomonas aeruginosa Isolated From Clinical Specimens. *Avicenna Journal of Medical Biotechnology*, *13*(2), 98–103. https://doi.org/10.18502/ajmb.v13i2.5529

Navarro, S. (2016). Historical compilation of cystic fibrosis. *Gastroenterología y Hepatología (English Edition)*, *39*(1), 36–42. https://doi.org/10.1016/j.gastre.2015.12.006

Nelson, C. E., Huang, W., Brewer, L. K., Nguyen, A. T., Kane, M. A., Wilks, A., & Oglesby-Sherrouse, A. G. (2019). Proteomic Analysis of the Pseudomonas aeruginosa Iron Starvation Response Reveals PrrF Small Regulatory RNA-Dependent Iron Regulation of Twitching Motility, Amino Acid Metabolism, and Zinc Homeostasis Proteins. *Journal of Bacteriology*, *201*(12), 10.1128/jb.00754-18. https://doi.org/10.1128/jb.00754-18

Ng, S. K. C., & Hamilton, I. R. (1971). Lactate Metabolism by Veillonella parvula. *Journal of Bacteriology*, *105*(3), 999–1005. https://doi.org/10.1128/jb.105.3.999-1005.1971

Nobbs, A. H., Lamont, R. J., & Jenkinson, H. F. (2009). Streptococcus Adherence and Colonization. *Microbiology and Molecular Biology Reviews : MMBR*, *73*(3), 407–450. https://doi.org/10.1128/MMBR.00014-09

Nordmann, P., Ronco, E., Naas, T., Duport, C., Michel-Briand, Y., & Labia, R. (1993). Characterization of a novel extended-spectrum beta-lactamase from Pseudomonas aeruginosa. *Antimicrobial Agents and Chemotherapy*, *37*(5), 962–969. https://doi.org/10.1128/aac.37.5.962

Ogawa, A. T., Brasil de Souza, T. de A. C., de Uzeda, M., Jankevicius, J. V., & Jankevicius, S. I. (2006). Characterization of proteolytic activities of Fusobacterium nucleatum. *Journal of Endodontics*, *32*(6), 521–523. https://doi.org/10.1016/j.joen.2005.10.045

Okuda, K., Chen, G., Subramani, D. B., Wolf, M., Gilmore, R. C., Kato, T., Radicioni, G., Kesimer, M., Chua, M., Dang, H., Livraghi-Butrico, A., Ehre, C., Doerschuk, C. M., Randell, S. H., Matsui, H., Nagase, T., O'Neal, W. K., & Boucher, R. C. (2019). Localization of Secretory Mucins MUC5AC and MUC5B in Normal/Healthy Human Airways. *American Journal of Respiratory and Critical Care Medicine*, *199*(6), 715–727. https://doi.org/10.1164/rccm.201804-0734OC

O'Toole, G. A. (2011). Microtiter Dish Biofilm Formation Assay. *Journal of Visualized Experiments : JoVE*, *47*, 2437. https://doi.org/10.3791/2437

Ozdal, M. (2019). A new strategy for the efficient production of pyocyanin, a versatile pigment, in Pseudomonas aeruginosa OG1 via toluene addition. *3 Biotech*, *9*(10), 374. https://doi.org/10.1007/s13205-019-1907-1

Palmer, K. L., Mashburn, L. M., Singh, P. K., & Whiteley, M. (2005). Cystic Fibrosis Sputum Supports Growth and Cues Key Aspects of Pseudomonas aeruginosa Physiology. *Journal of Bacteriology*, *187*(15), 5267–5277. https://doi.org/10.1128/JB.187.15.5267-5277.2005

Pang, Z., Raudonis, R., Glick, B. R., Lin, T.-J., & Cheng, Z. (2019). Antibiotic resistance in Pseudomonas aeruginosa: Mechanisms and alternative therapeutic strategies. *Biotechnology Advances*, *37*(1), 177–192. https://doi.org/10.1016/j.biotechadv.2018.11.013

Patterson, M. J. (1996). Streptococcus. In S. Baron (Ed.), *Medical Microbiology* (4th ed.). University of Texas Medical Branch at Galveston. http://www.ncbi.nlm.nih.gov/books/NBK7611/

Pedersen, R. M., Holt, H. M., & Justesen, U. S. (2011). Solobacterium moorei Bacteremia: Identification, Antimicrobial Susceptibility, and Clinical Characteristics ▿ . *Journal of Clinical Microbiology*, *49*(7), 2766–2768. https://doi.org/10.1128/JCM.02525-10

Pencharz, P. B., & Durie, P. R. (2000). Pathogenesis of malnutrition in cystic fibrosis, and its treatment. *Clinical Nutrition*, *19*(6), 387–394. https://doi.org/10.1054/clnu.1999.0079

Pereira-Marques, J., Hout, A., Ferreira, R. M., Weber, M., Pinto-Ribeiro, I., van Doorn, L.-J., Knetsch, C. W., & Figueiredo, C. (2019). Impact of Host DNA and Sequencing Depth on the Taxonomic Resolution of Whole Metagenome Sequencing for Microbiome Analysis. *Frontiers in Microbiology*, *10*. https://www.frontiersin.org/articles/10.3389/fmicb.2019.01277

Pérez-Sánchez, J., Estensoro, I., Redondo, M. J., Calduch-Giner, J. A., Kaushik, S., & Sitjà-Bobadilla, A. (2013). Mucins as Diagnostic and Prognostic Biomarkers in a Fish-Parasite Model: Transcriptional and Functional Analysis. *PLOS ONE*, *8*(6), e65457. https://doi.org/10.1371/journal.pone.0065457

Petrova, O. E., & Sauer, K. (2012). Sticky Situations: Key Components That Control Bacterial Surface Attachment. *Journal of Bacteriology*, *194*(10), 2413–2425. https://doi.org/10.1128/JB.00003-12

Pittman, J. E., Calloway, E. H., Kiser, M., Yeatts, J., Davis, S. D., Drumm, M. L., Schechter, M. S., Leigh, M. W., Emond, M., Van Rie, A., & Knowles, M. R. (2011). Age of Pseudomonas aeruginosa Acquisition and Subsequent Severity of Cystic Fibrosis Lung Disease. *Pediatric Pulmonology*, *46*(5), 497–504. https://doi.org/10.1002/ppul.21397

Pustelny, C., Komor, U., Pawar, V., Lorenz, A., Bielecka, A., Moter, A., Gocht, B., Eckweiler, D., Müsken, M., Grothe, C., Lünsdorf, H., Weiss, S., & Häussler, S. (2014). Contribution of Veillonella parvula to Pseudomonas aeruginosa-Mediated Pathogenicity in a Murine Tumor Model System. *Infection and Immunity*, *83*(1), 417–429. https://doi.org/10.1128/iai.02234-14

Razvi, S., Quittell, L., Sewall, A., Quinton, H., Marshall, B., & Saiman, L. (2009). Respiratory microbiology of patients with cystic fibrosis in the United States, 1995 to 2005. *Chest*, *136*(6), 1554–1560. https://doi.org/10.1378/chest.09-0132

Reid, D. W., Latham, R., Lamont, I. L., Camara, M., & Roddam, L. F. (2013). Molecular analysis of changes in Pseudomonas aeruginosa load during treatment of a pulmonary exacerbation in cystic fibrosis. *Journal of Cystic Fibrosis: Official Journal of the European Cystic Fibrosis Society*, *12*(6), 688–699. https://doi.org/10.1016/j.jcf.2013.03.008

Robinson, M., & Bye, P. T. B. (2002). Mucociliary clearance in cystic fibrosis. *Pediatric Pulmonology*, *33*(4), 293–306. https://doi.org/10.1002/ppul.10079

Rogosa, M. (1964). The genus veillonella i. *Journal of Bacteriology*, *87*(1), 162–170. https://doi.org/10.1128/jb.87.1.162-170.1964

Rojas-Tapias, D. F., Brown, E. M., Temple, E. R., Onyekaba, M. A., Mohamed, A. M. T., Duncan, K., Schirmer, M., Walker, R. L., Mayassi, T., Pierce, K. A., Ávila-Pacheco, J., Clish, C. B., Vlamakis, H., & Xavier, R. J. (2022). Inflammation-associated nitrate facilitates ectopic colonization of oral bacterium Veillonella parvula in the intestine. *Nature Microbiology*, *7*(10), Article 10. https://doi.org/10.1038/s41564-022-01224-7

Rolfe, M. D., Rice, C. J., Lucchini, S., Pin, C., Thompson, A., Cameron, A. D. S., Alston, M., Stringer, M. F., Betts, R. P., Baranyi, J., Peck, M. W., & Hinton, J. C. D. (2012). Lag Phase Is a Distinct Growth Phase That Prepares Bacteria for Exponential Growth and Involves Transient Metal Accumulation. *Journal of Bacteriology*, *194*(3), 686–701. https://doi.org/10.1128/JB.06112-11

Rose, M. C., & Voynow, J. A. (2006). Respiratory Tract Mucin Genes and Mucin Glycoproteins in Health and Disease. *Physiological Reviews*, *86*(1), 245–278. https://doi.org/10.1152/physrev.00010.2005

Rouillard, K. R., Kissner, W. J., Markovetz, M. R., & Hill, D. B. (2022). Effects of Mucin and DNA Concentrations in Airway Mucus on Pseudomonas aeruginosa Biofilm Recalcitrance. *MSphere*, *7*(4), e0029122. https://doi.org/10.1128/msphere.00291-22

Rowe, S. M., Zuckerman, J. B., Dorgan, D., Lascano, J., McCoy, K., Jain, M., Schechter, M. S., Lommatzsch, S., Indihar, V., Lechtzin, N., McBennett, K., Callison, C., Brown, C., Liou, T. G., MacDonald, K. D., Nasr, S. Z., Bodie, S., Vaughn, M., Meltzer, E. B., & Barbier, A. J. (2023). Inhaled mRNA therapy for treatment of cystic fibrosis: Interim results of a randomized, double-blind, placebo-controlled phase 1/2 clinical study. *Journal of Cystic Fibrosis*. https://doi.org/10.1016/j.jcf.2023.04.008

Rowntree, R. K., & Harris, A. (2003). The Phenotypic Consequences of CFTR Mutations. *Annals of Human Genetics*, *67*(5), 471–485. https://doi.org/10.1046/j.1469-1809.2003.00028.x

Sakanaka, A., Kuboniwa, M., Shimma, S., Alghamdi, S. A., Mayumi, S., Lamont, R. J., Fukusaki, E., & Amano, A. (2022). Fusobacterium nucleatum Metabolically Integrates Commensals and Pathogens in Oral Biofilms. *MSystems*, *7*(4), e00170-22. https://doi.org/10.1128/msystems.00170-22

Salgar-Chaparro, S. J., Lepkova, K., Pojtanabuntoeng, T., Darwin, A., & Machuca, L. L. (2020). Nutrient Level Determines Biofilm Characteristics and Subsequent Impact on Microbial Corrosion and Biocide Effectiveness. *Applied and Environmental Microbiology*, *86*(7), e02885-19. https://doi.org/10.1128/AEM.02885-19

Sanders, D. B., Bittner, R. CL., Rosenfeld, M., Redding, G. J., & Goss, C. H. (2011). Pulmonary exacerbations are associated with subsequent FEV1 decline in both adults and children with cystic fibrosis. *Pediatric Pulmonology*, *46*(4), 393–400. https://doi.org/10.1002/ppul.21374

Schoemig, V., Isik, E., Martin, L., & Berensmeier, S. (2017). Solid liquid liquid extraction of porcine gastric mucins from homogenized animal material. *RSC Advances*, *7*(63), 39708–39717. https://doi.org/10.1039/C7RA06594A

Schultz, J. E., & Breznak, J. A. (1979). Cross-Feeding of Lactate Between Streptococcus lactis and Bacteroides sp. Isolated from Termite Hindguts. *Applied and Environmental Microbiology*, *37*(6), 1206–1210. https://doi.org/10.1128/aem.37.6.1206-1210.1979

Scotet, V., Duguépéroux, I., Saliou, P., Rault, G., Roussey, M., Audrézet, M.-P., & Férec, C. (2012). Evidence for decline in the incidence of cystic fibrosis: A 35-year observational study in Brittany, France. *Orphanet Journal of Rare Diseases*, *7*, 14. https://doi.org/10.1186/1750-1172-7-14

Scott, J. E., & O'Toole, G. A. (2019). The Yin and Yang of Streptococcus Lung Infections in Cystic Fibrosis: A Model for Studying Polymicrobial Interactions. *Journal of Bacteriology*, *201*(11), e00115-19. https://doi.org/10.1128/JB.00115-19

Scott-Jupp, R., Lama, M., & Tanner, M. S. (1991). Prevalence of liver disease in cystic fibrosis. *Archives of Disease in Childhood*, *66*(6), 698–701. https://doi.org/10.1136/adc.66.6.698

Sellers, L. A., & Allen, A. (1989). Gastrointestinal mucus gel rheology. *Symposia of the Society for Experimental Biology*, *43*, 65–71.

Sheng, Y. H., & Hasnain, S. Z. (2022). Mucus and Mucins: The Underappreciated Host Defence System. *Frontiers in Cellular and Infection Microbiology*, *12*, 856962. https://doi.org/10.3389/fcimb.2022.856962

Shteinberg, M., Haq, I. J., Polineni, D., & Davies, J. C. (2021). Cystic fibrosis. *Lancet (London, England)*, *397*(10290), 2195–2211. https://doi.org/10.1016/S0140-6736(20)32542-3

Smith, A. L., Fiel, S. B., Mayer-Hamblett, N., Ramsey, B., & Burns, J. L. (2003). Susceptibility testing of Pseudomonas aeruginosa isolates and clinical response to parenteral antibiotic administration: Lack of association in cystic fibrosis. *Chest*, *123*(5), 1495–1502. https://doi.org/10.1378/chest.123.5.1495

Song, D., Cahn, D., & Duncan, G. A. (2020). Mucin Biopolymers and Their Barrier Function at Airway Surfaces. *Langmuir: The ACS Journal of Surfaces and Colloids*, *36*(43), 12773–12783. https://doi.org/10.1021/acs.langmuir.0c02410

Sriramulu, D. D., Lünsdorf, H., Lam, J. S., & Römling, U. (2005). Microcolony formation: A novel biofilm model of Pseudomonas aeruginosa for the cystic fibrosis lung. *Journal of Medical Microbiology*, *54*(7), 667–676. https://doi.org/10.1099/jmm.0.45969-0

Steffen, K. (2018). *Find your filter. What's best for your process?* https://www.slideshare.net/MilliporeSigma/find-your-filter-whats-best-for-your-process-125259240

Steinberg, D., Poran, S., & Shapira, L. (1999). The effect of extracellular polysaccharides from Streptococcus mutans on the bactericidal activity of human neutrophils. *Archives of Oral Biology*, *44*(5), 437–444. https://doi.org/10.1016/s0003-9969(99)00014-x

Strauss, J., White, A., Ambrose, C., McDonald, J., & Allen-Vercoe, E. (2008). Phenotypic and genotypic analyses of clinical Fusobacterium nucleatum and Fusobacterium periodonticum isolates from the human gut. *Anaerobe*, *14*(6), 301–309. https://doi.org/10.1016/j.anaerobe.2008.12.003

Takagi, J., Aoki, K., Turner, B. S., Lamont, S., Lehoux, S., Kavanaugh, N., Gulati, M., Valle Arevalo, A., Lawrence, T. J., Kim, C. Y., Bakshi, B., Ishihara, M., Nobile, C. J., Cummings, R. D., Wozniak, D. J., Tiemeyer, M., Hevey, R., & Ribbeck, K. (2022). Mucin O-glycans are natural inhibitors of Candida albicans pathogenicity. *Nature Chemical Biology*, *18*(7), Article 7. https://doi.org/10.1038/s41589-022-01035-1

Taylor, P. K., Yeung, A. T. Y., & Hancock, R. E. W. (2014). Antibiotic resistance in Pseudomonas aeruginosa biofilms: Towards the development of novel anti-biofilm therapies. *Journal of Biotechnology*, *191*, 121–130. https://doi.org/10.1016/j.jbiotec.2014.09.003

Taylor-Robinson, D., Whitehead, M., Diderichsen, F., Olesen, H. V., Pressler, T., Smyth, R. L., & Diggle, P. (2012). Understanding the natural progression in %FEV1 decline in patients with cystic fibrosis: A longitudinal study. *Thorax*, *67*(10), 860–866. https://doi.org/10.1136/thoraxjnl-2011-200953

Tett, A., Pasolli, E., Masetti, G., Ercolini, D., & Segata, N. (2021). Prevotella diversity, niches and interactions with the human host. *Nature Reviews Microbiology*, *19*(9), Article 9. https://doi.org/10.1038/s41579-021-00559-y

Thermo Fischer Scientific. (2009). Product Manual for Acclaim Organic Acid (OA). Jul 28; Doc No. 031996-02. Available from: https://tools.thermofisher.com/content/sfs/manuals/41786-Man-031996-02-Acclaim-OA-Jul09.pdf

Tildy, B. E., & Rogers, D. F. (2015). Therapeutic Options for Hydrating Airway Mucus in Cystic Fibrosis. *Pharmacology*, *95*(3–4), 117–132. https://doi.org/10.1159/000377638

Tony-Odigie, A., Wilke, L., Boutin, S., Dalpke, A. H., & Yi, B. (2022). Commensal Bacteria in the Cystic Fibrosis Airway Microbiome Reduce P. aeruginosa Induced Inflammation. *Frontiers in Cellular and Infection Microbiology*, *12*. https://www.frontiersin.org/articles/10.3389/fcimb.2022.824101

Truong, D. T., Franzosa, E. A., Tickle, T. L., Scholz, M., Weingart, G., Pasolli, E., Tett, A., Huttenhower, C., & Segata, N. (2015). MetaPhlAn2 for enhanced metagenomic taxonomic profiling. *Nature Methods*, *12*(10), Article 10. https://doi.org/10.1038/nmeth.3589

Tuon, F. F., Dantas, L. R., Suss, P. H., & Tasca Ribeiro, V. S. (2022). Pathogenesis of the Pseudomonas aeruginosa Biofilm: A Review. *Pathogens*, *11*(3), Article 3. https://doi.org/10.3390/pathogens11030300

Understanding Changes in Life Expectancy | Cystic Fibrosis Foundation. (n.d.). Retrieved May 3, 2023, from https://www.cff.org/managing-cf/understanding-changes-life-expectancy

Van der Hoeven, J. S., & Camp, P. J. (1991). Synergistic degradation of mucin by Streptococcus oralis and Streptococcus sanguis in mixed chemostat cultures. *Journal of Dental Research*, *70*(7), 1041–1044. https://doi.org/10.1177/00220345910700070401

Van Gool, K., Norman, R., Delatycki, M. B., Hall, J., & Massie, J. (2013). Understanding the Costs of Care for Cystic Fibrosis: An Analysis by Age and Health State. *Value in Health*, *16*(2), 345–355. https://doi.org/10.1016/j.jval.2012.12.003

Vandenbergh, P. A. (1993). Lactic acid bacteria, their metabolic products and interference with microbial growth. *FEMS Microbiology Reviews*, *12*(1–3), 221–237. https://doi.org/10.1111/j.1574-6976.1993.tb00020.x

Varki, A. (2017). Biological roles of glycans. *Glycobiology*, *27*(1), 3–49. https://doi.org/10.1093/glycob/cww086

Ventura, M., Turroni, F., Zomer, A., Foroni, E., Giubellini, V., Bottacini, F., Canchaya, C., Claesson, M. J., He, F., Mantzourani, M., Mulas, L., Ferrarini, A., Gao, B., Delledonne, M., Henrissat, B., Coutinho, P., Oggioni, M., Gupta, R. S., Zhang, Z., … Sinderen, D. van. (2009). The Bifidobacterium dentium Bd1 Genome Sequence Reflects Its Genetic Adaptation to the Human Oral Cavity. *PLOS Genetics*, *5*(12), e1000785. https://doi.org/10.1371/journal.pgen.1000785

Venturi, V. (2006). Regulation of quorum sensing in Pseudomonas. *FEMS Microbiology Reviews*, *30*(2), 274–291. https://doi.org/10.1111/j.1574-6976.2005.00012.x

Wang, B. X., Takagi, J., McShane, A., Park, J. H., Aoki, K., Griffin, C., Teschler, J., Kitts, G., Minzer, G., Tiemeyer, M., Hevey, R., Yildiz, F., & Ribbeck, K. (2023). Host-derived O-glycans inhibit toxigenic conversion by a virulence-encoding phage in Vibrio cholerae. *The EMBO Journal*, *42*(3), e111562. https://doi.org/10.15252/embj.2022111562

Wang, S., Liu, Y., Li, J., Zhao, L., Yan, W., Lin, B., Guo, X., & Wei, Y. (2021). Fusobacterium nucleatum Acts as a Pro-carcinogenic Bacterium in Colorectal Cancer: From Association to Causality. *Frontiers in Cell and Developmental Biology*, *9*, 710165. https://doi.org/10.3389/fcell.2021.710165

Wang, Y., Wilks, J. C., Danhorn, T., Ramos, I., Croal, L., & Newman, D. K. (2011). Phenazine-1-Carboxylic Acid Promotes Bacterial Biofilm Development via Ferrous Iron Acquisition ▿ . *Journal of Bacteriology*, *193*(14), 3606–3617. https://doi.org/10.1128/JB.00396-11

Wang, Y., Wu, J., Lv, M., Shao, Z., Hungwe, M., Wang, J., Bai, X., Xie, J., Wang, Y., & Geng, W. (2021). Metabolism Characteristics of Lactic Acid Bacteria and the Expanding Applications in Food Industry. *Frontiers in Bioengineering and Biotechnology*, *9*, 612285. https://doi.org/10.3389/fbioe.2021.612285

Wanner, A., Salathé, M., & O'Riordan, T. G. (1996). Mucociliary clearance in the airways. *American Journal of Respiratory and Critical Care Medicine*, *154*(6 Pt 1), 1868–1902. https://doi.org/10.1164/ajrccm.154.6.8970383

Waters, V. J., Kidd, T. J., Canton, R., Ekkelenkamp, M. B., Johansen, H. K., LiPuma, J. J., Bell, S. C., Elborn, J. S., Flume, P. A., VanDevanter, D. R., Gilligan, P., & Antimicrobial Resistance International Working Group in Cystic Fibrosis. (2019). Reconciling Antimicrobial Susceptibility Testing and Clinical Response in Antimicrobial Treatment of Chronic Cystic Fibrosis Lung Infections. *Clinical Infectious Diseases: An Official Publication of the Infectious Diseases Society of America*, *69*(10), 1812–1816. https://doi.org/10.1093/cid/ciz364

Westbrock-Wadman, S., Sherman, D. R., Hickey, M. J., Coulter, S. N., Zhu, Y. Q., Warrener, P., Nguyen, L. Y., Shawar, R. M., Folger, K. R., & Stover, C. K. (1999). Characterization of a Pseudomonas aeruginosa Efflux Pump Contributing to Aminoglycoside Impermeability. *Antimicrobial Agents and Chemotherapy*, *43*(12), 2975–2983. https://doi.org/10.1128/aac.43.12.2975

Wheeler, K. M., Cárcamo-Oyarce, G., Turner, B. S., Dellos-Nolan, S., Co, J. Y., Lehoux, S., Cummings, R. D., Wozniak, D. J., & Ribbeck, K. (2019). Mucin glycans attenuate the virulence of Pseudomonas aeruginosa in infection. *Nature Microbiology*, *4*(12), 2146–2154. https://doi.org/10.1038/s41564-019-0581-8

Whelan, F. J., & Surette, M. G. (2015). Clinical Insights into Pulmonary Exacerbations in Cystic Fibrosis from the Microbiome. What Are We Missing? *Annals of the American Thoracic Society*, *12 Suppl 2*, S207-211. https://doi.org/10.1513/AnnalsATS.201506-353AW

Wicaksono, D. P., Washio, J., Abiko, Y., Domon, H., & Takahashi, N. (2020). Nitrite Production from Nitrate and Its Link with Lactate Metabolism in Oral Veillonella spp. *Applied and Environmental Microbiology*, *86*(20), e01255-20. https://doi.org/10.1128/AEM.01255-20

Wickström, C., Herzberg, M. C., Beighton, D., & Svensäter, G. (2009). Proteolytic degradation of human salivary MUC5B by dental biofilms. *Microbiology*, *155*(Pt 9), 2866–2872. https://doi.org/10.1099/mic.0.030536-0

Wood, M. E., Stockwell, R. E., Johnson, G. R., Ramsay, K. A., Sherrard, L. J., Kidd, T. J., Cheney, J., Ballard, E. L., O'Rourke, P., Jabbour, N., Wainwright, C. E., Knibbs, L. D., Sly, P. D., Morawska, L., & Bell, S. C. (2019). Cystic fibrosis pathogens survive for extended periods within cough-generated droplet nuclei. *Thorax*, *74*(1), 87–90. https://doi.org/10.1136/thoraxjnl-2018-211567

Worlitzsch, D., Tarran, R., Ulrich, M., Schwab, U., Cekici, A., Meyer, K. C., Birrer, P., Bellon, G., Berger, J., Weiss, T., Botzenhart, K., Yankaskas, J. R., Randell, S., Boucher, R. C., & Döring, G. (2002). Effects of reduced mucus oxygen concentration in airway Pseudomonas infections of cystic fibrosis patients. *The Journal of Clinical Investigation*, *109*(3), 317–325. https://doi.org/10.1172/JCI13870

Yu, Y., Cheng, A. S., Wang, L., Dunne, W. M., & Bayliss, S. J. (2007). Hot tub folliculitis or hot hand–foot syndrome caused by Pseudomonas aeruginosa. *Journal of the American Academy of Dermatology*, *57*(4), 596–600. https://doi.org/10.1016/j.jaad.2007.04.004

Yung, Y. P., McGill, S. L., Chen, H., Park, H., Carlson, R. P., & Hanley, L. (2019). Reverse diauxie phenotype in Pseudomonas aeruginosa biofilm revealed by exometabolomics and label-free proteomics. *Npj Biofilms and Microbiomes*, *5*(1), Article 1. https://doi.org/10.1038/s41522-019-0104-7

Zaher, A., ElSaygh, J., Elsori, D., ElSaygh, H., & Sanni, A. (2021). A Review of Trikafta: Triple Cystic Fibrosis Transmembrane Conductance Regulator (CFTR) Modulator Therapy. *Cureus*. https://doi.org/10.7759/cureus.1614

Zemanick, E., Burgel, P.-R., Taccetti, G., Holmes, A., Ratjen, F., Byrnes, C. A., Waters, V. J., Bell, S. C., VanDevanter, D. R., Stuart Elborn, J., Flume, P. A., & Antimicrobial Resistance International Working Group in Cystic Fibrosis. (2020). Antimicrobial resistance in cystic fibrosis: A Delphi approach to defining best practices. *Journal of Cystic Fibrosis: Official Journal of the European Cystic Fibrosis Society*, *19*(3), 370–375. https://doi.org/10.1016/j.jcf.2019.10.006

Zhan, Z., Liu, W., Pan, L., Bao, Y., Yan, Z., & Hong, L. (2022). Overabundance of Veillonella parvula promotes intestinal inflammation by activating macrophages via LPS-TLR4 pathway. *Cell Death Discovery*, *8*(1), Article 1. https://doi.org/10.1038/s41420-022-01015-3

Zhu, W., Gao, J., Liu, H., Liu, J., Jin, T., Qin, N., Ren, X., & xia, X. (2022). Antibiofilm effect of sodium butyrate against Vibrio parahaemolyticus. *Food Control*, *131*, 1 08422. https://doi.org/10.1016/j.foodcont.2021.108422

APPENDICIES

Appendix A: Draft Genome Sequence of *Scheffersomyces spartinae* ARV011, a Marine Yeast

† Reprinted from *Journal of Medical Microbiology*. **Alex R. Villarreal**, Danielle E. Campbell, Shanice S. Webster, Ryan C. Hunter. “Draft Genome Sequence of *Scheffersomyces spartinae* ARV011, a Marine Yeast” © American Society for Microbiology. Originally published in *Microbiology Resource Announcements* 2021 Novermber 11;10(45):e0065221. DOI: https://doi.org/10.1128/MRA.00652-21

Abstract

We report the draft genome sequence of *Scheffersomyces spartinae* ARV011, which was isolated from the Great Sippewissett Marsh in Falmouth, Massachusetts. Sequencing was performed using the Illumina NovaSeq 6000 platform, yielding 7,598,030 read pairs 250 bp in length. This resulted in a total draft genome size of 12,132,557 bp.

Announcement

Previously assigned to the genus *Pichia* on the basis of phenotypic traits such as the ability to form ascospores, the species *spartinae* was assigned to its current genus *Scheffersomyces* in 2010 after large-subunit (LSU) rRNA (D1/D2) and small-subunit (SSU) rRNA gene sequencing provided support for its reassignment (1). Assignment of *Scheffersomyces spartinae* to its current genus remains controversial because of poor bootstrap support and, unlike other members of the genus, its inability to efficiently ferment d-xylose to ethanol (1, 2). However, *S. spartinae* is known to produce coenzyme Q9, fostering interest in the species for its potential biotechnological applications (1). The lack of sequenced *S. spartinae* genomes has limited progress in this area.

S. spartinae ARV011 was isolated from marine water and sediment collected from the Great Sippewissett Marsh in Falmouth, Massachusetts. The sample was composed of brackish water, sediment, plant matter, and macroscopic photosynthetic microbial aggregates known as “pink berries” (3). Microbial enrichment from this sediment was performed using yeast extract-peptone-dextrose (YPD) broth containing antibiotics (11 µg/ml carbenicillin, 25 µg/ml chloramphenicol, and 10 µg/ml tetracycline), with incubation at 30°C for 48 h prior to culture on YPD agar. An isolate of interest, based on the microscopic appearance of enlarged vacuoles containing fast moving volutin or “dancing bodies” (4) (**Fig. 1**), was selected for further characterization. Following overnight culture in YPD medium, genomic DNA was extracted using the Quick-DNA bacterial/fungal miniprep kit (Zymogen). Initial identification of the isolate as *S.*

spartinae was performed by Sanger sequencing of the internal transcribed spacer (ITS) region using the primer set ITS1-30F/ITS1-217R (5) and analysis via BLASTn against the standard nonredundant nucleotide database (6). Both the forward and reverse sequences best matched the same *S. spartinae* ITS and ribosomal subunit sequence (GenBank accession number KY105354.1), with the forward and reverse sequences exhibiting 98.94% and 99.20% identity, respectively. The same DNA extract was used to prepare a paired-end Illumina library using the TruSeq DNA PCR-free kit. Sequencing was performed using the Illumina NovaSeq 6000 platform, yielding 7,598,030 read pairs. Quality control was completed using KneadData v0.7.6 (https://github.com/biobakery/kneaddata), a wrapper for FastQC (7), Trimmomatic (8), and Bowtie2 (9), all with default settings. After quality control, 6,975,482 high-quality read pairs remained.

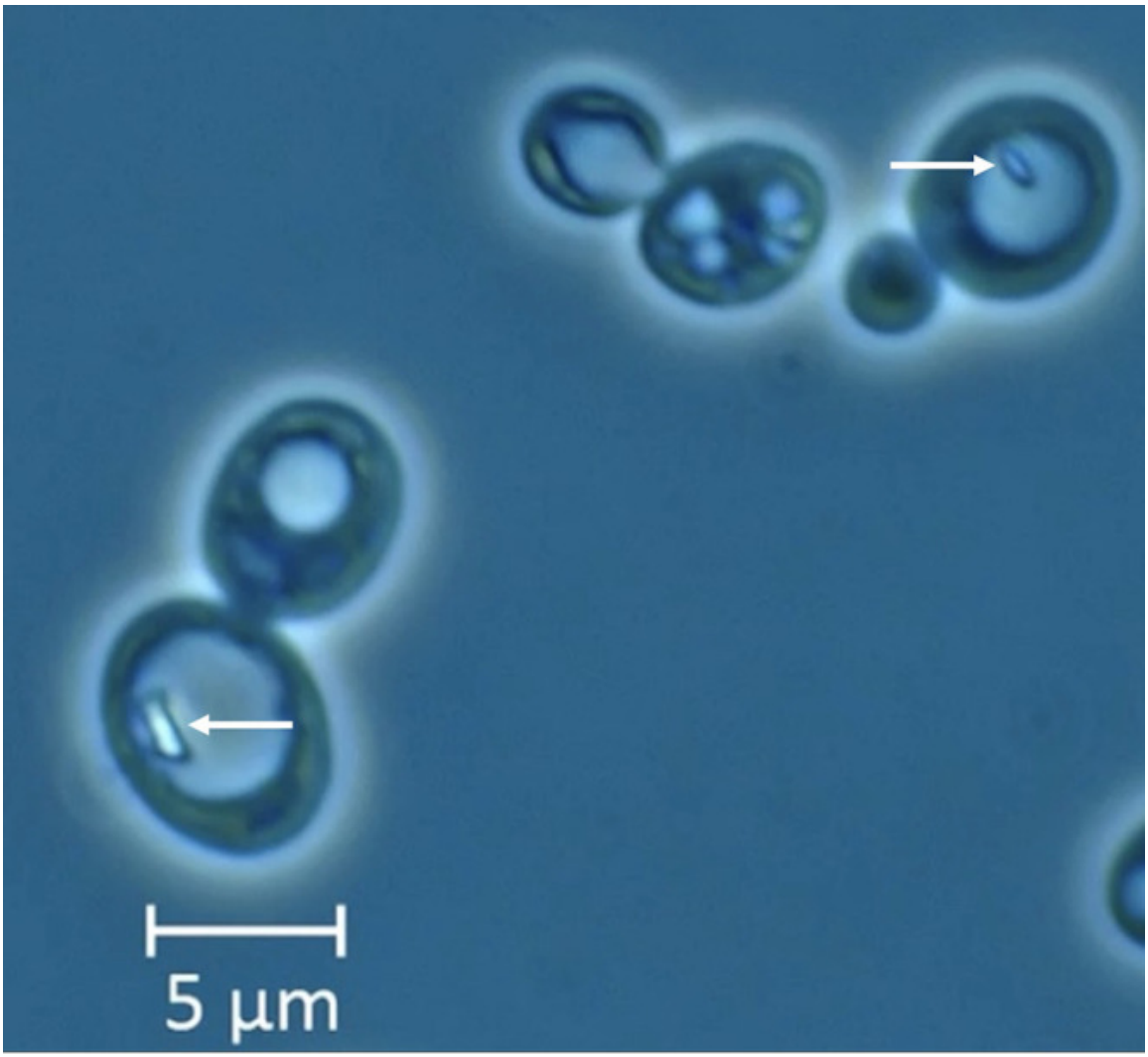

Figure 1 – Bright-field microscopy of isolate ARV011 at x1,000 magnification. Yeast isolate cells ranged from 4 to 10 µm in size, while the intracellular granules (white arrows) within enlarged vacuoles ranged from 1 to 2 µm in size.

Adapter-free and quality-filtered sequences were assembled *de novo* using the SPAdes genome assembler v3.10.0 with default settings and no additional pipeline options (10). The resulting assembly graph was visualized via Bandage v0.8.1 (11) using default settings, which resulted in a total of 646 contigs (nodes), 858 connections between those contigs (edges), 19 dead ends, an N_{50} value of 375,049 bp, a GC content of 38.39%, and a total length of 12,201,803 bp, including overlaps. Annotation through NCBI estimated a draft genome size of 12,132,557 bp, with 103 contigs and 165 scaffolds. BLASTn was used via Bandage to reconfirm the isolate identification as *S. spartinae*, finding a 100% identity match to the published *S. spartinae* ATCC 18866 (12) partial 18S rRNA gene (GenBank accession number HQ876044.1) and a 100% match to the D1D2 region of the 26S rRNA gene (GenBank accession number HQ876052.1). Gene prediction and functional annotation were performed using default settings with Funannotate v1.8.1, a software package for gene prediction, annotation, and comparison of small eukaryotic genomes (13). Through Funannotate, Augustus, Augustus HiQ, GlimmerHMM, and snap identified a total of 14,401 genes. Also through Funannotate, Diamond mapped 550,947 proteins to the isolate genome, and 2,014 final alignments were made via Exonerate. Default databases were used for identification of genes and proteins. The full list of databases used and their version numbers are associated with the default settings of Funannotate v1.8.1. Functional annotation completeness was estimated to be above 89.6% using BUSCO v3 (14) run in protein mode and 91.3% run in genome mode with the Ascomycota lineage and *Saccharomyces cerevisiae* species as references.

These data suggest that a nearly complete genome sequence was obtained for *Scheffersomyces spartinae* ARV011, which serves as a valuable resource for future studies of this organism.

Acknowledgments:

This work was supported by funds from the Marine Biological Laboratory, DOE (grant DE-SC0016127), NSF (grant MCB1822263), the Howard Hughes Medical Institute (grant 5600373), and a gift from the Simons Foundation.

We acknowledge the Woods Hole Microbial Diversity course directors (Rachel Whitaker and George O'Toole), course faculty Deborah Hogan, course staff, and lecturers for supporting this research. We acknowledge Alvaro Hernandez and Chris Wright at the Roy J. Carver Biotechnology Center at the University of Illinois in Urbana-Champaign for help with sequencing.

Data Availability:

This whole-genome shotgun project for *Scheffersomyces spartinae* ARV011 has been deposited in DDBJ/ENA/GenBank under accession number JAHMUF000000000. The version described in this paper is version JAHMUF010000000. The draft genome assembly and annotation can be found under BioProject number PRJNA738152 and BioSample number SAMN19714210.

References

1. Kurtzman CP, Suzuki M. 2010. Phylogenetic analysis of ascomycete yeasts that form coenzyme Q-9 and the proposal of the new genera *Babjeviella*, *Meyerozyma*, *Millerozyma*, *Priceomyces*, and *Scheffersomyces*. *Mycoscience* 51:2–14. doi: 10.1007/S10267-009-0011-5.

2. Jia R-R, Lv S-L, Chai C-Y, Hui F-L. 2020. Three new *Scheffersomyces* species associated with insects and rotting wood in China. *MycoKeys* 71:87–99. doi: 10.3897/mycokeys.71.56168.

3. Wilbanks EG, Jaekel U, Salman V, Humphrey PT, Eisen JA, Facciotti MT, Buckley DH, Zinder SH, Druschel GK, Fike DA, Orphan VJ. 2014. Microscale sulfur cycling in the phototrophic pink berry consortia of the Sippewissett Salt Marsh. *Environ Microbiol*16:3398–3415. doi: 10.1111/1462-2920.12388.

4. Kharchuk MS, Glushenkov AN, Gromozova EN. 2019. Analysis of the motion of vacuolar volutin granules in *Saccharomyces cerevisiae*. *Folia Microbiol (Praha)* 64:207–213. doi: 10.1007/s12223-018-0646-8.

5. Usyk M, Zolnik CP, Patel H, Levi MH, Burk RD. 2017. Novel ITS1 fungal primers for characterization of the mycobiome. *mSphere* 2:e00488-17. doi: 10.1128/mSphere.00488-17.

6. Altschul SF, Gish W, Miller W, Myers EW, Lipman DJ. 1990. Basic local alignment search tool. *J Mol Biol* 215:403–410. doi: 10.1016/S0022-2836(05)80360-2.

7. Andrews S. 2016. FastQC: a quality control tool for high throughput sequence data. http://www.bioinformatics.babraham.ac.uk/projects/fastqc.

8. Bolger AM, Lohse M, Usadel B. 2014. Trimmomatic: a flexible trimmer for Illumina sequence data. *Bioinformatics* 30:2114–2120. doi: 10.1093/bioinformatics/btu170.

9. Langmead B, Salzberg S. 2012. Fast gapped-read alignment with Bowtie 2. *Nat Methods*9:357–359. doi: 10.1038/nmeth.1923.

10. Nurk S, Bankevich A, Antipov D, Gurevich A, Korobeynikov A, Lapidus A, Prjibelsky A, Pyshkin A, Sirotkin A, Sirotkin Y, Stepanauskas R, McLean J, Lasken R, Clingenpeel SR, Woyke T, Tesler G, Alekseyev MA, Pevzner PA. 2013. Assembling genomes and mini-metagenomes from highly chimeric reads, p 158–170. *In* Deng M, Jiang R, Sun F, Zhang X (ed), *Research in computational molecular biology.* Springer, Berlin, Germany. doi: 10.1007/978-3-642-37195-0_13.

11. Wick RR, Schultz MB, Zobel J, Holt KE. 2015. Bandage: interactive visualization of *de novo* genome assemblies. *Bioinformatics* 31:3350–3352. doi: 10.1093/bioinformatics/btv383.

12. American Type Culture Collection. *Scheffersomyces spartinae* (Ahearn et al) Kurtzman et Suzuki:ATCC18866TM. https://www.atcc.org/products/18866.

13. Palmer JM, Stajich J. 2020. Funannotate v1.8.1: eukaryotic genome annotation. *Zenodo*. https://zenodo.org/record/4054262#.YXZmHhrMLIU.

14. Seppey M, Manni M, Zdobnov EM. 2019. BUSCO: assessing genome assembly and annotation completeness. *Methods Mol Biol* 1962:227–245. doi: 10.1007/978-1-4939-9173-0_14.